MATCHING OF WELL-LOGS AND SEISMIC FIELD DATA

A thesis submitted by

VINCENT I. EZEANYIM, B.Sc., M.Sc., D.I.C.,

for

the Degree of Doctor of Philosophy

of

the University of London

December, 1983

Geology Department,
Imperial College of
Science and Technology,
London SW7

ABSTRACT

The art of matching well-log data with field seismic data is complicated by a number of factors which are traced to the seismic data acquisition, processing, and synthetic seismogram generation systems. The limiting effects of these procedures and their effect on synthetic-field trace matching are reviewed. Demonstrations and applications with theoretical and real data are given whenever necessary.

A major problem in matching well-log generated seismograms with field observed seismogram is that of estimating the wavelet which ensures the best synthetic seismogram. The choice of waveform is the most critical aspect and the best method of making it is still a subject for research and development. Three different methods, the matrix partition technique, the method of straight residuals and the optimum least-squares technique, are introduced in addition to the method of White (1980), to overcome the wavelet estimation problems. Design examples and their applications to synthetic generation problems are demonstrated.

It is not always visually obvious that a match is of doubtful validity, White (1980). Other measures are therefore necessary. Some numerical matching or comparison measures are presented to give the most probable quantitative estimates of the relationship between a well-log generated seismogram and the corresponding field observed seismogram. These measures, such as γ_c

(the Pearson's product moment correlation coefficient), Ω(the goodness measure), α(the normalised mean-square error), coherence (the frequency domain measure), and such other statistics as X^2 (chi-squared), are discussed with examples. These methods increase the confidence we attach to our match.

New techniques for synthesising the reflection impulse responses, and for analysing the reflection responses generated from linear filter models are introduced in the present work. The first technique operates in the frequency - wave number domain. The second involves bandpass and time-variant filtering of reflection responses. The new techniques produce better matching than the unfiltered responses generated via a linear filter model.

ACKNOWLEDGEMENTS

I wish to express my thanks to Professor R.G. Mason (Head of Geophysics, Imperial College), and Dr. C.J. Hewlett for their encouragement during the course of this work. Dr. Hewlett spent a lot of time at the early stages of the research project and helped in the final reading of the manuscripts. I am also grateful to Dr. D.R. Cowan and Dr. Anna Thomas-Betts for their kind suggestions.

The continuing encouragement and help I received from a number of U.K. based oil companies and consultancies need some mentioning. Among these, the British Petroleum (BP), Texaco, Merlin, and Western Geophysical, did supply us with actual seismic and log data, at different stages of the work.

The stimulating discussions and communications I had with some members of the B.P. Geophysical group were very helpful. In this regard, I must mention Dr. R.E. White and A.T. Walden, C. Swaine and D. Dalchow. My special thanks go to Dr. B.L.N. Kennett (Dept. of App. Maths. and Theoretical Physics, Univ. of Cambridge) and P.N. Conn of Merlin Velocity profiling Co. Ltd. In addition to personal communications and suggestions,

Dr. Kennett, made available the layer matrix routine, while P. Conn, was very helpful for most of the log-field data analysis.

This project which is computer oriented owes much to the efficient facilities of the University of London and Imperial College computer centers with special reference to the advisories. Tape analysis, especially the reading of IBM tapes in CDC machines was about the most discouraging aspect of this project. As far as the author knows, there was no previous documented method of reading IBM seismic tapes on Imperial College CDC machines. To this end Mr. Peter Furnis (ULCC) and Thomas Sippel-Dau (ICCC) were most helpful.

I take this opportunity to thank all my colleagues, all members of the Geophysics section, and Royal School of Mines, for their cooperation I also thank Damian and Cyril Ezeanyim, who started my academic pursuits, the Commonwealth Council, the Federal Government of Nigeria, and the University of Calabar, for offering me sponsorships.

Finally, and not the least, I am grateful to Gill Davies for an efficient typing of the manuscripts.

CONTENTS

		PAGE
ABSTRACT		3
ACKNOWLEDGEMENTS		5
CHAPTER 1	Introduction	12
1.10	The Exploration Seismic Procedures	14
1.20	Seismic Data Processing	18
CHAPTER 2	Limitations of Exploration Seismic Methods	26
2.10	Limitations of Seismic Data Acquisition Techniques	26
2.1.1	Explosive Sources	27
2.1.2	Size of charge	28
2.1.3	Amplitude and Weight of Charge	29
2.1.4	Nature of the Explosive Impulse	31
2.1.5	The Vibroseis System	33
2.1.6	Marine Seismic Sources	36
2.1.7	Seisic Singal Receivers	38
2.1.8	Geophone plant and Ground Coupling	39
2.20	Limitations of Seismic Data Processing Techniques	42
2.2.1	Sampling Considerations	43
2.2.2	Effect of number of bits	43
2.2.3	Frequency Relations - Sampling Interval and Aliasing	45
2.2.4	Frequency Bandwidth	47
2.2.5	Seismic Filtering Methods	51
2.2.6	Deconvolution Filtering Technique	66
2.2.7	The Effect of NMO correction on a seismic pulse	62
2.2.8	The NMO Stretching Equation	65

PAGE

2.2.9 Effect of NMO Stretching on CPD stack 67
2.2.10 Multiples 69
2.2.11 Seismic Lateral Resolution - Wave Theory vs Ray Theory 72
Summary

CHAPTER 3 Generation of synthetic seismograms from well-log information 83
3.00 Synthetic Seismograms 83
3.10 The Fundamental Relations 87

3.20 The Synthetic Hypotheses 92

3.30 The General Methods of Synthesis 94

3.3.1 Synthesis Based on Filter Theory 94
3.3.2 Linear Filter and Convolution Process 96
3.3.3 Impulse Response Function 96
3.3.4 Linear Filter Model - Primaries Only 98
3.3.5 Linear Filter Model - All possible Reflections 100
3.3.6 The Layered System 102

3.40 Synthesis via Kirchhoffs Solution of Scalar Wave Equation 112

3.4.1 The Kirchhoffs Formulation of Diffraction 114
3.4.2 Kirchhoffs Reflections And Diffractions 117
3.4.3 The Weight Functions and Synthetic Seismograms 119
3.4.4 Plane Diffractor (Synthetic) Modeling 120
3.4.5 Computer Evaluation of the Synthetic Algorithms 122
3.4.6 Parameter specifications 124
3.4.7 Discussion of Kirchhoff's Seismograms 126

3.5.0 The Synthetic Generation problems and Limitations: 132

		PAGE
3.5.1	Inaccurate well-logs and Approximations	132
3.5.2	Problems of Velocity Measurements in Boreholes	135
CHAPTER 4	Misties between the Synthetic and Field Seismograms	139
4.10	Why Match Synthetic with Field Seimograms?	139
4.20	Causes of Misties Between Synthetic and Field Seismograms	141
4.2.1	Noise, Its Effects and Suppression	142
4.2.10	Recorded Noise	144
4.2.1.1	Ambient Noise	144
4.2.1.2	Source Generated Noise	145
4.2.2	Processing Noise	149
4.2.3	Anisotropy	152
4.2.3.1	Anisotropy and Velocity Measurements	154
4.2.3.2	Checkshot and Well-log Velocities	156
4.2.3.3	Anisotropy and NMO	157
4.2.4	Seismic Approximations and Assumptions	159
4.2.5	Amplitude Distortion	159
4.2.5.1	Spherical Divergence	160
4.2.5.2	Absorption	161
4.2.5.3	Multiples and Interfaces	161
CHAPTER 5	Similarity Measures and Quantitative Matching of Seismogram Traces	163
5.10	Similarity Measures	163
5.1.1	Correlation	164
5.1.2	Correlation Coefficient (γ_c)	166
5.1.3	Coefficient of coherence	168
5.1.4	Coefficient of Multiple Coherence	171
5.1.5	Coefficient of Partial Coherence	172

PAGE

5.20 Multiple Input Linear Systems - Application to Similarity Measurement, Wavelet Estimation and Synthetic Seismogram Generations: 173

5.2.1 The cross-spectra relations 175
5.2.2 Matrix Formulation of the multi-system of Linear Equations 175
5.2.3 Computational Procedures and Parameters 178
5.2.4 Two-input Linear Systems 181
5.2.5 Partial Coherence (Two-input Systems) 181
5.2.6 Method of Application 185
5.2.7 Generation of Synthetic Seismogram (Multiple-input) 187

5.30 Least-squares Measures 189

5.3.1 The optimum least-squares Analysis 191
5.3.2 Mathematical Theory 193
5.3.3 The Practical Optimum Filter Model 196
5.3.4 Practical Requirements 197
5.3.5 Practical Procedure 198
5.3.6 Goodness of Input and least-squares Measure 198

5.40 Statistical Measures 200

5.4.1 The X^2- (chi-squared) Measure 201

5.50 Matching with Similarity Measures 203

Summary 228

CHAPTER 6 Further Developments in Matching Analysis 230

6.10 Synthesis of Impulse Responses from a point-localised source with attenuation included in frequency - wavenumber domain 230

PAGE

6.20 Basic Theory 232

6.30 The theoretical synthetic seismograms and matching improvements 237

6.40 Matching Improvement from Filtered Impulse Responses Generated via Linear Filter model

CHAPTER 7 Conclusions and Suggestions for Further Works 267

REFERENCES 269

APPENDIX A-2 281

APPENDIX A-3 283

CHAPTER 1

INTRODUCTION

Exploration seismology is a very broad area of endeavour. A thesis about the matching of well-logs and field seismic data faces the great task of reviewing nearly every aspect of exploration seismic work. As such a task is obviously beyond the scope of a normal thesis, our emphasis will be on those areas of exploration seismic studies that are most relevant to synthetic and field trace matching. These areas include various aspects of exploration seismic data acquisition, processing, and synthetic seismogram generation systems. We shall study the major limitations of these systems as they affect synthetic-field trace matching.

In most cases we shall suggest possible ways of annulling or at least reducing the effects of these limitations. In this respect our work differs from that of White (1980), Walden et al. (1983). These authors laid more emphasis on the statistics of the match but said little about the physical causes of the mismatch or methods of reducing it. We will show in practice that it is possible to improve a match by reducing some of the seismic limitations, and the synthetic generation problems such as noise (especially the multiples), seismic approximations and assumptions, inaccurate well-log information, problems of velocity measurements in boreholes and in the field, NMO effects, aliasing, limited frequency bandwidth, etc. These seismic problems

and possible methods of elimination are presented in chapters two and three, while chapter four discusses the major causes of misties between the synthetic and the field observed seismogram.

One of the main problems in matching well-log generated seismogram with field observed seismogram is that of estimating the wavelet which ensures the "most probable" synthetic seismogram. The choice of this waveform is critical and the best method of generating it is still a subject of research and development. In chapter five, three different new techniques of wavelet estimation, in addition to White's model (1980) are introduced. The three techniques are; the matrix partition technique, the method of straight residuals, and the optimum least-squares technique. In addition, some numerical matching or comparison measures have been introduced to give the most probable quantitative estimates of the relationship between a well-log generated seismogram and a corresponding field observed seismogram. Such measures as γ_c (the Pearson's product moment correlation coefficient), Ω(the goodness measure), α(the normalised mean square error), coherence (the frequency domain measure), and other related statistics like X^2 (chi-squared), strengthen the confidence attached to any established match.

In chapter six, new methods are introduced to improve the match between the well-log generated seismogram and the field seismogram observed closest to the well. The methods include; (i) matching improvement by the method of generation of impulse responses from Fourier Synthesis

and far-field signature, and (ii) matching improvement by filtering the impulse responses generated from the linear filter models. The merits and demerits of these methods are also assessed.

For the last part of this chapter, it is appropriate to refresh our minds about basic exploration seismic procedures, in addition to some important steps in seismic data processing.

1.10 The Exploration Seismic procedures

As a convenient starting point we discuss the various stages necessary to develop a field seismogram, pointing out any of the limiting factors as we encounter them. We will leave detailed discussions on limitations to chapters two and three. This approach is necessary because it is easier to find a solution once the root-cause of any problem is known. For example, the best match between the field trace and synthetic trace may be obtained if we can know and control the effects of the limiting factors from the onset of data acquisition to the end of processing.

A typical seismic exploration set-up often looks very simple. Figure (1.00) is illustrative enough, it is a simple diagramatic cross-section which illustrates the requirements of the seismic technique. It is necessary that a method be derived that allows a cross-section of the earth to be drawn in sufficient detail to permit probable oil and gas reservoirs such as X, Y, Z or even any other structure of interest to be found. The sources and

receivers of acoustic energy must reside on or close to the surface. It is important to note, however, that the medium through which the energy travels is heterogeneous, laminated but subject to discontinuities such as the unconformity shown, or abrupt displacements due to faulting. In addition, the weathered layer is a layer of low velocity and density, of variable thickness and constitution, disconformable with the underlying consolidated rocks, and even subject to seasonal fluctuations in properties. We definitely must expect problems from such a complex medium.

A possible acoustic wavepath is that shown from the source to O, to the receiver (figure (1.00). It is immediately obvious that not just one echo is received at each receiver from a single input pulse, since each change in the elastic properties of the rocks should give an echo. The cross-section shown in figure (1.00) is most cases is exaggerated, bearing in mind that the change in the vertical sequence of rocks is not quite as rapid in the horizontal direction as shown in the figure. Thus most, but not all prospecting problems can be looked at in the first place as a challenge to measure the positions of rock boundaries vertically beneath the experimental equipment which can be moved along the surface from point to point. For one of these experimental positions on the surface, the problem then reduces to that shown in figure (1.01), determination of the co-ordinates (Xi, Zi) of the successive reflecting points. Figure (1.02) is a seismic cross-section. It consists of a large number

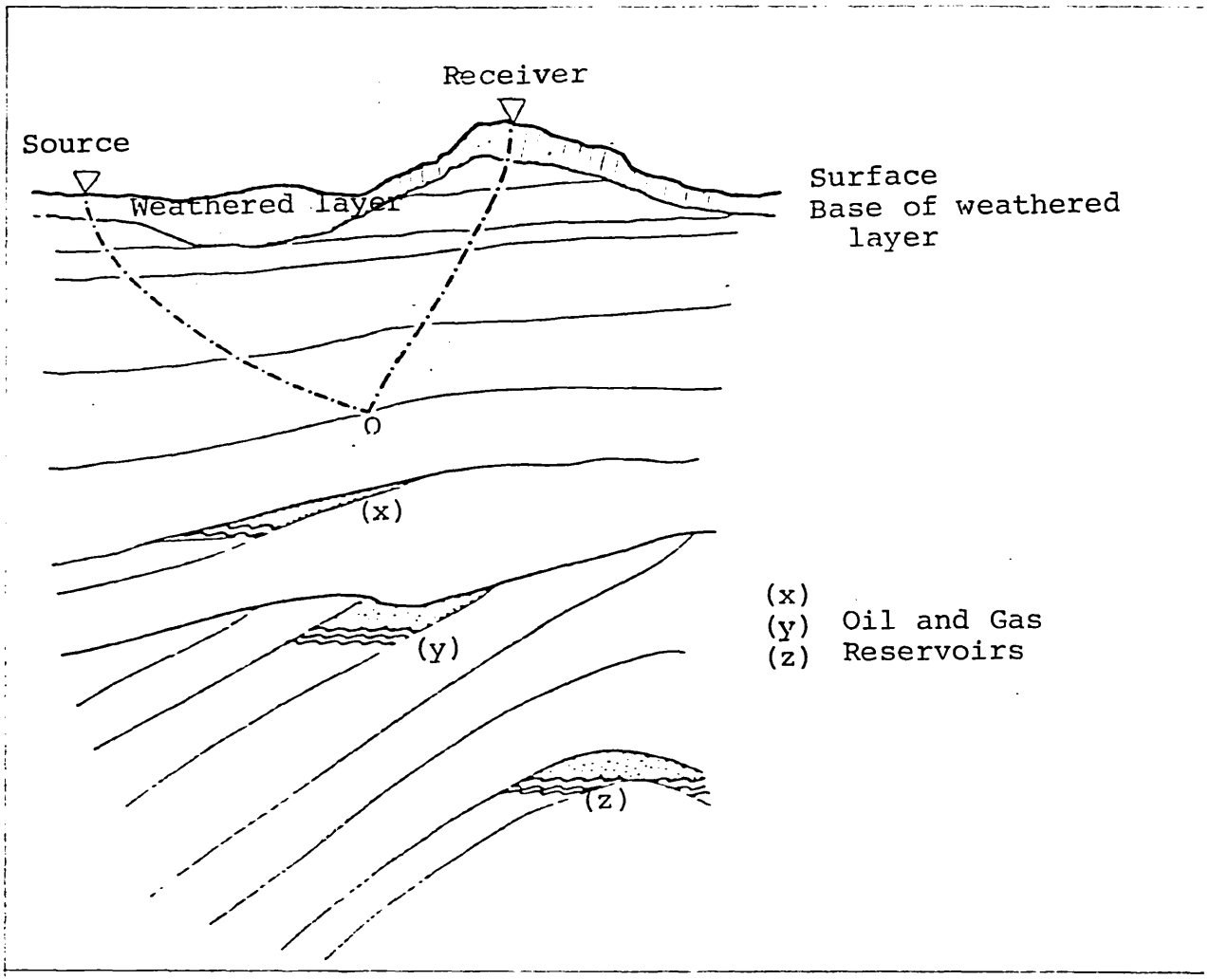


Fig. 1.00 Diagramatic cross-section showing trapping modes for oil and gas in the pores of rocks (Waters, 1979).

of vertical seismic traces, each of which shows the variation in received energy with time (the vertical coordinate). Thus any indication of suitable conditions (say of oil accumulation, such as the marked reflection near B) can immediately be related to the surface position on the earth and steps can be taken to make appropriate tests by well drilling.

The geological picture presented here is not yet true in all respects, nor are the steps and conditions of survey as simple and straight forward as illustrated.

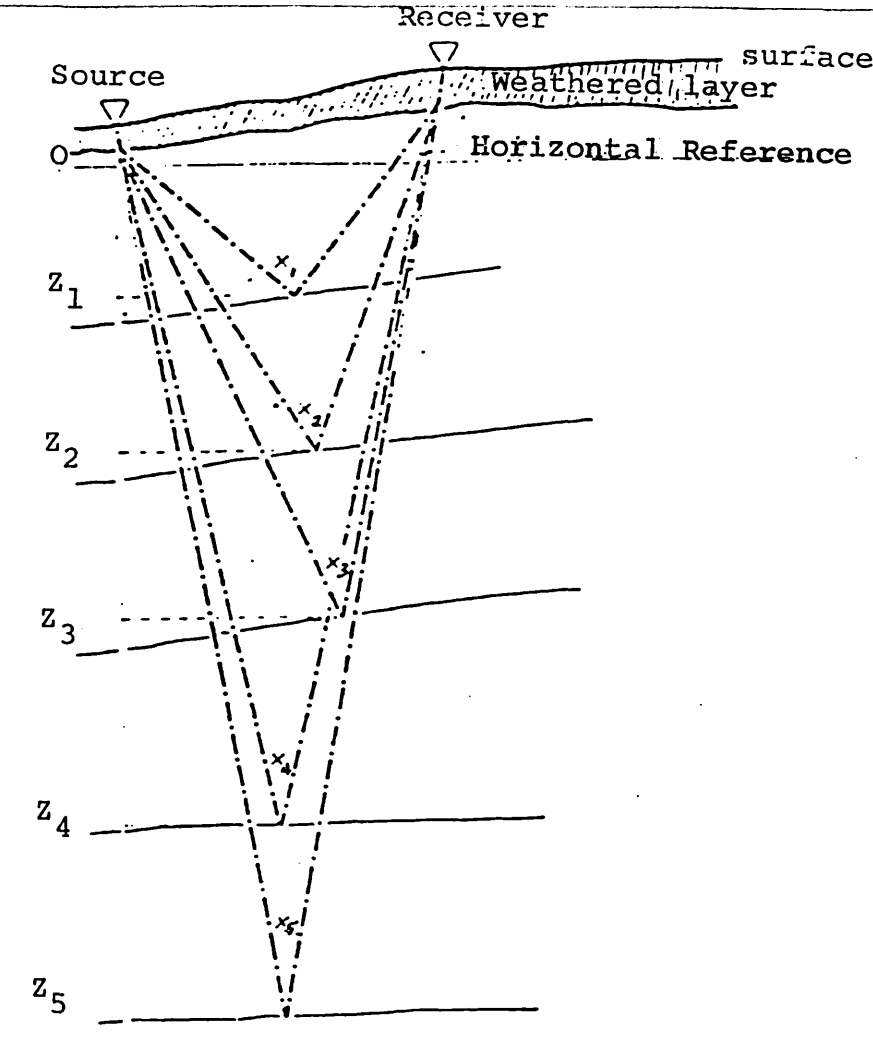


Fig. 1.01 The coordinates of reflecting points to be determined by reflection seismology (Waters, 1979)

The section is only the first indication of the geological structure beneath the sequence of experimental stations. We proceed to mention some of the major steps in processing before the discussion on the prevalent exploration seismic limitations and limiting factors.

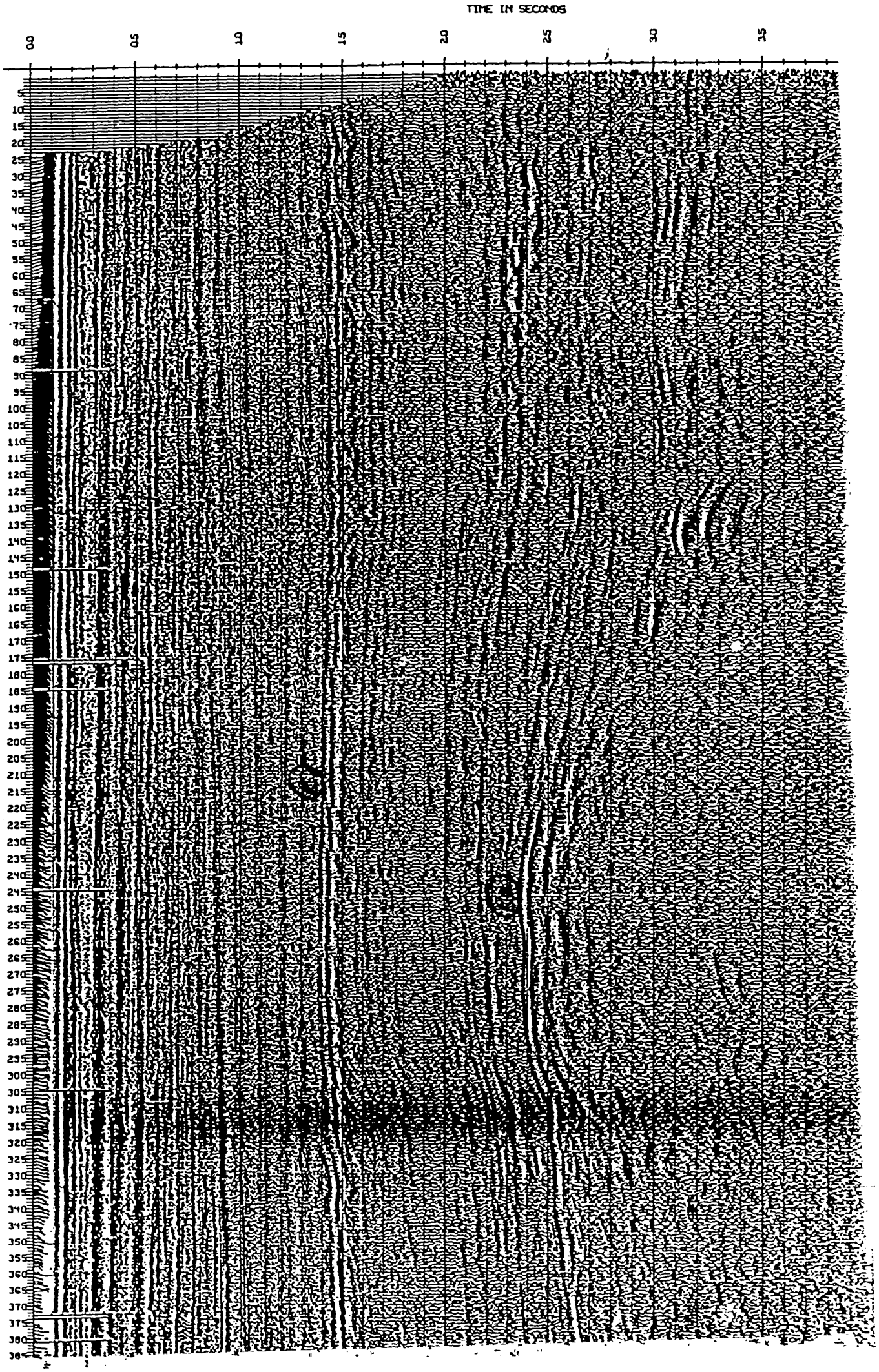
1.20 Seismic data processing

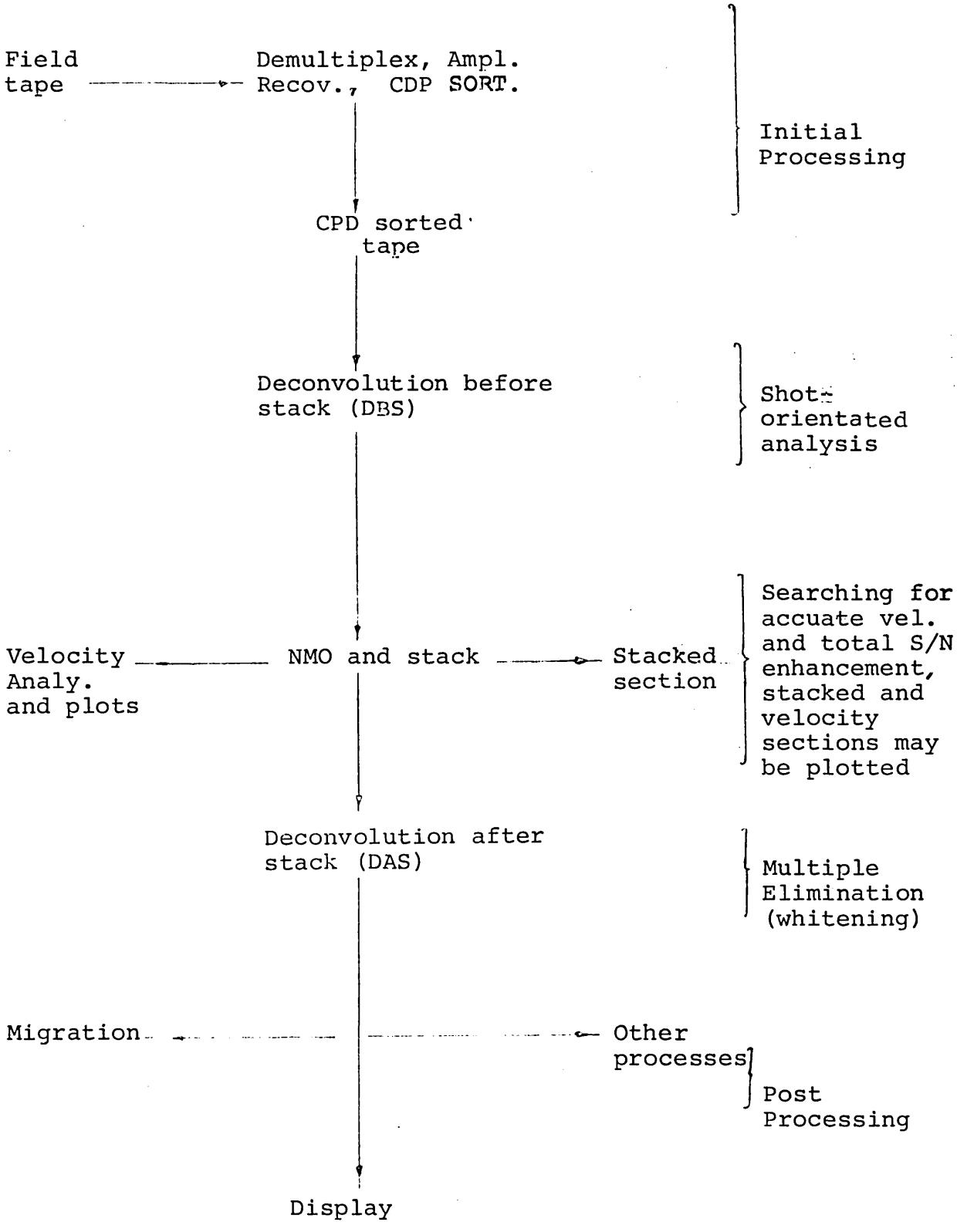
Our discussion of seismic data processing here, will be very brief. Detailed discussion may be found in text books on seismic data analysis, and geophysical periodicals. Reflection Seismology (K. Waters, 1979), Geophysical Signal Analysis (E.A. Robinson, 1980), Geophysics, and Geophysical Prospecting, may be very helpful to an interested reader.

Most seismic data is recorded digitally in the field. Seismic processing takes this data as input and produces as output a suitable product for interpretation (see block diagram A). Usually this consists of a vertical cross-section in time through the earth, of the seismic reflections. It may, also take the form of velocity information or even horizontal time slices (3-d seismic). Some parts of this procedure are essential (e.g., demultiplexing, move-out corrections prior to stack). other parts just improve the interpretability of the data, (e.g. deconvolution, migration) but this improvement can be vast.

The basic stages in seismic signal processing are now given. Each stage will be presented as a brief summary of a particular processing step. The term optional included with any stage of processing, implies that the application of that specific processing step is at the discretion of the seismic analyst.

Fig. 1.02 Seismic section- Forties (Courtesy, British Petroleum)





Block 1A: Seismic processing steps and procedures

(i) Field Tape Demultiplex and Edit

In the field, seismic data is recorded in multiplexed form (samples of all traces for one time step are recorded together, then followed by all samples for the next time step). On the other hand, seismic processing is carried out trace by trace (for ease of general data manipulation). The data, therefore, are demultiplexed into trace sequential format. In theory this process is a simple matrix transposition but in practice, owing to the large matrices involved, it turns out to be a demanding process. At this stage, the data are checked for tape errors, while test shots and misfires are muted or edited out.

(ii) Amplitude Recovery

On a modern floating point field system the changes in gain of the recording amplifier are written onto the field tapes, and the true amplitudes of the signal output from the detectors can therefore be recovered. To compensate for the effects of absorption and geometrical spreading the signal values are multiplied by some linear or exponential factors. Sometimes, data dependent scaling is applied. This is a form of automatic gain control whereby trace amplitudes within a (sliding) time gate are equalised, so that the r.m.s. or average amplitude within the gate is held constant.

(iii) Shot - Orientated processing - Optional

At an early stage in processing the traces are in gathers, each associated with a single shot. These gathers may be processed in a number of ways.

(a) Signature Deconvolution

If the outgoing seismic signal is known, it may be transformed into an approximation to a spike by inverse filtering. This step is particularly essential for sources with a long signature (Maxipulse, for example). The signature is either recorded or synthesised as it is often difficult to record the outgoing signal for a spatially large source (such as the airgun).

(b) Shot Noise Filtering

Noise peculiar to a specific shot (first arrivals, cable jerk, etc.) which has a particular velocity can be suppressed by two-dimensional filtering. A phase compensation filter can be applied to correct for instrument filtering or other phase effects.

(iv) Field Geometry Merge

Each trace is assigned a CMP number for the stacking process (see below). This requires definition of the shot and receiver positions for every trace. In marine seismic data acquisition, the spacings are often regular but in land acquisition and 3-d seismic work, we may need the detailed information of the position of each shot and geophone station, where the relevant

static corrections must also be specified. The necessary information is usually stored in the seismic trace header, the observer's log, or a separate navigation file.

(v) Cmp SORT

For convenience during stacking (and velocity analysis), all traces belonging to the same common mid point are sorted into the same group. This is usually another time consuming procedure and takes the form of a physical reordering of the traces on tape.

(vi) Deconvolution Before Stack (DBS) - Optional

The procedure is frequently applied for two main reasons - to remove multiples (dereverberation) and to equalise the frequencies in the traces (whitening) prior to velocity determination and stacking.

(vii) Velocity Determination

For a horizontally layered medium, seismic reflection times vary with offset along a hyperbola defined by the Normal Moveout (NMO) equation:

$$T^2 = T_o^2 + \left(\frac{X}{V}\right)^2 \qquad (1.00)$$

where, T is the travel time for the reflected wave, and T_o, the zero offset-time. For stacking to be successfully carried out, all reflection times must be NMO corrected to the zero offset time, To. This requires accurate knowledge of the velocities in the earth and is a critical part of processing. Accurate velocity

information may be of vital importance in predicting lithologies, and hence in synthetic-field trace matching. In general the accuracy and spatial frequency with which velocity determinations are made depends on the objectives which include: stacking (greater accuracy for high frequencies and shallow events), lithological predictions and depth conversions.

(viii) Normal Moveout (NMO) and Stack

The stack is a powerful processing operation which enhances the signal/noise ratio. In stacking we sum traces which share the same sequence of subsurface reflection points but are from different shots and have different distances between shot and detector (offsets). If NMO correction is properly applied, and velocity accurately determined, stacking will give a signal/noise enhancement of the order $\sqrt{n}$ for n fold stack. Actually the enhancement relies on the very ability to receive signals from one reflection point by more than one raypath so that the noise due to scattering along the raypath is random. Usually NMO corrections involve the corrections of the reflection times for the effect of shot-to-receiver horizontal distance.

(ix) Devonvolution After Stack (DAS) - Optional

This is a whitening and multiple elimination process. The signal spectrum is usually whitened to within a certain frequency band in order to shorten the reflection pulse length and stabilise the pulse shape. Usually, predictive deconvolution aims at removing multiples,

water reverberations, or any ringing tail to a reflection pulse. The "white noise" level is a noise suppression factor input to the deconvolution filter design, which effectively restricts the frequency band over which the signal spectrum is whitened.

(x) Migration - Optional

Migration is an imaging process whereby dipping reflections and diffractions are restored to their correct spatial configurations.

(xi) Display

The individual graph representing the motion of a geophone (or the average of a geophone group) is called a trace. The trace records the signal amplitudes in the form of wiggly-line. Sometimes variable-area or variable-density traces are used. In the field variable-density output is obtained by replacing the recording galvanometer component with a light source whose intensity is varied in accordance with the signal variations, so that the intensity might increase during signal peaks and decrease during signal troughs. A common computer method is to shade all the positive amplitudes making them more conspicuous relative to the negative amplitudes. The plots may be a combination of traces, a migrated or a simple stacked section. Visual analysis of seismic data is simplified by good plots and displays.

There are of course other processes which can be applied (Bandpass Filtering, autocorrelation, mixing. etc). Each of the above mentioned processes has its

merits and limitations as we shall see in coming chapters.

CHAPTER 2

The Limitations of Exploration Seismic Methods

In the last chapter we pointed out the need to check the many seismic limitations and limiting factors. For the present chapter we discuss some of these limitations, especially as they affect the various aspects of seismic data acquisition, and processing techniques. Well-log synthetics are left until the next chapter on synthetic seismogram generation.

2.10 Limitations of Seismic Data Acquisition Techniques

In nature, elastic waves are generated whenever a sudden change in stress occurs in the earth, usually in the form of a stress change due to strain relief by faulting. The tectonic forces acting on the earths crust build up strain energy, both compressive and shear, until the elastic limit of the material is exceeded. The change in strain energy often implies a change in gravitational potential energy of the rock masses as well as energy radiated in the form of various kinds of elastic waves.

Whereas the use of these natural sources of elastic energy supplies some general knowledge of the earth's structure, such sources are generally unsuitable for more detailed investigations. Some of these investigations have to take place beneath the land and others below the shallow seas overlying the continental shelves.

Enhancement of seismic signals can be achieved by improving the geometrical array configuration of the sources and receivers, and by choosing the seismic source that can provide good reflection signal-to-noise ratios at all times of interest. Such a source will produce the best results.

2.1.1 Explosive Sources

Explosive sources give rise to radiated seismic waves. The distribution of energy into different types of elastic waves varies considerably depending on the location of the explosion with respect to significant rock boundaries, as well as on the type and strength of the rock. The past (and present day) use of explosions to generate suitable waves for exploration is due to the very concentrated chemical energy available in high explosives. Dynamite and other high-energy explosive sources provide the simplest and most efficient means of releasing energy, but not without limitations.

The severity of the limitations has led to the development of many alternative sources; explosive air-guns, electrical sparkers, vibrating chirp systems (Crawford et al., 1960), and so on. In practice, charges are buried by drilling a suitable slot hole. The hole is usually deep enough to be below the weathered layer, a depth of few tens of metres. The signal produced by such an impulsive source is in the form of a "Dirac delta function". Owing to the transmission characteristics of the earth, the propagating pulse

broadens in time, and decays in amplitude. Sometimes, several shots are fired at different depths below the base of the weathered layer. The method generates waves of different forms due to the presence of a reflected wave from the base of the weathering. This affects the downward travelling composite pulse by introducing some unwanted variations in the spectrum.

2.1.2 Size of Charge

More often than not seismologists do not agree on the quantities of explosives they require most. Usually, they are particular about the physical characteristics of charges (diameter, weight, density ...) which affects the ease of handling in the field and determine the shooters maximum production. Sometimes, they have a feeling that one explosive is better than another but they cannot tell exactly why nor by how much. In an attempt to keep close to the realization of a point charge, it is customary to use high velocity, densely packed powerful explosives. However, in the desire for power, one is limited by the cost, and the cost of explosives is a considerable point of the total cost of seismic exploration. Besides, even if the cost is inconsequential, there are other limitations to the size of explosives to be used in exploration work. On the contrary, we should not take the strength of the explosives for granted and think that the seismic effects are directly related to it.

2.1.3 Amplitude and Weight of Charge

Striking a compromise between the amplitude of a seismic wave produced on explosion and the size or weight of charge causing the explosion has not been very easy. It is evident that the relation between charge weight and the amplitude of the reflected pulse will be complex, depending on the dimensions of the cavity both before and after the shot as well as the theoretical relation of energy and amplitude consequent on the shape of the pulse (Anstey, 1957).

Fig. 2.10 (O'Brien, 1967) shows the relationship between amplitude and weight of charge in a single hole, for shots fired in an actual refraction survey. If the charge of 1,320 lb weight had been divided into five equal parts and loaded into five holes, each separated from its neighbour by at least the diameter of the equivalent radiator, then the amplitude of the refracted arrival should have increased by a factor of about 2.5. From this, it follows that either the amount of dynamite could have been reduced in this proportion, or that readable records could have been obtained under noisier background conditions. In other words, under a noisy background, larger charges can always be used to operate successfully above the range of the noise. This, however, does not always follow. For sometimes (say nearer-surface (shallow) reflection, refraction works), of more interest to the seismologists is the energy in the low-frequency range. It can be shown that the low-frequency spectral amplitude should be directly proportional to

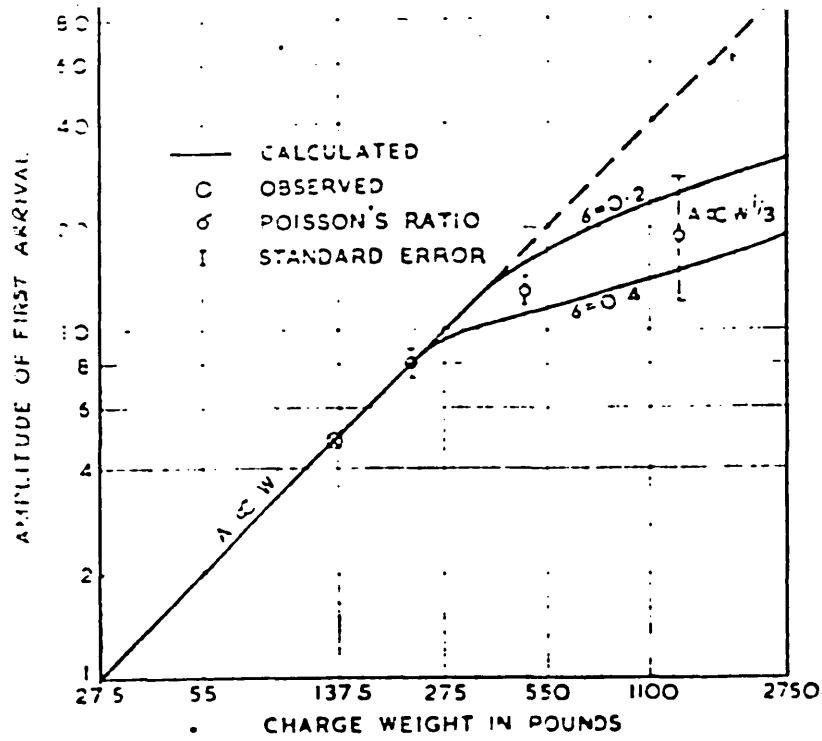


Fig. 2.10 Seismic amplitude as a function of weight of charge fired in a single hole (O'Brien, 1967).

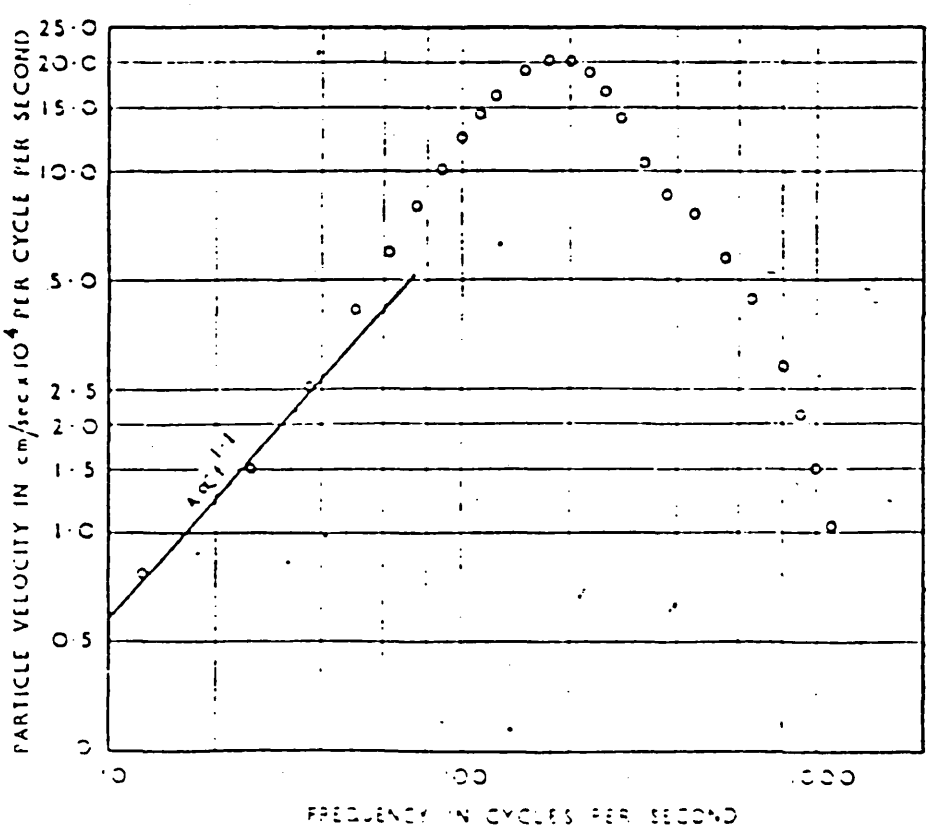


Fig. 2.11 Spectral amplitude for a pulse observed 100 ft from a one-lb charge in soft sandstone. No correction has been made for absorption

the frequency. Fig. 2.11, shows a Fourier analysis of a pulse observed 100 ft. from a one-lb charge in soft sandstone. The low-frequency amplitude is approximately proportional to $f^{1.1}$.

The spectral amplitude of an impulse is independent of frequency for periods long compared with its duration and we can show from Blake's equation* that the low frequencies of the wave radiated by an impulsive source should be proportional to f^2. On the other hand, if we accept the fact that the technique of reducing noise should be linked to signal strength, then we must remember that no good will come from increasing the source strength if the noise is ordinary interference (results from incoherent scattering of the signal).

When the change of pulse breadth with charge size is negligible over a range of operating conditions, the charge size may be determined as follows;

(1) If the solution of the geologic problem requires information only to a certain time, then the charge should be the smallest which will give information just beyond that time.

(2) If the problem requires as deep information as can be obtained, then the limit is that charge size at which the clarity of the early reflections begins to suffer on account of the lengthening of the pulse and then non-linear generation of noise in the region near the shot.

2.1.4 Nature of the Explosive Impulse

Many of the limitations encountered in seismic exploration may be traced to the nature of the source. The study of explosion-generated seismic waves may still be regarded as an empirical science. Unfortunately, it is difficult to observe the development of the complex disturbance that radiates from an explosion. The most extensive theoretical and experimental work is due to Sharpe (1946). Sharpe derived many well-known relations connecting the amplitude and dominant frequency of the radiated impulse with charge size, positioning, and the nature of the rock. He does not, however, explain the observed duration of the impulse. If we assume that the explosion suddenly increases the ambient pressure in a spherical cavity of raduis r and the elastic limits of the material surrounding the cavity are not exceeded, Sharpe showed that the shape of the elastic pulse generated a highly damped sinusoid is determined both

---

* Blake's theory shows that the amplitude A, of the particle velocity is given by

$$A = (P_w \; K/PV^2).W.(a^3/r)\left\{(W/V)^2+(1/r)^2\right\}^{\frac{1}{2}} \cdot \left\{1+(1-2K)\;(wa/c)^2 + K^2(wa/c)^4\right\}^{-\frac{1}{2}}$$

where P_w = amplitude of radial stress at w radians/sec.

$K = (1-\sigma)/_2(1-2\sigma)$

σ = Poisson's ratio

P = density

V = irrotational wave velocity

a = radius of equivalent radiator

by the radius of the cavity and the elastic constants of the material. It has also been suggested that an equivalent cavity can always be found to which the elastic limits are not exceeded. Thus a high frequency pulse is generated when the cavity radius is small. The actual mechanism, however, is much more complex, since almost always crushing of the rock takes place until the shock wave reaches a point where the behaviour of the rock is elastic.

In the absence of a complete theory of the processes that result in the radiated waves, progress is dependent on well designed experiments. Unfortunately, the complex properties of earth materials and the geologic structures in which full-scale tests must be carried out make the design of experiments difficult, hence we have to depend on approximations.

For the generation of high energy seismic waves exposive sources are quite commendable. The burying of sources below the weathered zone ensures relative freedom from surface waves. Explosive sources offer a good possibility of measuring the transit time through the weathered layer. On the other hand, the exact shape of the signal fed into the ground is neither controllable nor exactly reproducible. There are many cases where explosive sources turn out to be inefficient. For example, when confronted with a lossy overburden and a high noise level, one quickly reaches the point where the information is drowned in the background noise. The effect of these militate against our seismic accuracy using explosive sources.

2.1.5 VIBROSEIS SYSTEMS

A very important innovation in exploration seismology has been the development of systems in which the conventional explosive source is replaced by a vibratory signal source. The method is based on the use of mechanical vibrator which is hydraulically or electrically driven to exert a force of an oscillating magnitude. The source function (the sweep) is made up of force pulses generated at a frequency which increases linearly with time. A linear taper is often imposed at the begining and end of the applied sweep, while the sweep amplitude is constant through its lapse-time. The sweep signal is stored in a memory on each of the vibrator trucks and it is usually initiated by radio signal from the recording truck. The faithfulness with which the control signal is fed into the ground is limited by the vibrator-earth transfer characteristics. Sometimes, an array of vibrators may be used in place of a single vibrator.

The received signal represents the superposition resultant of all the wave trains which correspond to the individual reflections - different in amplitude and delayed in time. The record, at this stage is not well defined, because of the complexity of interference of the overlapping signals, where we define the recorded signal as shown:

$$F_y(t) = \sum_{j=1}^{N} b_j \, F_x(t-T_j)$$

and, bj, is the signal strength, $F_x(t)$ the initial source function and T the time delay. To extract the actual

reflection time, the recorded signal Fy(t) is cross-correlated with the applied source function $F_x(t)$, where correlation is equivalent to convolutions (see filtering technique) operation with signal turned around in time, hence;

$$
\begin{aligned}
{}_{yx}(t) &= F_y(t) * F_x(-t) \\
&= \sum_{j=1}^{N} b_j \, F_x(t-T_j) * F_x(-t) \\
&= \sum_{j=1}^{N} b_j \, \Psi_{xx}(Ti)
\end{aligned}
$$

where * denotes convolution operation. and $\Psi_{xx}(t)$, is the auto correlation pulse occuring with its maximum at the delay T.

Vibratory sources for seismic work have a number of advantages over conventional impulsive sources. A vibratory source signal can be chosen so that it contains only the desired frequencies. It is because no power is wasted crushing rock and generating frequencies which the earth cannot transmit that the enormous chemical energy of a charge of dynamite can be suitably replaced by a comparatively small vibrator. Unlike explosives or dropping weights, it is not disruptive to the environment, and can be applied in densely populated areas. The cost of operating the vibroseis systems is small when compared to conventional seismic field operations with impulsive sources.

---

* VIBROSEIS - Trade mark for the Continental Oil Company

There are however, some disadvantages. The vibroseis signal is of several seconds duration and travel time for the depths involved are less than this by one to three orders of magnitude, the wavelets in the received signal overlap each other considerably. Visual resolution of major wavelets, as done on conventional impulsive-source records is not possible. Other techniques, such as matched filtering must be applied to effect resolution. The rigid base plate and piston assembly of the system have a mass which is coupled to the impedance of the earth. For the seismic frequency range, the earth acts approximately as a spring, although the action is more complicated because of damping (both by radiation of energy and by heat loss) and because of the non-linear behaviour of the baseplate - earth system. In general the earth consolidates under the action of successive impacts and so presents a varying load to the force being impressed on it. From the point of view of signal shape, the effect of the non-linear behaviour is to introduce harmonics fig. (2.12) into the low-frequency signal generated, sometimes almost to the extinction of the desired fundamental. These harmonics may be detrimental to the quality of the seismograms eventually produced.

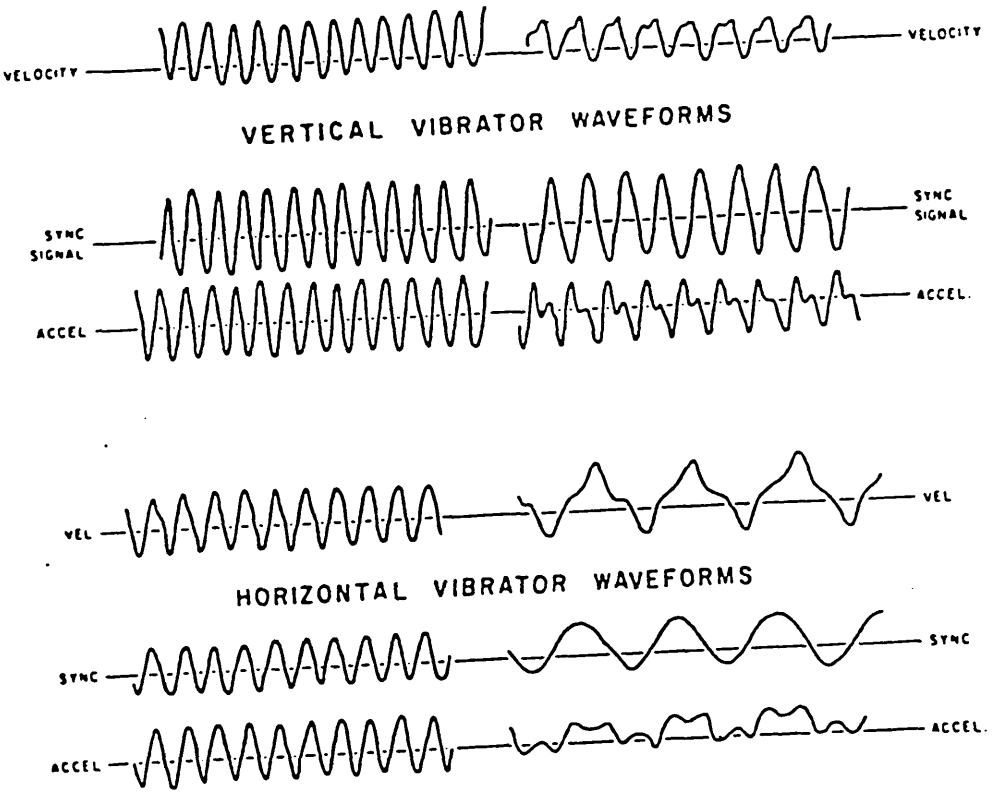


Fig. 2.12 The vertical and horizontal vibrator baseplate motions corresponding to a given synchronizing electric signal. High frequencies are on the left, and low frequencies on the right. Development of the double-frequency components as the frequency is lowered is evident. (Waters, 1979).

2.1.6 Marine Seismic Sources

Much seismic exploration is carried out in water-covered areas such as the continental shelves. In the early days of marine exploration unconfined explosive was used. The inefficiency of the unconfined explosives soon became apparent. A major disadvantage of some marine seismic sources is the bubble effects which generally accompany the recorded signals.

There are a number of solutions to the problem. Source wavelets may be generated regardless of the bubbles and then the recorded signals are debubbled at the end. The exposive source "Maxipulse" (Western Geophysical) belongs to this class of sources. In Maxipulse, small dynamite charges are exploded in the water. The idea of exploding the charges below the water surface is to improve the signal efficiency. This is not always successful.

The air-gun uses highly compressed air which is suddenly released into a chamber whose volume controls the frequency content of the pressure waveform. Sometimes the generation of bubbles may be suppressed by a suitable arrangement of air-gun array. Another possible solution to the problem imposed by bubbles is to use sources which inhibit or reduce bubble generation. In this group, we mention Aquapulse (Western Geophysical) and Vaporchoc (Compagnie Generale de Geophysique). For Aquapulse, a propane-oxygen mixture is exploded inside a steel mesh-supported cylindrical rubber sleeve. After detonation the sleeve expands from its initial cylindrical form but retains its cylindrical symmetry. This effectively reduces the bubble. Later the explosion generated gases are expelled, and a new charge enters. The Vaporchoc, unlike the air-gun uses compressed steam which is discharged into the water.

There are other sources such as the spark sources which rely on the creation of an acoustic wave in the air, while arc sources achieve their acoustic output by the ohmic heating of conductivity water between two

renewable electrodes. The high temperatures cause a steam bubble to be formed suddenly, which expands to give the seismic wave. Most of the successful sources have been the air-guns or gas guns for deep seismic prospecting, and sparker or Boomer for shallower, higher frequency work. We do not need to over-estimate these successes and assume that the best marine seismic sources had been developed. Those engaged in active processing of seismic data are aware of the fact that debubbling of marine seismic data is neither unnecessary nor is it a simple task. The discussed problems reduce our seismic accuracy.

2.1.7 Seismic Signal Receivers

The Earth's movement due to the arrival of seismic wave is sometimes small. A seismic receiver should have a high dynamic range and sensitivity in order to detect very small earth or water vibrations. On land the most common seismic signal receiver is the geophone while the hydrophone is the commonest receiver used in water. The geophone responds to the vertical component of the motion of the ground in which it is planted, and the hydrophone responds to the hydrostatic excess pressure exerted by the column of water. A seismic streamer is usually made up of a number of geophone elements encased in a fluid filled (kerosene or silicone liquid) flexible tube. The elements consist of piezo-electric (ceramic) devices in which the output voltage is

proportional to the stress (hydrostatic excess pressure) caused by the seismic wave. It has been found necessary to use many elements in parallel in order to achieve a reasonable impedance match to the cable-input transformer system, and some noise cancellation.

Most land geophones are electro-magnetic, and operate on the principle of voltage generation due to differential movement of a coil in a magnetic field. The generated voltage is proportional to the rate of change of flux caused by the movement of one part relative to the other. The resolution of most geophones may be increased by suitable damping.

The choice of Geophone is an important factor in applied seismology. In the field, care must be taken in the geophone plant, use of geophone groups and geophone spread.

2.1.8 Geophone plant

The coupling between the geophone and the ground is a resonant system. The behaviour of this system has been investigated by Wolf (1944), Pasechwik (1952). The resonant frequency and sharpness of tuning of this system are controlled by features which may seem insignificant to the man who plants the geophones, and in practice there is little hope of preserving these parameters identical from one geophone to the next. The effect of

this resonant system is of course, the same as that of a filter, so that each trace may be distorted and time-shifted by the geophone plant as though each one had been on a different filter setting. Where planting conditions on the spread vary widely (as often possible), this effect can seriously mar reflection alignments.

The "Bright spot" technique has been more successful in marine prospecting than in land prospecting (Safar, 1978). This is due partly to the problem of distortion of the seismic signal caused by the geophone - ground coupling, especially when carrying out high resolution shallow seismic surveys in swampy terrain. Though the effect of Geophone - Ground coupling on the response of a single geophone to the incident compressional waves has been treated by several authors, they have always neglected the influence of mutual interaction between an array of geophones on the response of each geophone forming the array.

It can be shown that mutual interaction which results from the re-radiation of the incident compressional waves by the geophones forming the array, can have considerable effect on the response of each geophone. This can be done by considering the effect of the geophone - ground coupling on the response of a seismic channel in the absence and in presence of mutual interaction between a group of geophones for the case when the shear wave velocity of the soil varies by a factor of three. It is also possible to increase the damping of the geophone-ground coupling system and consequently the undesirable distortion caused by the geophone-ground coupling is

reduced. The increase in the damping of the geophone-ground system is achieved by means of mutual interaction which results from the re-radiation of part of the incident compressional waves by closely planted geophones. Again we note the distortion is only reduced and not completely cancelled.

There are a lot of other problems that affect our Geophone usage in field exploration and which if not carefully avoided will reduce our seismic resolution. For example, if we are using a group of geophones, we must consider how far the geophones have to be separated so that the background noise is completely uncorrelated. Though we may plant the geophone firmly and even put them in small holes to minimize wind effects, we must take account of the fact that the elastic, transmitting characteristics of the material immediately underneath the geophone have direct influence on the arrival times. This is particularly important in land exploration and has been investigated by Koefoed (1954), Domzalski (1956).

The above mentioned are but few of the many problems we may expect while using most of our present day receivers, and in general we cannot completely remove their undesirable influences which do nothing except to reduce the limit of our field seismic accuracy.

Summary:

We have discussed the seismic acquisition systems pointing out the major limitations and limiting factors. Many authors (Kisslinger, 1963, Allen, 1956) have pointed

out in several ways, the many difficulties encountered in seismic surveying. It has come to be accepted that certain limitations of the seismic methods cannot be overcome, and others can be overcome though not economically. Some classes of problems are accordingly avoided and the possibility of devising radically new techniques has been largely neglected. Explosive impulse for example is inherently unsuitable for shallow surveys. We have little control over the nature of the explosive impulse signature. In marine work, bubble generation is still a problem to overcome. Recent researches have been directed towards the acquisition of sharp sources. In this respect the water gun is quite promising. Sources with sharp signals ensures higher resolution.

2.20 Limitations of Seismic Data Processing Techniques

The data obtained in a typical seismic survey consistsof measurements of the motion of the surface or pressure at a series of surface positions following the operation of a source of seismic waves. This motion may be particle displacement or velocity, which in its most general form is a vector function of time, or in certain cases the scalar excess pressure can be measured as a function of time. An important property of sets of time functions is that they are recorded simultaneously or at least have an indication of operation of the source.

For an exploration geophysicist, usually the most relevant data are from reflections from the geological strata and for this reason methods are needed for treating

the raw data which de-emphasise all but the reflection information. As the seismic reflection exploration method developed, more and more data processing became necessary. The advent of magnetic tape recording (early 1950s) began to demonstrate the possibilities of filtering, stacking and recording. Such methods dealt with continuous recordings of time functions (analog data). Some major processes of seismic data processing have been noted earlier in the chapter. We shall now discuss some of those factors in seismic data processing whose effects inhibit the attainment of high seismic resolution.

2.2.1 Sampling Considerations

The parameters associated with digitizing seismic data which are of greatest concern in processing are sampling interval and the number of bits (or binary digits) for each sample. The former quantity governs the frequency range over which the processing system gives usable results while the latter governs the dynamic range, resolution and precision of the processed information.

2.2.2 Effect of Number of bits

Seismic signals are stored digitally in binary code. The number of bits available for encoding the analog voltages at the sampling points sets a limit on the precision with which the data can be registered. If a voltage of 123.53 MV is to be encoded on analog tape with only 7 bits available, we would only express 123 MV

by the binary digits 11 1011 , but we cannot designate any values in between. With seven bits, our final result can be read only to the nearest millivolt, and this is not precise enough for most seismic registration.

The bits of each binary word are arranged according to a defined format (such as SEGY, SEGB, etc.). The formating procedure involves distribution of the bits of each binary word on a defined number of information tracks (seven or nine track tapes) as the case may be. There is always an error-checking bit for redundancy Two types of checking, vertical and longitudinal redundancy (parity) checks, are common. The longitudinal check accounts for missing bits while the vertical check shows whether the sum of ones recorded in a given tape is even or odd.

In modern equipment, the use of floating-point mode now ensures higher precision in data recording. Equipment of about 120 dB dynamic range and 18 bits precision is now common and can record information with higher accuracy so that the signal voltages are easily encoded with the degree of precision inherent in seismic data, which in most cases allows resolution to the order of microvolts. Seismic recording with high resolution instruments ensures better results.

2.2.3 Frequency Relations - Sampling Interval and Aliasing

In sampling, one of the major problems is to determine how often equidistant samples must be taken in order to describe adequately a given time function. Sampling has no adverse effect on the fidelity with which desired frequency components can be reproduced so long as the sampling frequency is more than twice the highest frequency component of interest in the signal. If the sampling frequency is less than this, one can expect a serious distortion of the output frequency which is generally referred to as aliasing. Aliasing is a potential source of error in seismic recording and processing, and aliasing noise can be detrimental. Anti-aliasing filters are generally designed to provide linear phase response and nearly flat amplitude response over the signal passband so that high attenuation is provided at and above the aliasing frequency.

The aliasing problems in the wave number domain are often much more severe. In order to explain the frequency - wave number relation, let us define the two-dimensional Fourier Transform of the continuous functions a(t,x) and A(f,k), where X, is distance and k, is wave number:

$$a(t,x) = \int_{-\infty}^{\infty}\int A(f,K)\, e^{2\pi i(ft+kx)}\, dfdk$$

$$A(f,K) = \int_{-\infty}^{\infty}\int a(t,x)\, e^{-2\pi i(ft+Kx)}\, dtdx \qquad (2.00)$$

Let us also assume that a(t,x) is sampled at N discrete points, ΔT units apart in the time direction and M discrete points, Δx units apart in the spatial direction. Within the seismic context, the spatial sampling is effected by the array of seismic detectors. Without loss of generality one may take $\Delta T = \Delta x = 1$ so that the discrete two-dimensional Fourier Transform pair is given by

$$a_{nm} = \sum_{p=0}^{N-1} \sum_{q=0}^{M-1} Apq\, e^{2\pi i(np/N+mq/M)} \qquad (2.00)$$

$$n = 0, 1, \ldots N-1$$

$$m = 0, 1, \ldots M-1$$

$$Apq = \frac{1}{NM} \sum_{n=0}^{N-1} \sum_{m=0}^{M-1} a_{nm}\, e^{-2\pi i(np/N+mq/M)}$$

$$p = 0, 1, \ldots, N-1$$

$$q = 0, 1, \ldots, M-1$$

The discrete frequencies are given by

$$f = np/N$$

and the discrete wave number by

$$K = mq/M$$

In order to avoid aliasing in the above sampling, the frequency wave number - values must lie within certain limits. A number of authors have suggested ways of dealing with this error source. The suggestions however, depend on problems in hand. Kennett (1979) reduced the

problem of wave number aliasing by introducing attenuation into his velocity model while making the distance spacing Δx equal to the geophone spacing or half of it. The introduction of attenuation leads to damping in both space and time and so reduces the problems due to aliasing. Owing to the periodicity of the 'F-K' plane (Bracewell, 1965) it is sufficient to describe A(f,K) in the region $0 \leq f \leq \frac{1}{2}$, $-\frac{1}{2} \leq K \leq \frac{1}{2}$, and in the formulation of equation (2.00), a criterion to avoid frequency - wave number aliasing is that $|F| \leq \frac{1}{2}$ and $|K| \leq \frac{1}{2}$.

2.2.4 Frequency Bandwidth

Sometimes, modern seismic reflection data may be processed to approximate closely the reflection coefficient series of a sedimentary section. Inversion of the series will produce a low-cut filtered impedance log. Extension of the technique to include density correction and replacement of missing low-frequency components leads to generation of a synthetic sonic log having dimensions and characteristics similar to a conventional borehole sonic log. When the goal is achieved, synthetic sonic log sections can be useful in stratigraphic exploration. The direct depth display of the logs largely eliminates the vertical scale distortion inherent in time sections, and integration with other subsurface data will be enhanced. Unfortunately, this goal will be only partially achieved and the major limitation is the limited frequency bandwidth of most

seismic recordings. The effects of bandwidth reduction on seismic signals are illustrated in Fig. (2.17), which compares a reflection coefficients and resulting synthetic seismograms (Lindseth, 1979).

The reflection coefficients are a sample-for-sample transformation of the sonic log samples and as such have the same resolution, and bandwidth. Accordingly, there is a direct correlation between the reflection coefficients and sonic log.

Convolution of the reflection coefficients with a wavelet to simulate the filter and phase shift effects of the earth and recording system produces the synthetic seismogram. Whereas the reflection coefficients in this example have a bandwidth extending from 0 to 250 Hz, the synthetic seismic trace is band limited to approximately 15 to 50 Hz. Although the synthetic seismogram is noise free, it is no longer possible to correlate it with the sonic log with precision and confidence. Widess (1973) demonstrated the time-shift and distortion of band-limited reflections from thin beds (closely spaced reflection coefficients). Comparison of the coefficients of fig. (2.17) to the synthetic seismogram reveals an abundance of similar effects.

A low-cut filter (6-250 Hz), applied to a sonic log in Fig. (2.19) illustrates the effect of missing low frequency components which evidently contain much of the essential velocity information. The sonic log may be considered as a low-frequency function modulated by a higher-frequency function, i.e. as a sum of frequency components above the $5H_Z$ added to those below

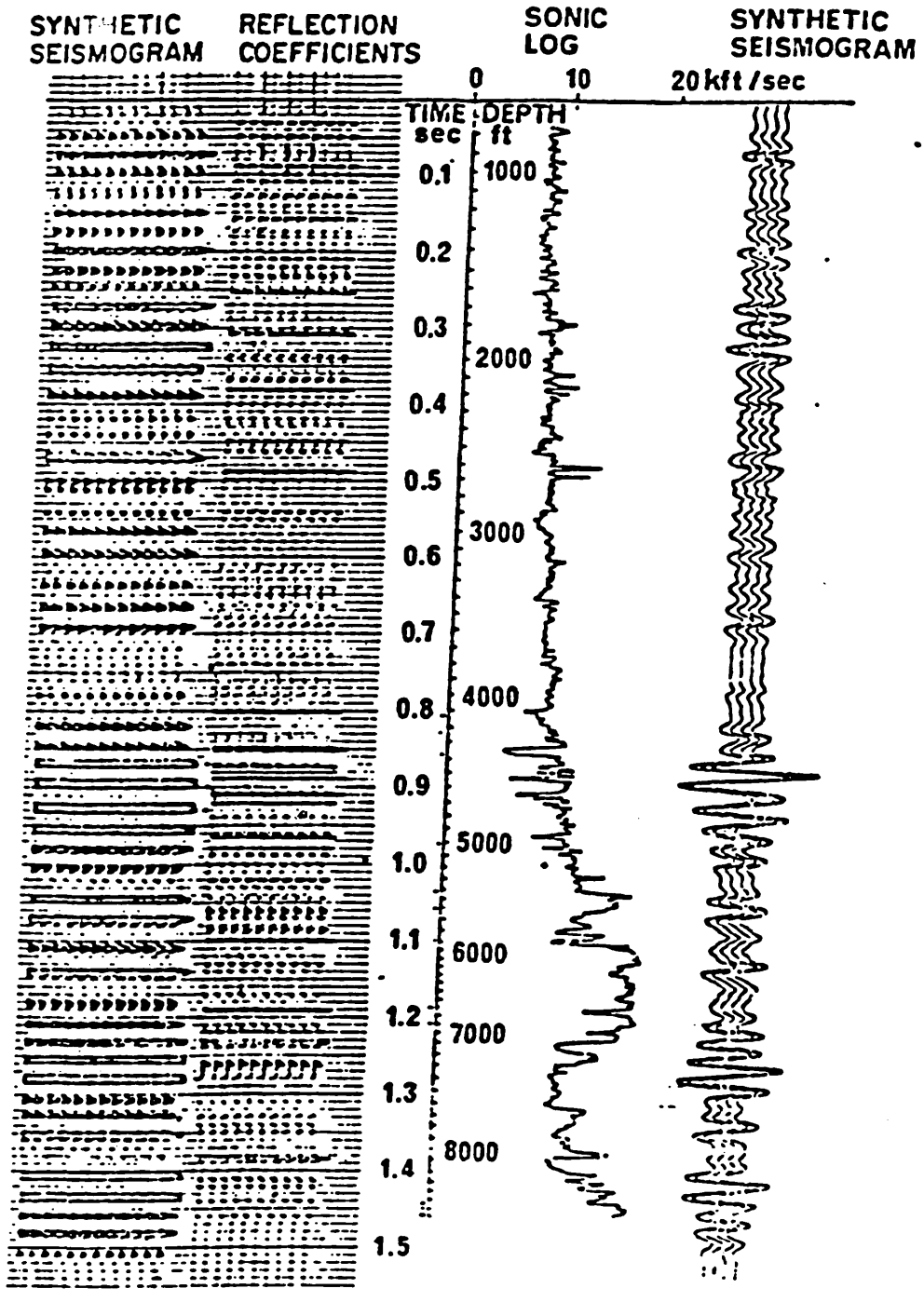


Fig. 2.17 A time-corrected ("integrated") sonic log and synthetic seismogram (right) derived from this log. The same synthetic seismogram and corresponding reflection coefficients are plotted (left) in variable area reverse polarity. The reflection coefficients are a direct transformation of the sonic log and, consequently, correlate closely to it. The poorer correlation of the synthetic seismogram illustrates the result of bandwidth reduction and phase distortion which occurs in the field recordings.

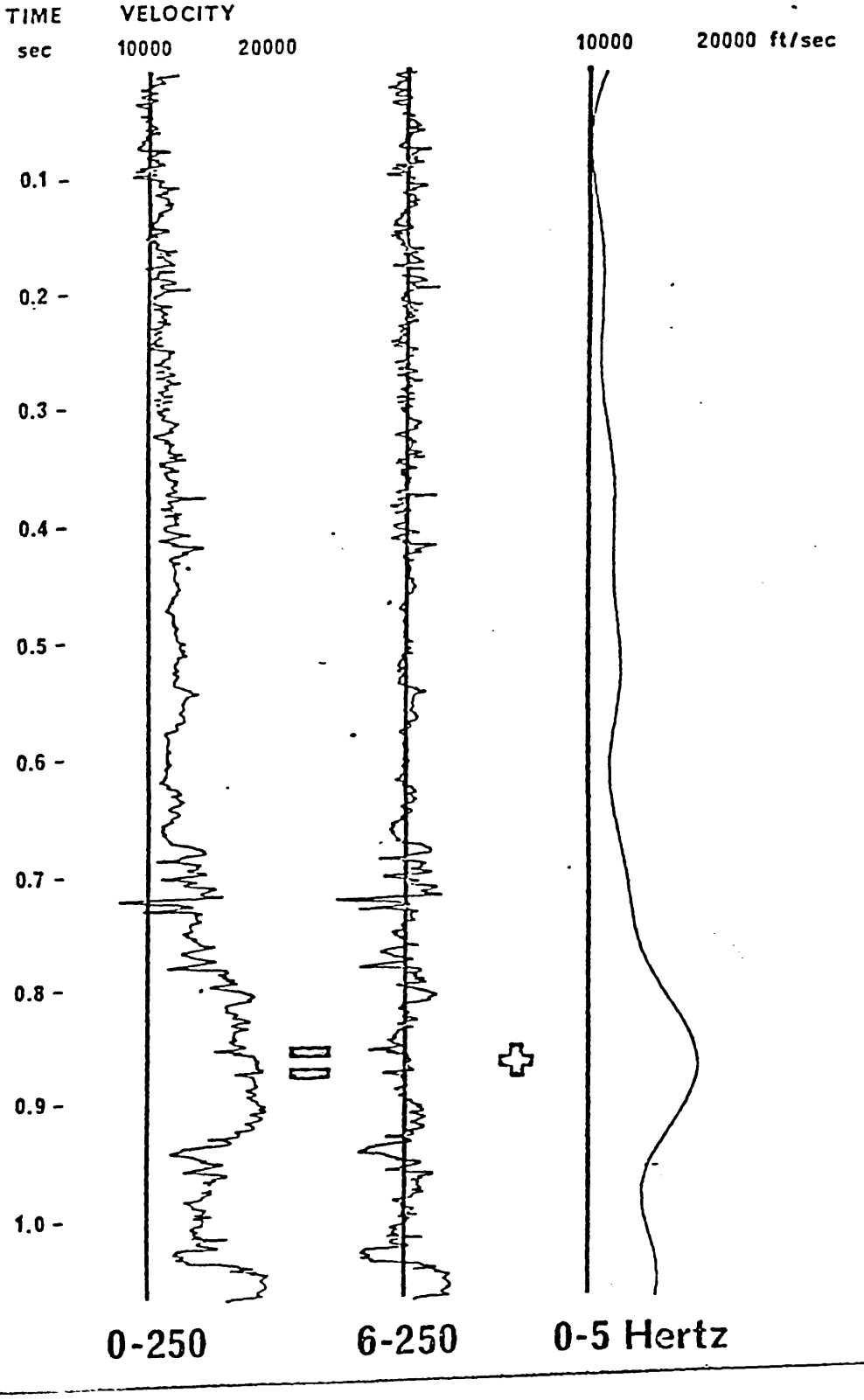


Fig. 2.19 A sonic log may be considered to be the sum of a gross velocity function (0-5 Hz) and a detailed velocity function (0-250 Hz). (Lindseth, 1978.)

$5H_z$. Without low-frequency components the synthetic sonic log values obtained from inverting seismic data do not closely approximate velocities measured on borehole sonic log.

2.2.5 Seismic Filtering Methods

In a seismic record, accompanying the seismic signal are a series of different unwanted signals (ranging from ghosts, multiples, etc.), generally called noise. We are not interested in the noise and therefore must separate it from our signals of interest. The operators, generally used in detecting and extracting the desired signal are called filters and the process filtering. A filter may be defined by its impulse response characteristics (see chapter three). The input for example, can be a seismic signal (source function, f(t)), the impulse response characteristics, may be represented by reflection response series, g(t), the output Y(t), of the filter which we call the convolution product of the two functions f(t) and g(t) can be expressed mathematically thus:

$$Y(t) = \int_{-\infty} f(s)g(t-s)\, ds$$

$$Y(t) = f(t) * g(t)$$

where the symbol * means 'convolved with'.

The above expression follows the definition of Jennison (1961) which states that convolution of two functions is the result we would obtain by scanning one function with each element of the other (from minus infinity to infinity) and summing the products at each

position of the scan. In discrete form y(t) is written:

$$Y_t = \sum_{s=0}^{n} fs\,g_{t-s} \qquad t = 0, 1, 2 \ldots, m+n$$

where $Y_t = 0$ when t lies outside the range $t = 0, 1, 2, 3, \ldots, m+n$

Designing Digital Frequency Filters

We shall consider the principles governing the design of filter operators by applying them to the relatively simple type of frequency filtering required in passing all signals above one specified frequency or removing all below another such frequency or both. Such filters are generally called high pass, low pass or bandpass. In designing digital filters that operate in the time domain, we express the desired filter characteristics as a function of frequency and then compute the Fourier transform of this function so as to set up a filter operator as a function of time.

Suppose we want to design a low-pass filter in the time domain that transmits all frequencies from 0 to 20 H_z without attenuation but allows no frequencies above 20 H_z to pass. The frequency characteristics curves must be symmetrical about zero, and since they apply equally to positive and negative frequencies, we can draw the characteristics curve for the desired filter in the form of the rectangle shown in Fig. (2.20 - right-up). This has uniform amplitude between

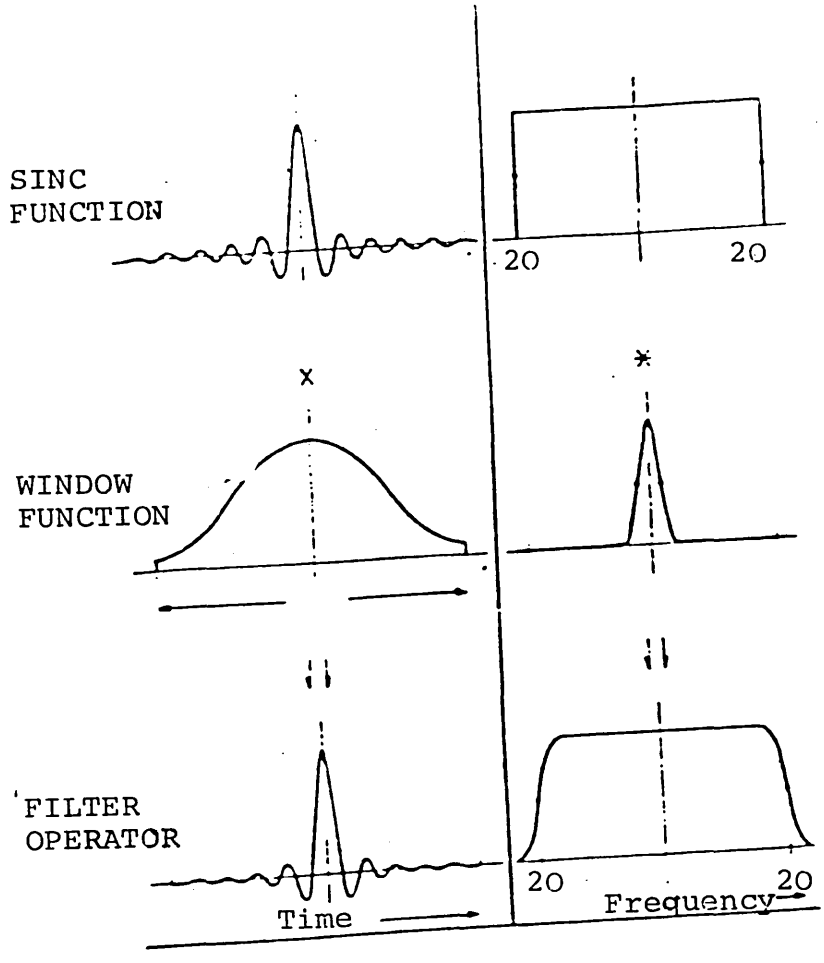


Fig. 2.20 Design of low-pass filter operator based on convolution theorem. Desired cutoff at 20 Hz cannot be achieved exactly because the operator must be of finite length and the frequency function in the form of the square wave shown at the upper right would require an infinitely long filter function (Dobrin, 1976).

frequencies of - 20 Hz and 20 Hz and zero transmission outside this range. The time representation of this rectangular frequency function, which is its Fourier transform, is a sine function, having zero crossings at $\pm$0.025, +0.050, $\pm$0.075, $\pm$0.10, ..., S. The times of these crossings are respectively equal to 1, 2, 3 ..., divided by the width, 40 H_z of the rectangular wave as measured on the frequency scale. The amplitudes of the

lobes thus obtained attenuate only as 1/t, and therefore have to be truncated.

One way of truncating the time operator would be to multiply it by a rectangular (square wave) function having a time duration of proper length. The sharp corner at the cut-off point would generally leave undesired side-band effects. A common solution to this problem is to truncate the operator more gradually by multiplying it by a Hamming window function, fig. (2-20, left-centre). The frequency transform of this window is shown adjacent to it. The transform consists of a peak at zero with a fairly sharp drop on either side. The window function aims to reduce the side bands to the point where they have no perceptible effect on the output. Now, multiplying the infinitely long sine function by this window function, we get a time domain operator (left-below). We can find the effect of the truncation on the frequency characteristics of the filter, if we convolve the original rectangular filter curve with the transform of the window in accordance with the convolution theorem. Instead of a vertical cut-off, we have an inclined cut-off curve centred at about 20 Hz, the slope depending on the width of the truncation window. The broader the window the steeper slope, and the longer the filter operator the sharper the cut-off at the desired frequency. Thus the convolution of what is effectively a single peak spectrum for the window function with the desired rectangular-wave frequency function yields a filter with a frequency characteristic that has sloping rather than vertical sides. Gibb's phenomenon (the name given

to the undesired side lobes) now becomes a restriction on the practical design of a truncated box car shaped bandpass filter.

It is also not possible to make a filter which exactly produces the gain characteristics of an ideal low pass. It is, however, possible to approximate this ideal low pass behaviour as closely as desired. The approximation may be approached in more satisfactory manner by a general function of the form.

$$\left|Y(\bar{\Omega})\right|^2 = 1/(1+An(\bar{\Omega}))$$

where $An \ll 1$ $\quad 0 \leq \bar{\Omega} \leq 1$

$An \gg 1$ $\quad \bar{\Omega} > 1$

$\bar{\Omega}$ is the normalised frequency defined

$\bar{\Omega} = W/W_L$

and $W_L = 2\pi f_L$ (f_L = cut off frequency)

Butterworth (1930), let $An = \bar{\Omega}^{2n}$

$n = 1, 2 \ldots$

to obtain a monotonic function as an approximation to the square response. We therefore define the Butterworth filter as shown:

$$\left|Y_L(\bar{\Omega})\right|^2 = \frac{1}{(1 + \Omega^{2n})}$$

$$= \frac{1}{1 + (W/W_L)^{2n}}$$

where n is the order of the filter. Using the appropriate frequency transformations (Kanasewich, 1975), Gold and Radar (1967), we can then obtain the ideal high pass,

and bandpass filters from the lowpass prototype. These filters contain less of the undesired side effects when compared to the ideal box car (rectangular) function. Fig. (2.21a) is the impulse response (time domain equivalent) of the Butterworth bandpass filter produced by the routine "Butter." "Butter" is a computer program which computes the Butterworth filter response functions given the cut-off frequencies and slopes. Options are available to generate either the lowpass, highpass or bandpass responses.

The computed bandpass impulse response is a useful minimum phase wavelet for the generation of theoretical synthetic seismograms (see chapter three). Another useful suggestion that often works while filtering in the frequency domain is to add zero amplitude in sufficient number to the end of the original trace before Fourier transformation. This will reduce the problem of wrap around which is another source of error. The more we reduce the disturbing filter effects the better our seismic resolution.

2.2.6 Deconvolution Filtering Technique

The output $h_1(t)$ of a filter having a given impulse response $g_1(t)$ when the input signal $f_1(t)$ is known can be computed by convolving the input with the impulse response, i.e.,

$$h_1(t) = g_1(t) * f_1(t)$$

Where * has the usual meaning.

If the output $h_1(t)$ is known and we wish to recover the form of $f_1(t)$, then we need to find another filter with a response $r(t)$ through which $h_1(t)$ might be passed to recover $f_1(t)$. $r(t)$ is the inverse filter of $g_1(t)$. The process of cancelling the effect of a filter with a second filter designed to be its inverse is called deconvolution. The equation for the deconvolution operation is:

$$f_1(t) = h_1(t) * \frac{1}{g_1(t)}$$

$$= h_1(t) * r(t)$$

or in the frequency domain

$$F_1(n) = H_1(n)/G_{1(n)}$$

$$= H_{1(n)} \; R_{(n)}$$

where the upper case characters are the respective Fourier Transforms of the lower case letters.

In practice we deconvolve seismic signals to convert the waveform of a reflection complicated by filtering that takes place in the earth (such as by reverberation within water layer) into a simple pulse representing the reflection waveform before the filtering took place. The signal generated by the shot ideally has the form of a very short pulse which was broadened by the filtering action of the earth with a consequent decrease in resolution.

To achieve the objective of a deconvolution process,

the first step is to measure the spectrum of the signal and to manipulate this spectrum in a way that makes it approach the uniform character of the transform associated with a single spike. Mathematically, the ideal reflection signal is a spike of zero time duration but even after deconvolution, our signal is limited to the narrowest breadth the earths filtering characteristics (and noise) allow. The resolution of such a signal must be limited. Fig. (2.23) illustrates an attempt to smooth the amplitude spectrum of a trace which with approximation would yield the amplitude spectrum of the convolving pulse.

In the time domain, we perform the auto-correlation of a given seismic trace by a convolution operation of the trace with the trace reversed in time. The auto-correlation then shows a peak (obviously) at a zero delay, followed by a decay and oscillation at nearby time delays - the shape of which is controlled by the average frequency content of the trace, followed by a series of peaks and troughs which mainly correspond to reflections correlating with each other. The small lags part of the autocorrelation contains the information needed for estimating the amplitude spectrum of the initial pulse. If the assumption is then made that the initial pulse has a minimum phase spectrum, the phase can be determined from the amplitude spectrum, and the problem of determining the initial pulse is formally solved. The actual methods of calculation have been described by Foster et al. (1968), Robinson et al. (1967). The method of Robinson incorporates the Wiener's double inverse method.

Fig. 2.23 The effect of predicting minimum-phase wavelets of different lengths (left), the corresponding spectra (center), and the spectrum of the deconvolved trace (right). (Waters (1979)).

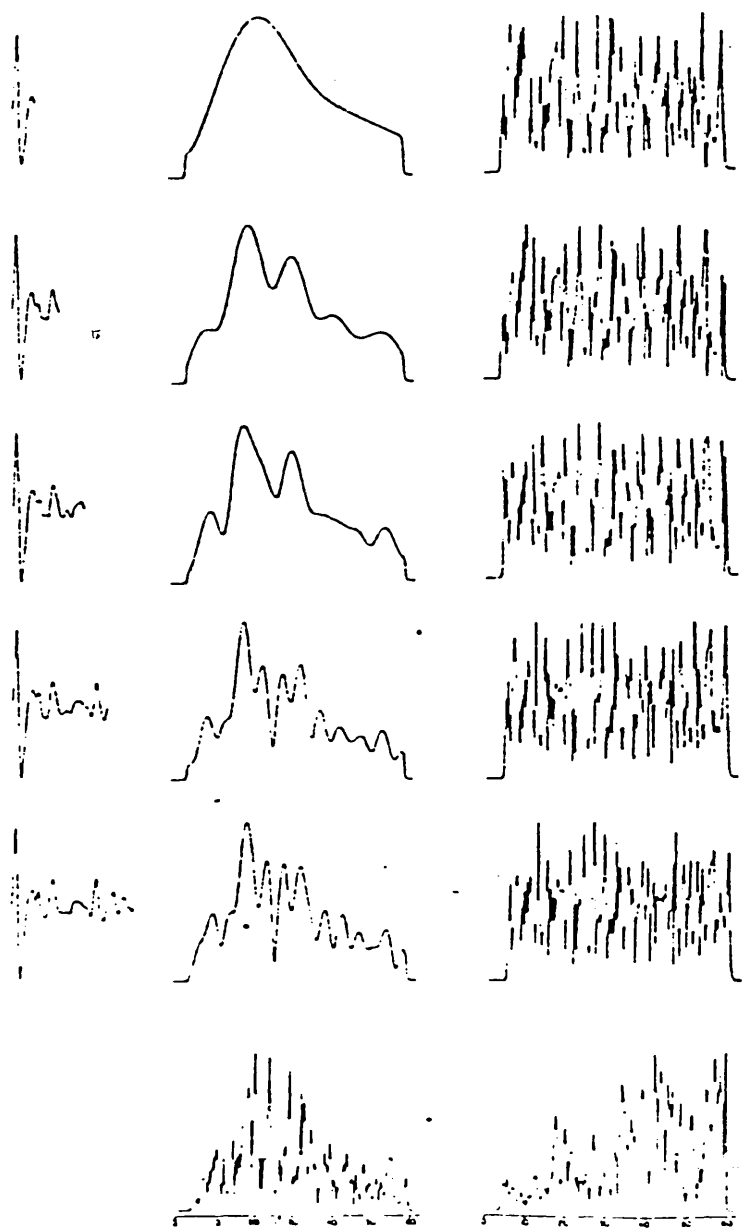


Fig. 2.24a: Estimating the initial pulse (double inverse)

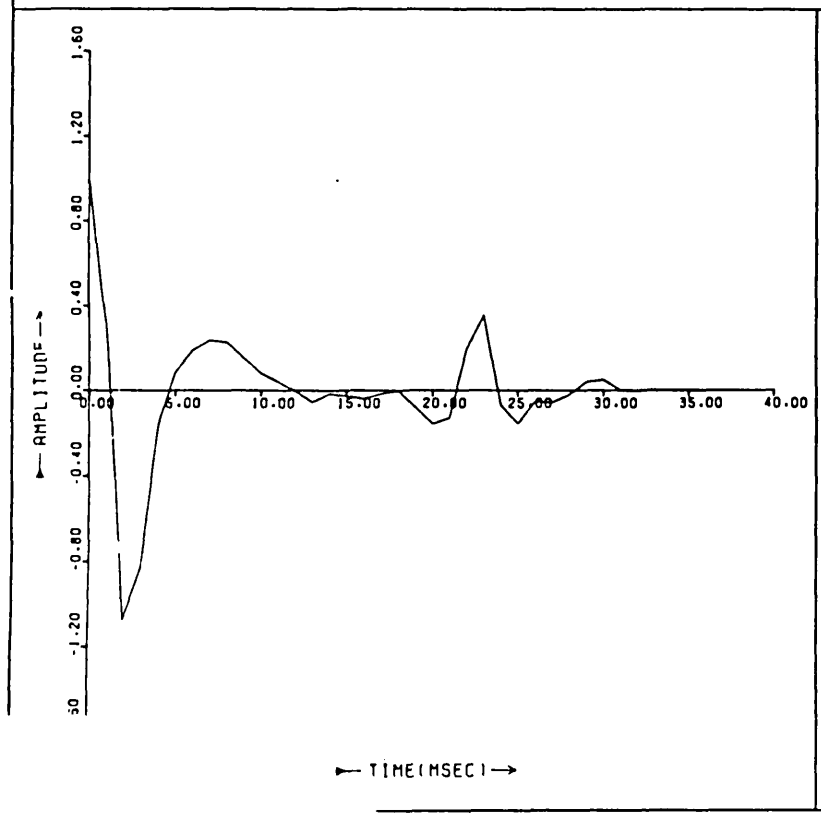


Fig. 2.21a Impulse Response (wavelet)

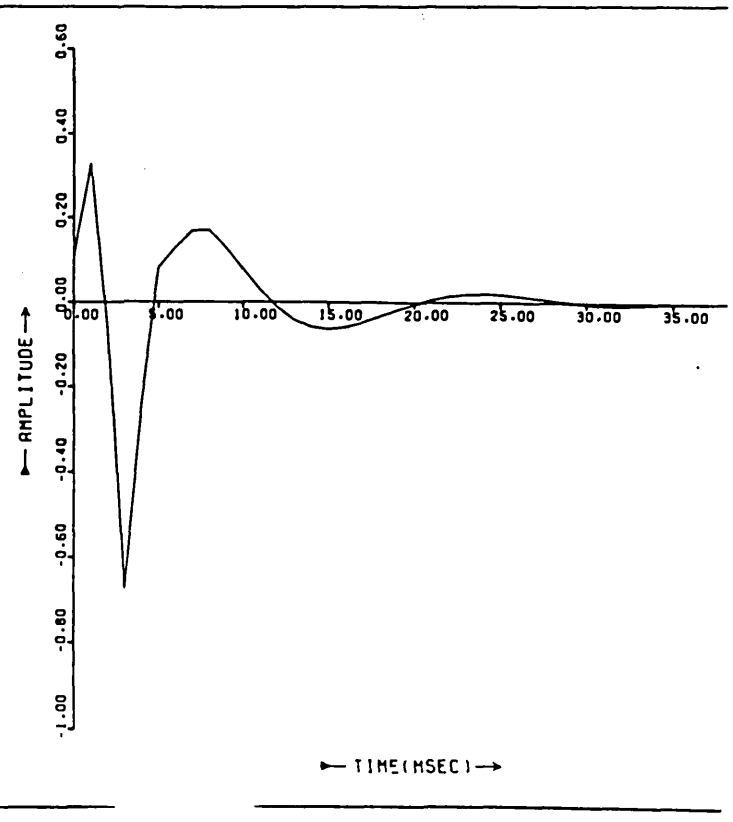


Fig. 2.24b Seismogram generated using the initial pulse

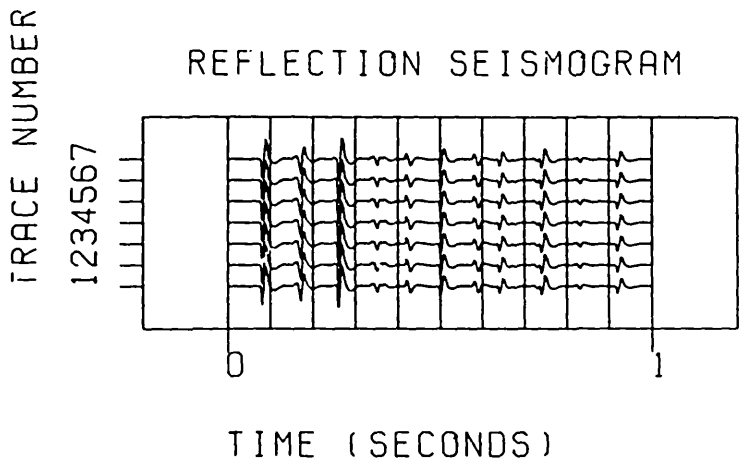


Fig. 2.21b Seismogram from which initial pulse was estimated

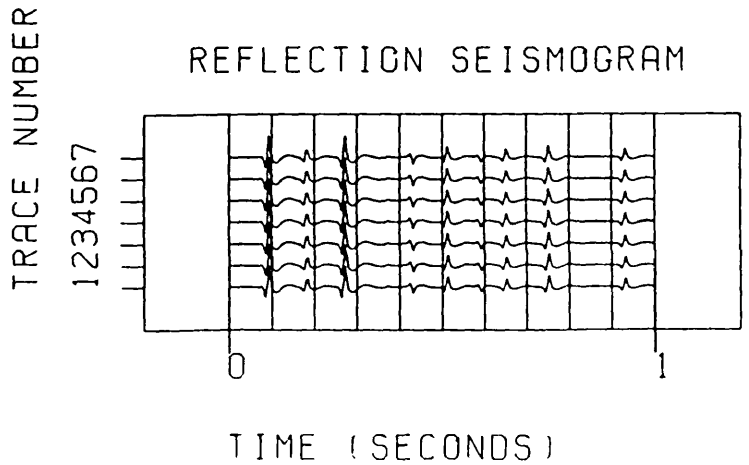


Fig. (2.24a) shows the result obtained using Wieners double inverse method to calculate the initial pulse from one of the traces in Fig. (2.21b). White and O'Brien (1974), however, has called attention to the danger of estimating the seismic pulse from a single trace (see Fig. (2.24b).

In the coming chapters, we shall see that the problem of estimating the accurate seismic pulse (wavelet) is one of the major problems in seismogram synthesis using well-log information. Given good data, it is straight forward to construct a synthetic seismogram which matches the field observation. Methods of estimating the optimum seismic wavelets for synthetic generations are presented in chapter five.

2.2.7 The Effect of NMO (Normal Moveout) Correction On a Seismic Pulse

The effects of NMO correction on a seismic pulse have serious consequences on the outcome of (seismic) sections obtained from the field seismic data. Fig. (2.25) shows a schematic set of impulses, such as might be received on a seismic record, with the offsets of the traces varying from 0 to 9,000 ft. and with a constant velocity of 10,000 ft./sec. The individual reflection layer impulses form a hyperbola. These successive hyperbolas are often closer together on the far offset traces than on the near offsets. Now, when impulses (infinite frequency response) are used, the removal of the correct amount of NMO simply places all

the impulses at a constant time for a given reflector regardless of the offset distance. When reflections have a finite bandwidth, they overlap one another on the field record, and all the traces are recorded with the same bandwidth. A serious wave shape and spectrum distortion (pulse stretching) then appears on the long-offset traces as NMO is removed. This is non-linear distortion, so that filtering again after NMO removal does not give the same result as would have been obtained if all the traces had been recorded at very wide bandwidth and the NMO removed, followed by bandpass filtering.

Usually, the seismic event is a pulse of the order of 0.1 sec in length, with only its begining occuring at the proper reflection time. The tail of the wavelet or pulse occurs at a later time, but its NMO is removed as though it were a later reflection. in fact all velocities are incorrect, as the main energy occurs with some delay after the true reflection time that applies to it (Waters, 1979). It is sometimes possible to correct impulsive-type records for pulse distortions by the filtering process - devonvolution, though deconvolution itself has its own problems. Predictive deconvolution (Robinson, et al., 1980) has been a satisfactory tool but its capability is limited when long-leg multiples are encountered. Other methods of long-leg multiple attenuation (Ursin et al., 1979, Kennett, 1978, etc.) may serve as useful alternatives though not without limitations either, so we still have to depend on approximations.

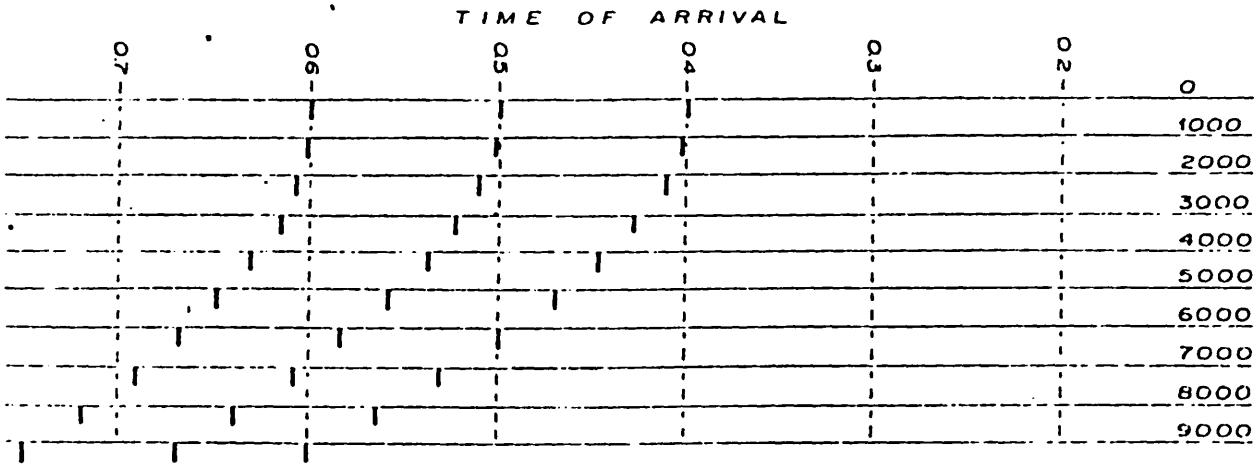


Fig. 2.25 **Schematic of an impulse (nonreal) record showing comparative times o: arrival. X = 0(1000)9000 ft and V = 10,000 ft/sec.(1)**

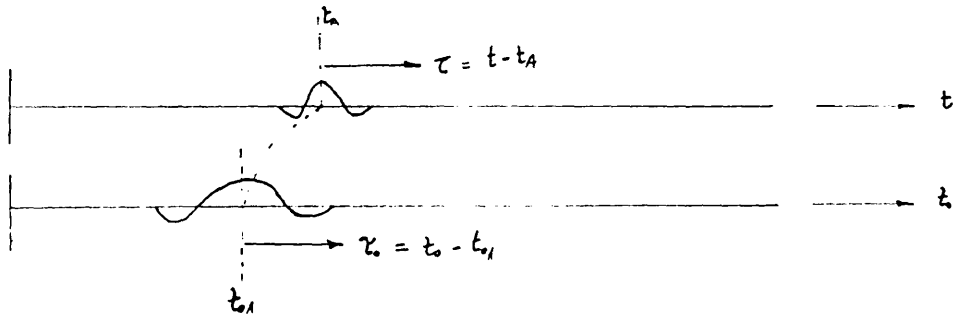


Fig. 2.26 Stretching of pulse by NMO Correction

2.2.8 The Nmo Stretching Equation

Let us consider a seismic trace from a detector, a distance X from the source. We assume the interval velocity depends only on depth, or equivalently t_o, where t_o is the time recorded for x = 0. The stretching of a reflected pulse caused by application of NMO correction is illustrated in Fig. (2.26). In the figure, a pulse centred at t_A is removed to a time t_o and stretched.

Nmo correction uses the relation,

$$t^2 = t_o^2 + X^2/V^2(t_o) \qquad (2.01)$$

t, is transformed into, t_o, in a non-linear manner. We also assume the pulse duration is small compared with t_o or t. We are therefore considering a transformation of variables that describes a localised stretching of the pulse at t_A. We define variables $T = t - t_A$ and $\tau_o = t_o - t_{oA}$ (Fig. 2.26) and study the transformation of τ into τ_o.

If we expand $t_o = t_o(t)$ in a Taylor Series around $t = t_A$, then

$$t_o = t_{oA} + \left.\frac{dt_o}{dt}\right|_{t_A} (t-t_A) + \tfrac{1}{2}\left.\frac{d^2t_o}{dt^2}\right|_{t_A} (t-t_A)^2 \qquad (2.02)$$

In terms of T and T_o, we have

$$T_o = \left.\frac{dt_o}{dt}\right|_{t_A} T + \tfrac{1}{2} \left.\frac{d^2 t_o}{dt^2}\right|_{t_A} T^2 + \ldots \qquad (2.03)$$

If we retain only the linear terms in (2.03), then from (2.01) we have

$$\left.\frac{dt_o}{dt}\right|_{t_A} = a = \frac{t_A}{t_{oA}} \left(1 - \frac{x^2}{v^3 t_{oA}} \left.\frac{dv}{dt_o}\right|_{t_{oA}}\right)^{-1} \qquad (2.04)$$

In this approximation our transformation is a simple uniform dilatation of time given by

$$T_o = aT \qquad (2.05)$$

Equation (2.05) implies that if $g(T)$ is the uncorrected pulse and $g_o(T_o)$ is the Nmo corrected pulse, then they are related by

$$g_o(T_o) = g(To/a) \qquad (2.06)$$

If we indicate Fourier transformation by the symbol ($\sim$) then:

$$\begin{aligned} \tilde{g}_o(f) &= \int_{-\infty} g_o(T_o) e^{-2\pi i f T_o} \, dT_o \\ &= \int_{-\infty} g(T_o/a) \, e^{-2\pi i f T_o} \, dT_o \\ &= \int_{-\infty} g(T) e^{-2\pi i f a T} a \, d_T \end{aligned} \qquad (2.07)$$

or

$$\tilde{g}_o(f) = a\tilde{g}(af)$$

Equation (2.07) shows that the spectrum of the NMO-corrected pulse is compressed and multiplied by the factor,"a" (Dunkin and Levin, 1973).

2.2.9 Effect of NMO Stretching on cDp stack

When cDp data are stacked, signals with different source detector separations are summed after NMO correction. We anticipate that the stacked pulse will be broader than pulses uncorrected for NMO but narrower than the far-trace, for NMO-corrected pulse. We might guess also that the summed pulses will be stretched versions of the original uncorrected pulses, but we have no assurance that this will be the case. Figure (2.27) is a suite of 12-fold cDp traces. Examining traces 23 and 24, which are full stacks for record times, greater than 1.5 secs, the reflections would resemble the symmetric input pulse. At shorter record times, the pulses are distorted slightly, presumably because NMO corrections did not line up the central peaks of the pulses precisely. The reflection between 0.8 and 0.9 sec. also suffers because some of the individual pulses that were summed were clipped.

We can now appreciate why the actual stacked pulse spectrum is richer in low frequencies than the spectrum we expected. This follows from the fact of stretching a pulse without reducing its amplitude, then we increase the area included within the pulse or equivalently, add energy to the system. This energy appears at low frequencies. In the case of sampled data, the stretched pulse develops gaps that are filled by interpolation of extra samples, a process again equivalent to adding energy.

In general pulse stretching or equivalently frequency scaling produced by NMO correction is linear, however,

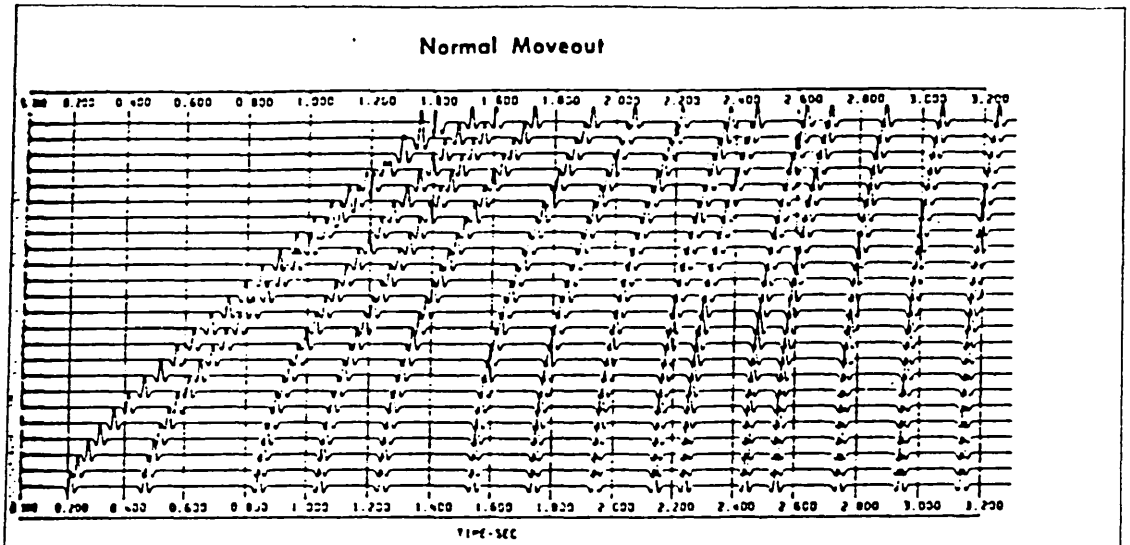


Fig. 2.27a The synthetic seismogram before NMO correction.

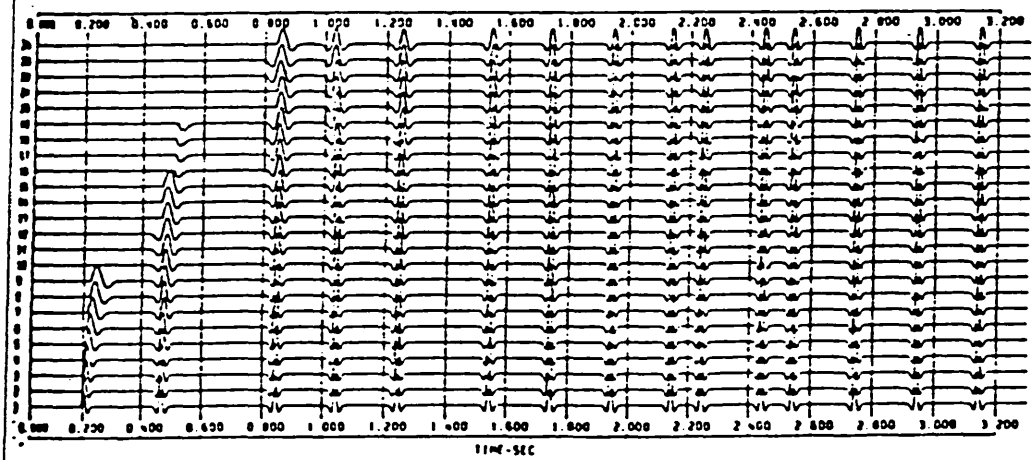


Fig. 2.27b The synthetic seismogram after NMO correction.

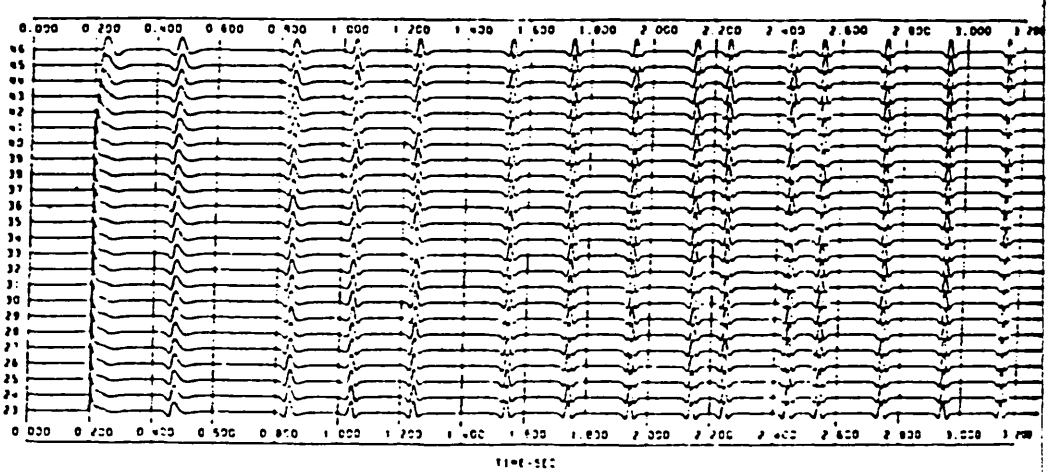


Fig. 2.27c 12-fold stacked synthetic seismogram. The unstacked traces are plotted in Fig. 2.27b.

it cannot be expressed as a convolution operation. Although the result of the process is deceptively simple (equations, 2.06, 2.07) subsequent processes such as stacking are not, hence the consequences of NMO corrections on a seismic pulse.

2.2.10 Multiples

Multiple reflections often impair seismic resolution and interpretation considerably. It is thus of paramount importance to free the primary reflections as far as possible from interfering multiples. Multiples are often subdivided into different kinds; Peg-leg multiples consisting of one long leg and one or more small legs, and long-leg multiple reflections which consist of two or more long legs, are all well known.

In the majority of recordings, due to the loss of energy (if this is not counteracted by automatic volume control) multiple reflections are not always observed on the seismogram, although they may have sufficient energy to distort the authentic reflections. Nevertheless, under favourable conditions in shallow beds, when a reflector is exceptionally good, strong multiple reflections may be generated up to the fourth or fifth multiple. These may have the same or even greater intensity than the true reflections which correspond to the same recorded time, and may be easily mistaken for legitimate reflections. If the arrival time is the same as that of deeper reflections, and if multiples combine

with these, the reflections are distorted in such a manner as to make their identification difficult or impossible or, if these are taken to be legitimate reflections and picked according to their arrival times, ficticious deep horizons are obtained. The identification of multiple reflections is often difficult and under certain conditions may be impossible as may be seen in Fig. (2.32a). Assuming a constant velocity V, if aC, is the surface with a shot-point at a, and with a geophone at C, and df, the reflector then the reflected wave follows the path abc but it is possible that a multiple reflection is also produced which follows the path adefc, and is recorded at c with a time almost double that of reflection abc. If we map the multiple reflection adefc as a legitimate reflection, we will obtain a ficticious horizon a point of reflection at g. Now, if a horizon g actually exists, this will be indistinguishable from the multiple reflection adefc, in that the wave in both cases will arrive at c with the angle i (Fig. 2.32b). It follows that when the second reflection is observed (the first reflection is the legitimate abc), it will be impossible to say that it is truly the horizon g or the multiple of the horizon df.

In general short period multiples can be attenuated by deconvolution, predictive or spike deconvolution can be very effective. When sufficient velocity differences exist between the multiple and the primary reflections, multiple coverage becomes an effective tool against long-leg multiple reflections. However, when the velocity differences are too small, or when the distance between

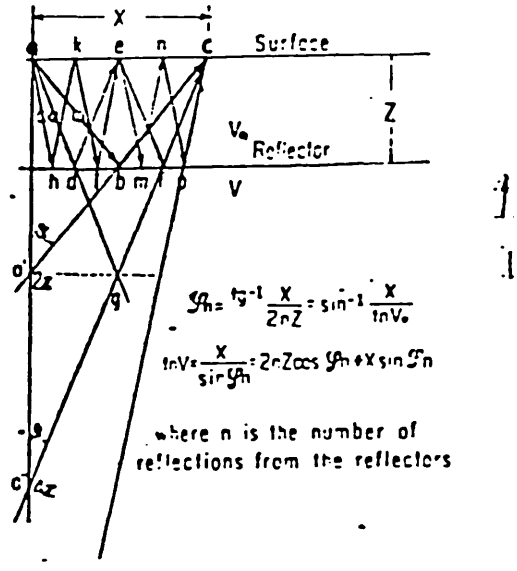


Fig. 2.32a: Single and Multiple reflection paths

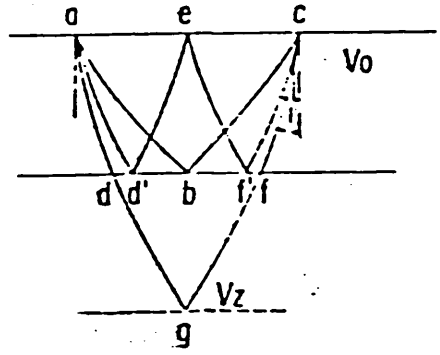


Fig. 2.32b: Curved reflection paths (Olhovich, 1964)

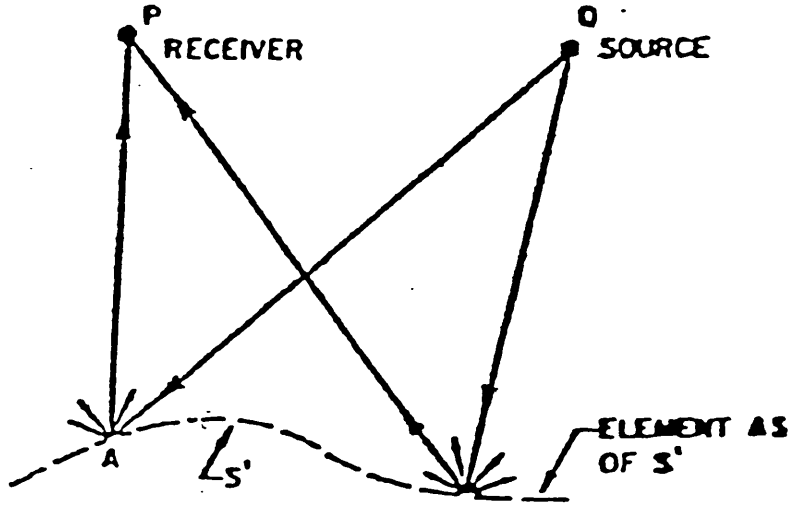


Fig. 2.33: Path of Incident ray from source to receiver

shot and farthest geophone cannot be made large enough, then other methods have to be looked for. Among such methods we include multiple cancellation using feedback technique (Koehler, et al., 1974), Long period multiple attenuation using the maximum likelihood approach (Ursin, et al., 1979).

2.2.11 Seismic Lateral Resolution

How small a feature in the subsurface can the reflection seismic method resolve? Simple Ray theory approximations are inadequate for answering this type of question. Only by using wave theory can satisfactory answers be provided.

In general any reflector may be thought of as an ensemble of diffractions each acting as a point source, emitting in all directions when struck by an incident ray. (Fig. 2.23). The rays which diffract towards a receiver p are summed to obtain the response at p. Each point on a reflector therefore, sends energy towards all receivers. For a plane reflector of infinite extent this approach yields the well known specular reflection model in which all the energy is reflected at a single reflecting point (A). This viewpoint is only partially correct. For a truncated or non-planar surface, diffraction always occurs and we may even argue that the term "reflection" is a misnomer.

The laws of propagation, reflection and refraction, all enable us to follow the usual rays from the source outwards, and determine where they go and what they produce. The usual laws fail to specify what happens to a ray which hits an edge or a vertex or grazes a boundary surface. Such rays will give rise to diffracted rays. In general, we get a reflected wave field and a diffracted wave - field, and diffraction itself is related to wavelength. Thus to get a true picture of a reflector we must focus more attention to wave theory than to Ray theory. The ray theory, however, works in a number of cases because if the reflector is infinite in extent, then all the contributions from points other than the geometrical midway point will interfere with complete destruction of each other's contributions. But the response from the geometrical midpoint is unique in that it is the shortest path of reflection from shot to reflector and to the geophone. Since it is the first arrival, there is no destruction. So in reality is is necessary to think of a reflector as an ensemble of diffractors each producing diffracted rays in all directions when struck by an incident ray from the source.

Suppose we consider the response from an infinite half plane (Fig. 2.34). Several half planes lie at different depths and extend from the center of the diagram to the right. The seismic section shows the reflections from these half planes (the flat events) and diffractions from the edges of the planes - the curves. Huggen's principle has the particles near

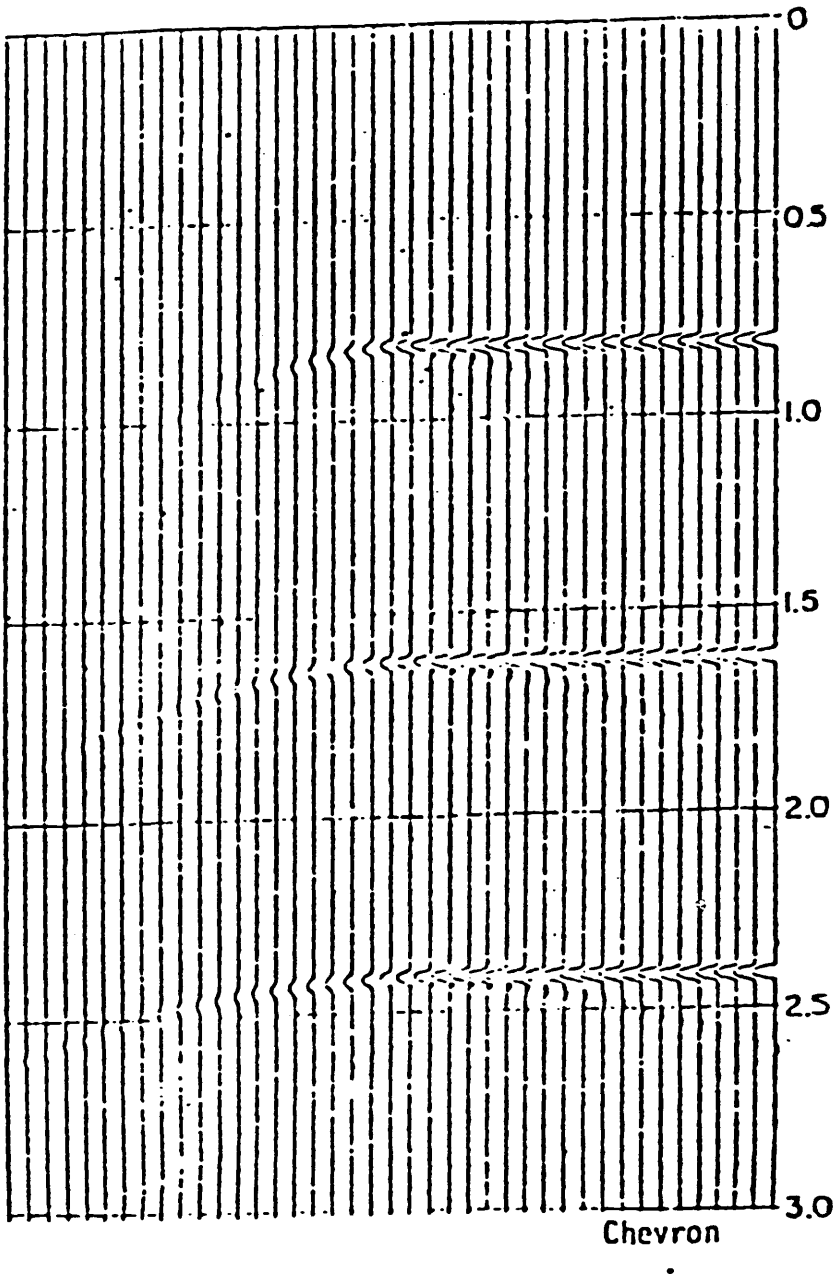


Fig. 2.34 Response from an infinite plane (Trorey, 1970)

the edge of the reflecting planes radiating energy in all directions and the position of the energy with lateral components will not cancel as would be the case if the reflecting planes were continuous. There is no phase break to indicate the termination of the reflector. The wave is continuous where the reflection is tangent to the diffraction curve. The amplitude of the reflection decreases before the end of the reflector is reached and is only half as strong at the end of the reflector as it is remote from the edge. The energy which disappears from the reflection is the energy which subsequently appears in the diffraction.

For any general trace near the middle of the cross section (as seen in our present example or in Fig. 2.35), there are three events, the reflection and two diffractions of opposite sign and different amplitudes and times of arrival. Under this condition, the lateral resolution of a strip width then turns into a problem of vertical resolution of the pulses coming from three different processes. The depth controls the curvature of the diffracted events, hence the differences in arrival times of the events on any given seismic trace. Details of these events near the strip are shown in Fig. (2.36) for a particular strip. Further discussions are deferred until chapter three on seismic diffractions.

With the above concepts in mind, the effective zone which can be said to be responsible for the seismic reflection can be readily defined. This zone is termed the Fresnel zone.

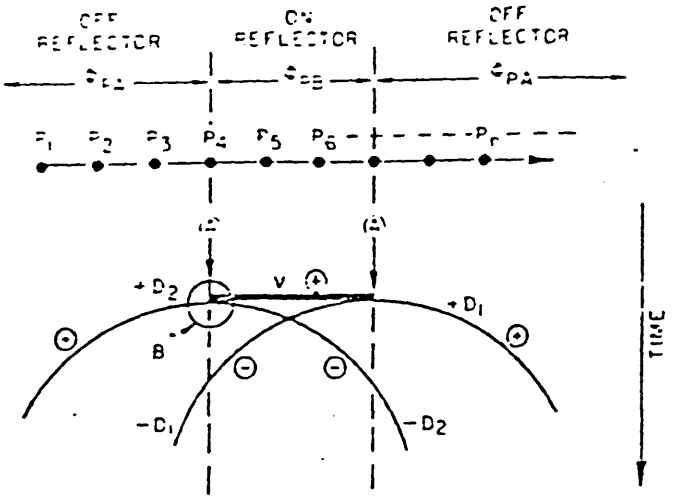
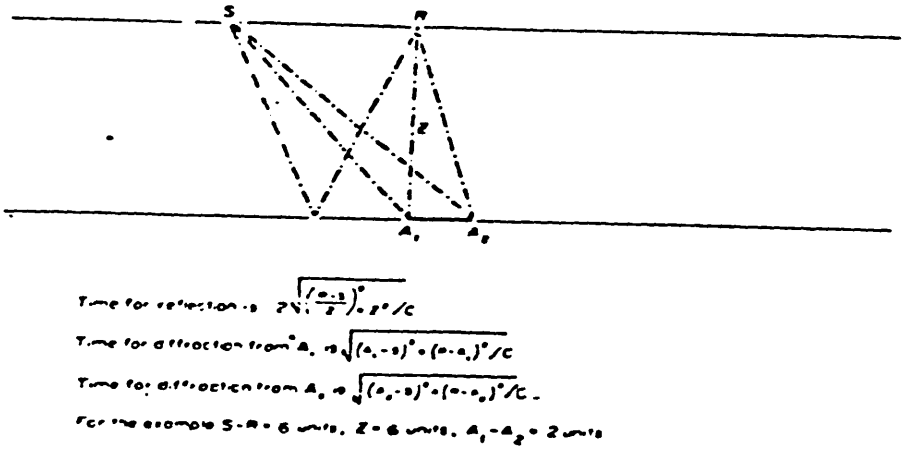


Fig. 2.35 A diffraction must undergo a 180 phase change on either side of a diffracting edge. P_1 and P_2 are successive source or receiver locations. D_1 and D_2 are diffractions. The circled signs show the phases of the various parts of the response (After Trorey (1970). Reprinted with permission from Geophysics).



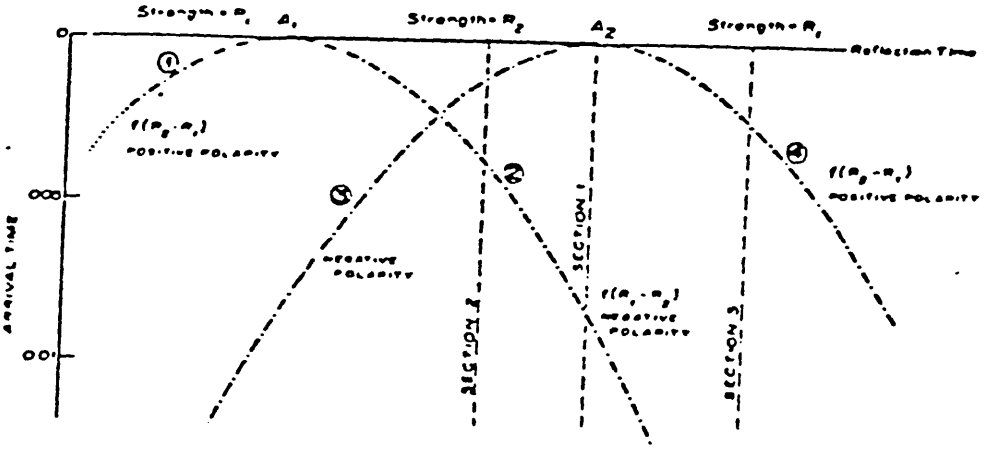


Fig. 2.36 Events and times of arrival of reflections and diffractions from an infinite strip. Times are in seconds for 1 unit = 100 ft. and velocity = 10,000 ft/sec.

Fig. (2.38) illustrates the Fresnel Zone. We observe spherically radiating wave-motion as it encounters a flat acoustic impedance boundary. The maximum-sized region of this boundary, over which the particle motion is all in the same direction, is indicated. A Fresnel Zone, although directly related to the size of this region, has a somewhat smaller value since some allowance must also be made for the respective magnitudes of particle motion within this region. If the source is at a distance R from the reflecting boundary where R represents travel distance at a velocity V over a two-way time of t seconds, and the dorminant frequency content of the seismic data is f_c, then a Fresnel zone radius r_f is approximated by:

$$r_f \simeq {}^{V}/_{4}(t/f_c)^{\frac{1}{2}}$$

This mathematical relation is derived using basic geometry and an empirical weighting. For the values V = 3,000 m/sec, t = 1 sec, and f_c = 25 H_z, r_f = 150 m. Thus we can say that the seismic illumination of the subsurface may be considered analogous to a 'search light beam', and the sub-surface area illuminated by this beam is considered to be the Fresnel zone.

With such an intuitive point of view, we can go further to consider fundamental questions such as how small in extent a subsurface feature must be as compared to a Fresnel zone in order to be detectable, and perhaps what the nature of its seismic expression must be for it to be detected. Fig. (2.39) may offer a possible

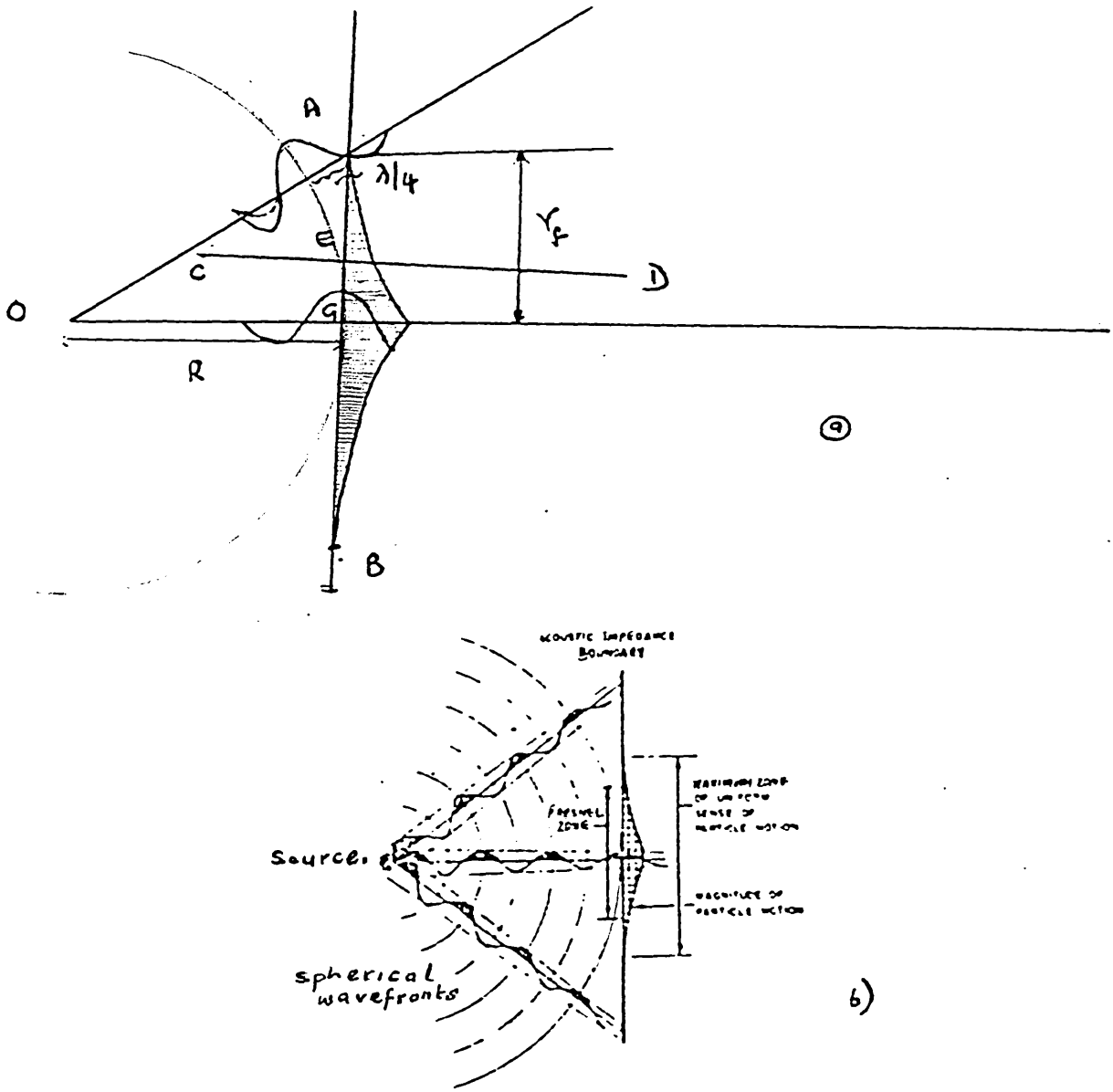


Fig. 2.38 Spherical wave motion encountering a flat reflector illustrating Fresnel zone region which is principally responsible for reflection event

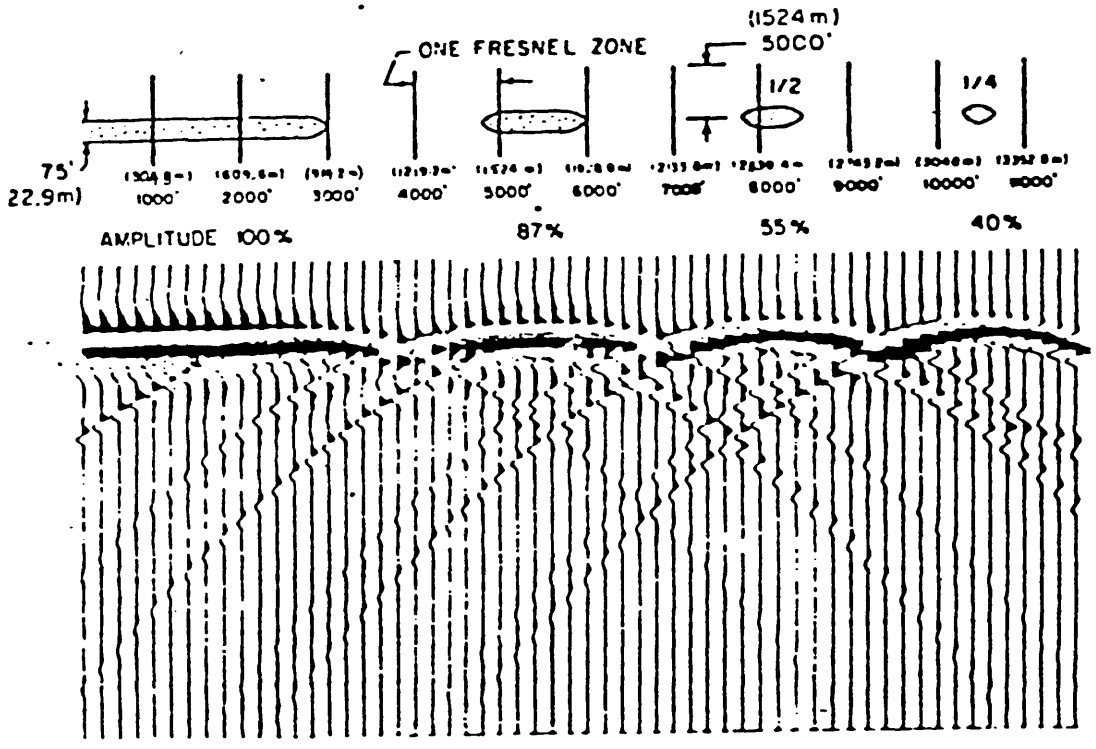


Fig. 2.39 Wave-theory model response for sandstone bodies of varying lateral extents illustrating significance of Fresnel zone size (Neidell, 1977).

explanation. As the size of a sandstone body decreases below the size of the Fresnel zone, the seismic signature loses all reflection character and tends towards the diffraction form corresponding to a reflecting point. The lessons are obvious,

1) Thin beds of small spatial extent have a seismic expression, but not dominantly of reflective nature.

11) Although the forms of the signature are alike for sandstone bodies smaller than the Fresnel zone, their size can be guaged by noting the differences in the strengths of the seismic events. The smaller extent bodies produce weaker events by occupying only

portions of the full Fresnel zone.

In general, "True Amplitude processing" is concerned with the preservation of seismic strengths. So with the mechanism just observed it was seen that where relative amplitudes have significance, they may be related to the identification of small lithologic inhomogeneities.

As a practical matter, the size of the Fresnel zone is initially related to the quarter wavelength of the dominant frequency component of the seismic waveform and the subsurface velocity. For the expression for r_f, the size of the Fresnel zone grows in proportion to the stacking velocity which may be determined readily from seismic data. The illustration using Fig. (2.39) is a typical one for intermediate - depth, Gulf Coast sandstone. If we consider Fig. (2.38a) we can show that r_f is proportional to $\frac{\lambda}{4}$ (quarter wavelength) for large λ .

$$(R + \lambda/4)^2 = R^2 + r_f^2$$

$$R^2 + \lambda/2 R + \lambda^2/16 = R^2 + r_f^2$$

$$r_f^2 = \lambda/2\, R + \lambda^2/16$$

$$r_f \propto \lambda/4 \quad \text{(for large } \lambda \text{)}$$

For a point O the reflector part AB will contribute a constructive response for a reflection and hence will have the highest amplitude. But if the reflector terminates at CD, then the response at O from the reflector is only from the part EB. It is then clear

that for a truncated reflector the full amplitude will be obtained only up to a Fresnel zone radius away from the edge A, and the amplitude will decrease until at the edge where it is one half due to the portion corresponding to GB. The other part of the energy will appear as diffraction at the edge. Thus we can say that for all practical purposes, the precise size of a feature in the subsurface that can be resolved by the reflection seismic method is limited to the size of Fresnel zone, beyond this limit not very much may be expected.

There are many other seismic distortions. In seismic interpretation for example, one finds several pitfalls. For this subject, the interested reader is referred to "pitfalls in Seismic Interpretation", Tucker et al. (1973). Limitations due to inaccurate well-logs, velocity, density, and noise will be discussed in chapter three.

Summary:

We have presented some of the limitations of seismic methods. An exhaustive treatment of this subject is beyond the scope of this chapter.

The general inability to control or reproduce the exact shape of the signal fed into the ground by explosive sources. presence of a weathered layer or lossy overburden, the absence of complete theory of processes that result in the radiated wave, and bubble effects (marine seismics), all have contributed to limit

the efficiency of explosive sources. It is clearly worthwhile to search for seismic sources which will offer sharper seismic signatures. It would seem that sharp, controlled signatures may provide the means of studying aspects of elastic propagation that have hitherto been beyond our reach.

Limited frequency bandwidth, aliasing, filter effects, multiples, and NMO effects contribute to reduced seismic resolution, either by broadening the observed pulse or by introducing undesired energy into the recorded or processed signal. In general, filter effects may be minimized using spike or predictive devonvolution (Robinson et al., 1980), while multiples may be estimated and removed using the maximum likelihood technique (Ursin et al., 1979, Kennett, 1978) and more often velocity F/K filters (Wiggins, 1966). The limitations have made it difficult for us to apply the principle of one-to-one correspondence between a field observed seismogram and an equivalent geologic section. In the coming chapters, we shall see how these limitations combine with those due to synthetic seismogram generation to reduce the accuracy with which the present state of the art matches a field observed seismogram and that constructed via the well-log information.

CHAPTER 3

Generation of Synthetic Seismograms From Well-log Information:

3.00 SYNTHETIC SEISMOGRAMS

The use of synthetic seismograms is a relatively recent innovation. Before the advent of synthetic seismogram generation, the knowledge that sound waves could be generated, reflected from geological discontinuities or strata, and recorded at the surface by suitable instruments was all that was required to sustain a very active seismic exploration program. The reflections (although their characteristics had not been related in any way to the lithological sequence) were similar enough to be correlated by eye, and the relative time of occurence at sequential subsurface points could be determined. After suitable corrections, and analysis, a structural map could often be made. This was the era of the search for structural hydrocarbon traps, a period which has not actually ended. However, in more intensively investigated areas, this approach is rapidly becoming less fruitful.

Using a continuous velocity log (CVL), it is possible to compute the acoustic impedence of the earth layers. Seismic reflections arise from changes in the acoustic impedance ρv of the rocks; if the density of the subsurface ρ, and the velocity of sound through it, V, are known continuously as function of depth, it is possible to calculate the exact form of an ideal, noise-free

or noise-inclusive seismic reflection trace. The synthesis of seismic reflection records has become a standard procedure as an aid to seismic interpretation since the initial publication of Peterson et al. (1955). The need in stratigraphic interpretation to correlate borehole data and reflection coefficients has provided a stimulus to improve synthetic seismogram techniques.

Synthetic seismograms are theoretical seismic traces or sections constructed or computed for use in studying correlation between borehole data and the reflected record. They are the main vehicles by which real seismic traces can be correlated with a subset of log data and an appropriate description of the geology of the earth. The synthetic is generally a seismic-response model based on an assumed seismic source-pulse and a hypothetical geological sequence. Like all models, it is precisely defined mathematically, but while the mathematical expressions remain exact, they do not always conform to reality in all conditions.

The Peterson approximation gives a reflectivity that is directly proportional to the amplitude of the velocity log when the latter is plotted on a linear logarithmic scale. In general, the generation of the reflectivity sequence constitutes the principal data set for the construction of a synthetic seismogram (exact or approximate). Once available, the assumed seismic pulse is then scaled in magnitude and polarity by the reflectivity spike of each reflector. The time-shifted and scaled versions of the source-pulse are then

compounded to give the required synthetic. Figure (3.01) shows some possible stages in synthetic generation.

Following the early work of Peterson et al. (1955) this method has been constantly improved (see Durshner (1958), Dennison (1960), Anstey (1960), etc.) Techniques based on the plane-wave solution by the method of finite differences, matrix propagators, and operational methods have been described by Berryman et al. (1958), Wuenschuel (1960), Baranov and Kunetz (1960), Trorey (1962), Robinson et al. (1966), plane wave solution in the frequency domain, Kennett (1979).

The earliest synthetics involved analogue techniques, using mechanical or electrical analogues. The mechanical analogue uses a metal rod of variable diameter - the analogue rod (Sacony Mobil Oil Company, Angona, 1958). The electrical analogue uses some electrical networks and like the Peterson's technique synthetics without multiples can be obtained easily and cheaply by appropriate filtering of the reflectivity series.

Modern methods of synthesis are computational in origin, giving synthetics with and without multiples, sometimes including the effects of absorption, attenuation, geometrical spreading, etc. Synthetic generation in this thesis is all based on computational methods. The emphasis is on synthesis based on filter theory (Robinson, et al., 1966), Wuenschel (1960, 1958), Kirchhoff's solution of acoustic wave equation (Buchen et al., 1980), and the frequency domain solution of a plane wave equation, Kennett (1979).

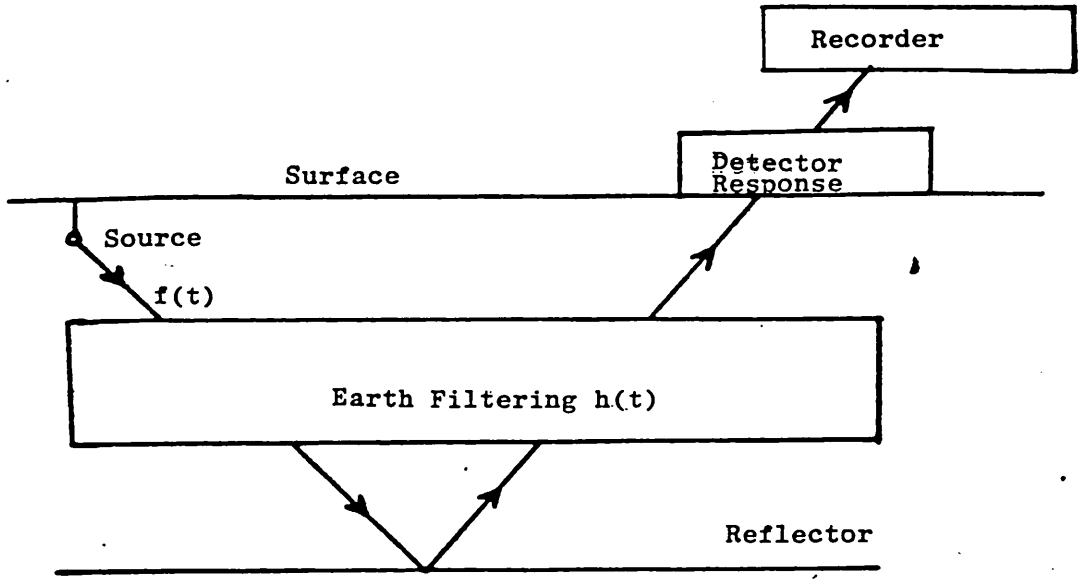


Fig. 3.03 Showing the sequence of filtering effects a seismic pulse encounters on its source-to-recorder wavepath.

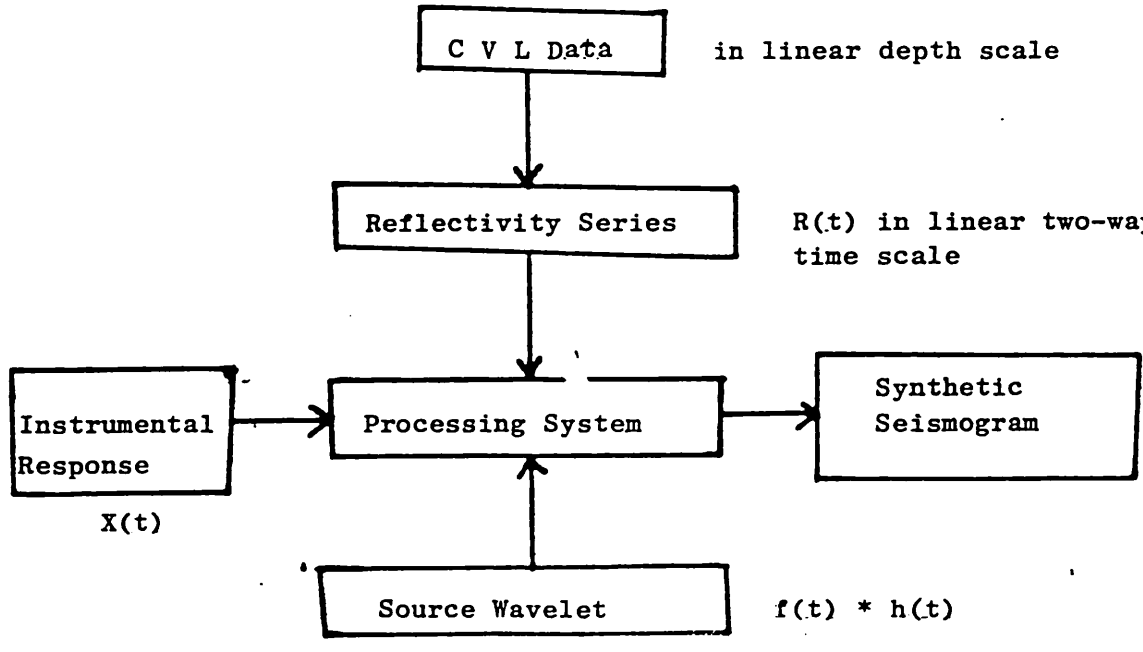


Fig. 3.01 Flow chart to show the basic data sets required to generate a synthetic seismogram.

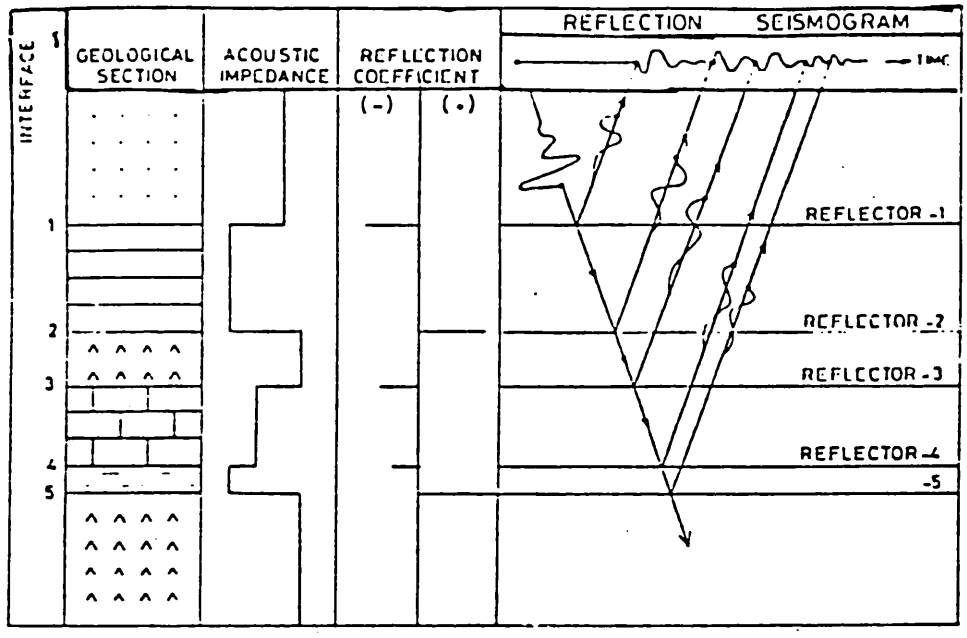


Fig. 3.02 A set up to simulate the seismic process n layers (n = 5, Al-Sadi, 1980)

3.10 The Fundamental Relations

The fundamental assumption underlying the synthesis of 1-dimensional synthetic seismograms is that the geological structure (earth) is made up of a finite number of thin horizontally laid strata each of which is characterized by an acoustic impedance which is a function of depth only. These beds are separated by a finite number of reflectors (their boundary surfaces). When an incident downward travelling-pulse encounters a reflector, a portion of its energy is reflected while the rest is transmitted into the next layer. The amount of reflected energy, hence the amplitude of the reflected pulse as well

as its phase relative to the incident pulse, depends on a single parameter, the acoustic impedance contrast at the interface. There is reflection at all interfaces such that the observed reflection at the surface is visualised as the result of the interference of all the individual reflections placed properly in time. These include, primary reflections, multiple reflections, and all other possible events. Figure ($3\text{-}O_2$) shows a simple set up to simulate the seismic process for a case of n layers (n=5). The model requires the incident pulse to arrive normally at each interface. The figure has it inclined to ensure the reflected pulse is placed in proper time sequence.

The set of strata is characterised by a reflectivity sequence $R_1(t)$ which becomes a reflectivity function for a continuous variation of acoustic impedance with depth, R_1 is a function of two-way travel time t and not of depth. This change of independent variable from depth to two-way travel time is effected in order to place the signals in the correct order in time when constructing a trace.

In a real experiment, the reflectivity effect (depicted by the illustration above) is accompanied by a modification of the seismic pulse. This modification is brought about by detector - response characteristics, transmission losses, and all other forms of earth filtering encountered by the pulse as it propagates through the earth (Fig. 3.03). Let this pulse filtering along its source-to-detector wavepath by represented by a time series $h_1(t)$, the seismic pulse by $f_1(t)$, and the modification of the detector-recorder system by $X_1(t)$. The synthetic seismogram, $S_1(t)$ is then mathematically represented by a

convolution of $f_1(t)$ with all the other effects along the ray path, hence;

$$S_1(t) = f_1(t) * R_1(t) * h_1(t) * X_1(t) \qquad 3.01$$

where * stands for convolution

$f_1(t)$ the source waveform

$R_1(t)$ Reflectivity function

$h_1(t)$ Internal Earth filtering

$X_1(t)$ Detector-recorder effects

At the beginning of synthesis, the reflectivity series $R_1(t)$ which is generated from well data, is usually available. The synthetic $S_1(t)$ is thus a mathematical solution of equation (3.01).

As earlier mentioned, the reflectivity series $R_1(t)$ is generated from the well data, usually velocity and density logs. The reflectivity R_1, for normal incidence of a seismic pressure pulse on a boundary separating two media of parameters.

$$Zi = \rho_i \, Vi$$

and $$Z_{i+1} = \rho_{i+1} \, V_{i+1}$$

is defined thus, (Kanasewich & Agarwal, 1973)

$$R_1 = \frac{Z_{i+1} - Z_i}{Z_{i+1} + Z_i} \qquad (3.02)$$

$$= \frac{\rho_{i+1} \, V_{i+1} - \rho_i \, Vi}{\rho_{i+1} \, V_{i+1} + \rho_i \, V_i}$$

Where Z, P, V are the medium acoustic impedance, density, and velocity. In reality the variation of velocity within an infinitesimal depth extent is much more than that of density so that the absence of density is not often of great importance, hence equation (3.02) may be approximated to obtain:

$$R_1 = \frac{V_{i+1} - V_i}{V_{i+1} + V_i} \qquad (3.03)$$

and from Peterson et al. (1955), R_1 may further be approximated as:

$$R_1 = \frac{Z_{i+1} - Z_i}{Z_{i+1} + Z_i}$$

$$\simeq \Delta Z/2Z$$

or $$R_1 \simeq \tfrac{1}{2}\Delta \ln Z$$

Similarly, we can define the transmission coefficient T_1 as follows:

$$T_1 = \frac{2\ Zi}{Z_{i+1} + Z_i}$$

A number of important deductions may be made from (3.02). Suppose there are two layers, of parameters Z_1 and Z_2, so that our equation (3.02) becomes:

$$R_1 = \frac{Z_2 - Z_1}{Z_2 + Z_1} \qquad (3.05)$$

From (3.05) it is easy to see that R_1 depends on acoustic impedance contrast ΔZ defined

$$\Delta Z = Z_2 - Z_1$$

(and which is the numerator of equation (3.05) hence,

1) IF $Z_1 < Z_2$ then $R_1 > 0$

When $R_1 > 0$, the reflection coefficient occurs without a change in polarity of the pulse.

2) IF $Z_1 > Z_2$ then $R_1 < 0$

In this case the reflection results in a change of amplitude and a phase reversal.

3) IF $Z_1 = Z_2$ then $R_1 = 0$

When $R_1 = 0$, no reflection occurs, rather all the incident energy is transmitted into the medium of parameter Z_2.

Sometimes, certain parameters of equation (3.02) such as velocity may be derived from an electrical resistivity log, if this is available, then from Faust (1953) we have

$$V = \gamma(Z/R_t)^{\frac{1}{6}}$$

where Z = depth

R_t = time formation resistivity

γ = 1948 (constant)

3.20 The Synthetic Hypotheses

In the last chapter we noted that the entire seismic process is a complex one. In setting up a model for it, certain simplifying assumptions have to be made. In order that the seismograms generated from the model might give useful information in the stratigraphic interpretation of real stacked records, it is necessary that the hypothesis used in creating the model be as close to reality as possible. However, the simplicity depends on the available computational techniques, for there are always some limitations as the last chapter has shown. Generally, the hypotheses can be varied if need be to obtain a reasonable variety of synthetics that closely approximate the real earth conditions.

One-dimensional synthetic seismograms are made subject to the following general assumptions:

a) There is a plane wave propagating at normal incidence to a finite number of thin layers (stratified earth) each of which is laterally homogeneous.

b) The transit time T of the seismic pulse is the same for all the layers.

c) The continuous velocity log (CVL) required as input is assumed to be flawless.

d) The velocity is a function of depth only and seismic pulses are propagated in plane wavefronts parallel to the layers of the earth.

e) The density is uniform in the subsurface.

f) The subsurface is perfectly elastic and obeys Hooke's law in its linear form.

Assumptions, d , e, and f lead to a very simplified scheme of the seismic process. They are equivalent to neglecting lateral variations in velocity, the broadening of the pulse with increasing distance away from the source, seismic ray curvature, all refraction and diffraction effects of obstacles, density variations, and possibly absorption effects.

Given a CVL (continuous velocity log) some of the assumptions can be varied to prepare the best possible reflectivity series.

Now, to admit that the transit time T_i for the i^{th} layer is the same for any other layer, and that the velocity V is a function of depth only, is equivalent to saying that:

$$Ti = \int_{Zi}^{Zi+1} dZ/V(Z) \qquad (3.06)$$

is a constant, while, twice this transit time (2Ti) is the two-way travel time of the pulse for layer i. Since Ti is constant, it will hence be referred to as T. However, in order to place the reflected pulse in correct time order, the continuous velocity in linear depth scale may be altered to a function that gives velocity in linear time scale, a CVL may then be represented as V(Z) or V(t) - as depth or time-function. The requirement for quantizing the time is a computational feature and not a physical requirement. This is analogous to the frequency domain computation of the complex wave amplitudes for a large but finite

number of frequencies.

Finally, we can represent the continuous earth by the continuous function U(t) such that

$$U(t) = \log Z(t)$$

where

$$Z(t) = \rho_{V(t)}$$

is the acoustic impedance, and

$$t = \int_0^z dZ/V(Z)$$

But for a discontinuous earth made up of a series of thin layers of equal transit time T, U(t) is replaced by $\bar{U}(t)$ with a sampling interval T. Then for such a sampling to preserve the pertinent information on the real earth, aliasing must be avoided so that

$$T \leq \frac{1}{2} f_{max}$$

The above condition requires that the layer thickness should be of the order of the wavelength of the pulse. The smaller T, the better U(t) is represented by $\bar{U}(t)$, (Woodward, 1953).

3.30 The General Methods of Synthesis

3.3.1 Synthesis Based on Filter Theory

The problem of plane wave propagation in layered media may be restated in terms of filter theory, e.g., Baranov et al. (1960), Wuenschel (1960), Trorey (1962),

Treitel et al. (1966). The method originated through Abels (1946) and Crook (1948) who applied it to optical systems. The technique among earth scientists has had its most immediate success in attacking problems of generating synthetic seismograms and removing unwanted reverberations from the field seismograms.

A linear filter model of the seismic reflection process can be derived from the following assumptions:

(1) The layering of the earth can be described by a CVL (continuous velocity log).

(2) The shot pulse is time-invariant and propagates as a plane wave at normal incidence to the stratified stack of layers.

There is often a third assumption, namely all multiples, ghosts and other kinds of noise are negligible (primaries only, Peterson et al., 1955), or not negligible (Primaries plus multiples, etc., Wuenschel (1960), Treitel et al. (1966), Kennett (1979).

A horizontally stratified earth can be replaced by a linear time-invariant filter whose transfer function is the Z-transform of the set of reflection coefficients. The filter input to the system is the invariant seismic pulse while the output is the synthetic seismogram. It can be shown for example that the synthetic process of Peterson et al. (1955) is equivalent to linear filtering in the time domain (Sengbush et al., 1961). In the same manner, Treitel et al., have shown that the response of a layered system may be represented as a dispersive all pass system with positive phase lag. Robinson (1967)

implemented this technique and generated a set of synthetic seismograms which contain all possible reflections. The seismograms are similar to those of Wuenschel (1960) except that the latter computations, particularly made allowance for inclusion of source ghosts.

3.3.2 Linear Filter and Convolution process

A given filter shows various properties. For example, it can be linear or time-invariant. A filter is linear if its output is always directly proportional to the input. If $Z_1(t)$ and $Z_2(t)$ are the outputs for the respective inputs $X_1(t)$ and $X_2(t)$, then for a linear filter we should expect an input $S_1(t) = \gamma_1 X_1(t) + \gamma_2 X_2(t)$, to give rise to an output $\mathcal{D}_1(t) = \gamma_1 Z_1(t) + \gamma_2 Z_2(t)$, for all complex constants γ_1, γ_2.

On the other hand, a filter is time-invariant if the properties of the filter do not vary with time. If $X_1(t)$ is the input at time t - producing an output $Z_1(t)$, then at time $(t+T)$, $X_1(t+T)$ will give an output $Z_1(t+T)$.

3.3.3 Impulse Response Function and Convolution

Let us recall the function $\delta(t)$ often called the impulse function (delta function) and defined:

$$\delta(t) = \begin{cases} \infty & t = 0 \\ 0 & t \neq 0 \end{cases}$$

and $$\int_{-\infty} \delta(t)\, dt = 1$$

If the input to a given linear time-invariant filter is $\delta(t)$, the output will be a characteristic transient waveform say, $g(t)$, called the impulse response function of the filter. All the effects the filter produces on a given input are a consequence of the form of $g(t)$. This function $g(t)$ is not arbitrary and cannot represent a physically realisable filter, unless it satisfies the relations:

(1) $g(t) = 0 \qquad t < 0$

(2) $g(t) \longrightarrow 0$ as $t \longrightarrow \infty$

Condition (1) implies that $g(t)$ must be one-sided in time (causal). The filter therefore cannot respond before the input is applied. The second condition states that $g(t)$ must be stable - ensuring that the effect of the filter must eventually die out.

In the light of the above, we can picture a linear filter as a black box with an input and an output, while the filter characteristic $g(t)$ is the effect of the box. So, given a box of characteristic $g_1(t)$ and an input $f_1(t)$, the output $S_1(t)$ is a convolution of $f_1(t)$ and $g_1(t)$.

$$S_1(t) = f_1(t) * g_1(t) \qquad (3.07)$$

where * as usual denotes convolution.

Equation (3.07) may be written in integral form:

$$S_1(t) = \int_{-\infty}^{\infty} f_1(\alpha)\, g\,(t-\alpha)\, d \qquad (3.08)$$

and since convolution is commutative,

$$f_1(t) * g_1(t) = g_1(t) * f_1(t) \qquad (3.09)$$

hence $$S_1(t) = g_1(t) * f_1(t) \qquad (3.10)$$

Equation (3.09) suggests that $S_1(t)$, the output, is unchanged in form, even when the box characteristics and the input are interchanged. Seismogram synthesis based on linear filter model is thus a convolution between the filter input (the desired wavelet), and the impulse response of the layered medium.

3.3.4 Linear Filter Model - Primaries only

Peterson's synthesis technique generates a synthetic that approximates the true reflected signal. The method neglects the effects of multiples, transmission losses and absorption. The reflection coefficient at each interface or at each change of acoustic impedance is approximated using the difference in the logarithm of velocity across the boundary. Analogue techniques are expensive and not easy to realize in practice (see McDonald et al., 1983).

Figure (3.04) shows a suite of seismogram traces generated through a computational method. The method follows a linear filter model (after Peterson, 1955). The response of the earth or the reflectivity sequence

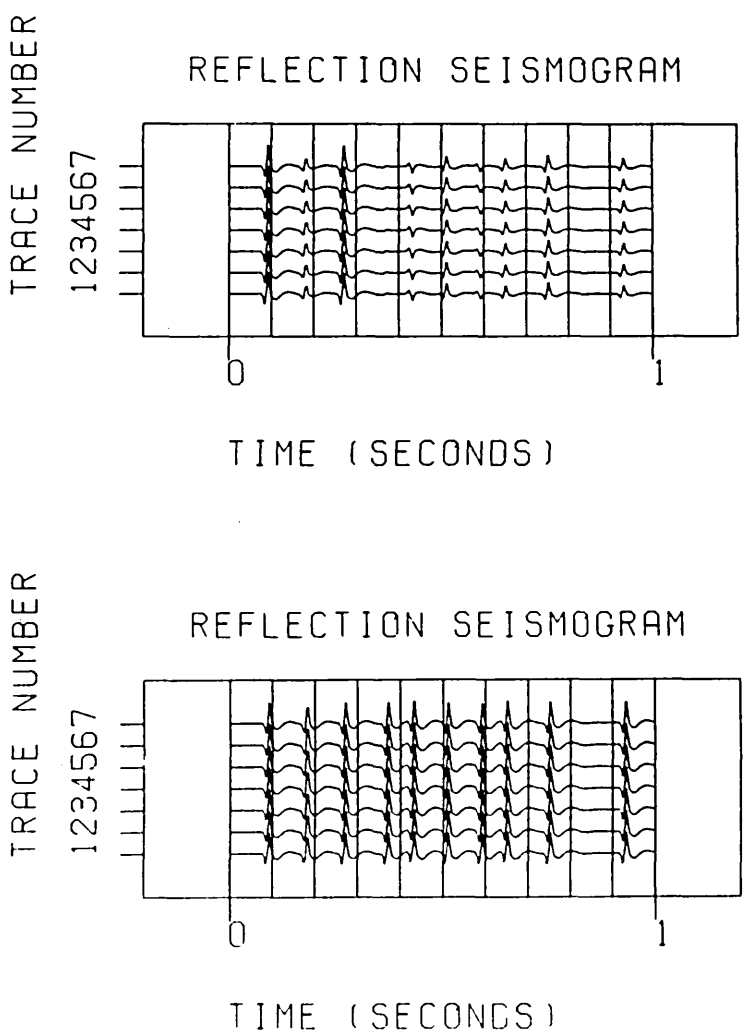


Fig. 3.04

a) A suite of seismogram traces generated using linear filter model

b) The same theoretical traces with amplitudes equalised to the highest absolute value

contains primaries only. The primary spike sequence is obtained using a random number generator - RANDOM. The generated random numbers are drawn from a population of zero mean and unit variance.

Each random spike amplitude arrives at a given time (the arrival time). We have therefore, two arrays representing the spike sequence and then the arrival times. A computer routine, FILT, performs the equivalence of convolution between the desired wavelet and the spike amplitudes. The result is the synthetic seismogram without multiples. The entire process is controlled by the routine HOMO, which acts as a manager program, co-ordinating the rest of the routines. The desired wavelet is the impulse response of a Butterworth band-pass filter (discussed in chapter two) with 15-85 Hz passband, while the low-cut/high cut slopes band edges are 24 (dB/Octave).

Table (3.1) shows the spike amplitudes and arrival times. It is easy to follow from the plots, the events as they arrive. The routine XPGRAM scales and plots the seismograms as desired.

3.3.5 Linear Filter Model; all Possible Reflections:

We now discuss a synthesis technique which includes: all possible reflections and transmission effects. We assume the earth is made up of a horizontal stack of layers and the signal recorded at the surface of this stack is exactly computed for a source of plane - waves at normal incidence to the stack. The response of

Spike Amplitudes	Arrival Times
-1.71716	80.00
-0.78199	170.00
-1.67762	260.00
-6.10528	360.00
0.54804	420.00
-0.79003	500.00
0.37256	580.00
-0.65543	640.00
-0.89532	740.00
-0.65775	920.00

Table 3-1: Spike Amplitudes and Arrival times for synthetic generation

the stack (the impulse response) is determined by assuming a source behaving as a unit impulse; the synthetic for an arbitrary source is then generated by convolution with the impulse response of the stack where the arbitrary source here represents the desired wavelet. A number of computational methods of estimating the best possible wavelets are described in chapter five. These estimations are done in both frequency and time domain.

The exact computation of synthetic seismogram with all reflections and transmissions included, follows the method of Treitel, S. et al. (1966) and Wuenschel (1960). We shall use both techniques in our synthetic generations.

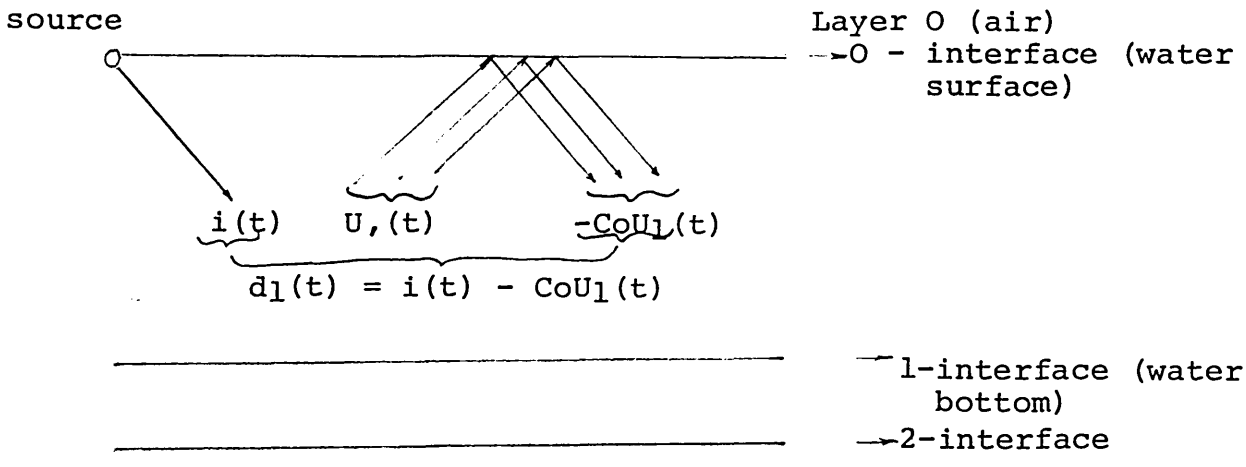


Fig. 3.05 The Layered System

Treitel's method follows from the assumption that a layered medium bounded by a perfect reflector at depth constitutes a dispersive, all-pass system with positive phase lag. The computation of the response is achieved using the Z-transform.

3.3.6 The layered System

Let us suppose that our layered system is such that the upper interface (O-interface) is a perfect reflector with coefficient Co = -1 (Fig. 3.05). This is particularly typical of marine seismic exploration, the first layer being the water layer and the subsurface of the water bottom acts also as a perfect reflector. We suppose too that a source located on the O-interface gives rise to an initial downgoing waveform i(t) at the top of layer 1, while an upgoing waveform $U_1(t)$ at the top of layer 1 is reflected at the water surface (interface O) to yield a downgoing waveform, $-CoU_1(t)$

at the top of the water (Fig. (3.05)).

$$\Longrightarrow D_1(t) = i(t) - CoU_1(t) \tag{3.11}$$

Since the water layer is perfect reflector then

$$D_1(t) = i(t) + U_1(t) \tag{3.12}$$

If the initial downgoing waveform i(t) is a single positive spike ψ_o at time O, then the upgoing waveform $U_1(t)$ will be a time series of the form:

$$\psi 1, \psi 2, \psi 3, \psi 4, \ldots, \psi n$$

The series starts at time 1, and

$$\psi_1 = U_1(1), \psi_2 = U_1(2), \ldots, \psi_n = U_{1(n)} \tag{3.13}$$

$$n = t$$

Similarly starting at time O, the downgoing waveform $D_1(t)$ becomes:

$$\psi_o, \psi_1, \psi_2, \ldots, \psi_n$$

Where

$$\begin{aligned} \psi_o &= D_{1(o)} = i(o) \\ \psi_1 &= D_{1(1)} = U_1(1) \\ \psi_2 &= D_{1(2)} = U_1(2) \\ \psi_3 &= D_{1(3)} = U_{1(3)} \end{aligned} \tag{3.14}$$

$$n = t$$

Hence a seismic receiver monitors the sum of the upgoing and downgoing waveforms which is the time series,

$$\psi_o, 2\psi_1, 2\psi_2, 2\psi_3, 2\psi_4 \ldots 2\psi_n$$

$$n = t$$

which is the response of the layered system due to a

source which is a unit spike. We shall give a brief mathematical detail which applies the Z-transform and matrix analysis to obtain a set of normal equations which are solved to obtain the up and down going waveforms, so that the layer response is expressed in a form easily programmed for computer evaluation.

Mathematical Theory

The Z-transform of the upgoing and downgoing waveforms at the top of layer 1 are,

$$\bar{U}_1(Z) = \psi_1 Z + \psi_2 Z^2 + \psi_3 t^3 + \psi_4 Z^4 \ldots$$

$$\bar{D}_1(Z) = \psi_0 + \psi_1 Z + \psi_2 Z^2 + \ldots$$

$$= \psi_0 + \bar{U}(Z)$$

From Robinson (1967b), the Z-transform of the downgoing and upgoing waveforms at the top of layer K+1 are:

$$D_{K+1}(Z) = D_{K+1}(K/2) Z^{K/2} + D_{K+1}(K/2+1) Z^{(K/2)+1} + \ldots$$

(3.15)

$$\bar{U}_{K+1}(Z) = U_{K+1}(K/2+1) Z^{(K/2)+1} + U_{K+1}(K/2+2)$$

$$Z^{(K/2)+2} + \ldots$$

The Z-transforms, equation (3.15), may be presented in matrix form; such that

$$\begin{bmatrix} \bar{D}_{K+1}(Z) \\ \bar{U}_{K+1}(Z) \end{bmatrix} = \frac{Z^{-k/2}}{(1-C_k)..(1-C_2)(1-C_1)} \begin{bmatrix} P_k^{R(z)} & Q_k^{R(z)} \\ Q_k(z) & P_k(z) \end{bmatrix} \begin{bmatrix} \psi_0 + \bar{U}_1(Z) \\ \bar{U}_1(z) \end{bmatrix}$$

(3.16)

where the C-values denote the interface reflection coefficients, $P_k(Z)$, $Q_k(z)$ are characteristic polynomials.

The matrix equation (3.16) may be represented in terms of two scalar equations defined:

$$\bar{D}_{k+1}(z) = \frac{z^{-K/2}}{(1-C_k)\ldots(1-C_2)(1-C_1)}\left\{\left[P_k{}^R(Z) + Q_K{}^R(z)\right]\right.$$

$$\left.\bar{U}_1(z) + \psi_o P_K{}^R(z)\right\}$$

$$\bar{U}_{K+1}(z) = \frac{z^{-k/2}}{(1-C_k)..(1-C_2)(1-C_1)}\left\{\left[P_K(Z) + Q_k(z)\right]\right.$$

$$\left.\bar{U}_1(z) + \psi_o Q_k(z)\right\} \qquad (3.17)$$

Where we define the $P_k(z)$, $Q_k(z)$, and $A_k(z)$ polynomial as follows:

$$P_k(z) = P_o(K) + P_1(K)\ Z + \ldots\ P_k(K)z^k$$
$$= P_o + P_1Z + P_2Z^2 + \ldots\ P_k\ z^k$$

$$Q_k(z) = q_o(k) + q_1{}^{(k)}\ Z + \ldots\ Q_k(k)\ z^k \qquad (3.18)$$
$$= q_o + Q_1Z + Q_2Z^2 \quad \ldots\ Q_k\ z^k$$

$$A_k(z) = a_o(k) + a_1(k)\ Z + \ldots\ a_k(k)z^k$$
$$= a_o + a_1Z + a_2Z^2\ Q\ \ldots\ a_kz^k$$

The operator $\{a_o(k), a_1(k) \ldots a_k(k)\}$ is the so-called prediction error operator of length K+1. Also $A_k(z)$ is defined:

$$A_k(z) = P_k(z) + Q_k(z)$$

If we multiply both sides of our scalar equations by $z^{k/2}$, then we have

$$D_{k+1}(k/2)z^k + D_{k+1}(\tfrac{k}{2}+1)z^{k+1} + D_{k+1}(\tfrac{k}{2}+2)z^{k+2} + \ldots$$

$$= \frac{1}{(1-C_k)..(1-C_1)}\left[(ak + ..a_o z^k)(\psi_1 z + \psi_2 z^2 + \ldots)\right.$$

$$\left. + \psi_o(P_k + \ldots P_o z^k)\right] \qquad (3.19)$$

and

$$U_{k+1}(\tfrac{k}{2}+1)z^{k+1} + U_{k+1}(\tfrac{k}{2}+2)z^{k+2} + \ldots =$$

$$\frac{1}{(1-C_k)..(1-C_1)}\left[(a_0 + .. a_k z^k)(\psi_1 z + \psi_2 z^2 + \ldots) + \right.$$

$$\left.\psi_o(q_o + \cdots + q_k z^k)\right. \qquad (3.20)$$

We can now identify the coefficients of powers of Z in equations (3.19) and (3.20). The coefficients of z^o, z^1, z^2, z^3 z^k in (3.20) and the coefficients of z^o, z^1, z^2, z^3 ..., z^{k-1} in (3.19) are zero so that the coefficients of z^o in (3.20) and z^k in (3.19) are respectively defined:

$$q_o \psi_o = 0$$

$$P_o\psi_o + a_1\psi_1 + a_2\psi_2 + a_3\psi_3 + \ldots a_k\psi_k = (1-C_k)..(1-C_2)(1-C_1)D_{k+1}(k/2)$$

If we recall

$$a_o\psi_o = P_o\psi_o + q_o\psi_o$$

and sum the two equations we have

$$a_o\psi_o + a_1\psi_1 \cdots + a_k\psi_k = (1-C_k) \ldots (1-C_2)(1-C_1)D_{k+1}(k/2)$$

Similarly the coefficients of Z in (3.20) and Z^{k-1} in (3.19) may be found. We can continue the process upto the coefficients of Z^k in (3.20) and Z^o in (3.19) which give:

$$a_o \psi_K + a_1\psi_{k-1} + a_2\psi_{k-2} + a_3\psi_{k-3} + \ldots + a_k \psi_o = 0$$

If we collect all the above coefficients we can generate a set of normal equations defined as follows:

$$a_o \psi_0 + a_1 \psi_1 + a_2 \psi_2 + a_3 \psi_3 + \ldots a_k \psi_k = V$$

$$a_0 \psi_1 + a_1 \psi_0 + a_2 \psi_1 + a_3 \psi_2 + \ldots a_k \psi_{k-1} = 0$$

$$a_o \psi_2 + a_1 \psi_1 + a_2 \psi_0 + a_3 \psi_1 + \ldots a_k \psi_{k-2} = 0$$

$$\vdots$$

$$a_o \psi_k + a_1 \psi_{k-1} + a_2 \psi_{k-2} + a_3 \psi_{k-3} + \ldots a_k \psi_0 = 0$$

when V is the so-called prediction error variance,

$$V = V(k) = (1-C_k)(1-C_{k-1})\ldots(1-C_2(1-C_1)\ D_{k+1}(k/2)$$

It can also be shown (Robinson, 1967*b*) that

$$D_{k+1}(k/2) = \psi_o(1+C1)(1+C_2)(1+C_3)\ \ldots\ (1+C_k)$$

hence $V = \psi_o(1-C_1^{\,2})(1-C_2^{\,2})(1-C_3^{\,2})\ \ldots\ (1-C_k^{\,2})$

The up and downgoing waveforms may be obtained if the coefficients for higher powers of Z (Z^{k+1}, Z^{k+2} ... Z^{k+n}) are determined from equations (3.19) and (3.20). A general relation for the downgoing and upgoing - waveforms expressed in terms of higher Z-coefficients may be written as follows:

$$D_{k+1(k/2+t)} = \frac{1}{(1-Ck)..(1-C_2)(1-C_1)}\left[a_k\psi_{k+1} + a_{k-1}\psi_{k+t-1}+\ldots\ a_o\psi_t\right]$$

$$U_{k+1}(k/2+t) = \frac{1}{(1-Ck)..(1-C_2)(1-C_1)}\left[a_o\psi_{k+t}+a_1\psi_{k+t-1}+\ldots+a_k\psi_t\right] \quad (3.21)$$

where (t = 1, 2, 3, 4, ..., n)

The expressions in square brackets are the reverse prediction error operator (a_k, a_{k-1}, a_{k-2}, a_{k-3}, ..., a_o) and the predictor error operator (a_o, a_1, a_2, a_3, ..., a_k), each convolved with the autocorrelation (ψ_{k+t}).

Recall, the pulse is a unit spike, hence the problem of computing the impulse response of the layered system is resolved. We can then obtain our synthetic seismogram if we convolve the responses with our desired wavelet. Wuenschel (1960) has treated similar synthetic generation process. His method did not only generate primaries, various levels of multiples, and transmission losses, but source ghosts are also included.

There is basically not much difference between the model just described and that presented by Wuenschel (1958, 1960). The two models have the same properties as Peterson's except that the continuous velocity function from the CVL is sampled to give an "n layered" earth and all reflections (primaries, multiples) are obtained by solving the one-dimensional wave-equation, and at the same time accounting for the transmission losses encountered at every boundary. We do not intend to discuss the Wuenschel model to another detail rather an interested reader may find the papers by Wuenschel (1958, 1960) quite elucidating.

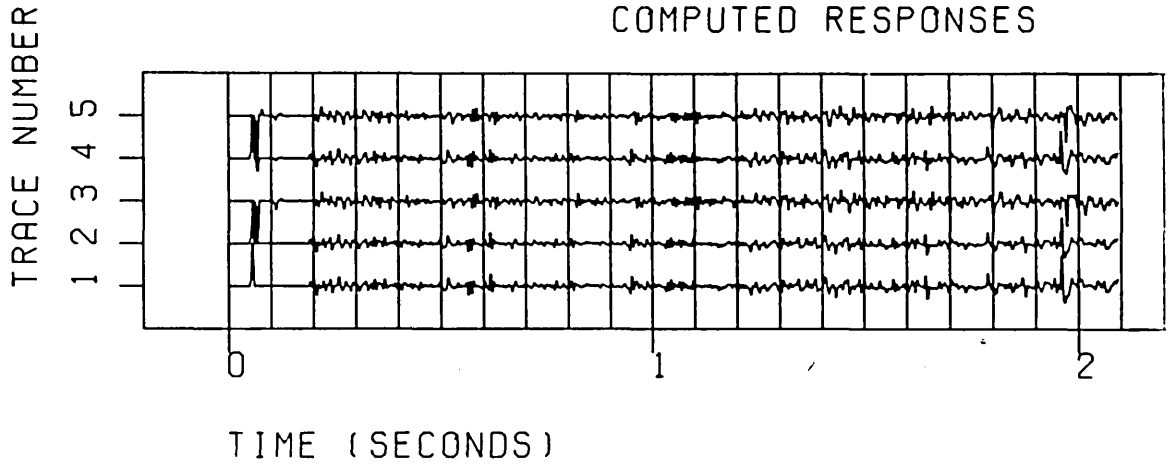
In our practical synthesis, the Treitel/Robinson (1966) model which we have discussed, and the Wuenschel (1960) model, were used. The Wuenschel model was particularly useful when the effects of source ghosts and direct computation of transmission losses were needed, otherwise the two methods were used interchangeably. The computer subroutines, LAYER, and SGEN were used in the computations. SGEN, is a fast routine which utilizes the Wuenschel algorithm to compute the various responses. The routine is used by VELPRO (Merlin velocity profiling) and is more efficient than LAYER in that it computes the source ghost contributions and transmission losses without undue modifications of the programs.

Figures (3.06) - (3.08) show a series of reflection responses computed from information based on the wells. In chapter five the responses will be used in conjunction with the field stacked traces to estimate the best wavelets which in turn will convolve with the reflection responses to produce the most probable synthetics used in our matching analysis. Most of the well-logs are from the Southern area of the N. Sea. Fuller descriptions of the individual logs are given in chapter five.

The computer routines are specifically arranged to accommodate various options. For example, if the option without multiples or ghosts is desired, the work of computing the impulse responses of the layered system is by-passed and the desired result obtained from the sequence of reflection coefficients (or from reflection coefficients plus transmission losses) as the case may be. Every attempt was made to ensure that the log data

The traces are scaled individually with respect to the maximum absolute peak-values.

Fig. 3.06 Synthetic Responses well (cpv-12)
(T_5) All possible multiples plus source ghosts
(T_4) Primaries plus all multiples
(T_3) All possible multiples
(T_2) Primaries plus transmission loss
(T_1) Reflection coefficients



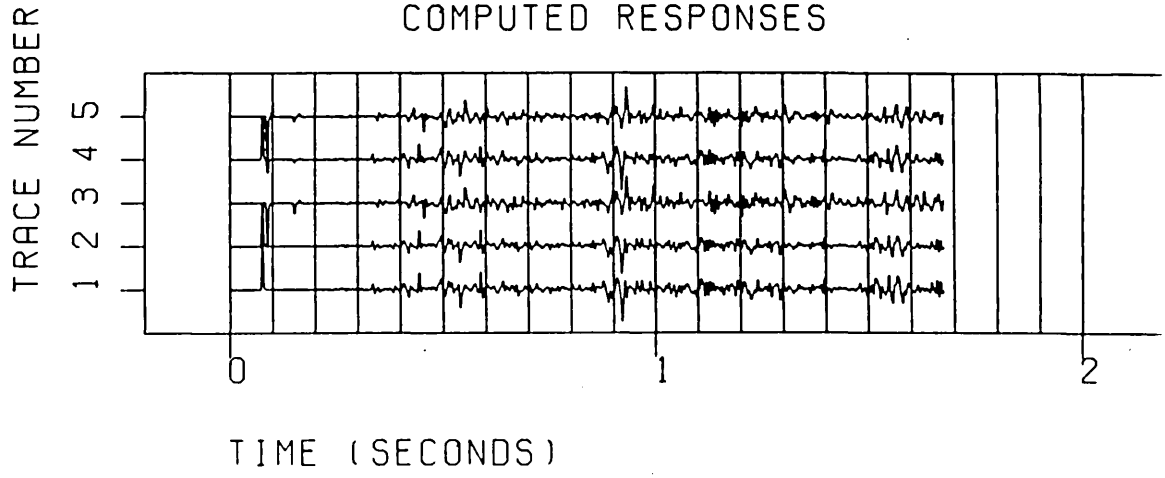
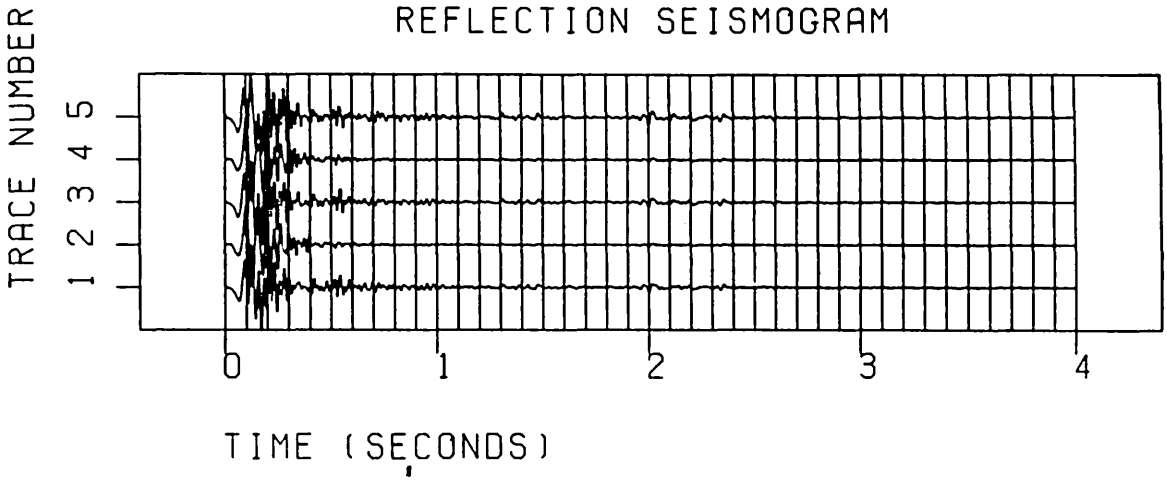


Fig. 3.07 Synthetic Responses (Well, cpv-108)
Traces (1-5) are described as in fig. (3.06)

Fig. 3.08a: Field stacked traces used in matching (line, Cpv-12A)



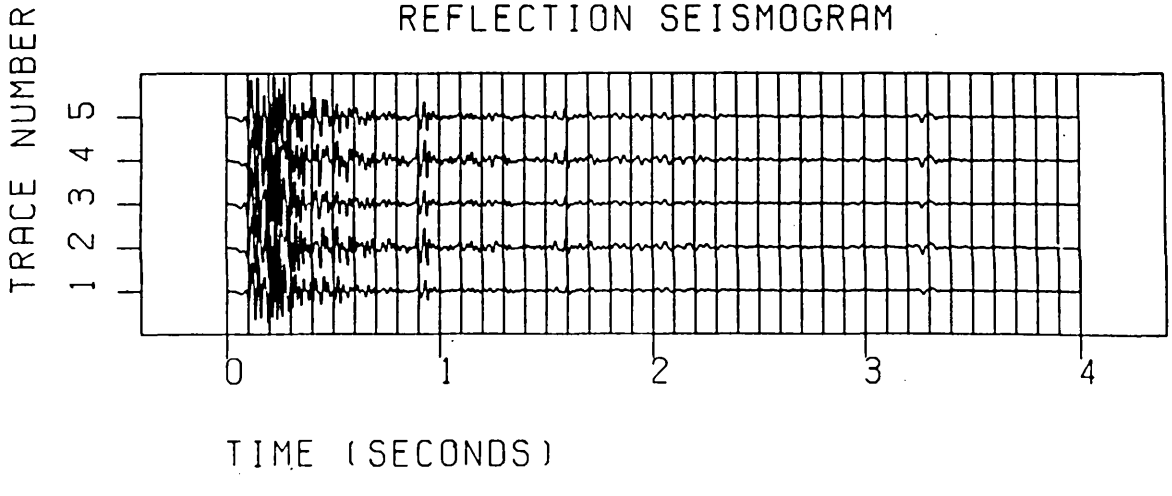


Fig. 3.08b: Field stacked traces (line, cpv-1ØB)

were without errors. They are resampled to 4 ms. sampling interval, after editing, calibration , and depth-time conversions.

We shall see later that the notion of obtaining error free log data is not always completely realized. Some inherent limitations are often encountered, and we only have to depend on best possible approximations.

3.40: Synthetics via Kirchhoff's solution of Scalar Wave Equation:

General Discussion

The main emphasis on the remaining sections of this chapter is on further understanding of diffractions and the accompanying interference and focussing phenomenae. Such understanding is important in seismic analysis of noise events which will form a major point of discussion in chapter four. Our reader is, therefore, reminded not to confuse the 2-dimensional synthetic analysis about to be discussed with the one-dimensional case completed in the last section.

Within the last decade, the Geophysicist has advanced steadily in his understanding of the nature of seismic wave diffraction phenomenon. In the highly original approach of Claerbout (1970, 1972) the wave equation is decomposed into upgoing and downgoing waves, and this has given some valuable insight into such wave effects as interference focussing, geometrical spreading,

refraction and diffraction. Kirchhoff's surface integral representation of scalar waves is a formalism which has been found useful in this understanding of seismic wave diffraction phenomenon. Some works which have been outstanding in this context include, Hilterman (1970, 1975), Trorey (1970, 1977), and Berryhill (1977). Their individual interpretations of seismic diffraction, in particular depends largely on what co-ordinates are chosen to compute the surface integral. Hilterman discussed diffraction in terms of solid angles contained at source by model obstacles at depth, while Trorey considered only planar structures (and combinations of them). He therefore discussed diffraction in terms of plane polar coordinates, as Berryhill gave a third interpretation of seismic diffraction by parametrizing the surface integral in terms of prolate spheroidal coordinates.

However, we can logically argue that a parameter - the two-way travel time from source to receiver, is common to all these time domain applications of the Kirchhoff's integral. Buchen et al. (1980) exploited this parameter to advantage and showed how seismic wave diffractions from arbitrary shaped obstacles could be represented. The result of the presentation is not only computationally feasible but has lead to an efficient numerical algorithm for computing and identifying reflection and diffraction events on field seismic sections. It is therefore more easy to separate a noise event from a diffraction event.

3.4.1 The Kirchhoff's Formulation of Diffractions

A good starting point for the generation of synthetic seismograms with diffraction events is the Kirchhoff's time dependent solution of the standard scalar wave equation (Baker et al., 1939) written:

$$U(p,t) = B\iint_s \left\{ [U]\partial/\partial n\left(\frac{1}{r}\right) - \frac{1}{Cr}\partial r/\partial n\left[\frac{\partial U}{\partial n}\right] - \frac{1}{r}\left[\frac{\partial U}{\partial n}\right]\right\} ds \qquad (3.23)$$

The complete solution to (3.23) follows the method of Buchen et al. (1980). Equation (3.23) says that U(P,t) is the wavefield evaluated at any point P, and time t. The point P is outside an arbitrary closed surface s of outward normal n, ds is the surface element, r is the distance between P and an element ds at Q, $\partial/\partial n$, denotes the directional derivative along the normal to s, c is the wave speed of the medium (assumed uniform), $B = \frac{1}{4\pi}$, is a constant, and

$$[U] = U[Q, t] = U[Q, t - r/c]$$

is the time-delayed or retarded field on s.

In general, only a limited portion of S will contribute to U(P,t) at a particular time, t = tp. That is, we are only concerned with the solution for $tp < t < t + T$ for some small enough T. Thus in practice, it is of little consequence how s closes in detail. The usual approximations in Kirchhoff's diffraction theory is to assume that the field is known everywhere on S. This approximation yields excellent results for diffraction from obstacles with linear dimensions of the order of a wavelength or more. In the seismic exploration case with

source pulses of 10-20 ms, this would correspond to structural inhomogeneities with linear dimensions of only a few meters or less.

In many practical cases, the field on s may be represented by

$$U(Q,t) = A(Q)f(t-\Upsilon(Q)) \tag{3.24}$$

where A(Q) is the amplitude distribution of the wave on S, $\Upsilon_{(Q)}$, the corresponding phase distribution and f(t) is the source function, so that after partial differentiating and substituting from (3.24) into (3.23) we can express (3.23) in the form

$$U(P,t) = U_1(P,t) + U_2(P,t)$$

where

$$U_1(P,t) = B\int_S \left\{A\partial/\partial_n\left(\frac{1}{r}\right) - \frac{1}{r}\frac{\partial A}{\partial n}\right\}\left[f\right] ds \tag{3.25}$$

and

$$U_2(P,t) = B\int_S A/r\left\{\frac{\partial \Upsilon}{\partial n} - \frac{1}{c}\frac{\partial r}{\partial n}\right\}\left[f^1\right] ds$$

where the retarded value is:

$$\left[f\right] = f\left[(t - \Upsilon_{(Q)} - r/c\right]$$

and r = PQ

Now changing to a new set of variables

$$\theta, \Upsilon = \Upsilon + r/c$$

and Υ is the retarded time (time-delay) between the surface element at Q on S and the observation point P, then we have

$$ds = |J|\, d\Upsilon\, d\theta$$

where $J = J(\Upsilon,\theta)$ is the surface Jacobian associated with these coordinates. Often J can be evaluated easily

enough when the specific geometry of the problem is stated. In general terms, if S is represented vectorially by say $\underset{\sim}{X} = \underset{\sim}{X}(T,\theta)$ then

$$J = \left| \frac{\partial X}{\partial T} \times \frac{\partial X}{\partial \theta} \right|$$

The Kirchhoffs formulation now reduces to the sum of two standard time domain convolutions, one over the source function f(t), and the next over its derivative $f'(t)$

$$\Longrightarrow U(P,t) = U_1(p,t) + U_2(p,t)$$

where

$$U_1(P,t) = \int w_1(T)\ f\ (t-T)\ dT \qquad (3.26)$$

$$U_2(P,t) = \int w_2(T)\ f'(t-T)\ dT \qquad (3.27)$$

$$W_1(T) = B \int_{\delta(t)} \left\{ A\, \partial/\partial n\left(\frac{1}{r}\right) - \frac{1}{r}\frac{\partial A}{\partial n} \right\} |J|\ d\theta \qquad (3.28)$$

$$W_2(T) = B \int_{\delta(t)} \left\{ \frac{A}{r}\left(\frac{\partial Y}{\partial n} - \frac{1}{c}\,\partial r/\partial n\right) \right\} |J|\ d\theta \qquad (3.29)$$

and the integrations are performed around the curves $\delta(t)$ on S defined by $t = T$ or $t = Y + r/c$. Such constant travel time curves are here called isochrons. In particular the t-isochron $\delta(t)$ is that curve on the given control surface, all of whose points contribute to the seismic signal at the specific time t. Before we discuss the weight functions along with the generated reflection and diffraction events, let us first present how these events are formed in the Kirchhoff's formulation.

3.4.2 Kirchhoffs Reflection and Diffraction

To understand how reflections and diffractions are formed in the discussed formalisation, let S coincide with the reflector assumed to be plane (just for simplicity).

For a distinct source/receiver pair above the reflector, the isochrons form a family of confocal ellipses on S. The central point of this family of ellipses is a singular point, the t_o-isochron, which corresponds to the true reflection point and gives rise to an observed reflection at time $t = t_o$. If the plane reflector under consideration has uniform reflectivity the contributions from $\delta(t)$ where $t > t_o$ arrive in phase and constructively interfere. Similar in phase contributions arriving from neighbouring isochrons, however, are relatively displaced in time and in general will destructively interfere. Interference contributions from the vicinity of $\delta(t_o)$ - the true reflection point, are exceptional in that no earlier arrivals exist to effect destructive interference. The resultant field at the receiver thus appears as a simple reflection from the single point defined by $\delta(t_o)$.

Similarly, the concept of diffraction can be explained if we assume that our hypothetical plane reflector contains regions of arbitrary shape across which there exist discontinuities in reflectivity. A given t-isochron $\delta(t)$ say, might intersect a number of such regions. Contributions from $\delta(t)$ still arrive

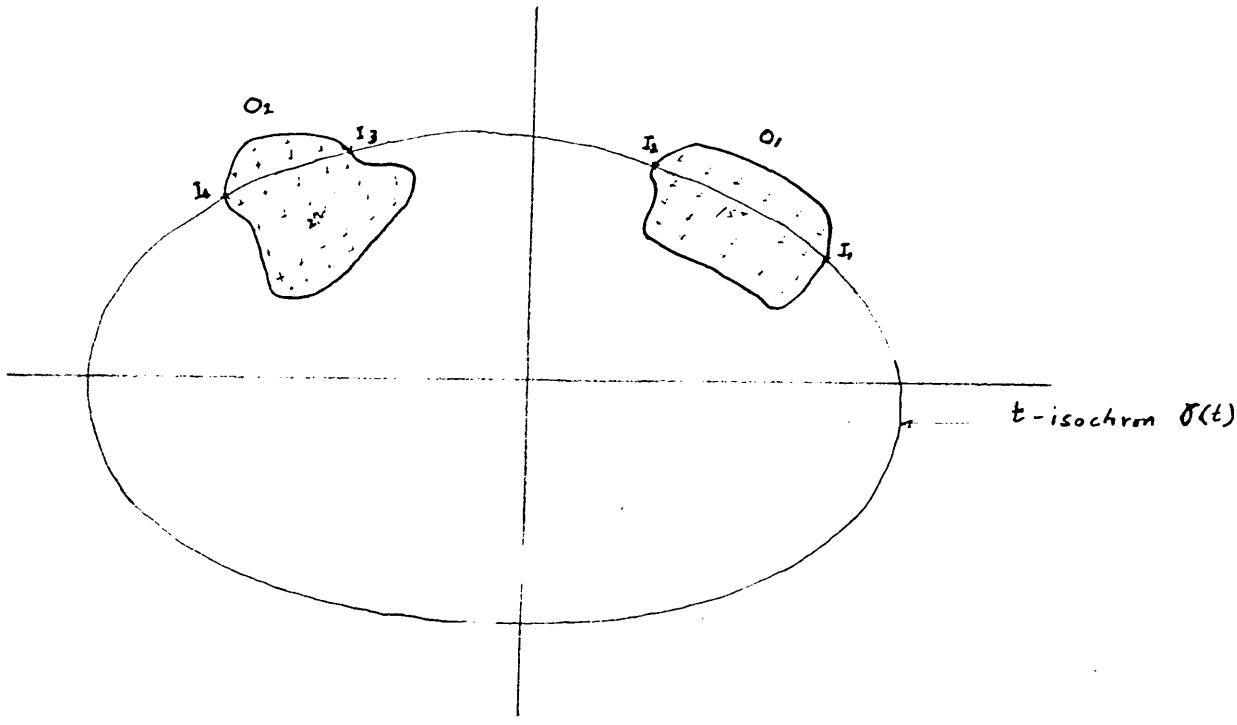


Fig. 3.10A Intersections of diffracting obstacles (O_1, O_2) with elliptic isochron $\sigma(t)$ absence of obstacles give rise to reflections only.

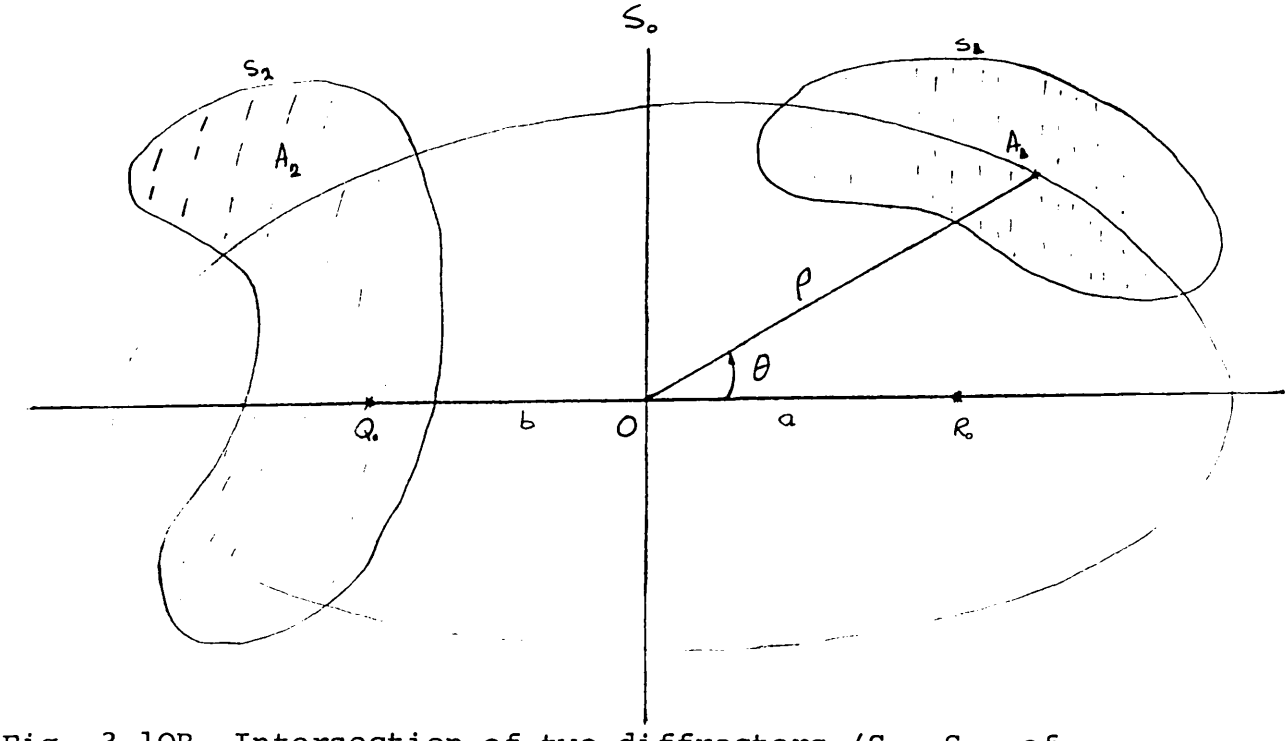


Fig. 3.10B Intersection of two diffractors (S_1, S_2, of reflectivities A_1, A_2) with elliptic isochron $\sigma(t)$. Q_o, R_o, are projections of the source and receiver onto the base reflector plane 'S_o' and $a = OR_o$, $b = OQ_o$.

in phase but the relative amplitudes of contributions arriving from neighbouring isochrons will be greatly affected and so the conditions for exact destructive interference will no longer apply. The non-cancelling contributions effectively originate at all points of the boundaries of the regions of laterally varying reflectivity and so give rise to boundary or edge diffracted waves (Figure 3.10A).

3.4.3: The Weight Functions and Synthetic Seismograms

Having explained the principles and methods of generation of reflection and diffraction events, we can return to our convolution integrals and hence to equations (3.28) and (3.29).

Equations (3.28) and (3.29) are called the weight functions (system responses). We can observe that the integrands for the representation of $W_1(\tau)$ and $W_2(\tau)$ are respectively of order (J/r^2) and (J/r). This suggests that whenever the receiver is more than a few wavelengths from the diffractors. we may neglect the term in W_1 relative to that in W_2.

The above approximation has proven its validity. Our representation of the seismic response therefore becomes a single convolution.

$$U(P,t) \simeq W_2(t) * f^1(t) \qquad (3.30)$$

The weight functions (3.28) and (3.29) depend on the source/receiver location, the velocity of wave propagation, and the distribution and shape of contributing diffractors.

We shall next illustrate the method of Buchen et al. (1980) by describing the properties of the weight function for the case involving a collection of planar but arbitrary shaped diffractors buried at depth in an otherwise homogeneous medium.

3.4.4 Plane Diffractor (Synthetic) Modelling

We here considered very simple models of planar surfaces or their combinations. The assumption of planar structures of arbitrary shape leads to easily manageable theoretical results that could be compared with other works - Trorey (1977), Hilterman (1978).

Let r. r_o. respectively stand for the distances of an arbitrary diffracting point P of the control surface s from the receiver R and source Q. We assume S coincides with a plane reflector which is laterally heterogeneous in the sense that it consists of a given number n of arbitrary shaped sub-regions S_k of reflectivitv A_k where K = 0, 1, 2. ... n. We define K = 0, so that it corresponds to the base reflector and K = 1, 2, 3 ... correspond to the diffractors contained within it. For simplicity we assume the reflector to be horizontal. We also choose (ρ, θ) as plane polar co-ordinates in S relative to the true reflection point O as origin (Fig. 3.10B).

After some elementary analysis, equation (3.29) reduces to the form (see Fig. (3.11)).

$$W_2(T) = B\int \frac{1}{K}(Z_o/r_c + \frac{1}{c} Z/r) \mid J \mid d_\theta \qquad (3.31)$$

where K = r r_o

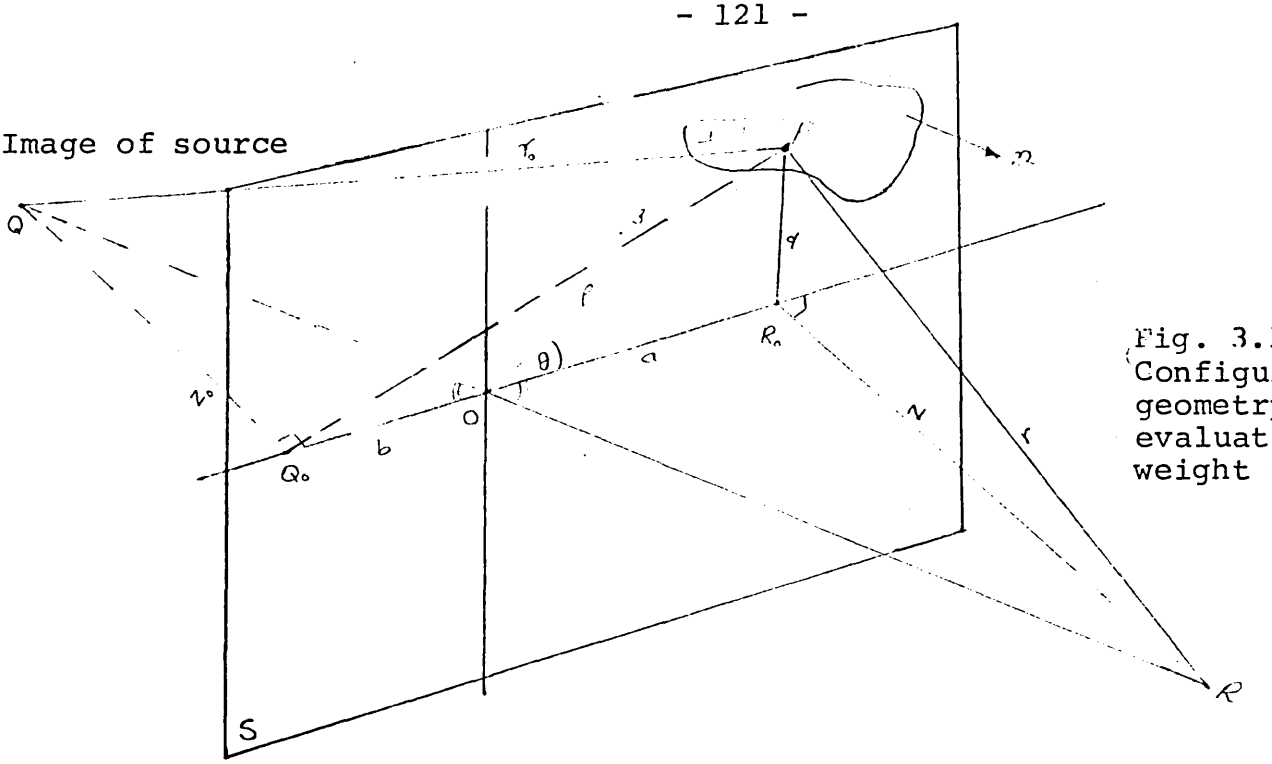


Fig. 3.11 Configuration geometry for evaluation of weight fns.

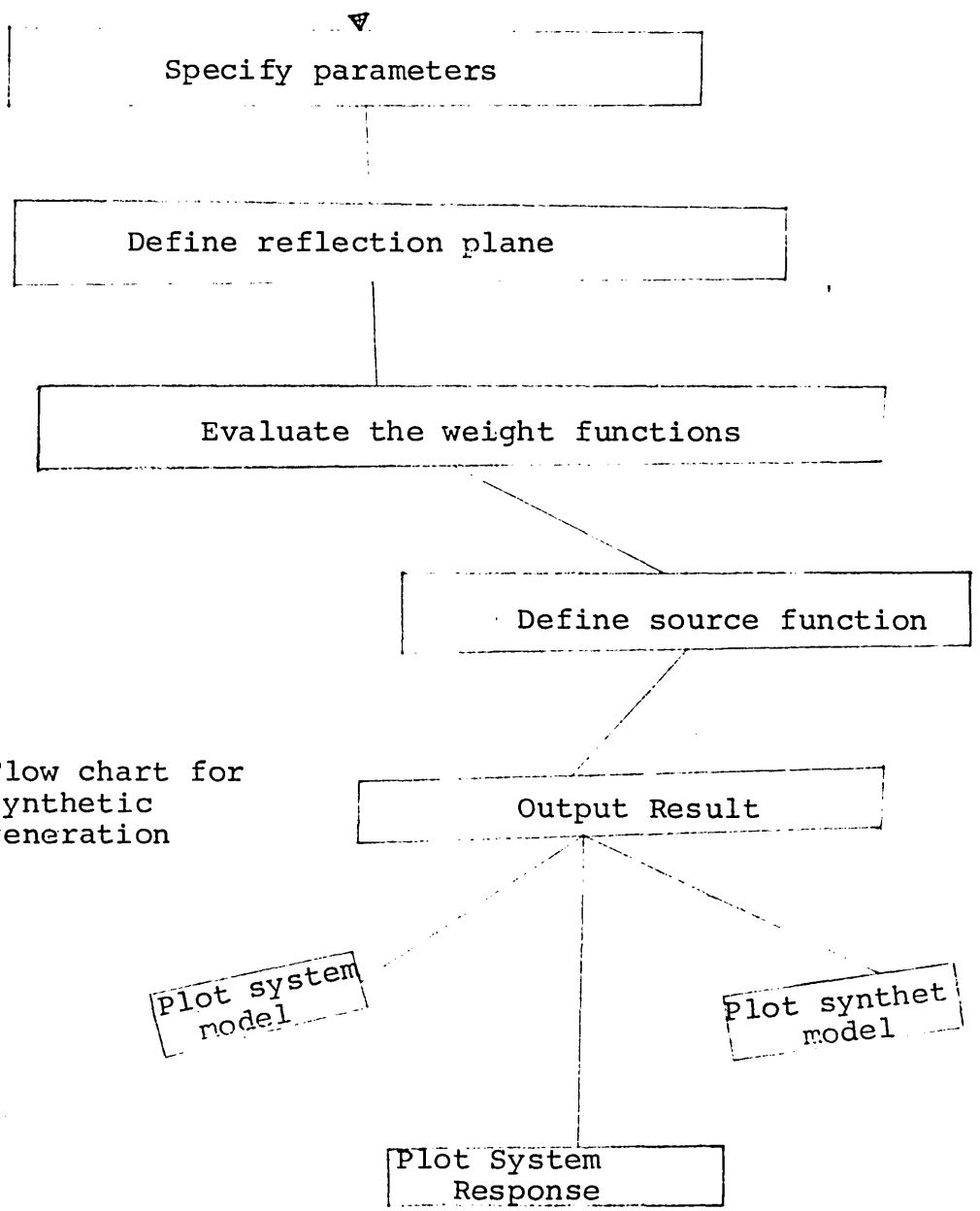


Fig. 3.12: Flow chart for synthetic generation

Similarly, the surface Jacobian $J(\mathcal{P},\theta)$ is readily evaluated from the geometry (Fig. 3.11) and gives

$$|J| = \frac{\rho_c}{\left| \frac{\rho + b\cos\theta}{r_o} + \frac{-a\cos\theta}{r} \right|} \qquad (3.32)$$

Where a and b are defined in the figures.

We can now use equations (3.29) through (3.30), (3.31) and (3.32) to evaluate the wavefield U(P,t) at any point p and time t. The result yields a synthetic seismic section with reflection and diffraction events.

3.4.5 Computer Evaluation of the Synthetic Algorithms

Having obtained some algorithms with which the weight functions and the wavefield U(P,t) could be computed, the next step is to develop some computer routines which would carry out the necessary computations. Figure (3.12) is a flow chart for the computer evaluation of Buchen et al. Algorithms to generate some synthetic seismic sections with reflection and diffraction events. We shall treat each member of the chart in turn. Using this chart a computer program is designed to generate the weight functions and the synthetic seismic section for specific source/receiver locations, with respect to a given subsurface formation. It is assumed that the series of receiver points (for which the output traces are required) are in a straight line, at a given distant apart. This is the normal procedure in seismic work. Figure (3.12A) shows a possible shooting

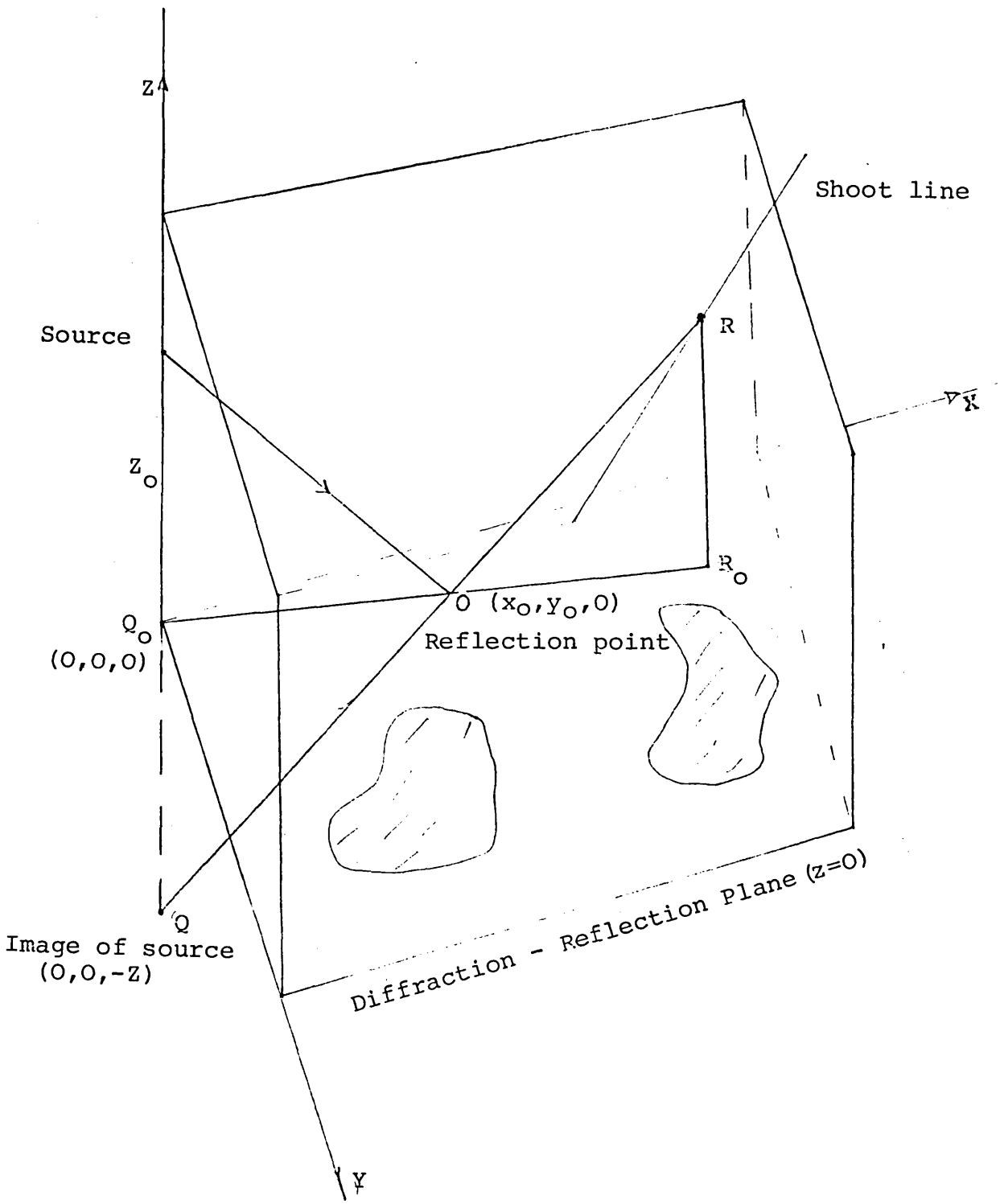


Fig. 3.12a: Shooting Configuration Geometry

configuration geometry as may be used in the modelling process. We take the modelling steps and discuss them.

3.4.6 Parameter Specifications:

Parameter specifications as required by the program are as follows; wave propagation speed, distance of shot and receiver from diffraction plane, receiver line, and shot geometry.

Define the Reflecting (Diffracting) Plane

The obstacle on the reflecting plane is defined by cartesian co-ordinates with respect to Q_o as origin (Fig. 3.12A), and are approximated by straight lines by joining the co-ordinate points (Fig. 3.14).

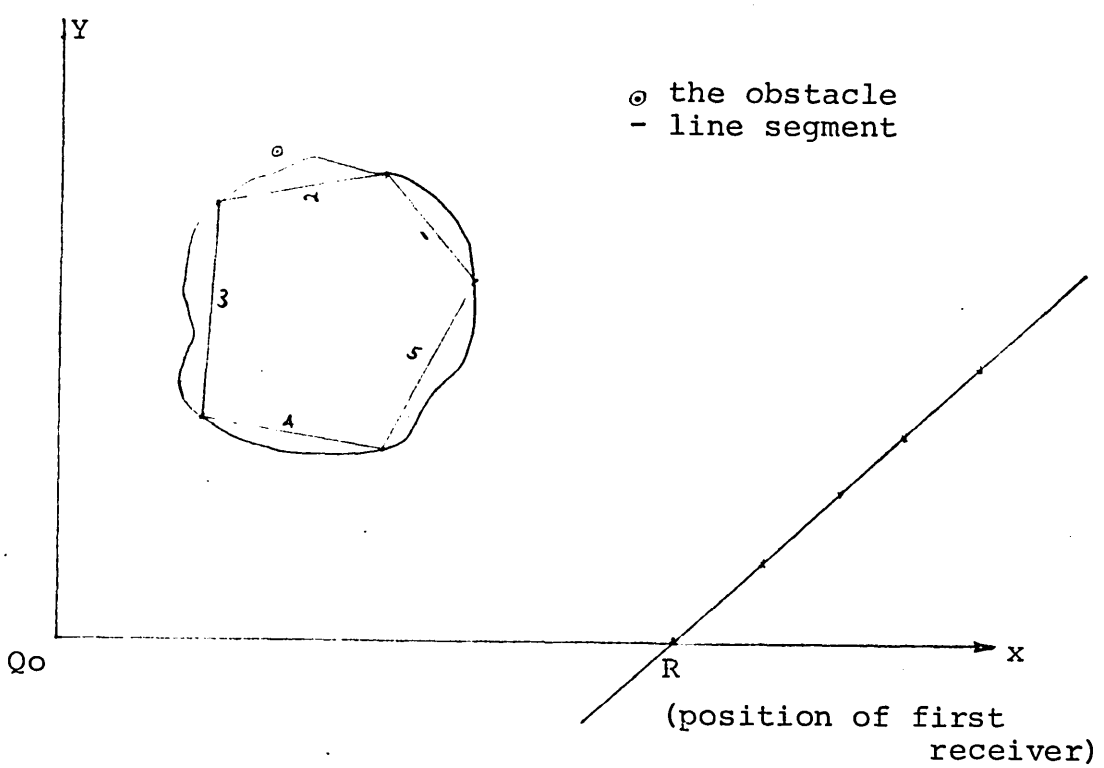


Fig. 3.14 Representation of obstacle

Evaluation of Weight Function

The first thing to do in evaluating the weight function is to convert the obstacle co-ordinates to polar co-ordinates (ρ,θ) with origins at O (see fig. (3.12A)). The weight function is then obtained by evaluating the integral equation (3.31) along a curve of constant T (Figs. (3.10A)). It is a good idea to locate the intersection of the constant T curve with the given set of obstacles first. This can be achieved by a search through the value of T for the co-ordinates of points of a given obstacle in pairs and testing whether T lies between any particular pair of points. The actual points of intersection are then obtained by linear interpolation. The interpolated values are finally re-ordered so as to facilitate the integration. so that while the obstacle integration is say from $I_4 \rightarrow I_1$ and then from $I_2 \rightarrow I_3$, the intersection order is I_1, I_2, I_3, I_4 (Fig.(3.15). The weight function is evaluated as summation using (3.31) and (3.32) while Simpsons rule is used for this numerical process.

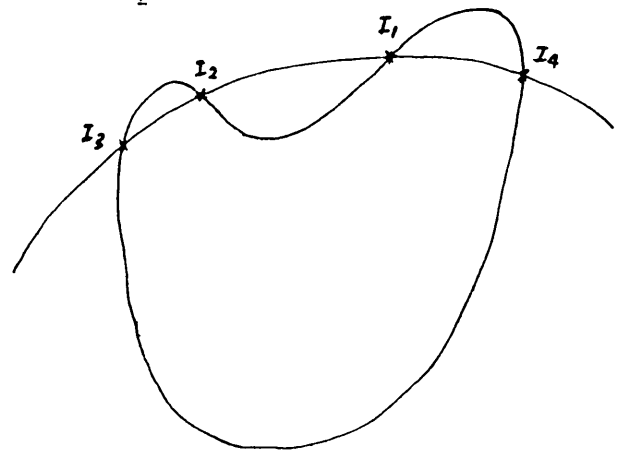


Fig. 3.15 Model of obstacle integration

Final Output

The final output is obtained through a convolution of the weight function with the derivative of the input source function, equation (3.30). The output results may then be displayed as desired. Figures (3.16) - (3.19), show a selection of results of the discussed computational process. The three portions of each figure are;

(1) The specified model showing the relative shot point and true reflection point positions.

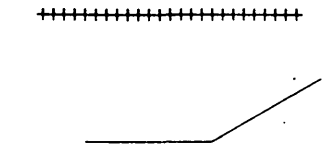
(2) A plot of the weight function $W_2(T)$ for each of the receiver locations.

(3) The synthetic seismic section showing reflection and diffraction events.

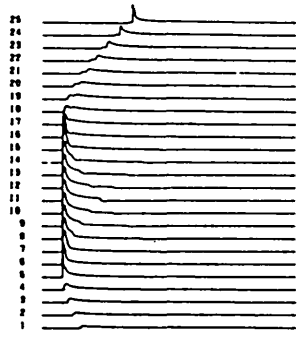
The seismic source is a single swing of a 10 millisecond sine-wave pulse.

3.4.7 Discussion of Results

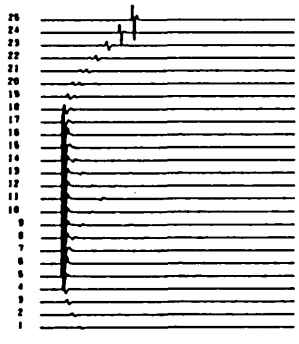
A close study of the weight function for the models reveals a number of interesting features. Figure (3.16) is a typical problem of diffraction by single straight edges (which might correspond to a fault model). Traces (1$\longrightarrow$4) correspond to receivers in the shadow and edge of the reflector so that the only contribution is pure diffraction, where as traces (5-17) are made up of both reflection and diffraction events. In the first 4 traces, diffractions are identified by positive discontinuity in



(a) Field configuration



(b) Weight Functions



(c) Seismic section

Fig. 3.16 Diffractions - reflections from straight-edges (case of fault model).

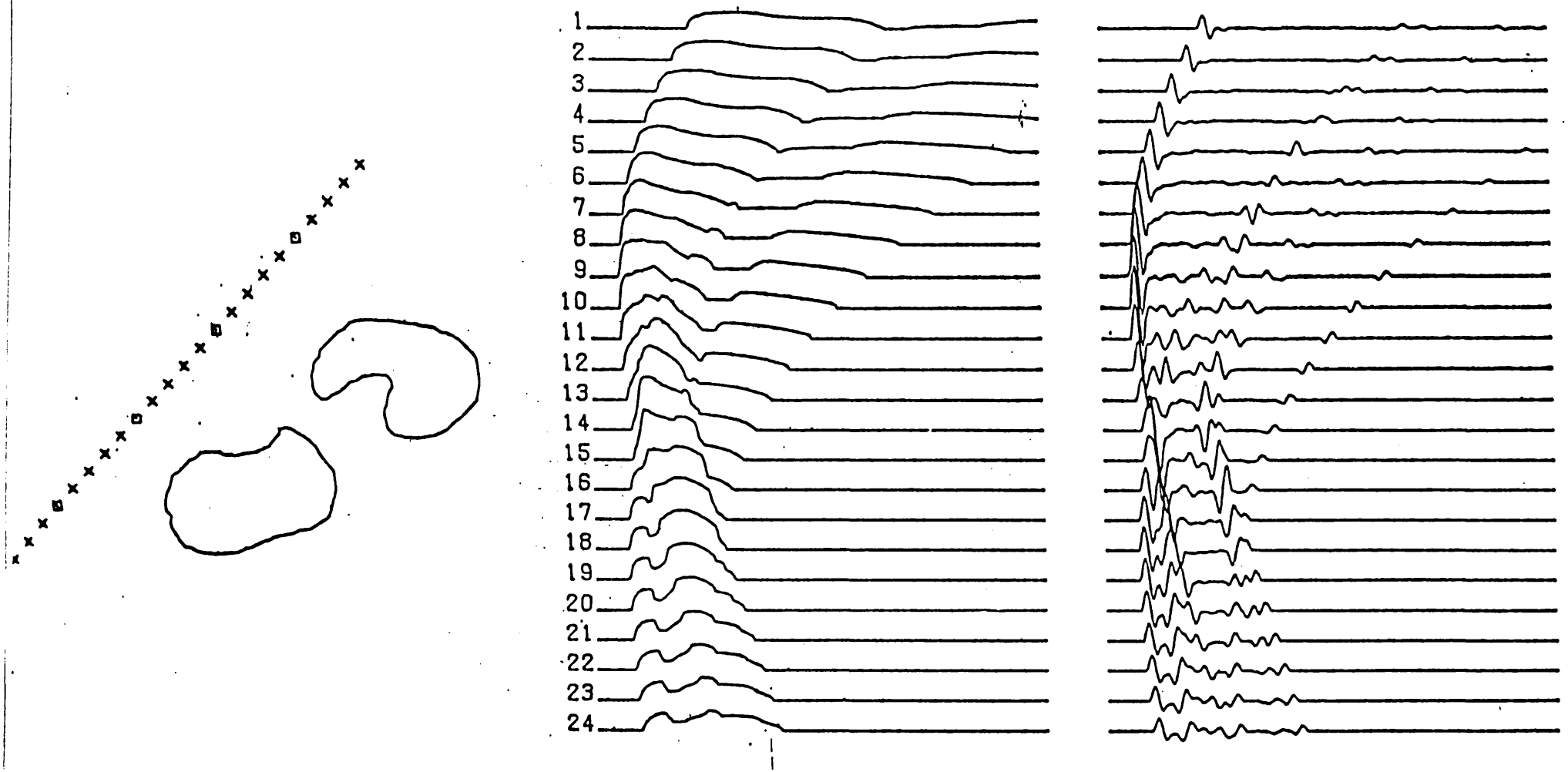


Fig. 3.17 Buried Reef structures (Buchen et al., 1980)

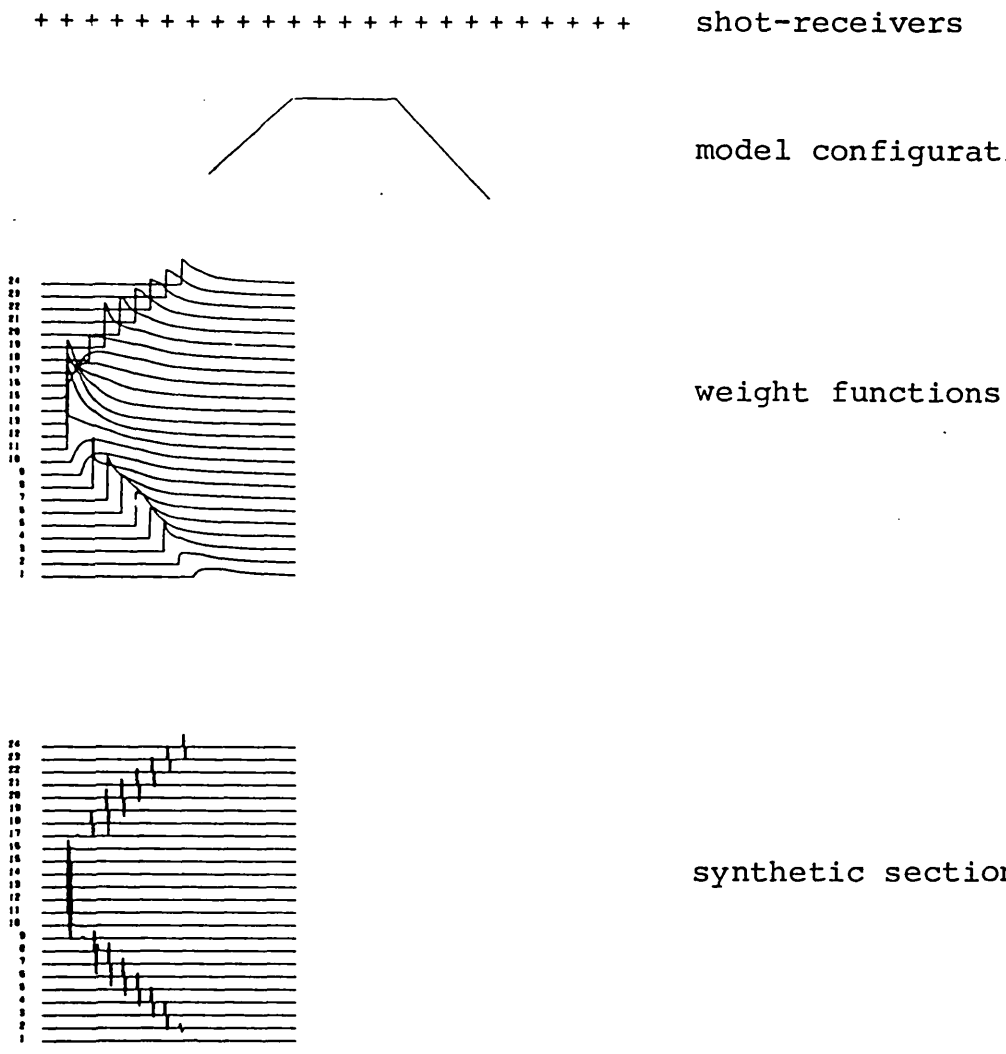


Fig. 3.18: An anticlinal model

slope of the weight function. The discontinuity occurs at the time where the $\sigma(t)$-isochron first cuts into the edge of the reflector. This positive discontinuity may be attributed to the fact that the cutting of $\sigma(t)$ across the edge is from a region of low reflectivity (which is zero for the shadow region) to a region of higher reflectivity.

In the lit region of the reflector traces (5→17), say, the weight function is first seen to suffer a finite jump at a time $t = t_o$. Corresponding to a reflection arrival.

Figure (3.17) illustrates the case of two arbitrary shaped diffractors which might correspond to a pair of buried reef structures. This model is taken from Buchen et al. (1980). The line of theoretical reflection points in figure (3.17) lies completely outside the region of the obstacles and so no reflections are generated for the model. The outcome is no more than pure complex diffraction events. We may notice here that some of the diffraction branches cross-over. For example, the first arrival branches correspond to diffraction from one of the obstacles and then to diffraction from the other obstacle with the cross-over point somewhere around trace 14. However, it is noteworthy that diffractions are generated not just when the $\sigma(t)$ cuts across the near edge of the diffracting body, and no more. It is also produced when $\sigma(t)$ cuts across intermediate and distant back edges of the diffractor.

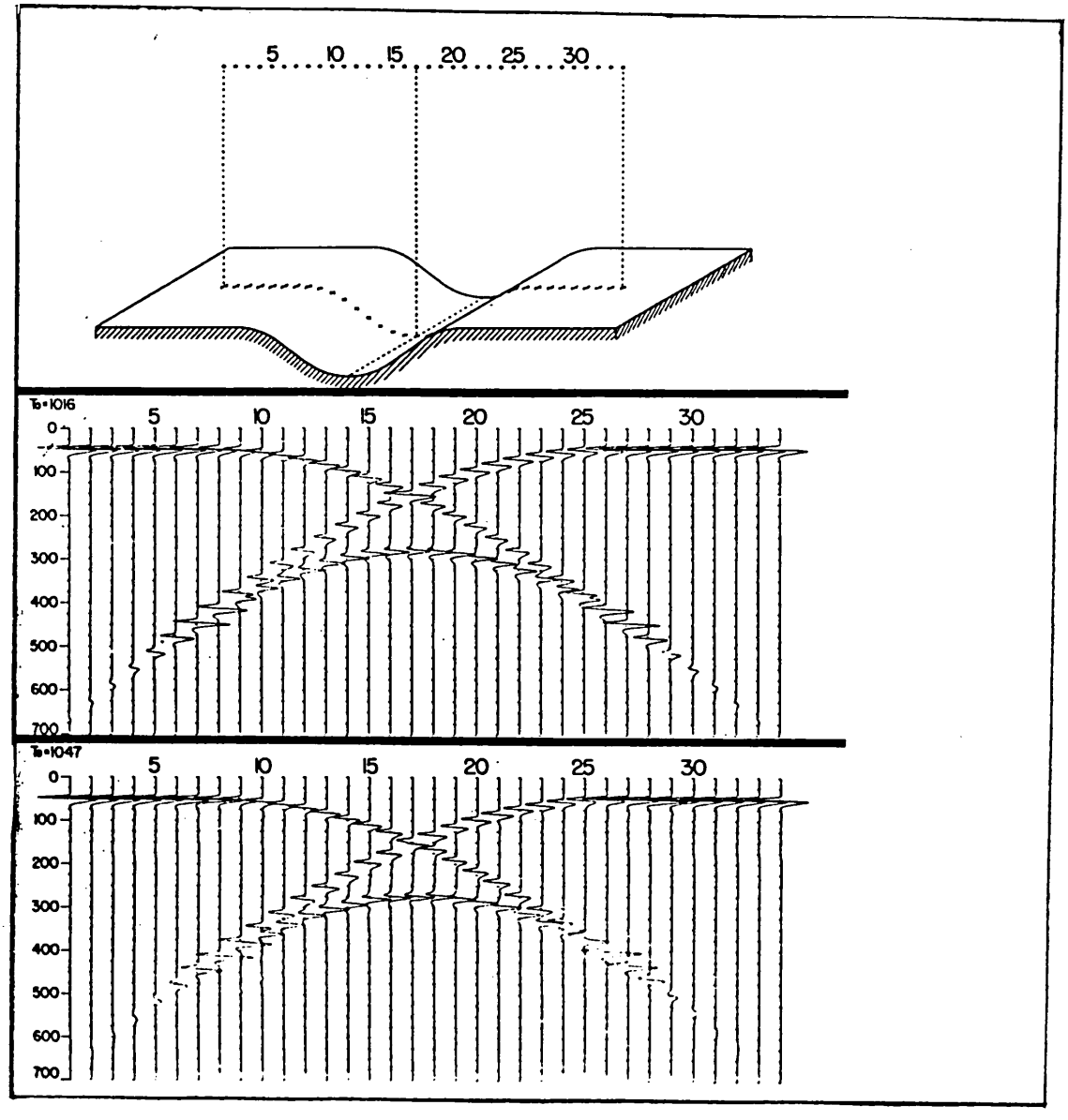


Fig. 3.19: Case of buried focus (Hilterman, 1970)

In Fig. (3.1) we show the case of an anticlinal model, approximated by three segments of a straight line. Once again, the reflection and diffraction events are obvious, and are less complex than those of fig. (3.17).

We have discussed the Kirchhoff's formulation of diffraction and reflection and show how using this approach Buchen et al. (1980) have developed some algorithms with which we generated some seismic sections containing diffraction and reflection events. The effects of these diffraction events are usually present in field sections (e.g., the bow tie effect of a buried focus - fig. 3.19b). These effects are sometimes treated as noise events, however, knowledge of diffraction patterns produced by structures (faults, anticlines and synclines, etc.) may enable us to recognise their presence within a seismic section, or perhaps migrate them.

3.50 The Synthetic Generation problems and limitations

We have presented methods of generation of synthetic seismograms, and illustrated them with some examples. Many of the problems are due to the seismic approximations and the complex nature of the earth.

3.5.1 Inaccurate Well logs and Approximations

The two main parameters obtained from well-logs for the construction of synthetic seismograms are; velocity and density. The accuracy of the velocity and density information obtained from well-logs is limited. So far

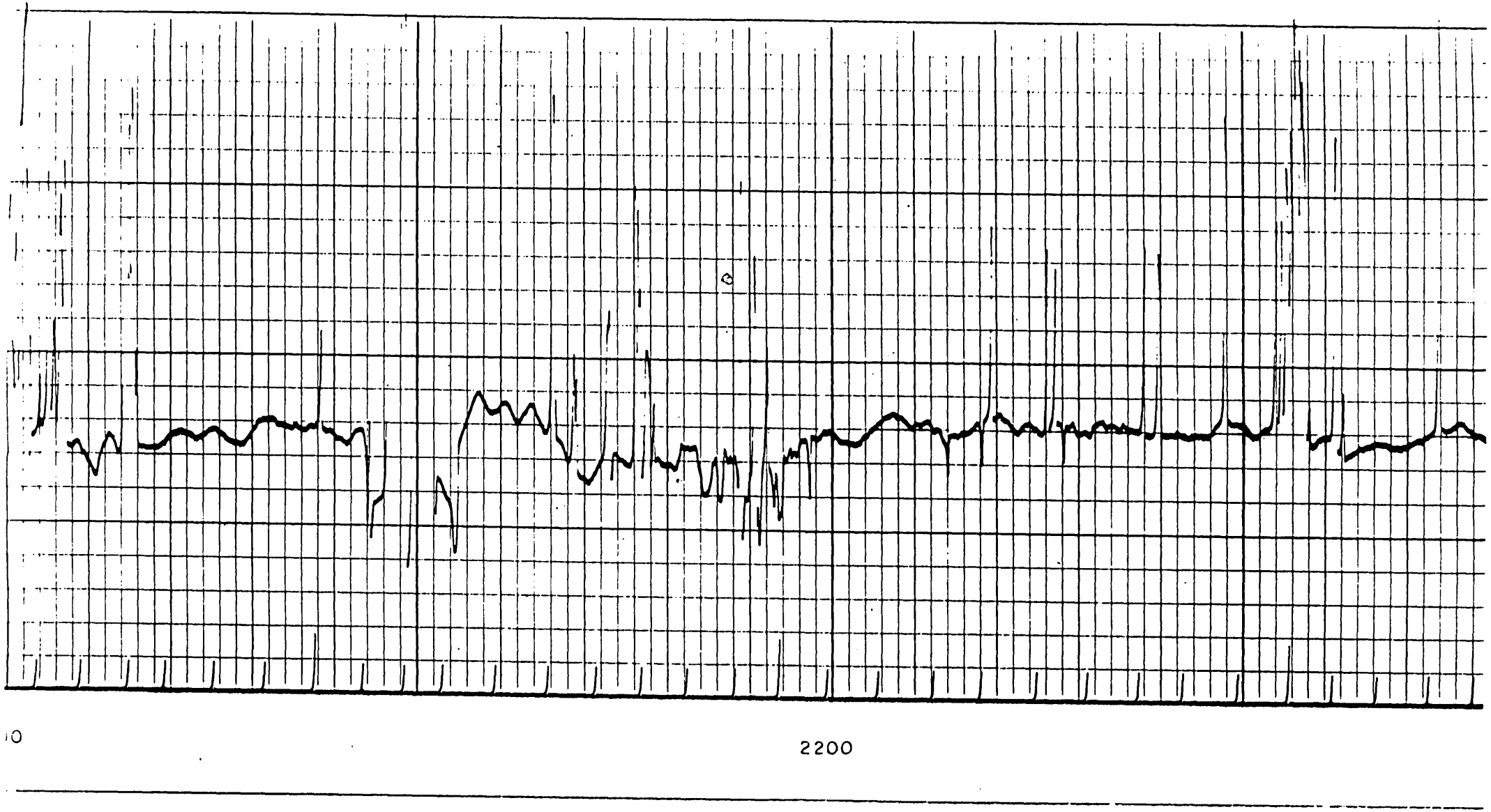


Fig. 3.20a Uncalibrated log - Mid North Sea High (Courtesy, Texaco)
From (2100 - 2250 ft, Sonic transit time).

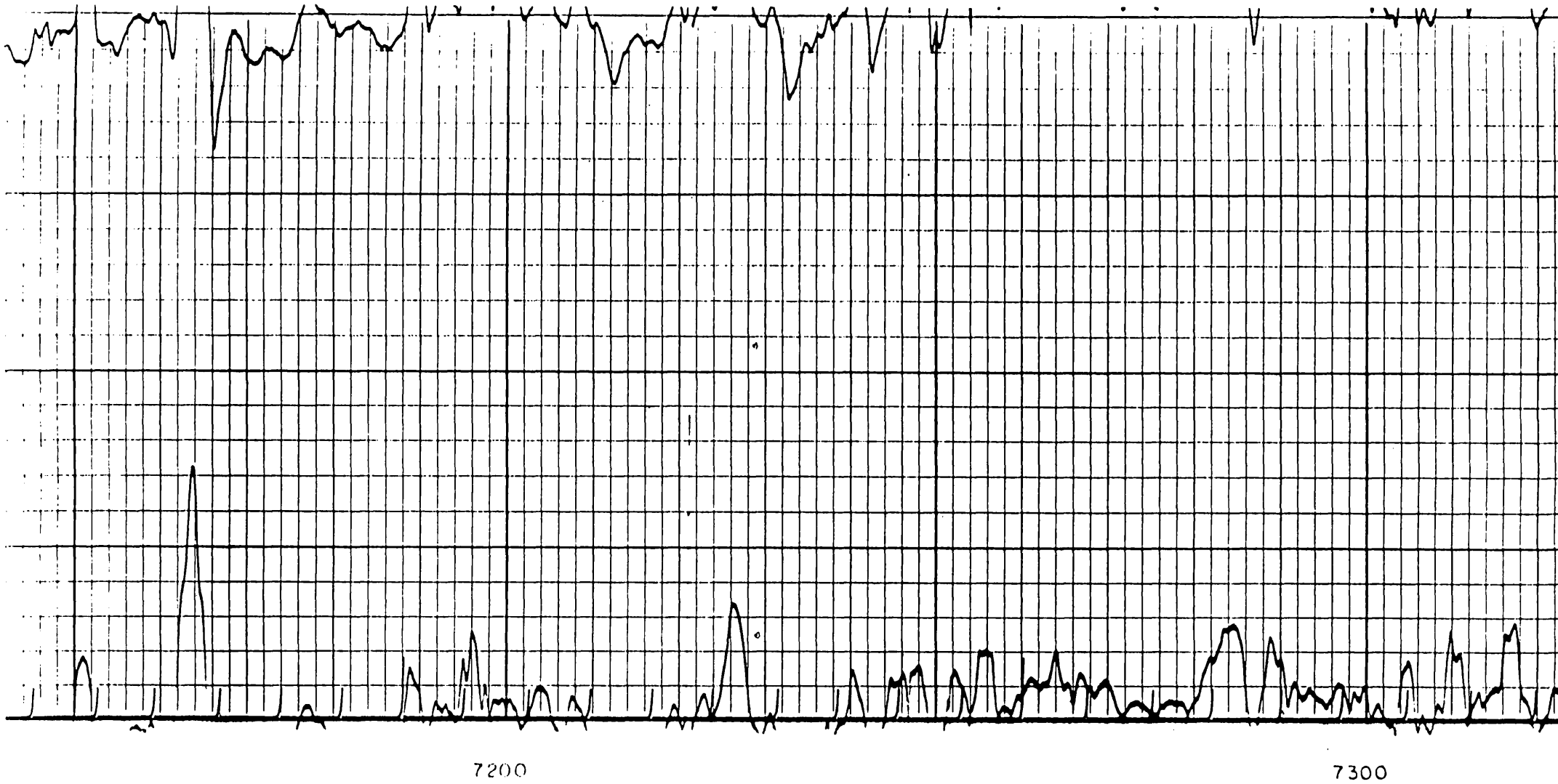


Fig. 3.20b Same log at different depth

we have assumed that our raw parameters (velocity and density from log information) are very accurate. Fig. (3.20) is an uncalibrated sonic log (mid-North Sea High). This Log (as is often the case) has a very noisy character. Opinions vary as to how best to deal with this high frequency character of most logs. Use of anti-alias filters and visual filtering have been suggested though visual filtering is often unreliable.

However, even after the log has been properly sampled over the interval logged, additional problems arise because of the lack of information in the near surface and the need to ensure that the travel times to certain depths agree with any measured times available. These measured times may come from actual check shots made at the time of the well survey. It may be based on statistically derived velocities from reflection data. An estimate must be made of the thickness and velocity applicable to the weathered layer. Then a smooth velocity-depth function is derived which:

(i) Is in agreement with the probable subweathering velocity.

(ii) Blends smoothly into the known interval velocities near the top of the logged interval.

(iii) Finally, integrate to give the correct arrival time of a wave starting from the base of the weathering and ending at a known checkpoint.

In the present work, we have followed the suggestions and methods of Wuenschel (1960), Schoenberger et al. (1979), so that the raw log information after necessary checks

and editing are digitized as finely as possible (1 ft. apart) before some integration and interpolation procedures are applied to achieve a depth-time conversion. The result after proper calibration was resampled in time as desired (in our case, 4 ms sampling was used to compare favourably with the field observations also recorded at 4 ms sampling).

3.5.2 Velocity Measurements in Boreholes

P-wave velocities and approximate S-save velocities can be measured continuously in boreholes over small intervals of a few feet. Such measurements are subject to errors when the rocks are altered by drilling fluid either chemically or by invasion of the pores. It is important to recall that a rock is not the homogeneous isotropic medium of theory but an aggregate of mineral particles which have been compressed and cemented, subjected to heat and stress cycles which are not well known. As a consequence, the rock may (and often does) show different velocities for p-waves depending on their direction of travel, and waves can be modified by non-linear stress-strain relationships or because of scattering. In most rocks, the variation of velocity with frequency is negligible in the seismic frequency range. Consequently much work has been done to measure both the P- and S-wave velocities at ultrasonic frequencies, using small samples taken from cores (Wyllie et al., 1958, Banthia, 1965). These experiments have shown that the measured

velocities both P and S are highly dependent on both the external pressure P_e applied to the matrix of rock particles, and also on the internal pressure P_i of the fluid content. The effects of pore fluids on rock velocities has been well treated by Wyllie et al. (1958), Dominico (1974), Geerstma (1961).

The most common way of measuring P-wave velocities is by ultrasonic logging in a hole. With this system (see Fig. 3.22) velocities can be measured continuously as the sonde is pulled up the hole.

Velocities obtained in this manner are reasonably representative of the velocities of seismic waves through the corresponding formation except:

(i) When invasion of the porous formation by drilling fluid is great or the formation is altered by drilling fluid, and the source is at an insufficient distance from the receivers. If this occurs, the fastest time path has to be through the altered formation and the velocity acquired is in error.

(ii) When there is cycle skipping. If large or irregular hole diameter is present the effect results in unequal times through the fluid at receivers (S_1, S_2) or it causes the level of the signal to get so low such that the electronic counter is triggered by later larger arrivals instead of the weak first arrival. In some places, the problem of cycle shipping has been solved by employing stronger sources but when the formation velocity is near that of the borehole fluid nothing much can be done.

(iii) When the formation velocity is lower than the P-wave velocity through the drilling fluid or when there is the occasional problem due to cave-in or wash-out zones.

Dix (1955) has dealt in detail with the problems of velocity measurement by shooting in holes. The experimental method is no way fool proof and care has to be taken when it is used to calibrate a CVL (continuous velocity log). The last two conditions of inaccurate velocities (due to rapid changes in hole diameter) or the actual rock velocity being close to that of the drilling fluid, can sometimes be discovered by the use of check-shots though this procedure again must be carried out with care. It can give rise to considerable error.

The effects of water invasion particularly in long shale sections can be very serious. Special long tools have been used so that the first arrival corresponds to a wave that has travelled for at least part of its path in unaltered shale. This has been found useful and the use of these long interval logging devices are to be preferred from strictly seismic point of view. Hick (1959) showed that the invasion effect occurred between two and six-hole diameters into the shale and that source - receiver spacings of 2.5 m upward are necessary to obtain the true shale velocity. Every precaution must be taken to ensure accuracy in our log-information including, editing and writing. In the present work, there were no Caliper Log to check for possibilities of cave-in or washed out zones. We therefore assume that the effects if present should be minimal.

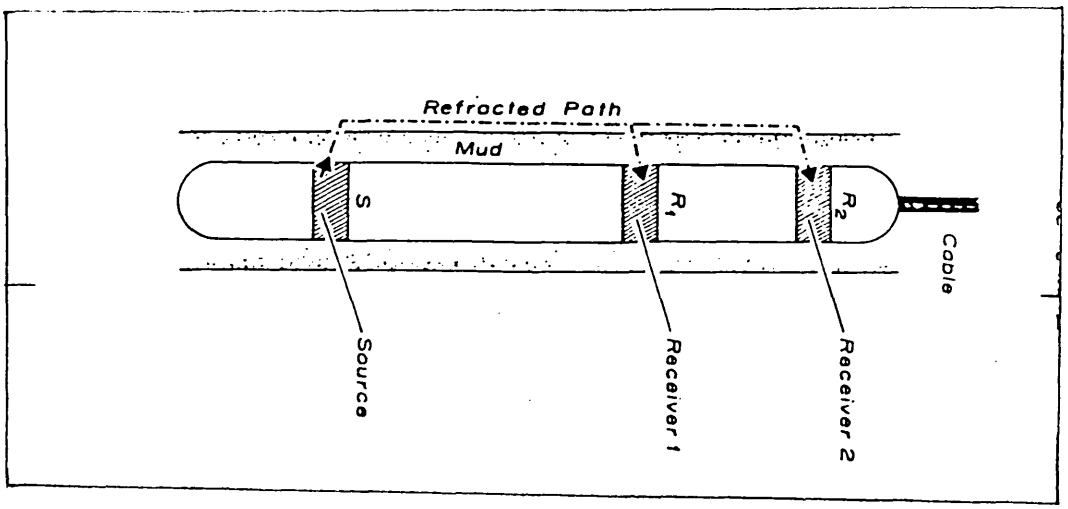


Fig. 3.22 Ultrasonic Logging Sonde

In this chapter, we have discussed with illustrations the various methods of seismogram synthesis. We have emphasised the computational methods in preference to the analogue methods. The former techniques yield synthetics that are easy and cheap to produce hence their dominance over the later techniques. There are many sources of error which reduce the quality of our results.

CHAPTER

Misties Between the Synthetic and Field Seismograms

This chapter discusses the accuracy of the match between synthetic and field seismograms, and suggests possible ways of dealing with matching problems. First, we discuss why matching seismograms and well logs is important.

4.10 Why Match Synthetic With Field Seismograms

Even if the methods of generation of synthetic seismogramswere perfect, the assumptions and parameters correct , and if all the methods of data acquisition and processings are accurate, the synthetic seismogram may still not be identical in every respect with the corresponding noise-free field observed seismogram. In the present state of the art, only a fractional part of the possible correspondence has been realizable. A detailed comparison or adequate matching of synthetic seismograms with field seismograms enables a realization of any of the following goals (how reasonable a match is may be indicated by the similarity measures treated in the next chapter).

(i) Identification of those parts of the subsurface which generated the recorded reflections or diffractions. In our analysis of Kirchhoff's formulation of diffraction, it is possible to deduce the sources of reflections and diffractions by studying the weight functions and the synthetic

sections, and tying them with the field observed seismic sections. Similarly, by plotting synthetic and field seismograms side by side, the arrival times of events can be used to estimate the true positions of the reflectors in depth. To ensure reliability, synthetic-field matching is an important tool to the seismic interpreter. He can simulate the effects of a suspected structure, and by varying the necessary parameters, approximations to the events on the field sections can be determined.

(ii) Identification of multiples on the field section. It is common practice to compute and display multiples along with primary, synthetics and field traces, for visual identification.

(iii) As an aid to deciding whether the total recording and processing system has sufficient resolving power and noise rejection capability to solve a given geological problem.

(iv) As an aid to deciding whether the data processing has been optimized, particularly with regard to deconvolution and bandpass filtering.

(v) To predict how the field trace will alter should the subsurface alter in some particular way.

(vi) Analysis of matched synthetic and field seismograms may be used to ascertain the existence of a potential reservoir for oil and gas. Delaplanche et al. (1965) studying the reflections from matched synthetic and field seismograms (obtained from Paris Basin), inferred the presence of pinchout.

Synthetic Seismogram are useful in planning a survey (especially for designing source and receiver array configurations). In conventional field surveys, one considers the following:

(a) The anticipated signal/noise ratio based on the surface conditions in the area under study.

(b) How to improve this signal/noise ratio through control of the field factors such as, source and receiver array patterns, number of geophones, the spread length, number of shotholes, use of horizontal stacking, etc.

(c) Whether the application of the necessary field techniques is economically worthwhile.

A synthetic seismogram with primaries, multiples, etc., enables one to make the proper decision concerning the above points. For example a study of the synthetic seismogram for a given area can give some idea about the surface and multiple noise levels, which could be suppressed by proper source-receiver array configuration or through stacking. Matching is improved when these error sources are known and are properly suppressed.

4.20: Causes of Misties Between Synthetic and Field Seismograms

For a number of reasons, the match between synthetic and field observed seismograms is limited in accuracy. The problems may be classified into three main headings:

(i) ACQUISITION PROBLEMS

Under this heading we include; the complex earth, the general inability to control or reproduce the exact shape of the signal fed into the ground by explosive sources, presence of a weathered layer or lossy overburden, geophone plant, bubble effects, attenuation, and multiples.

(ii) PROCESSING PROBLEMS

The processing problems discussed in chapter two are;

limited frequency bandwidth, filter effects, 'Noise', Aliasing (frequency-wave number), pulse stretching due to NMO and stack, inaccurate velocities.

(iii) WELL LOG PROBLEMS

The essential problems encountered in using well log data are; inadequacy of the measurements (due to caving, invasion, etc.), sampling problems, absence of upper layer information, wavelet estimation, etc.

4.2.1: Noise, Its Effects and Suppression

For all the many types of waveforms that arrive at the surface, and are observed on a seismogram, only a few are utilized in practical seismology. We can call these useful arrivals. The other arrivals may interfere with the useful ones damaging them and interfering with their recognition or having the complete appearance

of useful longitudinal arrivals, they may be interpreted as such, and as a result a number of errors are introduced into the interpretation. Such arrivals are undesirable, and attempts are made to suppress them throughout acquisition and processing.

However, the above division of reflected arrivals into useful and detrimental categories is somewhat arbitrary and conditional. The division actually depends upon what is to be determined, for example, the first longitudinal reflection arrival on a reflection seismogram is useful when the velocity in the first consolidated layer is to be determined but may be considered as noise when it inteferes with later events. Diffractions may or may not be regarded as noise depending on whether they can be migrated.

In this thesis we define all unwanted arrivals under the common name noise. The matching between the synthetic and field seismograms will be limited if the noise component is not properly suppressed. The ease of separation of signal from noise depends on the degree of coherence. In general seismic noise is a combination of recorded noise and processing noise. The former has very often a spectrum that overlaps that of the signal, however, the ratio of the two spectral distributions is generally not constant within the bandwidth of the data and spectral bands exist where the S/N (signal/noise) ratios are relatively high. On the other hand processing noise introduced by prematching analysis such as (deconvolution before or after stack) has a spectrum that may or may not overlap the signal

spectrum to such an extent. Although its introduction changes (whitens) the spectral density distribution of the data, the data still retains a spectrum with bands of high S/N ratio.

4.2.10 Recorded Noise

The nature and spectrum of recorded noise depends on its origin. Anstey (1972) grouped recorded noise origin into the following categories:

(1) Source-generated noise (2) Ambient noise
(3) Man-made noise (4) Power-line noise
(5) Electrical storms (6) Instrument noise

We can also include all classes of multiples and reverberations as noise.

4.2.2.1 Ambient Noise

This contributes a large proportion of the recorded noise. In marine exploration for example, the common ambient noise sources is due to the following; tow noise, shipping traffic, and marine life. Another serious source of ambient noise in the seismic passband is the condition of the sea surface. Marsh (1963) presented a theory on the origin of the Knudsen spectrum which he ascribed to the generation of sound by surface waves. Rough sea conditions, over which there is no control, can cause excessive tow noise.

When the spectrum of the noise is outside the recorded passband, it may be attenuated by frequency

filters. Narrow band noise, such as powerline interference within the seismic passband can be attenuated with notch filters in the field. Instrument noise is inherent in the recording amplifiers and is defined by the instrument characteristics.

4.2.1-2 Source Generated Noise

Source generated noise is almost always the strongest of all noise and includes all energy of source-origin scattered from local inhomogeneities in the earth such as, caves, fissures, fault zones, dykes, reefs, etc. Since its origin is the same source as that of the signal it has a spectrum that overlaps that of the latter to a considerable extent. However, within this overlap the S/N ratio is not constant and spectral bands of dominant S/N are present (Fig. 4.02), and may be utilized for signal detection.

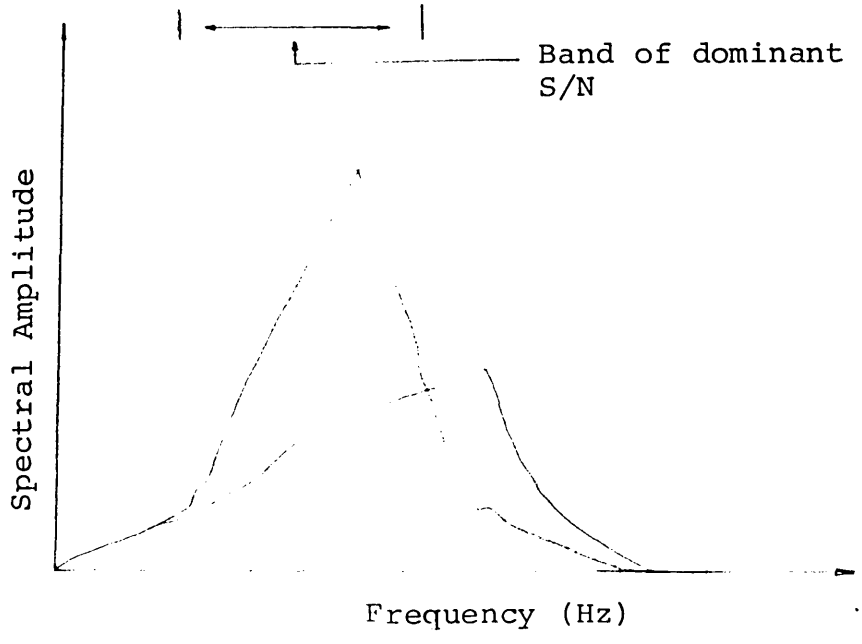


Fig. 4.02 Amplitude Spectrum showing Band of dominant (S/N)

Ideally, a seismic source should produce only compressional waves in the input signal. This may be possible at sea and in other bodies of deep water. At the sea-bottom, there is some partition of energy between compressional wave motion and other forms but this seems rarely to cause problems in practice. On land, all seismic sources and particularly surface sources generate other types of vibration. Surface waves of various kinds are very powerful often more than many times the amplitude of the reflection arrival that they mask. Shear waves are generated and as are refraction arrivals from near surface layers which often obscure the earlier reflections. All these arrivals are functionally related to the geological configuration and rock parameters of the near-surface. Because the near-surface stratification can vary so much from place to place, a great variety of surface waves is encountered. These include refracted shear waves, coupled airwaves, multiple-reflected refractions and normal mode wave-guide propagation in the low-velocity layer. In practice, these and the other arrivals are regarded as being summed with the signal which is of interest, and all the conventional methods of treatment deal with them as such.

Noise (such as surface waves, ghosts, multiples and other source-generated waves) is called coherent or systematic noise because it occurs similarly on all the CDP traces.

Surface wave noise is predominantly of low frequency and although its spectrum overlaps that of the

signal it is minimized by appropriate array - geometry and sometimes low-cut field filtering. In recent times very long source and receiver arrays have also been used to reduce the effects of waterbottom multiples (Ursin, 1978).

Two dimensional linear operators have been highly successful in detecting and extracting desired signals from a background of similar coherent noise. These operators are sometimes called 'velocity filters' (see, Embree, Burg et al., 1963). Wiggins calls the 2-dimensional operators 'w-k filters'. Velocity filters operate in the frequency and wave-number domain and therefore require a spatial array of sensing devices. It is often found that plane waves of the signal have different apparent velocities from those of coherent noise. The filter is designed to pass the signal without distortion but reject the noise. Several traces of data recorded at different locations are used in the analysis. Velocity operators based on the Wiener-Hopf optimum filter theory have been derived by Foster (1964), Schneider et al. (1965). These are generally more elaborate and are used to deghost seismic records and to reduce multiple reflections.

There are other forms of recorded noise which are purely random. These are: local disturbances around the geophones, innumerable diffractions and reflections (with their multiples) from irregularities and from velocity changes of the subsurface, which interact in an erratic and confused manner. The common depth point and stack technique are very effective for the suppression of such random noise. After proper

time corrections, signal reflections from different ray paths are summed together to form one composite trace. The stacked traces all have different sources and receivers as well as different paths through the upper formations. On stacking therefore, the random events increase as $\sqrt{N}$ (N is the total number of traces). The reflection amplitude common to all the traces at the same time would add up linearly as the number of traces. Ground-roll, interface waves, reverberations, ghosts, and other various multiple reflections are not generally brought into coincidence during NMO and stack, and this forms a basis for separating the signals from such a background noise (see Robinson, 1968, Foster et al. (1964), Burg et al. (1963)).

Sometimes, in the case of random noise, the shape, the time of occurence on any one trace and the pattern of arrival times are all unpredictable. If we define a seismic trace to consist of the time reflection signal and additive noise, we can represent the frequency domain equivalence of this trace as:

$$T_1(f) = S_1(f) + N_1(f)$$

where T_1, S_1 and N_1 represent the trace, signal and noise respectively. Following the method of Foster et al. (1967) we can deduce that an event on a trace is either noise or probably related to geology. This evidence can be obtained by computing the coefficient of coherence (also treated in next chapter) and signal/noise ratio using the given seismic data. The coefficient of coherence (Foster et al., 1967) is given by:

$$\gamma_{xy}(f) = \frac{\left| F_{xy}(f) \right|}{\sqrt{F_{xx}(f)\, F_{yy}(f)}}$$

Where $x(t)$ and $y(t)$ are time series with power $F_{xx}(f)$, $F_{yy}(t)$ and cross-power $F_{xy}(f)$. The coefficient of coherence is then related to the signal/noise ratio. Thus:

$$\frac{S_1(f)}{N_1(f)} = \frac{\gamma_{xy}(f)}{1 - \gamma_{xy}(t)}$$

It follows that if the coherence is estimated, the average noise power can be estimated in terms of the average signal. This provides a condition which may be applied to predict the quality of a seismic event. The computational approach has been treated in the above reference and chapter five of this thesis.

4.2.2 PROCESSING NOISE

A standard procedure in data processing is to deconvolve the data before stacking or velocity analysis. The natural filtering effect of the earth together with the limitations imposed by the recording instruments give seismic data a band limited spectrum. In the time domain, this means that the natural processes broaden and delay the primary seismic pulse, i.e. add a tail to it. Natural and man-made phenomena, add more noise. Processing, therefore, aims to shorten the pulse, to reduce the noise in relation to the signal thereby

enhancing seismic resolution. Methods for pulse compression are well established and they are described in the literature under the general heading of deconvolution. They are fairly effective but the model used is a gross simplification of the complex earth, and the process is further degraded by the noise in the traces which leads to noisy estimates of the tail or some function of it.

The reduced effect of most deconvolution operation lies in the weakness of some of the concepts and assumptions. Predictive deconvolution for example, assumes the following conditions;

(i) Stationarity

(ii) Minimum-delay

(iii) Random Reflectivity Sequence (white series)

Treatment based on these assmputions has an impressive mathematical solution (see Robinson, 1969). The treatment leads to a situation in which the input is a pulse with a tail and the output is a pulse without one. In real practical situations the above assumptions are not always completely satisfied, but predictive deconvolution has found wide application in the industry because the method is robust (its practical uses offset the errors).

The first weakness of the concept is that the input pulse is of constant shape. The changing geometry of multiple reflections with time and offset, and the effect of absorption ensures that the reflection pulse varies with time. In regions of complex folding and faulting, the multiple relationships are so complicated that the real reflection pulse on any one trace may be

far from constant.

A second weakness arises in assessment of the input pulse. The assumption often made is that the auto-correlation of the seismic trace is the same as the auto-correlation of seismic pulse and its tail. Even if the tail were constant, this would not be valid. The geological sequence (expressed by change in acoustic impedance), and noise, both contribute to the auto-correlation, and this must corrupt the assessment of the tail. Usually, the shorter the prediction-lag used in deconvolution the more noise from regions of the spectrum having poor S/N ratio is emphasised (see Douze, 1971, Robinson, 1969). This is not a complete disadvantage because the noise added by deconvolution, for example, is random (incoherent) noise, while the one it removes is aligned (coherent) noise which is more detrimental. The extra noise obscures the remaining low amplitude alignments, reflections are therefore given a more uniform character across the section and so improving their continuity. One way we can reduce the error due to deconvolution operation is to filter the output of the prediction error filter with a low-pass filter. The second method Robinson, (1966) is to use prediction error filters with prediction distances greater than unity.

The general effect of noise is to reduce the fidelity with which the true primary seismic pulse may be recovered or extracted from the recorded field seismograms, the attainment of high resolution is therefore limited. When the S/N ratio is very low, the

desire for high resolution must be abandoned. The synthetic seismogram can only compare well with the field observation if the S/N ratio is high.

4.2.3 ANISOTROPY

Seismologists have long recognized that seismic waves propagated by sedimentary rocks do not always behave as if the medium were isotropic. This property of velocity anisotropy often referred simply as anisotropy is characterized by variations of velocity with direction of propagation. A detailed analysis of anisotropy was published by Dunoyer de Segonzac et al. (1960). They presented a method of determining A (anisotropy factor - 'ratio of horizontal to vertical velocity') as a function of depth by using a velocity log together with first arrival times recorded at several geophone levels from shotpoints varying in distance from the well head. After surveying some wells in the North of Sahara, they came to a conclusion that anisotropy is primarily a function of lithology (table 3, below).

Lithology	Anisotropy Factor (A)
Sandstone, Sand	1.00
Salt	1.00 - 1.05
Limestone	1.08 - 1.12
Anhydrite	1.15 - 1.20

Table 3: Anisotropy as function of Lithology (Sahara wells, only - Dunoyer (1960)

In their analysis, the velocity log was segmented into layers of constant velocity, then theoretical travel time curves were computed with several values of A in the first layer, followed by the next layer and so on. The value of A giving the best fit was selected each time. They derived a 'generalised Snell's Law' for elliptically anisotropic media to compute their travel time curves. This is given by the relation:

$$\text{Sin } \gamma_k / V_k \, A_k = \text{Sin } \gamma n / Vn \, An$$

Where V_n and A_n are the velocities and A factors for the layers.

VanderSTOEP (1966) followed a different approach to compute the A factor as a function of depth. He also used well information. His analyses were carried out in wells in Mexico and Texas. The method assumed an n-layered system, with the base of layer i at a distance, Z_i, where the vertical velocity and anisotropy factor of i^{th} layer are Vi, Ai respectively. The X-Z plane is then transformed to an equivalent isotropic plane by stretching the thickness of each layer by its respective A factor. This follows from the fact that any problem involving elliptic anisotropy can be handled by reduction to an equivalent isotropic case simply by changing scale in the Z-direction by the factor A, which stretches or squeezes elliptically shaped wave-fronts into circular arcs, so that rays and wavefronts which are not orthogonal in the anisotropic medium become orthogonal by this transformation. Using this

technique, Vander Stoep (1966) derived and computed the numerical values of A factor in the named areas. In Lea county (New Mexico) the value of A factor range from (1.00 - 1.077), and in Waller County (Texas), the range was (1.05 - 1.025).

4.2.3-1 Anisotropy And Velocity Measurements

Velocity measurements are limited in accuracy due to a lack of knowledge of the true path of the energy travelling from the source to the receiver. This problem may be traced to velocity anisotropy. Fig. (4.03) is the result from a case study (after Waters, 1979). A series of plane-parallel layers (sands and shales or evaporite sequence) of alternating velocities is presented. The ray paths suffer refractions at the boundaries. As the offset is increased, the ratio of the paths in the higher velocity material changes. The composite material, therefore acts as though it were a single material having anisotropy. The average velocity for a composite ray at an angle to the vertical is higher than the velocity vertically through the layered system. In the given illustration, the shale velocity is higher than that of the sand, thus causing the shale paths to take a shorter time, the higher the angle of incidence.

Wave propagation in an anisotropic medium has been

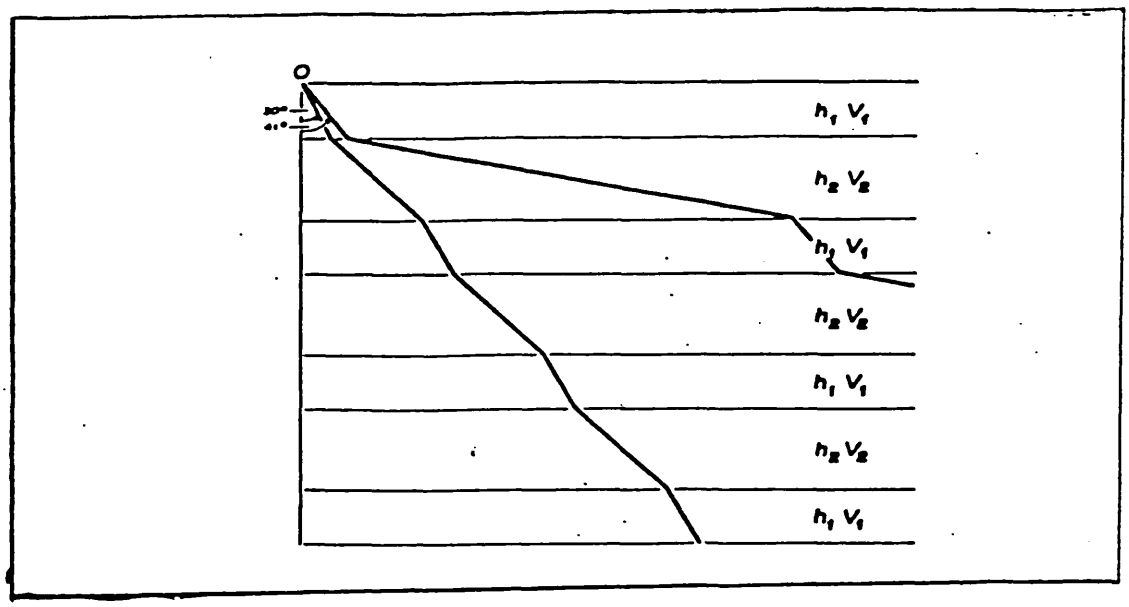


Fig. 4.03: Ray paths in Layered medium, showing the pseudo-anisotropy caused by p-wave velocities in the layers. The example is for $h_1/h_2 = {}^2/_3$, V_1 = 8000 ft/sec, and V_2 = 12,000 ft/sec. Average vertical velocity is 10,000 ft/sec; average velocity at 30^o incidence is 10,267.9 ft/sec; at 41^o is 11,235 ft/sec. (Waters, 1979).

the subject of several experimental and theoretical papers (Uhrig et al., (1955), Stoep, (1966), Daley, (1979), Berryman (1979)). One way to relate the time for a undirectional inclined path to the vertical average velocity, the anisotropic ratio, depth, and the offset distance is defined (see, Cressman, 1968).

$$T^2 = \frac{X^2}{A^2V^2} + \frac{Z^2}{V^2} \qquad (4.02)$$

For reflections from a constant depth reflector, we have

$$T_R^2 + \frac{X_R^2}{A^2V^2} + \frac{4Z^2}{V^2} \qquad (4.03)$$

where T_R (is the reflection time at offset X_R) A plot of T_R^2/X_R^2 will have a slope of $1/A^2V^2$, so that the

anisotropic ratio is not separated from the vertical velocity. This confirms to Postma's (1955) observation that the anisotropic ratio can never be determined from surface work alone, a knowledge of the actual depth of the reflector is also necessary. Knowledge of the depth can be obtained only by drilling a well which also determines the rock type, it then follows that anisotropy cannot be good rock type indicator.

4.2.3.2 Checkshot and Well Log - Velocities

Another error in seismic data analysis which may be attributed to velocity anisotropy is the lack of correspondence between the velocity measured in boreholes by the conventional check shot technique and that determined by logging. The two time determinations will not agree and discrepancies up to some tens of milliseconds for deep wells have been observed. Gretener (1961) measured the velocities in several wells using the two mentioned techniques to study the discrepancies. He explained the effect of anisotropy in the shallow layers using a conventional well velocity survey and a form of fig. (4.04).

For the very shallow check-shot positions the angle γ is large and the ray travels at a velocity V_p which is about $(V_h + V_z)/2$ while for the deep levels the angle γ becomes small and the ray travels through the same shallow layer at a velocity very close to V_z. As a result an error is introduced when correcting the shallow check shot times to vertical times by a simple

multiplication with $\cos\gamma$. The times for the shallow check shot positions will be short if no allowance is made for anisotropy, while the times for the deep check shot positions will be correct.

In practice when the velocity from the checkshot survey and logging are interpreted the logged data are adjusted to the conventional checkshots (during calibration). The usual argument for this adjustment is that the checkshot survey approximates more closely to the conditions encountered in conventional seismic shooting.

4.2.3.3 Anisotropy and NMO

Usually Normal Moveout (NMO) may be used to distinguish primary from multiple reflections when the average velocity changes with depth. In practice the approximate values of normal moveout may be found using an average velocity formula and such values are often large.

The effect of anisotropy to NMO has been investigated by Cressman (1968) From the NMO Equation

$$V^2 t_y^2 = V^2 t_o^2 + X^2$$

and

$$\begin{aligned} \Delta t &= t_y - t_o \\ &= X^2/(V^2(2t_y - \Delta t)) \\ &= X^2/(V^2(2t_o + \Delta t)) \end{aligned}$$

where t_o (vertical time), V (average vertical velocity), X (offset distance), and t_y (slant time),

Cressman, obtained the NMO equation in terms of A factor, for an oblique path, which is equation (4.02). He further went to deduce the Dix's factor for small offset - A_o (the quasi anisotropy) so that he defines the square of A_o in terms of V and σ,

$$A_o^2 = 1 + (\sigma/V)^2 \qquad (4.04)$$

and

$$ty^2 = t_o^2 + X_o^2/(A_o^2 V^2)$$

$$\Delta t_o = X^2/(Ao^2 V^2 (2t_o + \Delta t))$$

where σ is the standard deviation.

Equation (4.04) suggests that apparent anisotropy factor is most sensitive to changes in velocity contrast when the average velocity is low. Thus the introduction of say, a limestone bed into a low velocity section reduces the NMO not only by increasing the average vertical velocity but also by increasing the apparent anisotropy factor. It follows that all changes of NMO may not be attributed to changes in vertical velocity alone, anisotropy may be contributing.

Recent studies involving the inclusion of anisotropy in seismic studies is becoming common. Daley et al. (1979) derived expressions for the computation of reflection and transmission coefficients for seismic waves in ellipsoidally anisotropic media. Such an approach to elastic wave propagation may be advantageous in generating synthetic seismograms in anisotropic media which probably will yield a better approximation for the complex earth.

4.2.4: Seismic Approximations and Assumptions

The common assumptions and approximations which contribute to reduced accuracy in seismic data analysis are:

(1) The theoretical Earth Model - this models the complex Earth into thin parallel layers.

(ii) The assumption that each thin parallel layer of the Earth is homogeneous and isotropic within the layer.

(iii) The assumption of modeling the Earth as a fluid medium - acoustic approximation, in which only normal incidence pulses (energy) are considered.

The earth is far from being completely homogeneous and isotropic. Sedimentary rocks as we may recall do exhibit the phenomenon of anisotropy. Our results are therefore limited only to the best possible approximations.

4.2.5 Amplitude Distortion

Modern seismic recording instruments allow more accurate measurements of the amplitude of reflected signals. The amplitude on the other hand varies over a large range. A number of factors which are responsible for Amplitude variation and distortions do not contain subsurface information; they include, source strength and coupling, geophone sensitivity and plant, instrument errors, and scattering in the near-surface, etc. Methods of suppressing these effects have been dealt with already. There are other factors which do not convey information regarding lithology, such as spherical

spreading, raypath curvature, transmission loss, effect of multiple reflections.

4.2.5-1: Spherical Divergence

Geometrical divergence refers to the phenomenon of wavefronts expanding as they travel farther from the source. The source energy is spread over an ever increasing larger area. Consequently, the energy density decreases as the inverse square of the distance travelled. For a constant velocity medium, the energy density decreases inversely as the square of distance travelled, that implies, the amplitude varies inversely as the distance. If the velocity shows some variation, the raypaths curve. As velocity increases with depth the area over which the energy spreads increases faster than the square of the distance, so that the energy decay is more rapid than might be expected. Spherical divergence and hence amplitude attenuation may be expressed as functions of velocity and time. Attenuation due to spherical divergence therefore, varies as velocity for different raypaths. Compensation is always given for spherical divergence but not without limitations. When primary reflections and long-period multiples arrive together, but with different effective velocities, it is not possible to provide exact compensation for both. Proper compensation for the primaries ordinarily leaves the multiples too large. On the other hand compensation on the basis of horizontal layering ordinarily results in an excess of amplitude for reflections showing strong dip.

4.2.5.2 Absorption

Absorption is not a well understood phenomenon. Whereas divergence does not involve any loss of energy, for absorption energy is converted into heat. Opinions vary as to the mechanism by which seismic energy is converted into heat. Internal friction, anelasticity, etc. are all connected with absorption. Some geophysicists feel that absorption is approximately an exponential decay, involving the first power of the frequency or that absorption is inversely proportional to wavelength. It can often be expressed as a 'constant Q', where Q is proportional to the ratio of the peak energy periodic motion to the energy lost in one cycle. There is, however a common agreement that high frequencies are attenuated faster than low frequencies and hence absorption acts essentially as a low-pass filter. Absorption therefore contributes to pulse broadening and loss of resolution.

4.2.5.3 Multiples and Interfaces

The fractional part of the energy transmitted through an interface is smaller than one by the fraction of the reflected energy. Even good reflectors divert just a small part of the energy. Since the energy has to pass through many interfaces, the combined effect may be appreciable. More often, part of the energy diverted by reflection is reflected again as a short-period (peg-leg) multiple so that energy losses

by transmission through the interfaces and short-period multiples are intimately related. This process of removing energy from the primary and delaying it slightly adds a tail to a wavelet. The explanation that primary paths are systematically reinforced by very short-period (peg-leg) multiple paths was given and developed by Anstey (1960), Trorey (1962), Berzon (1967).

Modern procedure in synthetic generation is to display primaries only, primaries plus all order multiples, all order multiples plus source ghosts, etc. This is an attempt to ensure proper assessment. In seismogram synthesis, multiples are important. This is because if the omission of multiple reflections has even a slight effect, there is a risk that the best match may not be the right match; in this case conclusions drawn from the synthetic record may be misleading. Sometimes multiply reflected pulses will be of small amplitude and will not be noticeable on the field record, but may overlay a primary to produce a marked change in amplitude Methods of suppressing these multiples have been suggested but even after the suppression some residual multiples always remain and can be difficult to identify.

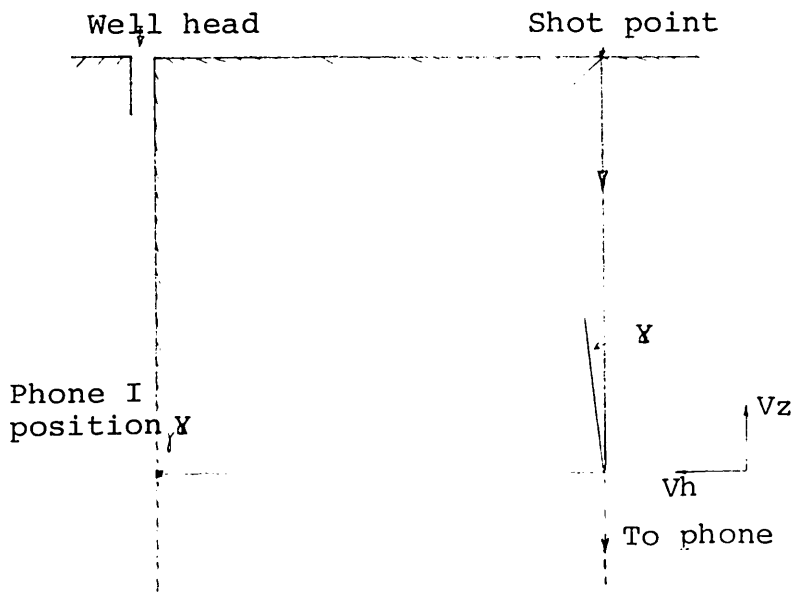


Fig. 4.04

Anisotropy in shallow layers on conventional well velocity survey

CHAPTER 5

Similarity Measures And Quantative Matching of Seismogram traces

In the remaining chapters of this thesis, our emphasis is on the methods of estimating the optimum wavelets (to assure the generation of the best possible synthetics), multiple-ghost inclusion, geometrical spreading, and attenuation (to improve the synthetics), residual analysis of the synthetic-field data components to ensure that each component contributes to the general result but without itself affected by any other data-component. Methods of matching analysis are also developed. By so doing our work goes further than that of White (1980). This is the first detailed analysis on seismogram matching - 'Partial Coherence Matching'. It did not fully address the causes of reduced match between seismograms, or the methods of removing them. Matches are often improved when the known error sources are removed or reduced from the seismograms of interest.

5.10 Similarity Measures

In this chapter, we present some possible ways one can identify the relationship between field and well-log generated synthetic seismograms.

By similarity measures, therefore, we mean those

processes by which we can quantify the relationship between two time series. There are a number of these similarity measures which we can apply to seismic time series. These include, correlation functions - correlation coefficients, coherences, and least-squares measures. Some statistics like, the X^2, F, and t statistics, which indicate statistical significance may be used as measures of similarity. The weakness, however, of the three statistics as similarity measures is that they tell us nothing about the degree of correlation between the quantities but in a quick way they can provide a test of independence between some observed and expected seismic data set. These will be discussed in later sections. We shall also observe that some of these similarity measures, such as coherence and least-squares measures, all come out as intermediate products during the wavelet estimation procedures.

5.1.1 Correlation

For the purpose of this thesis, we define correlation as a concept by which we measure the degree of parallelism between two time series. The process is auto-correlation if the two time series consist of a series f(t), and the same series displaced along the t-axis an amount T relative to itself, while the process is cross-correlation if the two series consist of two different time series f(t) with arbitrary relative time shifts, so that for each shift T there is a corresponding value

of the correlation. For two seismic traces, the process is one by which we measure the similarity in waveform shape between two traces for different relative displacements of the two traces.

Now, if $X_i(t)$ and $X_j(t)$ are two seismic traces, sampled at intervals $\Delta t = 1$ and if the second trace is displaced by an amount s relative to the first trace, then the cross correlation function $C_{ij}(s)$ for the two traces is defined thus;

$$C_{ij}(s) = \frac{1}{m-s} \sum_{t=1}^{m-s} X_i(t)\ X_j(t-s) \qquad (5.01)$$

$$(s = 0,1,2 \ldots n)$$

Where n = the maximum lag or length of correlation

m = length of each trace.

The Geophysical definitions of correlations generally correspond closest to the concepts of variance and covariance usually found in text books of statistics, hence $C_{ij}(s)$ is an estimate of the covariance function for which the traces $X_i(t)$ and $X_j(t)$ each have a zero mean value. In this work, we assume the trace mean-values are zero or at least nearly so while hereafter, the term cross correlation function replaces covariance function.

Actually, equation (5.01) is a sample function. It gives an unbiased estimate of the cross correlation function with some degree of variance. The variance, however, could be reduced if we can introduce even a small bias in the estimate. This compromise may be achieved using some window functions, such as the

Bartlett window which weights the estimates, thereby reducing the amplitude of spurious peaks at large lag. This modification reduces the above expression to the form;

$$C_{ij}(s) = \frac{1}{m} \sum_{t=1}^{m-s} Xi(t)\ X_j(t-s) \qquad (5.02)$$

The bias becomes negligible for $m \gg n$.

In this thesis, most of the traces are assumed long enough but not too long to contravene the stationarity conditions (Wadsworths, 1953). Besides, all of the comparing traces of a given record used in the present work are virtually of equal length, hence the division by 'm' in equation (5.02) is not very necessary, hence we can write

$$C_{ij}(s) = \sum_{t=1}^{m-s} Xi(t)\ X_j(t-s) \qquad (5.03)$$

Equation (5.03) is in reality the un-normalised one-sided cross-correlation function as defined by Robinson (1967a).

5.1.2 Correlation Coefficient (γ_c)

The general equation for a normalised cross correlation is written;

$$\bar{C}_{ij(s)} = \frac{\int_{-\infty}^{\infty} fi(t) f_j(t-s)\ dt}{\left[\int_{-\infty}^{\infty} \{fi(t)\}^2 dt \int_{-\infty}^{\infty} \{fj(t)\}^2 dt\right]^{\frac{1}{2}}} \qquad (5.04)$$

$$= 1 \text{ (if } s = 0)$$

Equation (5.04) agrees with the expression for correlation coefficient γ_c found in text books of mathematical statistics (where γ_c is the Pearson product moment correlation coefficient).

$$\gamma_c = \frac{\sum (x-\bar{x})\ (y-\bar{y})}{\left[\sum (x-\bar{x})^2 \sum (y-\bar{y})^2\right]^{\frac{1}{2}}}$$

$$= \frac{fi(t)\ f_j(t)}{\left[fi(t)^2\ f_j(t)^2\right]^{\frac{1}{2}}}$$

and for continuous functions,

$$\gamma_c = \frac{\int_{-\infty}^{\infty} fi(t)\ f_j(t)\ dt}{\left[\int \{fi(t)\}^2 dt \int \{(f_j(t)\}^2 dt\right]^{\frac{1}{2}}} \qquad (5.05)$$

$$\Rightarrow C_{ij}(0) = \frac{C_{ij}(0)}{\left[C_{ii}(0)\ C_{jj}(0)\right]^{\frac{1}{2}}}$$

where x, y, $\bar{x}$, $\bar{y}$ are the two time series and their means. The statistical correlation coefficient γ_c, therefore agrees with the normalised cross-correlation at zero-lag. The value of γ_c lies between zero and one,

$$\Rightarrow 0 \leq \gamma_c \leq 1$$

If $\gamma_c = 1$

then $f_i(t)$ is very similar to $f_j(t)$. That is to say, $f_i(t)$ matches $f_j(t)$ exactly, the reverse is true when

$$\gamma_c = 0$$

In practice, however, the value of γ_c lies between the two extremes.

Apart from computing correlation coefficients,

auto and cross correlations contain information about periodicity of the function. They also constitute the first step in the calculation of power, cross power and coherences. Coherences in themselves are similarity measures. In the frequency domain coherence measures the degree of closeness between sets of frequency dependent observations. Before we discuss coherence as a similarity measure, we must not however forget the old time method of measuring similarities - the well known visual correlation. Though we cannot quantify this relationship, the method compares two time series time-point after time-point to observe how close the wave peaks and troughs of one series coincide with those of the second series. This is not a very objective way of measuring relationships, because in most instances judgement depends on how the eye and the brain see and interpret the waveform.

5.1.3 Coefficient of Coherence

Following the method of Foster et al. (1967), Hinich et al. (1968) we define coherence in terms of power and cross power spectra, for two different frequency transformed time series as shown;

$$\gamma_{12}(w) = \frac{\left|F_{12}(w)\right|}{\left[F_{11}(w)\, F_{22}(w)\right]^{\frac{1}{2}}}$$

$$= \left[\frac{\tilde{C}^2_{12}(w) + \tilde{Q}^2_{12}(w)}{C'_{11}(w)\ C'_{22}(w)} \right]^{\frac{1}{2}} \qquad (5.06)$$

where

F_{11}, F_{22}, F_{12}, are the auto and cross-spectra of the two time series $f_1(t)$ and $f_2(t)$. $\tilde{C}_{12}(w)$ is the cospectrum - the real component of the cross power and $\tilde{Q}_{12}(w)$ is the quadrature or imaginary component of the complex cross power for the two series.

As we present the multiple input linear systems in the future section, we shall observe that for a Fourier decomposition of two or more time series, other forms of spectral coherences exist as modifications of expression (5.06). In this section we shall give the general definitions of these coherence functions and leave their applications for future sections. If for example, we consider a - time invariant system of inputs $f_i(t)$, i = 1, 2, 3 ..., m, and output g(t) such that

$$g(t) = \sum_{i=1}^{m} gi(t)$$

where gi(t) is that part of the output obtained from the i^{th} input $f_i(t)$ when $f_j(t) = 0$

$$j = 1, 2, 3, \ldots, m \ (j \neq i)$$

then the classical coherence of Wiener (1930) measures the correlation between any pair of inputs $f_i(t)$, $f_j(t)$ of the system as a function of frequency and is defined as

$$\gamma_{i,j}(w) = \frac{\left|F_{ij}(w)\right|}{\sqrt{F_{i,i}(w)\ F_{jj}(w)}} \qquad (5.07)$$

$F_{i,i}(w)$, $F_{jj}(w)$ and $F_{i,j}(w)$ are as previously defined. Similar relations exist between the output $g(t)$ and each of the inputs, $f_i(t)$. Equation (5.07) is identical to (5.06) if we set i = 1 and j = 2. From the two expressions, it follows that:

$\gamma_{i,j}(w)$ has non-zero values for $F_{i,i}(w)F_{jj}(w) > 0$ but for $F_{ii}(w)\ F_{jj}(w) = 0$, then $\gamma_{ij}(w) = 0$

i.e. $\gamma(w)$ exists in the interval $0 \leq \gamma(w) \leq 1$. and being a stationary normalised coefficient it is insensitive to variations in the amplitudes of $f_i(t)$ or $g(t)$. The coefficient of coherence apart from its normalising denominator, is infact the spectrum of the cross-correlation. Thus if the cross-correlation $C_{12}(T)$ - in the time domain exhibits large values at certain regularly spaced time shifts, T, this will correspond to a maximum of the coherence $\gamma_{12}(w)$ at the corresponding frequencies.

Sometimes, $F_{i,j}(w)$ replaces the absolute value $\left|F_{i,j}(w)\right|$ in (5.06) and (5.07), i.e. $F_{i,j}(w)$ appears with its real and imaginary parts and has often been referred to as cross-correlation spectrum (Davenport, 1961, Rudnick, 1969). Robinson (1967) called it the coefficient of coherence or just coherency. Often, Coherence is defined as the square of the quantity in (5.06), (5.07) or their equivalent. This is the form of expression for coherence as used in this thesis. Theoretically, the coherence function as we have described it would be equal

to unity, and independent of frequency. This is not so in practical applications, mainly due to windowing or smoothing effects (Bendat and Piersol, 1971), and probably due to errors inherent in the data sets.

5.1.4 Coefficient of Multiple Coherence

This measures the degree of correlation between one input $f_i(t)$ and the rest of the inputs $f_j(t)$ $j = 1, 2, 3 \ldots, m$, $j = i$ as a function of frequency. For such a multiple input-system we quantify the coefficient of multiple coherence thus,

$$\gamma_{i,j}(w) = \sqrt{1 - (F_{i,i}(w)\ F^{ii}_{(w)})^{-1}} \qquad (5.08)$$

where $F^{ii}_{(w)}$ denotes the i^{th} diagnonal element of the inverse matrix $(F_{ii}(w))^{-1}$, and $F_{ii}{}^{(w)}$ is the (m x m) matrix of the power and cross-power spectra of all the inputs $f_i(t)$ defined as;

$$\begin{bmatrix} F_{11}(w) & F_{12}(w) & \ldots & F_{1m}(w) \\ F_{21}(w) & F_{22}(w) & \ldots & F_{2m}(w) \\ F_{31}(w) & F_{32}(w) & \ldots & F_{3m}(w) \\ \vdots & & & \\ F_{m1}(w) & F_{m2}(w) & \ldots & F_{mm}(w) \end{bmatrix} = Fi,i(w)$$

A similar function exists between the output $g(t)$ and all the inputs $f_i(t)$, hence we have;

$$\gamma_{i,g}(w) = \sqrt{1 - (F_{gg}(w)\ F^{gg}_{(w)})^{-1}}$$

where $0 \leq \gamma_{ig}(w) \leq 1$

$F_{gg}(w)$ is the power spectrum for the output and $F^{gg}_{(w)}$ denotes the first diagonal element of the inverse matrix $(F_{i,g}(w))^{-1}$.

$F_{i,g}(w)$ is the (m x m) matrix of the power and cross-power of the output g(t) and input $f_i(t)$ combinations defined below,

$$\begin{bmatrix} F_{gg}(w) & F_{g1}(w) & \cdots & F_{gm}(w) \\ F_{1g}(w) & F_{11}(w) & \cdots & F_{1m}(w) \\ F_{2g}(w) & F_{21}(w) & \cdots & F_{2m}(w) \\ \vdots & & & \\ F_{mg}(w) & F_{m1}(w) & \cdots & F_{mm}(w) \end{bmatrix} = F_{ig}(w)$$

5.1.5 Coefficient of Partial Coherence

The coefficient of partial coherence measures the correlation between one input $f_i(t)$ and the output g(t), conditioned to the remaining (m-1) inputs as a function of frequency and is defined thus;

$$\gamma^{p}_{i,g}(w) = \frac{\left|F_{i,g}(w)\right|}{\left[F^{p}_{i,i}(w)\ F^{p}_{g,g}(w)\right]^{\frac{1}{2}}} \qquad (5.09)$$

where as in (5.06), (5.07) $\gamma^{p}_{i,g}(w)$ lies in the range $0 \leq \gamma^{p}_{i,g}(w) \leq 1$

but the suffix P denotes partial spectrum, which is the spectrum calculated from residual $f_i(t)$ and g(t) after the effects of the remaining components have been

removed from them. In this thesis we shall be more concerned with this last form of coherence function, especially as it helps us to estimate the optimum wavelet necessary for synthetic generations.

5.20 Multiple Input Linear Systems: Applications to similarity measurement, wavelet estimation and synthetic seismogram generation

As a convenient starting point let us consider a model of a linear system responding to multiple inputs. For simplicity we assume that n inputs exist, while a single output is measured - Figure (5.01).

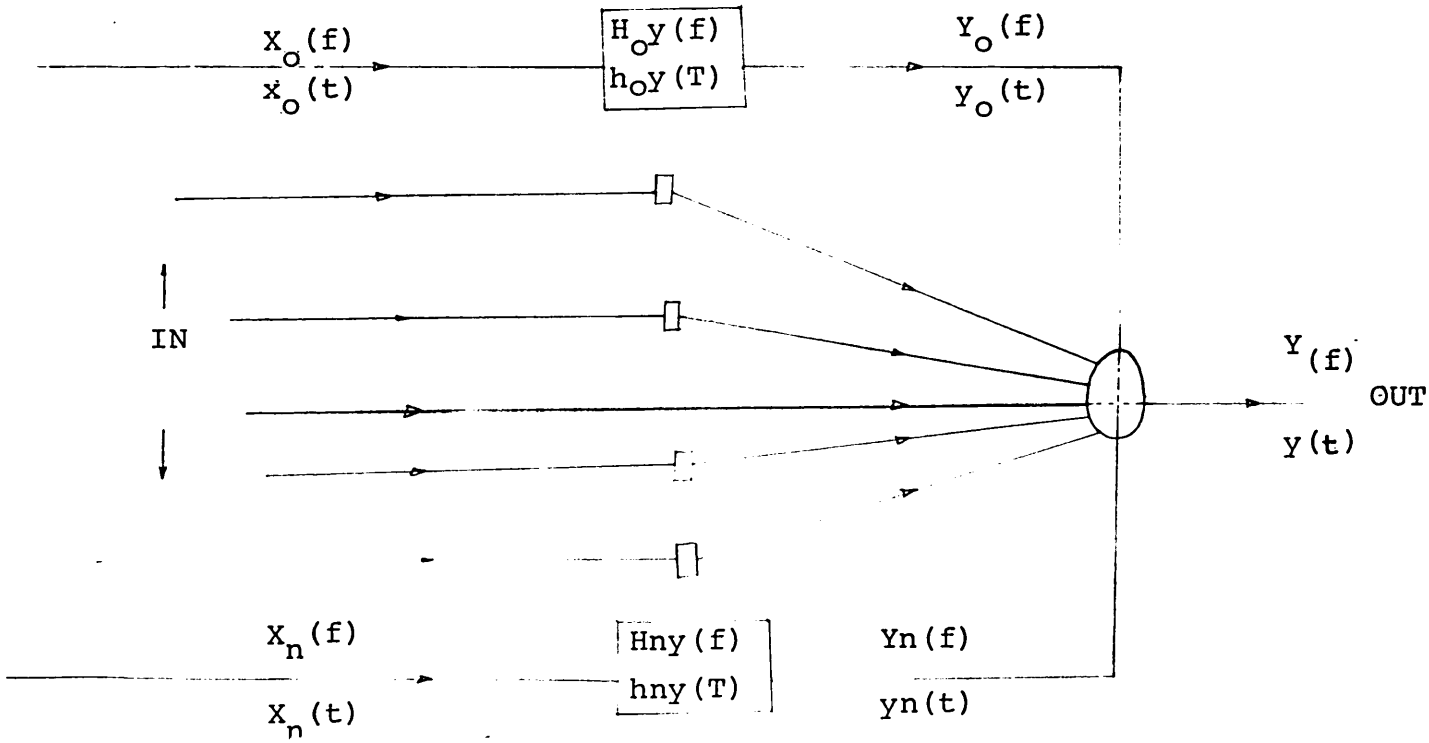


Fig. 5.01 Multiple input linear system, inputs/output and weighting functions expressed in frequency and time.

The multiple input linear system as we here described, is represented in both frequency and time domains where $h_o y(T)$, for example is the weighting function associated with the system between the input $X_o(t)$ and the output component $Y_o(t)$. In general three common types of coherence functions exist as similarity measures when multiple input linear systems are considered. These are already mentioned in the last sections, they include, the ordinary, multiple and partial coherence functions. This section will emphasise the evaluation, and use of these functions with special reference to partial coherence.

Let us consider at this point, an n constant parameter (time - invariant) linear system with n defined inputs $\bar{x}i(t)$, (i = 0, 1, 2, ..., n-1) and one measured output y(t), see Figure (5.01). It then follows that

$$y(t) = \sum_{i=0}^{n-1} \bar{y}i(t) \qquad (5.10)$$

so that $\bar{y}i(t)$ is that component of the output produced by the i^{th} input when all the other inputs are zero. If we define $h_i(T)$ as the weighting function associated with the ith input $x_i(t)$, we can hence express $\bar{y}_i(t)$ in terms of the well known convolutional relation;

$$\bar{y}i(t) = \int_0 hi(T)\ \bar{x}i(t-T)\ dT \qquad (5.11)$$

(Note the system is physically realisable if the lower limit of our integration is zero). The Fourier transformation of (5.11) will give

$$Yi(f) = Hi(f)\ Xi(f) \qquad (5.12)$$

where upper case letters are the Fourier transforms of the lower case letters, Hi(f) is the frequency response function corresponding to transform of hi(T). The FT (Fourier transform) Y(f) of the total system output then becomes;

$$Y(f) = \sum_{i=0}^{n-1} Yi(f)$$

$$= \sum_{i=0}^{n-1} Hi(f)\ Xi(f) \qquad (5.14)$$

5.2.1 The Cross-spectral Relations

The cross-spectral relations for a multiple input linear system may be obtained from the cross-spectral density function ($G_{iy}(f)$) of the output Y(t) with any one of the i-inputs. If the inputs are correlated, we can define a general relation for this density function,

$$G_{iy}(f) = \sum_{j=1}^{n} H_j(f)\ G_{ij}(f) \qquad (5.15)$$

where $G_{ij}(f)$ is the cross spectral density function between the ith and jth inputs. A method of derivation of equation (5.15) has been efficiently dealt with by Bendat et al. (1971).

5.2.2 Matrix Formulation of Results

The results of the preceding section may be made more concise through matrix notation besides, other intermediate results may become more readily apparent from the matrix formulations. Let us

at first define an n-dimensional input vector

$$X(t) = \left[x_1(t),\ x_2(t),\ x_3(t),\ \ldots x_n(t)\ \right] \quad (5.16)$$

where our index has changed (1→n) instead of (0→n-1). The effect is the same but the former facilitated computer programming. Again, we define an n-dimensional transfer function vector,

$$H(f) = \left[H_1(f),\ H_2(f),\ H_3(f),\ \ldots,\ H_n(f)\ \right] \quad (5.17)$$

Similarly, we define an n-dimensional cross-power spectrum vector of the output Y(t) with the inputs $x_i(t)$;

$$G_{xy}(f) = \left[G_{1y}(f),\ G_{2y}(f),\ G_{3y}(f),\ \ldots,\ G_{ny}(f)\right] \quad (5.18)$$

where

(1,2,3, ...,n) represent (x_1, x_2, x_3, ... x_n)

Finally we define the n x n matrix of cross-spectra of all the inputs $x_i(t)$ by;

$$G_{xx}(f) = \begin{bmatrix} G_{11}(f) & G_{12}(f) & G_{13}(f) & \ldots & G_{1n}(f) \\ G_{21}(f) & G_{22}(f) & G_{23}(f) & \ldots & G_{2n}(f) \\ G_{31}(f) & G_{32}(f) & G_{33}(f) & \ldots & G_{3n}(f) \\ \cdot & & & & \\ \cdot & & & & \\ \cdot & & & & \\ G_{n1}(f) & G_{n2}(f) & G_{n3}(f) & \ldots & G_{nn}(t) \end{bmatrix}$$

Where $G_{ij}(f) = G_{x_i x_j}(f)$ $(i, j = 1,2,3, \ldots, n)$

The matrix $(G_{XX}(f)$ is Hermitian (it equals its conjugate transpose). The Hermitian symmetry enables an efficient use of the escalator method to do the matrix inversion of (5-19).

Now, returning to equation (5-12) the system of linear equations to obtain a least squares solution for Hi(f) is the matrix equation defined,

$$G_{xy}(f) = G_{xx}(f)\ H(f) \tag{5.20}$$

which when expanded reads;

$$\begin{bmatrix} G_{1y}(f) \\ G_{2y}(f) \\ G_{3y}(f) \\ \vdots \\ G_{ny}(f) \end{bmatrix} \quad \begin{bmatrix} G_{11}(f) & G_{12}(f) & G_{13}(f) & \cdots & G_{1n}(f) \\ G_{21}(f) & G_{22}(f) & G_{23}(f) & \cdots & G_{2n}(f) \\ G_{31}(f) & G_{32}(f) & G_{33}(f) & \cdots & G_{3n}(f) \\ & & & & \\ G_{1}(f) & G_{2}(f) & G_{3}(f) & \cdots & G_{nn}(f) \end{bmatrix} \quad \begin{bmatrix} H_1(f) \\ H_2(f) \\ H_3(f) \\ \\ H_n(f) \end{bmatrix} \tag{5.21}$$

On solution.(5.21) yields the following result

$$H(f) = G^{-1}_{xx(f)}\ G_{xy}(f) \tag{5.22}$$

It therefore follows that the frequency response functions $H_k(f) = H(f)$ can be obtained by solving the frequency domain normal equations (5.20), and the coherence functions may also be computed as intermediate results. When the frequency response function $H_1(f)$, say, is inverse transformed, back to the time domain we obtain a "most probable" estimate of the desired seismic wavelet necessary for synthetic generation. This is the procedure adopted by White (1980), in his paper on partial coherence matching of synthetic seismograms with seismic traces.

5.2.3 Computational Procedures and Parameters

The four main parameters commonly computed for a multiple input linear system may be summarized as follows;

a) Transfer Functions between each of the inputs and the output.

b) Ordinary coherence functions between all pairs of variables

c) The multiple coherence function between the output and all the inputs

d) Partial (conditional) coherence functions between each input and the output while conditioning on the other inputs. Method of conditioning and residual analysis has been mathematically derived in Appendix A-3.

The computational procedures for the evaluation of (5.22) may be divided into three main steps.

i) Acquisition of power and cross-spectral density function computation routines.

ii) Acquisition of efficient techniques for simultaneously handling of (n+1) variables to obtain the spectral density functions among all these variables.

iii) Acquisition of efficient complex variable routines to enhance computation of complex matrix operations necessary to determine the desired linear system parameters.

In general, the required spectral density functions can be generated either by FFT or by correlation-power spectral density procedures. It is, however, important that all possible combinations of cross-spectral relations are computed. The Hermitian symmetry implies that only the diagonal and upper right portion of the matrix need be calculated, since

$$G_{ij}(f) = G^{*}_{ji}(f) = G_{ij}(-f)$$

A program for multiple-input linear system analysis operates on the (n+1) x (n+1) spectral density matrices, one matrix for each frequency value. The data is a set of spectral density matrices at frequencies indexed as below:

$$Gyi = \begin{bmatrix} G_{yyi} & G_{yli} & G_{y2i} & \cdots & G_{yni} \\ G_{iyi} & G_{ll}{}^{i} & G_{l2i} & \cdots & G_{lni} \\ \cdot & & & & \\ \cdot & & & & \\ G_{nyi} & G_{nli} & G_{n2i} & \cdots & G_{nni} \end{bmatrix} \qquad (5.24)$$

$$(i = 0,1,2, \ldots m)$$

The m separate (n+1) x (n+1) spectral density matrices can be visualised in the three-dimensions as shown in figure (5.02).

The relations necessary to evaluate the system parameters are summarized as follows;

1) We recall equation (5.21) is the necessary matrix equation whose solution yields the frequency response function, and we require complex arithmetical operations

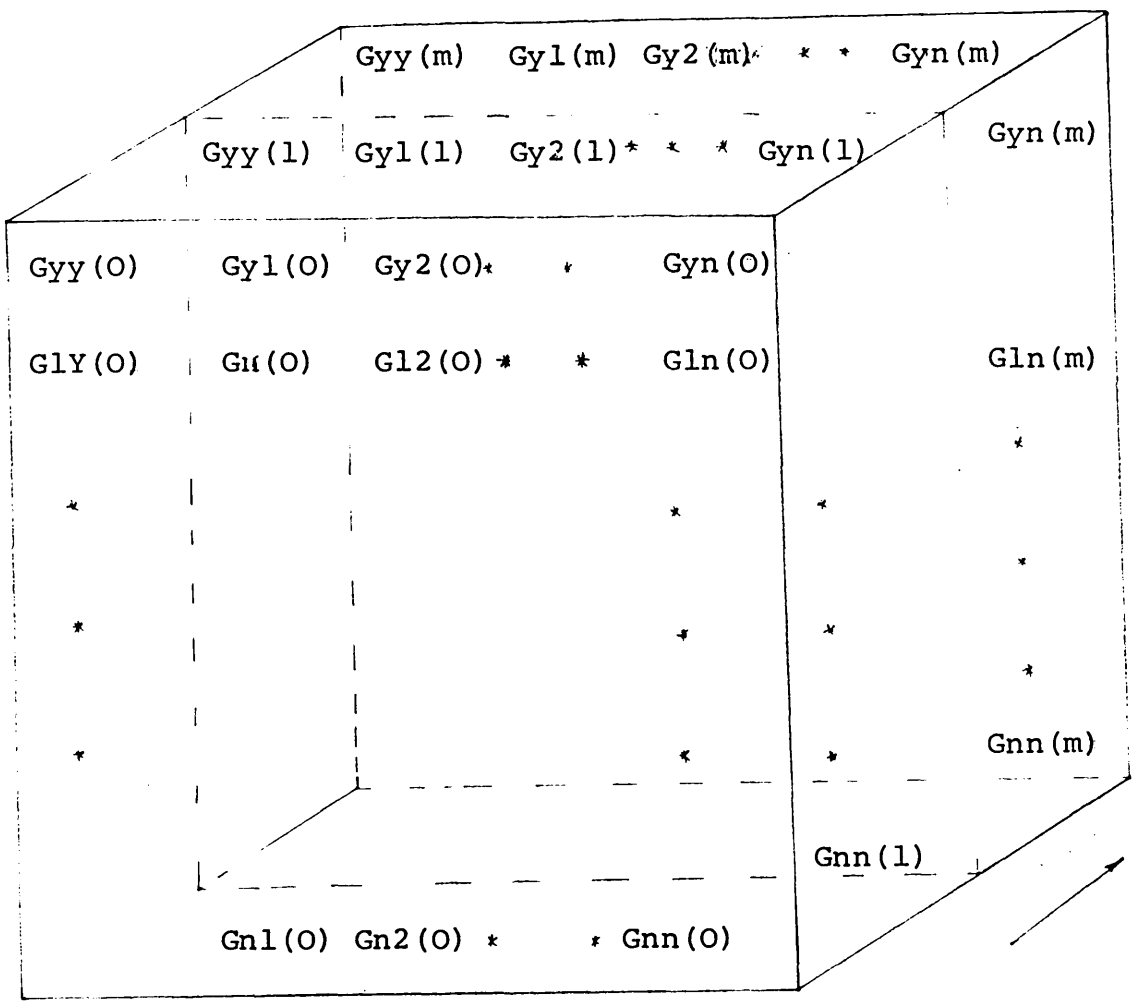


Fig. 5.02 Viewing spectral matrices in 3-dimensions. Each slice represents a frequency component.

to evaluate the complex matrices and vectors.

2) The ordinary coherence functions between the output y and each input Xi are computed from the relation

$$\gamma^2_{iy} = \frac{|G_{iy}|^2}{G_{ii}G_{yy}} \qquad (5.26)$$

$$(i = 1, 2, 3, \ldots, n)$$

(3) The multiple coherence function between the output Y and all the inputs, x_1, x_2, x_3, ... x_n is computed from

$$\gamma^2_{yx} = 1 - (G_{yy}\, G^{yy})^{-1} \qquad (5.27)$$

Where G^{yy} denotes the first diagonal element of the augmented spectral matrix (5.24).

4) Following Otnes et al. (1972), and White (1980), we can calculate the partial coherence function from the relation:

$$\gamma^2_{ky}/q\text{-}1 = \left[1 + \frac{\phi^{kk}}{|Hk|^2 \phi^{yy}}\right]^{-1} \qquad (5.28)$$

where computation was carried out after conditioning for the rest of the remaining (q-1) inputs.

5.2.4 Two Input Linear Systems

Earlier, Bendat and Piersol (1966, 1971) had developed equivalent formalisms as Otnes et al. (1972) and had treated in detail coherency and frequency response function computations for the special case of two-input linear systems. For a two-input linear system, the two methods will yield the same results, and the method of Bendat et al. (1971) will not be as complicated, as noted in White's paper (1980).

5.2.5 Partial Coherence for Two-Input Systems

We may recall that coherence functions are related

to correlation functions through time - frequency transformations. Following Bendat et al. (1981), the partial correlation function coefficient at T = 0, is defined according to the relation:

$$\rho^2_{1y.2} = R^2_{1y.2}/R_{11.2}\, R_{yy.2} \qquad (5.29)$$

($\rho^2_{1y.2}$ is the partial correlation function coefficient)

Now for a two-input linear system where the inputs $X_1(t)$ and $X_2(t)$ are correlated, we can define a partial coherence function between $X_1(t)$ and $y(t)$, with $X_2(t)$ removed at every t by least-squares prediction from $X_1(t)$ and $y(t)$. This partial coherence function is analogous to the definition of equation (5.29) - the partial correlation function coefficient except that partial coherence is expressed as frequency function while (5.29) is a time function, hence we can write:

$$\gamma^2_{1y.2}(f) = \frac{\left|G_{1y.2}(f)\right|^2}{G_{11.2}(f)\, G_{yy.2}(f)} \qquad (5.30)$$

the symbols $G_{yy.2}$ and $G_{11.2}$ indicate that the residuals are obtained by removing the effects of $X_2(t)$ by least-squares prediction from $X_1(t)$ and $y(t)$. We, therefore, call the terms in (5.30) the residual (or conditional) spectra. The terms in equation (5.30) are easily obtained from matrix analysis such that

$$G_{1y.2}(f) = G_{1y}(f)\left[1 - \frac{G_{12}(f)\, G_{2y}(f)}{G_{22}(f)\, G_{1y}(f)}\right]$$

$$G_{11.2}(f) = G_{11}(f)\left[1 - \gamma^2_{12}(f)\right]$$

$$G_{yy.2}(f) = G_{yy}(f)\left[1 - \gamma^2_{2y}(f)\right] \qquad (5.31)$$

$$\gamma^2_{12}(f) = \frac{|G_{12}(f)|^2}{G_{11}(f)\,G_{22}(f)}, \quad \gamma^2_{2y}(f) = \frac{|G_{2y}(f)|^2}{G_{22}(f)G_{yy}(f)}$$

We can briefly deduce the matrix relation.

Now equation (5.31) may be obtained from the augmented spectral matrix by partitioning as shown:

$$G_{yxx} = \left[\begin{array}{c|cc} G_{yy} & G_{y1} & G_{y2} \\ \hline G_{1y} & G_{11} & G_{12} \\ G_{2y} & G_{21} & G_{22} \end{array}\right] \qquad (5.32)$$

We can also define the residual spectral matrix between $X_1(t)$ and $y(t)$ as in (5.33)

$$G_{xy.2} = \begin{bmatrix} G_{yy.2} & G_{y1.2} \\ G_{1y.2} & G_{11.2} \end{bmatrix} \qquad (5.33)$$

By expanding the partitioned matrix (5.32) we come up with the result,

$$G_{xy.2} = \begin{bmatrix} G_{yy} - \frac{G_{y2}G_{2y}}{G_{22}} & \frac{G_{y1} - G_{y2}G_{21}}{G_{22}} \\ G_{1y} - \frac{G_{12}G_{2y}}{G_{22}} & G_{11} - \frac{G_{12}G_{21}}{G_{22}} \end{bmatrix} \qquad (5.34)$$

Since $G_{y1.2}(f)$ is the complex conjugate of $G_{1y.2}(f)$ it is easy to see the correspondence between the elements in the last two matrices and the quantities defined in (5.31). The frequency dependence in the matrices has been dropped to reduce notations. The expressions in (5.31) show how to compute each term in the residual matrix, and from which the frequency response function $H_1(f)$ and partial coherence function $\gamma^2_{1y.2}(f)$, are easily obtained, so that

$$H_1(f) = G_{1y.2}(f)/G_{11.2}(f) \qquad (5.35)$$

while $\gamma^2_{1y.2}(f)$ is computed from equation (5.30).

On the other hand it is also an easy matter to get a straight forward computation of $H_1(f)$ and $Y^2_{1y.2}(f)$ by calculating the power and cross power spectra from the auto and cross-correlation functions of the residuals $DX_1(t)$ and $DY_1(t)$, and using expressions (5.30) and (5.35) to obtain the required functions. The method of estimating the residuals $D_{X1}(t)$ and $D_{y1}(t)$ has been derived in the appendix - A3.

This work, however, has not pursued further the method of partitioning the augmented spectra matrix and the consequent complex analysis for the general case of more than two inputs. The method is particularly unattractive, commercially. This is due to the complexity and high computer time necessary to achieve the necessary results. White (1980) pointed out this fact in his paper on partial coherence matching. On the other hand, if we confine our analysis to a two-input linear system

consisting solely of the signals in one channel and the noise components in the second channel (and by noise we mean every undesired signal), then equations (5.30) and (5.35) as here defined become very attractive.

The methods as we have described are simple and straight forward to apply.

5.2.6 Method of Application

Generally with the aid of expressions (5.30) and (5.35) the partial coherence functions and the frequency response functions for the two-channel systems which we have described may be computed as follows;

a) The input and output residuals, $D_{X1}(t)$ and $D_{y1}(t)$ are found by the method described in the appendix-A3. The residual (conditioned) power and cross-spectral density relations between DX_1DX_1, DY_1DY_1, and DX_1DY_1 are obtained through fourier transformation of their auto- and cross-correlation relations, to obtain, $G_{11.2}(f)$, $G_{yy.2}(f)$ and $G_{1y.2}(f)$ respectively, where:

$$G_{11.2}(f) = G_{DX_1DX_1}(f)$$

is the power spectrum of the conditioned X_1-input,

$$G_{yy.2}(f) = G_{DY_1DY_1}(f)$$

is the equivalent power of the conditioned output Y, and

$$G_{1y.2}(f) = G_{D_{X_1}D_{y1}}(f)$$

is the cross power between the residual (conditioned) input and output.

The straight application of equations (5.30) and (5.35), therefore, produces the desired partial coherence and frequency response functions, the frequency response of which transforms into the time domain to yield the best estimate of the synthetic waveforms.

(b) In our second approach, the frequency response and the partial coherence functions are computed through a different method. This method utilizes the matrix partitioning technique as described in the previous section, so that all the components of equations (5.30) and (5.35) for the computations of partial coherence and the frequency response functions are obtained from (5.31) which is a simplified version of the matrix representation, equation (5.34). Once more the estimate of the best waveform may be obtained by an inverse transform of the frequency response function.

The results obtained from each of the two methods may then be compared with each other and with that obtained by the method of White (1980). In White's paper as we may recall, the Hermitian symmetry was used to solve the system of frequency domain normal equations (5.20), where the matrix inversion is by the escalator method.

The subroutines BENSOL, OTNES, and FAITH (developed by the author), were used to carry out the three methods of analysis. As we shall see in the section, on matching with similarity measures, the three methods gave the same degree of accuracy for a two-channel system. On the other hand, the first two methods require less computer time than the third method. The time difference follows

from the total number of multiplications and complex operations required to bring each method to completion. In addition, each of the first two computer subroutines is easily adapted for use in the absence of complex arithmetical operations, and complex variable routines. This is an obvious advantage in places if the compiler has no in built routines for analysis of complex variables. In general it will not be very easy to adapt the last package in the same manner. However, the first two methods need amendment when dealing with more than two-channel systems and in which case the last method becomes indispensable. For purposes of general seismic matching of traces, the above two methods (as we shall see) are as efficient as White's model.

5.2.7 Generation of Synthetic Seismograms

We have discussed how to compute the frequency response functions whose inverses in the time domain generate the desired seismic wavelet. The coherences estimate the statistics of the match , All computations are made for a multiple input system. In our discussed models, the inputs are calculated from the well log information which may be any of the following; Primaries (with or without transmission, absorption or geometrical spreading effects and attenuation), then the multiples (which may include some multiples only, all possible multiples, all multiples plus some ghost, etc.). The desired output of the

models is the observed stacked field seismogram. Using a set of input/output combinations, we calculate the frequency response of the best fit wavelet where the statistical evidence of this goodness of fit is determined by the estimate of partial coherences, values of which must lie between 0 and 1 for the frequency range of interest.

In the frequency domain, the computed frequency response function will multiply with the Fourier transform of the equivalent input to yield a characteristic output. An inversion of this frequency dependent output yields the synthetic seismogram in the time domain (consisting, say of primaries only, multiples only or their combinations). Alternatively, we can invert the calculated frequency response function and then convolve it with an equivalent input, both in the time domain, to yield the synthetic seismogram. Computation of the Pearson's product moment correlation coefficient, γ_c, (between the computed synthetic and the observed field seismogram), tells us quantitatively how well the synthetic seismogram matches the field observation. As mentioned earlier, the Routines; BENSOL, OTNES, and FAITH, are used to carry out all the computations. The results as well as the plots from each Routine will be displayed in the section on matching with similarity measures.

5.30 Least squares measure

In many areas of study the least squares technique has been employed as a very useful and versatile tool for numerical analysis of data. In nuclear engineering and instrumentation for example, this method has been used in the analysis of complex Gamma-ray spectra (Robert et al., 1964), Analysis of Pulse-height spectra containing gain-shift and zero-drift compensation (Trombka et al., 1968). In both cases detection of Nuclear components from their energy contents has been enhanced.

In the social sciences, economic experts have long utilised this method to their advantage. Their major areas of interest include the processes of regression analysis, curve fitting and general predictions of events.

In electrical engineering, the role of the method in signal analysis has long been established and most of these engineering techniques have equally found proper utilization among the earth scientists. We cannot overemphasize the role of regression analysis, trend surface analysis (curve surface fittings) etc., in time series analysis. These are all techniques based on the least squares criterion. Indeed it may be true to say that the least-squares technique is a major contributor to the

successful application of the statistical theory of random variables to discrete data. Bendat and Piersol (1966) applied the technique to derive expressions for discrete residual random variables and the accompanying partial coherences computed in the frequency domain.

Following the mathematical deductions of the mathematician, Nobert Wiener (1949) who developed the theory of Optimum filters based on least-squares criterion, this theory has been extended and expanded, and among other disciplines has found wide applications in Geophysical studies. Schneider et al. (1965), Backus et al. (1964), used these filters on seismic data, while Foster et al. (1962), George et al. (1964) applied them to well logs. Detailed mathematical treatment of the theory as applied to exploration industries for single and multi-channel time series have been given by Wiggins et al. (1965), Robinson et al. (1969). The general processes of deconvolution signal-noise enhancement , signal estimation , prediction , and smoothing, as applied in oil and gas exploration, often utilize the least-squares technique. For more information on general theory of least squares approximation and smoothing, the interested reader may find the mathematical literature very helpful - Ralston (1965), Hildebrand (1956), and Lee (1960).

If we know the past history of a time series, it is an easy matter under the least-squares criterion to generate operators

which make predictions of future values of the time series possible. Claerbout (1976) called the least-squares technique, a ubiquitous tool which fulfils the essence of science.

In this thesis, use is made of the least-squares criterion to study the relationship between the input and the desired output to a least-squares filter. The technique shows how close a well-log generated data (the filter input) approximates a field seismic data (the desired output). The seismic field data is observed closest to the well of interest. A matching criterion has been developed from this study, hence the least-squares measure. A brief theory of the method is given in the next section.

5.3.1 The Optimum Least-squares Filter Analysis

In general, the design of least-squares optimum filters is based upon minimizing a suitably defined error criterion. A typical model, figure (5.04) will incorporate three main signals viz;

(m_1) Input Signal

(m_2) Desired Output (observed) signal)

(m_3) Actual Output (expected) signal

The last component, the expected value is easily obtained once the coefficients of the optimum filter have been determined.

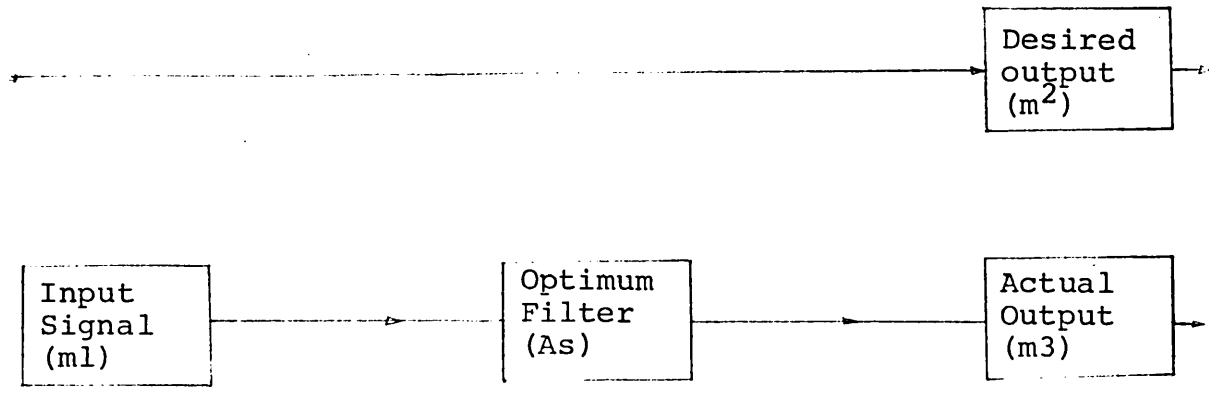


Figure (5.04) - Optimum Filter Model

The mathematics of the discrete least-squares optimum filters assumes that:

(a) the signals are discrete and time-sampled

(b) the observed component may contain only signals or may be an additive combination of signal and noise

(c) the expected signal is a convolution of the input with the filter coefficients

(d) We minimize the expected value of the error process.

In addition to the above mentioned assumptions we add the following:

(e) That each of the seismic time sequences is regarded as being only one out of a large number of possible observations that could have been observed. This collection of observations is termed an 'ensemble', X(t), and our sequence is a particular realisation of X(t), i.e. $xi(t) \in X(t)$.

(f) Each seismic sequence constitutes a stationary time series, i.e. that measurements of correlation functions, mean, spectral power estimaes, and so on, do not depend

upon the time origin chosen for their measurement. Such an assumption is generally true in real data for not very long record lengths (Wadsworth et al., 1953).

(g) We also assume the ergodic hypothesis, which is to say that the time average and ensemble average are the same, i.e., that the average value of some quantity, obtained by averaging any one specific sequence over all times is equal to that obtained by averaging over all the possible sequences at one time hence

$$\overline{Xi(t)} = \overline{\{X(ti)\}}$$

These notions of average behaviour form the cornerstone of statistical communication theory, from which much of our current data processing is derived. The last three assumptions particularly apply to all seismic data used in the thesis. Further discussion may be found in Lee (1960).

5.3.2 Mathematical Theory

According to least-squares principle, the optimum filter coefficients, a_o, a_1, ... a_n which operate on the input to generate the actual output, are determined such that the sum of squared errors e is a minimum, where

$$e = E\{(Dt - Pt)^2\} \qquad (5.36)$$

The smallest achievable value of e for a given situation yields the optimum linear filter in the least-squares

sense. Dt, is the observed or desired output, Pt, the expected, computed or Actual Output, defined;

$$Pt = \sum_{s=0}^{n} a_s C_{t-s} = C_t * a_s \qquad (5.37)$$

where * signifies convolution, hence

$$e = E\left\{ (Dt - \sum_{s=0}^{n} as(C_{t-s})^2 \right\} \qquad (5.37a)$$

The error e is minimized if the partial derivative with respect to each of the filter coefficients equals zero. Setting the partial derivative with respect to ai (i = 0, 1, ..., n) equal to zero we have;

$$de/d_{ai} = E\left\{ 2(Dt - \sum_{s=0}^{n} a_s (C_{t-s})(-C_{t-i}) \right\} = 0 \qquad (5.38)$$

$$\Rightarrow 2\left[-E\{D_t C_{t-i}\} + \sum_{s=0}^{n} a_s E\{C_{t-s} C_{t-i}\} \right] = 0 \qquad (5.39)$$

If we define the second expectation term in (5.39) as the autocorrelation R(i-s) (for index (i-s)) of the filter input, and the first expectation term as the cross correlation G(i) of the desired output with the filter input, then;

$$R(i-s) = E\{C_{t-s} C_{t-i}\} \qquad (5.40)$$

$$G(i) = E\{D_t C_{t-i}\} \qquad (5.41)$$

If we put back in (5.39), the last two equations then;

$$2\left[-G(i) + \sum_{s=0}^{n} a_s R(i-s)\right] = 0$$

$$\rightarrow \sum_{s=0}^{n} as\, R(i-s) = G(i) \qquad (5.42)$$

$$(i = 0, 1, \ldots, n)$$

Equation (5.42) defines a set of (n+1) simultaneous linear equations, the solutions of which give the (n+1) coefficients of the optimum filter. The set of (n+1) equations is the so-called time-domain normal equations.

Robinson et al. (1969) expanded equation (5.37a) thereby defining a more convenient expression for e, in terms of the main design parameters (see appendix A-2) so that e_{min}, (the minimum error) is defined thus;

$$e_{min} = E\{Dt^2\} - 2\sum_{s=0}^{n} asG(s) + \sum_{s=0}^{n} asG(s) \qquad (5.43)$$

or put differently;

$$e_{min} = R_D(0) - \sum_{s=0}^{n} a_s G(s) \qquad (5.44)$$

where $R_D(0)$ is the autocorrelation at zero lag of the desired filter output. If we normalize expression (5.44), with respect to $R_D(0)$, then the minimum error will always have value between zero and 1 hence;

$$e_{min}/R_D(0) = 1 - \sum_{s=0}^{n} asG(s)/R_D(0) \qquad (5.45)$$

If we set $\alpha = e_{min}/R_D(0)$

then $\alpha = 1 - \sum_{s=0}^{n} asG(s)/R_D(0) \qquad (5.46)$

α, is often called the normalised mean square error. If it is zero, the agreement between the desired output and the actual output is complete. The reverse follows when α is 1. In practice, however, α lies between the two limits. For a given set of filter parameters, required to solve a given problem, the best filter is one for which α is a minimum. The ability of the optimum filter to achieve the least possible minimum error depends on the problem, the nature of the input, and desired output (e.g., the desired output shape and the relative positioning in time between the desired output and input, etc.). Wiggins (1969) noted that the delay of the filter input strongly affects the expected error minimum, while the closer the spectrum of the filter desired output is to that of the input, the better the error minimum. He, however, noted that expected error is a non-increasing function of filter length for any particular lag of the desired output relative to the input. With these in mind, we designed an experiment wholly to emphasise the effect of the filter input on the error minimum. This will enable us to define a general matching criterion - the least-squares measure , between the desired output (observed field seismogram) and the actual output (the synthetic seismogram).

5.3.3 Practical Filter Model

In our practical use of the discussed filter model, the following definitions are given to our model parameters:

(P1) The filter input, is the calculated well-log information. This may be any of the following primaries only, some multiples, all possible multiples, or all possible multiples plus source ghost.

(P2) The desired output, is the observed stacked field trace with noise and multiples attenuated.

(P3) The actual output is the expected or computed synthetic trace. This as earlier mentioned, is obtained by convolution between the input (P1) and the computed filter coefficients.

(P4) Residual (conditioned) inputs and desired output can replace (P1) and (P2) above. This permits the effect of each component to be treated in isolation.

5.3.4 Practical Requirements

(R1) The filter is expected to convert the input as much as is theoretically possible to a prototype of the desired output.

(R2) In each experiment, the desired output is always the same while the input may be any of the options in (P1).

(R3) For any data input, we compute the filter coefficients for the optimum positioning in time of the desired output relative to the input. This is done by searching through the errors for the different lag positions and picking the one with the most minimum value.

(R4) The length of input equals the length of the desired output.

5.3.5 Practical Procedure

For any of the input components recorded in (P1) we computed three inputs:

(i) The input as originally computed from well-log information.

(ii) A randomised component of the input. This is obtained by adding to (1) a set of random numbers (pure noise) drawn from a population of zero mean and unit variance.

(iii) An array of complete random numbers (similar to components added to (1) above).

Finally, our computer program, with its routines uses Levison's recursion technique to solve the normal equations (5.42). It also solves equation (5.46) to obtain the normalised mean square error. The same procedure is repeated for any of the 3-component inputs, taking one component at a time.

5.3.6 Goodness of Input and Least Squares Measure

As already mentioned each defined input, received the same treatment as any other one, in order to yield the desired results, mainly, the filter coefficients, the actual output and the minimum error. We also recall that for each of (i), (ii), (iii) as defined in the last section the same constant filter length and desired output are used by the program to search and pick the new optimum position, and the new error

minimum. From the foregoing, it is therefore evident that for each optimum position calculated for any of (i), (ii) or (iii), the input is the most varying parameter and will have the most registered effect on the calculated minimum error, hence, we define the measure of goodness of input (the least-squares measure), Ω, in this situation as follows;

$$\Omega = 1 - \alpha \tag{5.47}$$

where α is the normalised mean square error. Ω, is very similar to the so-called filter performance and has a value between 1 and 0. If it is 1, we should expect the input to be much related to the desired output, and we conclude that the actual output matches the desired output in the least-squares sense. The reverse is the case when the value of Ω is 0, and we say there is no match between the expected and observed seismograms. The value of Ω for pure noise (the generated random spike series) from (iii), Ωr, defines the practical limit of good and poor match. This is because, experience has shown that Ω, like other related measures, such as γ_c (the product moment correlation coefficient) rarely give non-spurious values at the two extremes (1, 0). Since we cannot expect a pure random noise (white series) to yield a high value of Ω, we must therefore be very critical in interpreting any value of $\Omega r \geq \Omega$, as good match, rather we must resort to possible ways to improve the match.

Further quick checks on the accuracy of Ω, may be carried out by computing the correlation coefficient, γ_c and X^2 (chi-squared) using the observed and calculated seismograms. The method of computing and interpreting γ_c and X^2, follows the definitions given in the appropriate sections on similarity measures. We can also quickly calculate γ_c from the relation;

$$\gamma_c = \pm \sqrt{\frac{\sum\{Yest - \bar{Y}\}^2}{\sum(Y-\bar{Y})^2}}$$

where Yest is the estimated (actual output) seismogram, Y, the observed or field stacked seismogram, and $\bar{Y}$ the mean value of Y. If the values of γ_c and X^2 support the calculated low value of Ω, then bearing in mind, the seismic limitations, steps should be taken to check on the appropriateness of the models or the computations that generated the signal components. We must check on the errors due to inaccurate log analysis, velocity and reflection coefficients, as well as multiple computations, above all we must consider errors from the general seismic data processing of the original field seismograms. These and all the discussed sources of mismatch could lead the way to probable remedies and possible improvements.

5.40 Statistical Measures

Some statistics like the X^2, F, and t statistics which indicate statistical significance may be used as measures of similarity since they often indicate to some

degree, the relationships between quantities of interest. We shall here give a brief summary of the type X^2 statistics used in this thesis.

5.4.1 THE X^2 - MEASURE

In this work, the X^2 measure is simply a fast but crude method of similarity measurement which utilizes the X^2 (chi-square) distribution. In using the method we may compute the residual between the observed and expected seismograms. The field seismogram is the observed and the synthetic is the expected seismogram. The computed residuals are then squared, dividing each time with the variance of the expected value and finally summing. This follows directly from the statistical definition of X^2

$$X^2 = \sum_{j=1}^{k} (D_j - P_j)^2 / P_{var}$$

Where D_j is the observed field data, and P_j is the expected synthetic seismogram. P_{var}, is the variance of the expected values.

$$STD(P_j) = \left(\sum_{j=1}^{N} (P_j - \bar{P})^2 / N \right)^{\frac{1}{2}}$$

$$VAR(P_j) = (STD(P_j))^2$$

$\bar{P}$ is the mean of the expected values. STD (denotes standard deviation), and VAR (variance), N is the total number of expected values or total number of observations. A similar method has been applied by Trombka et al. (1969) to test the match due

to some channels of radiometric data. The value of X^2 depends on the observed/expected values, the number of degrees of freedom (N-I, where I, is the number of measured parameters - mean, variance, etc.), and the level of significance (degree of confidence) attached to our observations. A(Ø.Ø5) level of significance was used in our analysis.

The weakness, however, of X^2 and other related statistics as similarity measures, is that they do not tell us much about the degree of correlation between the quantities, though they are quite fast and quick in determining a test of independence between the quantities. In later section - matching with similarity measures, we shall see how these discussed measures are used in practical analysis and matching of seismic time series (the well-log generated and field observed seismograms).

5.50 Matching with Similarity Measures

We have presented several similarity measures and their uses for assessing a match. In this section, we present the practical use of these measures in construction and numerical analysis of seismogram traces. The confidence attached to the results depends on the statistics and magnitude of the measures - γ_c (product moment correlation coefficient), Ω (goodness measure), coherences, or the X^2 measures, as defined in the previous sections. As we earlier stated, source wavelets are estimated via four main ways: 1) the matrix partition technique, (2) the method of straight residuals, 3) the normal equation - evaluation technique White (1980), and 4) the method of optimum - least squares analysis. There are also four main computer programs, each of which carries out the necessary computer evaluations to obtain the desired wavelet. This wavelet convolves with a given reflection response series to yield the 'most probable' synthetic seismogram, so that a confident match between this well-log generated synthetic seismogram and a field seismogram observed closest to the well is obtained.

In this first three methods, the useful statistic which determines the confidence attached to the computer estimations is the partial coherence, while α (the normalised mean square error) serves equally as the statistic attached to the fourth technique. Each of the four computer programs is designed to estimate the

necessary wavelet, compute the necessary statistics and generate the synthetic seismogram by convolving the estimated wavelet with the reflection impulse responses. It then prints out a numerical estimate of the measure of similarity between the well-log generated seismogram and the field seismogram observed closest to the well. The basic numerical (estimate printed out by each program) is the Parsons product moment correlation coefficent (γ_c), referred in the programs as CCOEF. Other numerical measures such as, Ω , X^2, etc, may be printed out as desired. The results from the first two programs, using the residual and matrix partition techniques, compare with each and with the third - the frequency domain normal equation evaluation technique, White (1980). The three are then compared with the fourth result from the optimum least-squares technique.

Three main well-logs were used in this analysis. These include; well cpv-1Ø, cpv-12, cpv-Ø3. These three wells in particular were supplied by Merlin Velocity profiling Company Ltd. (VELPRO), and are from the southern portion of the North Sea. Four seismic lines were again of prime importance to us. Each of the stated wells was shot at little or no offset distance from one of the lines. The lines are as follows, spec-line, cpv-1ØA, cpv-1ØB, cpv-12A, cpv-Ø3A. The nomen-clature is aimed to bring the wells and the lines to close correspondence so that well cpv-1Ø for example, lies directly on line cpv-1ØA (see Appendix, A-1).

Well cpv-1Ø is known to lie closest to line cpv-1ØA,

or cpv-1ØB. When compared to other wells, well cpv-1Ø has the least offset from its lines. It is about 200 m from cpv-1ØA and 100 m or less from cpv-1ØB. The four seismic lines are of the same origin as the wells and were kindly supplied by Merlin Geophysical. We shall now discuss the models and the results they produce.

Figure (5.05) - (5.08) show the plot and related results obtained by estimating the wavelet and generating the synthetic seismogram using;

(i) The matrix partition technique

(ii) The method of straight residuals

(iii) White's model

In figure (5.05a), T_5 is the required computed synthetic seismogram. This synthetic has been plotted with the rest of the stacked traces for visual comparison. The match between the synthetic and the field stack closest to well-cpv-1Ø may be described as an average match. This is seen from the visual plot and from the estimate of CCOEF (the Parson's product moment correlation coefficient) which is 0.4. Strikingly, Figure (5.06) - (5.08), seem to give approximately the same results. This is actually what we should expect from an intuitive view point. The first three methods for example, basically estimate the best possible wavelets in the frequency domain, by analysis of the power and cross power spectral relations. It is actually the mathematical techniques and the methods of evaluation of these results that differ. If these mathematical approaches and applications are accurate enough

then we should expect the results from the three methods of synthesis to be virtually the same. This is what our results have shown, so that using the matrix partition technique or by the straight application of residuals we can estimate the best possible wavelets which could generate in either frequency or time domain, the same synthetic seismograms as those obtained by the method of White (1980). Figure (5.05b) - figure (5.08b), show the segments of the well-log information as used in the synthesis. The first three traces are the field observations. Traces (4-8) are;

(4) Reflection coefficients

(5) Depths to subsurface

(6) Acoustic impedance

(7) Velocity

(8) Density

This enables one to compare the reflection changes relative to the subsurface parameters producing them. The remaining figures in this chapter will follow a similar pattern.

Figure (5.08) is the result from the fourth main computer program, which employs the optimum least-squares technique in its computation. In the analysis, α(the normalised mean-square error), and Ω(the goodness measure), for each of the three component inputs are as follows;

(1) Primaries only; $\alpha_1 = \emptyset.6\emptyset$, $\Omega_1 = \emptyset.4\emptyset$

(2) Primaries plus white noise; $\alpha_2 = \emptyset.7\emptyset$, $\Omega_2 = \emptyset.3\emptyset$

(3) Random White Series; $\alpha_3 = 0.8\emptyset$, $\Omega_3 = \emptyset.2\emptyset$

Fig. 5.05a Plots of synthetic and field seismograms (matrix - partition) correlation = Ø.4 (well , cpv-1Ø). T_5 & T_7 are the synthetics, other traces are field stacks. When 11 traces are used, T_4, T_6, and T_8 are skipped to facilitate visual analysis.

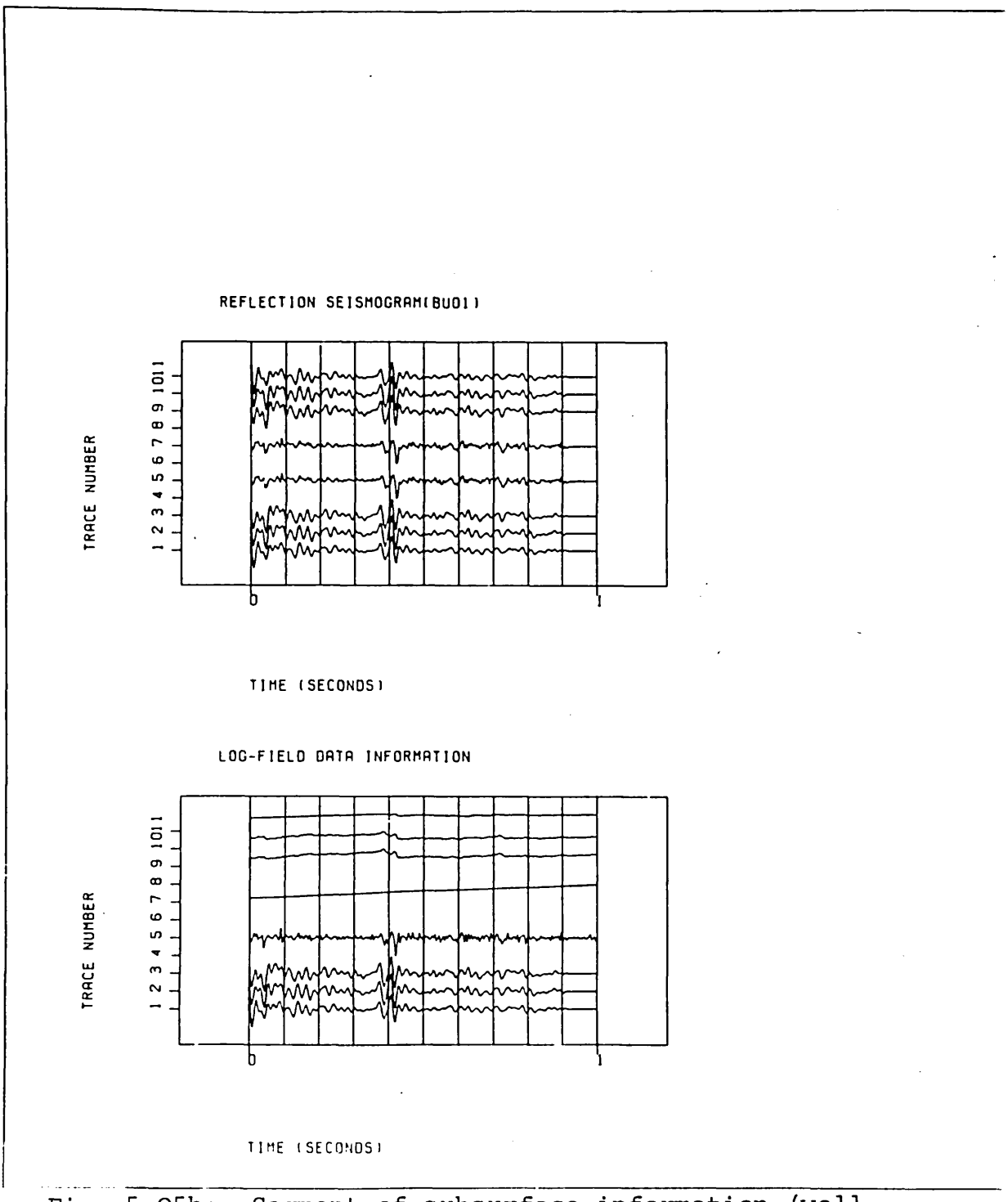
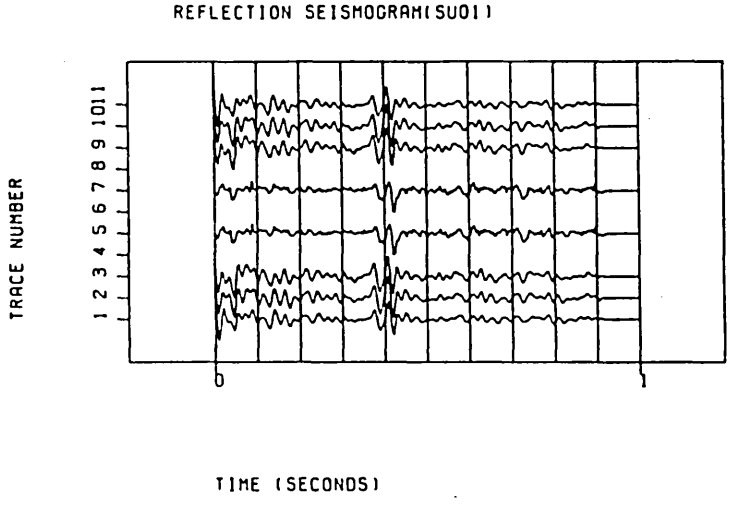


Fig. 5.05b: Segment of subsurface information (well-log Analysis)
(T_{11}) Density
(T_{10}) Velocity
(T_9) Acoustic Impedance
(T_7) Depths to subsurface
(T_5) Reflection coefficient
(T_1-T_3) Field stacks

All plots in chapter five follow similar pattern

Fig. 5.06a: Synthetic Result (Residual Analysis)
T_5 & T_7 are the synthetics
Other traces are field Stacks
Correlation = Ø.4
When 11 traces are used, T_4, T_6, and T_8, are skipped to facilitate visual analysis.



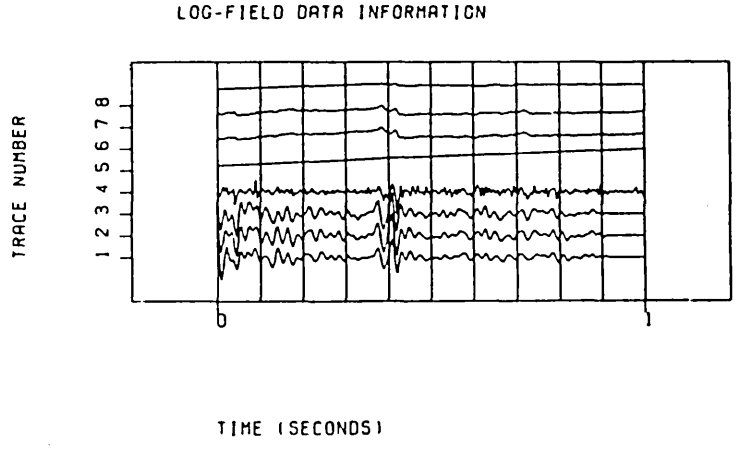
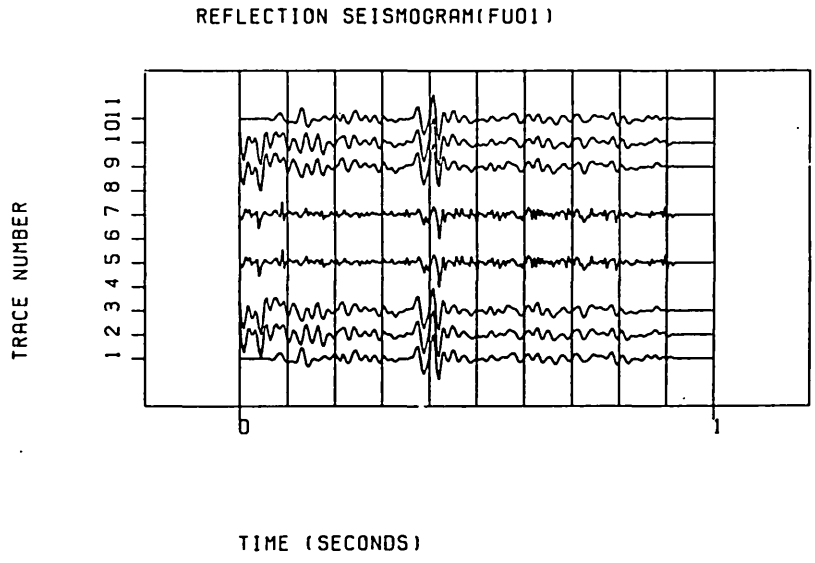


Fig. 5.06b: Subsurface Information (well-cpv-1Ø)
(T_8) Density
(T_7) Velocity
(T_6) Acoustic Impedance
(T_5) Depths to subsurface
(T_4) Reflection coefficients
(T_1-T_3) Field stacks

Fig. 5.07a: Analysis of Synthetic and Field Observations (White's Model) Correlation = Ø.4 (well-cpv-1Ø)



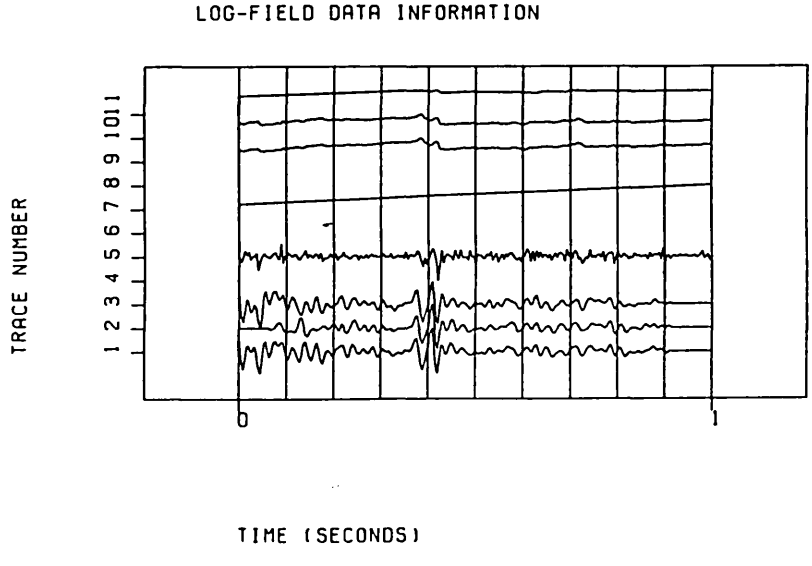


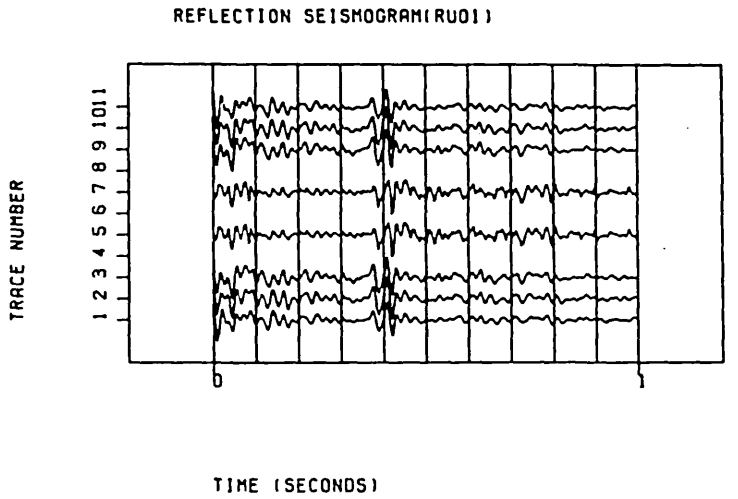
Fig. 5.07b: Segment of Subsurface Information (Well-log Analysis)

Fig. 5.08a Comparing Synthetic and Field plots (optimization - least squares)

$a_1 = 0.60$ $\Omega_1 = 0.40$

$a_2 = 0.70$ $\Omega_2 = 0.30$

$a_3 = 0.80$ $\Omega_3 = 0.20$



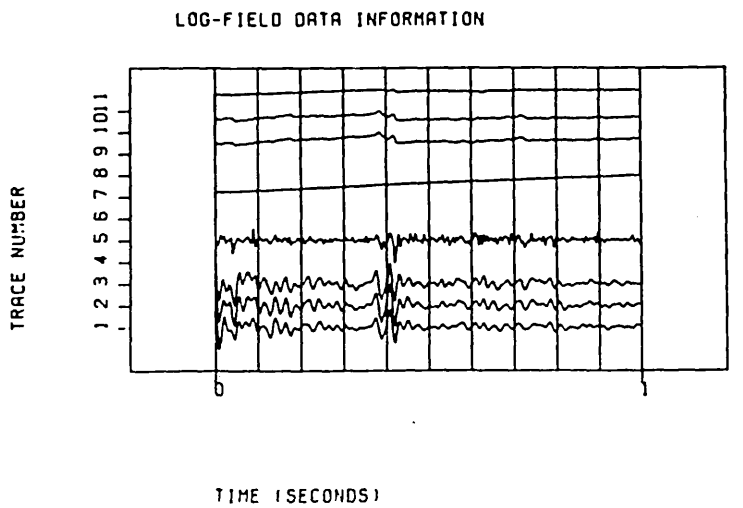


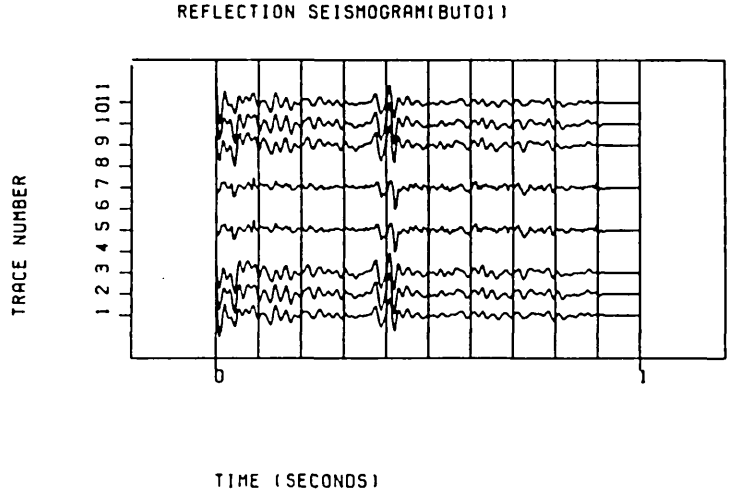
Fig. 5.08b: Subsurface segments (well-log Analysis)

The above three results suggest that as much as is theoretically possible, the match between the synthetic and the field observed seismogram is of the order of Ø.40 (as shown by the values of α_1 and Ω_1). The limit of poor match as we recall, is determined from the results in (3).

Generally, the match depends on the length of data segment. Short segments often give high values. If the match is confined to a short inverval of interest or if the seismic reflection wavelet is allowed to be unduly long, there is considerable danger of forcing a spurious fit that treats the noise on the trace as part of the seismic reflection signal (Walden et al., 1983). White and Walden (1980, 1983) suggested that a data segment at least should be of the order of 500 ms or more. In this thesis, each data segment is at least of 800 ms duration. When comparing results from the different techniques, each technique is allowed to operate only on the same length of well and seismic data segments. The best correlation in the acceptable gate is taken. What each technique measures may therefore be regarded as a confidence match.

In our second test, instead of using primaries only, and all possible multiples, we decided to include the transmission effects. Our inputs to the four techniques now become, primaries plus transmission loss, all possible multiples. Figures (5.09) - (5.12) show the computed results. As in the first example, the four results are similar. The change in the magnitude of the results due to the inclusion of transmission effects is not very marked nor is it very significant.

Fig. 5.09a Synthetic (Primaries and Transmission Loss) - Matrix-Analysis Correlation 0.41



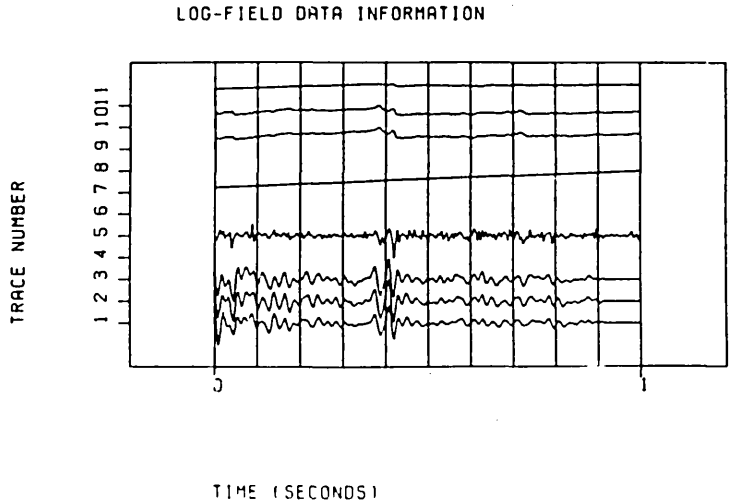
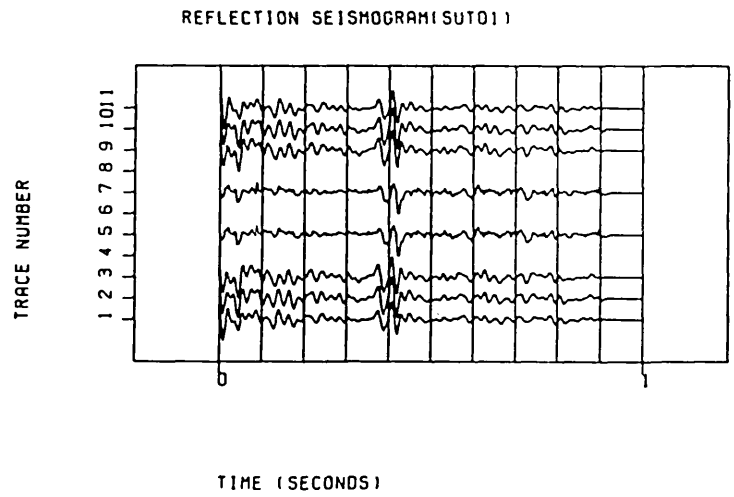


Fig. 5.09b Subsurface Segments (from Log Analysis)

Fig. 5.10a: Synthetic - Primaries and Transmission loss (Residual Analysis) correlation = 0.41



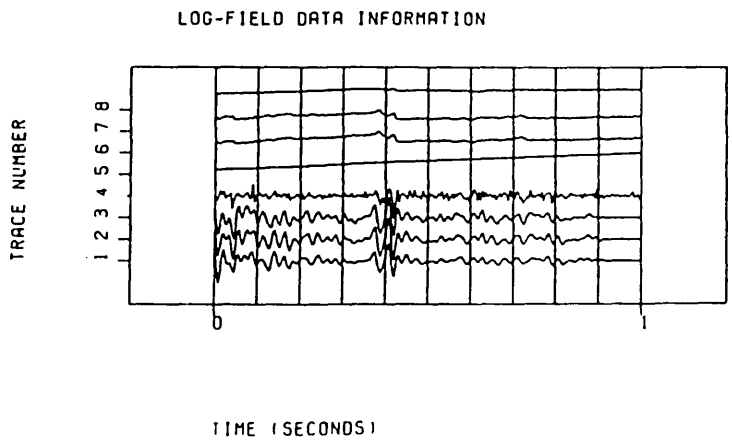
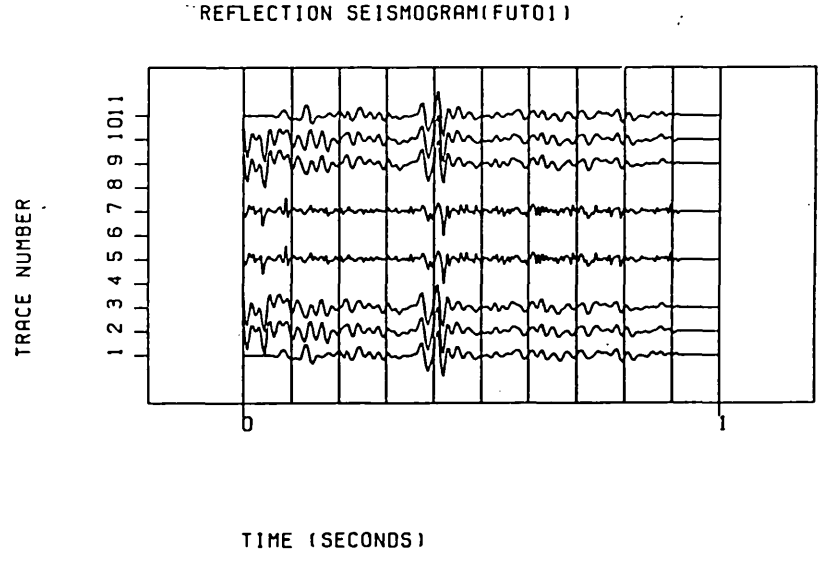


Fig. 5.10b: Subsurface segment (Log Analysis)

Fig. 5.11a: Synthetic: Primaries and Transmission loss (White's model).
$\gamma_c = 0.41$



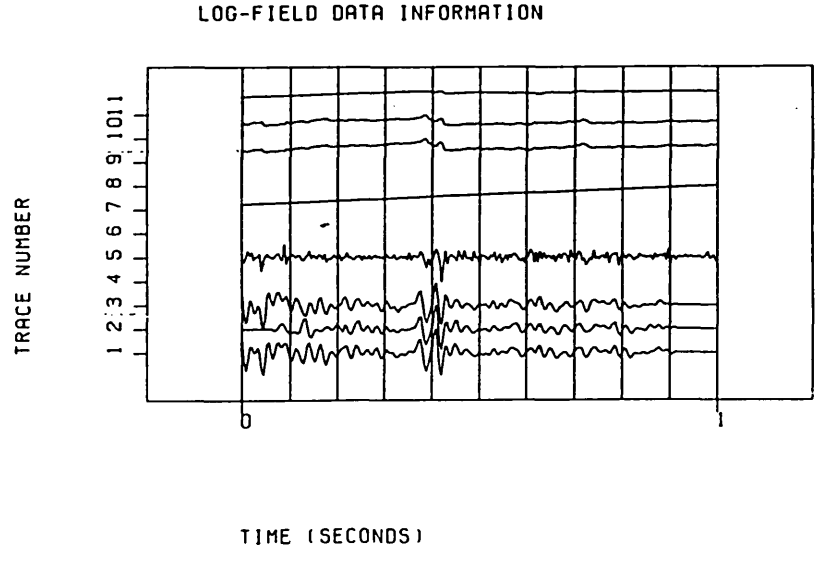


Fig. 5.11b: Subsurface Information (from Log-Analysis)

Fig. 5.12a Synthetic: Primaries and Transmission Loss (least squares optimization)

$a_1 = 0.58$ $\quad \Omega_1 = 0.43$

$a_2 = 0.65$ $\quad \Omega_2 = 0.35$

$a_3 = 0.80$ $\quad \Omega_3 = 0.20$

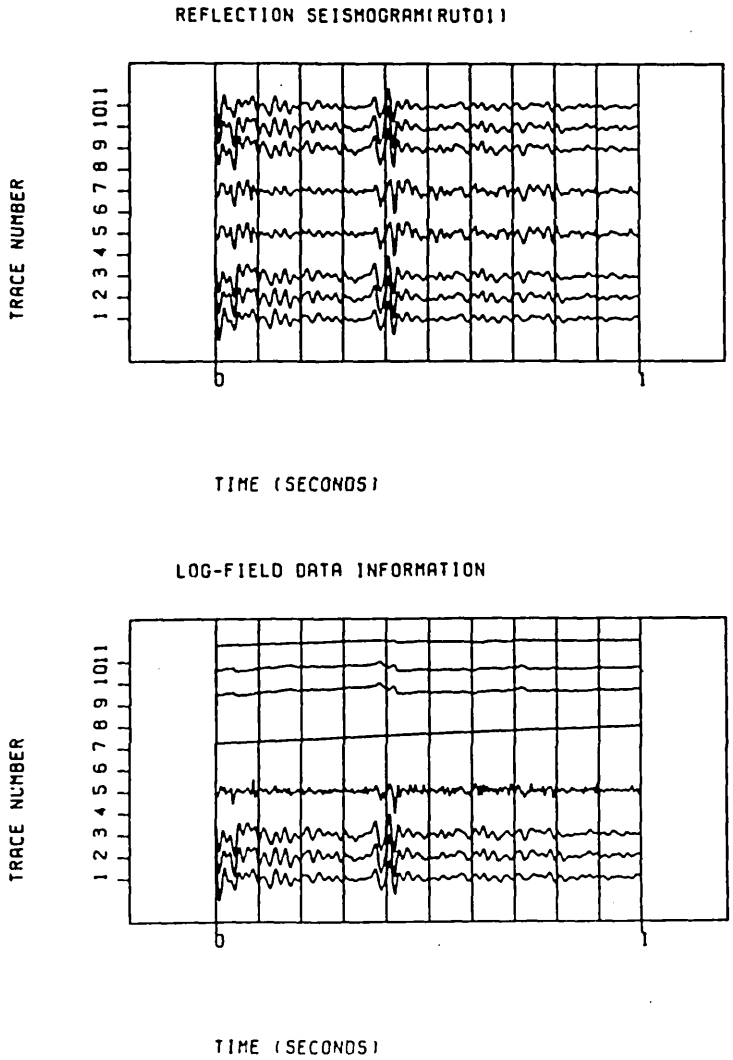


Fig. 5.12b: Subsurface Information (Log Analysis)

Fig. 5.13a Synthetic: Primaries, Multiples and Source Ghosts (Matrix - Analysis) Correlation = 0.40

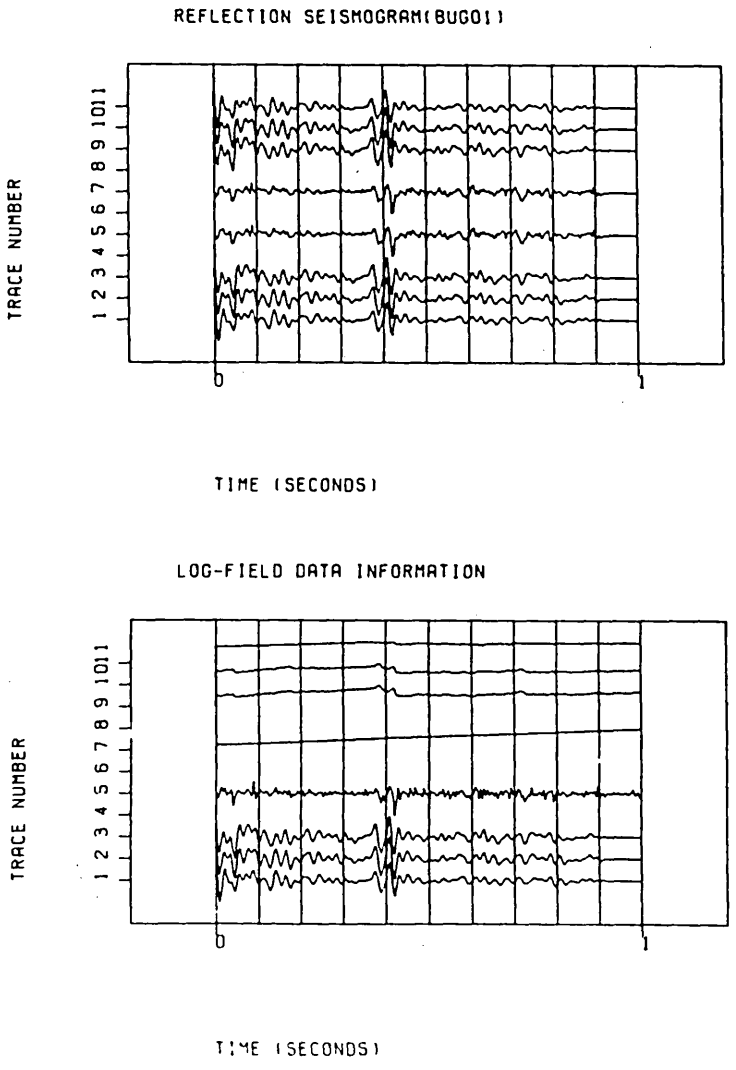
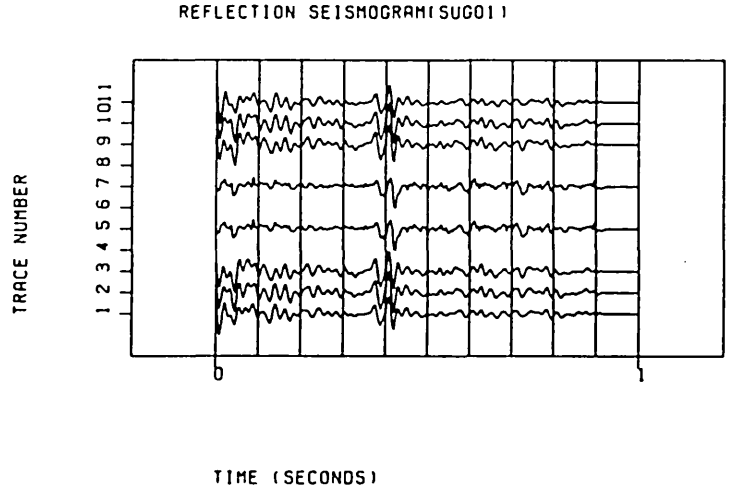


Fig. 5.13b: Subsurface Information (Log Analysis)

Fig. 5.14a: Synthetic: Primaries, Multiples & Source Ghosts (Residual - Analysis) Correlation = 0.40



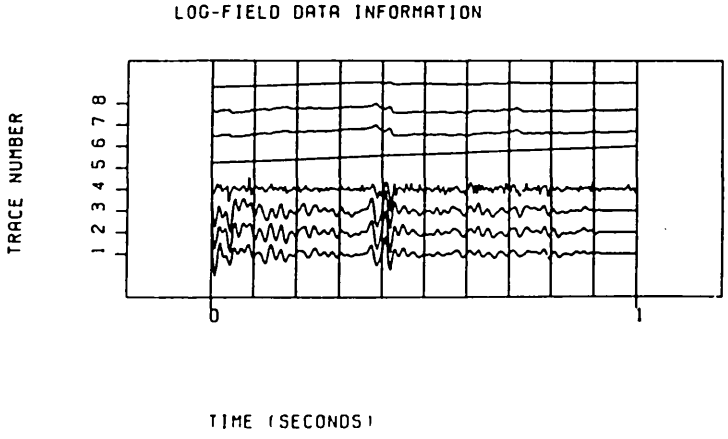
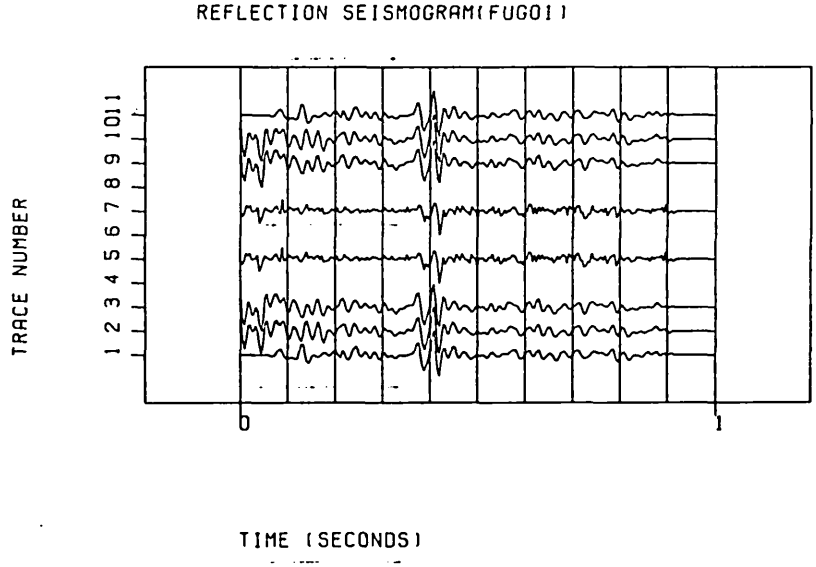


Fig. 5.14b: Subsurface Information (Log Analysis)

Fig. 5.15a: Synthetic Primaries, Multiples and Source ghosts (White's Model, Y_c = 0.40)



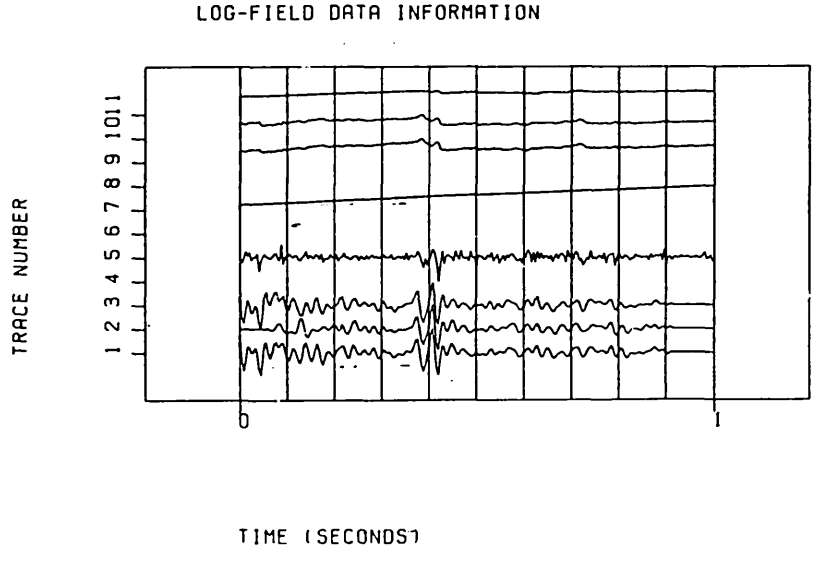


Fig. 5.15b: Subsurface Information (Log Analysis)

Fig. 5.16a: Synthetic: Primaries, Multiples and Source Ghosts (least-squares optimization)

$a_1 = 0.60$ $\quad \alpha_1 = 0.40$

$a_2 = 0.20$ $\quad \alpha_2 = 0.30$

$a_3 = 0.80$ $\quad \alpha_3 = 0.20$

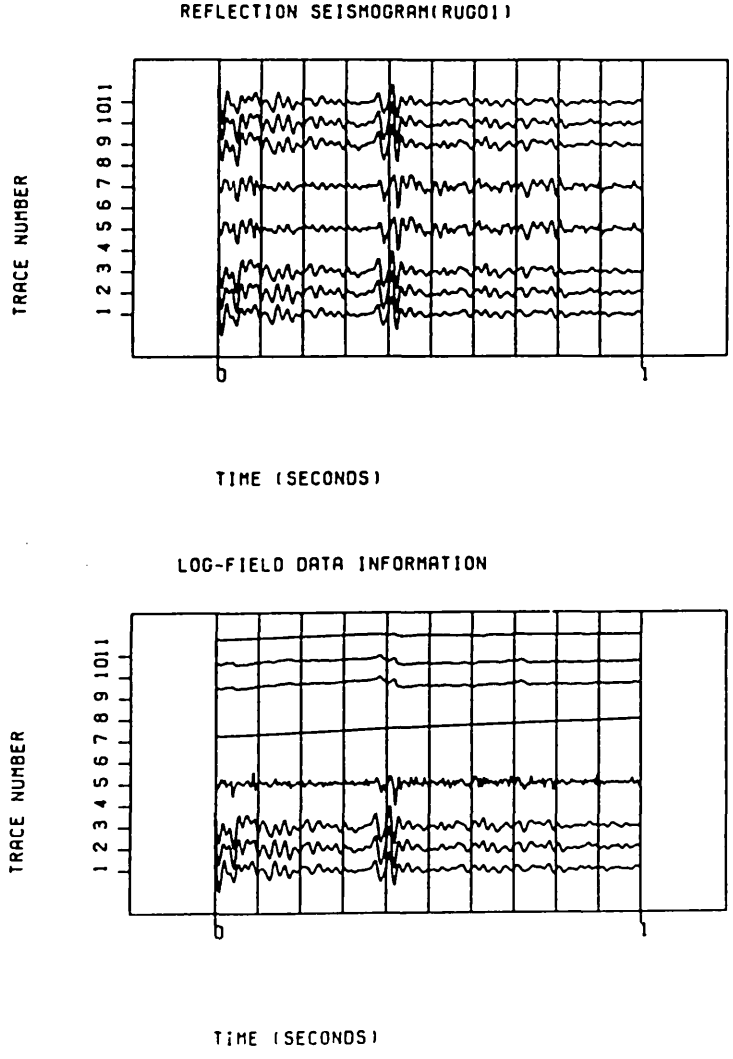


Fig. 5.16b: Subsurface Information (Log Analysis)

The change in magnitude is about Ø.Ø2.

In a third experiment, we included the effect of the source ghosts to the multiples. We again used our four test programs. The inputs are, primaries only, all possible multiples plus source ghosts, and the results are shown in figures (5.13 - 5.16). The results suggest that the effect of source ghosts is again not marked. The magnitude of γ_c, in each case is approximately the same as in experiment one.

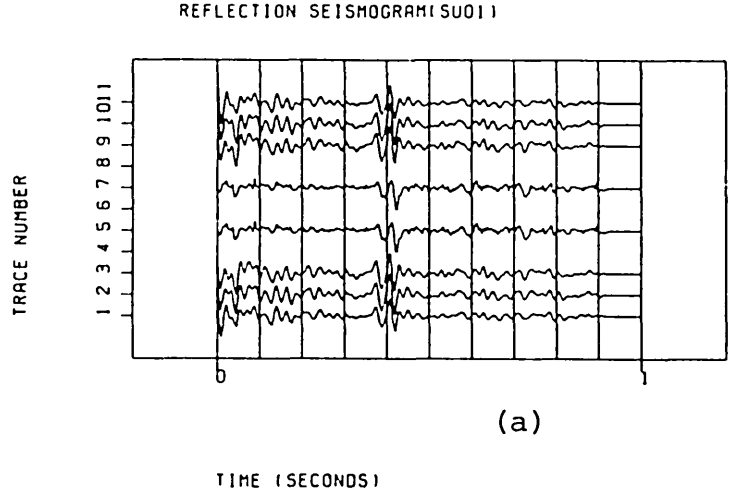
We have tested all the methods using one well. For effective comparison we decided to test all the wells using one technique. The method of straight residuals is applied to all the wells. Figures (5.13-1-5.16-1) show the results. Wells (cpv-12 and cpv-Ø3) each has γ_c-value of Ø.40 and Ø.22 respectively, while line cpv-1OA has γ_c-value of Ø.4 with well cpv-1Ø. The results compare favourably with the previous experiments.

The fifth and final experiment was carried out with all the wells and all the seismic lines. The order of distribution of wells, seismic lines and computer programs are as follows;

(1)	BENSOL	CPV-Ø3	CPV-Ø3A
(2)	OTNES	CPV-12	CPV-12A
(3)	FAITH	CPV-1Ø	CPV-1ØB
(4)	DESIGN	CPV-1Ø	CPV-1ØA

The first configuration (1) for example, implies that the computer program, BENSOL, used the information from well, cpv-Ø3, and spec line cpv-Ø3A to estimate

Fig. 5.13.1 Method of S Residuals for all wells. Well, cpv = 10(Yc = 0.4)



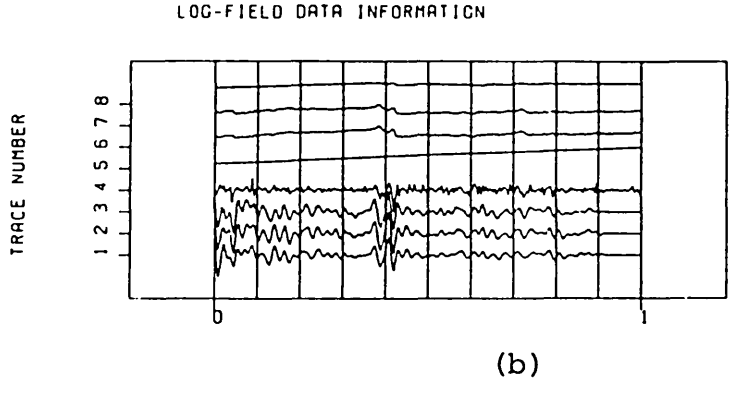
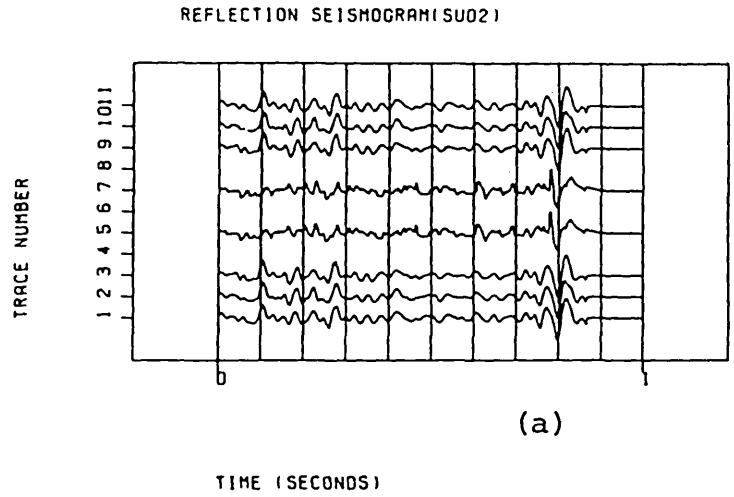


Fig. 5.14.1: Method of S. Residual, well, cpv-12 (γ_c = 0.4)



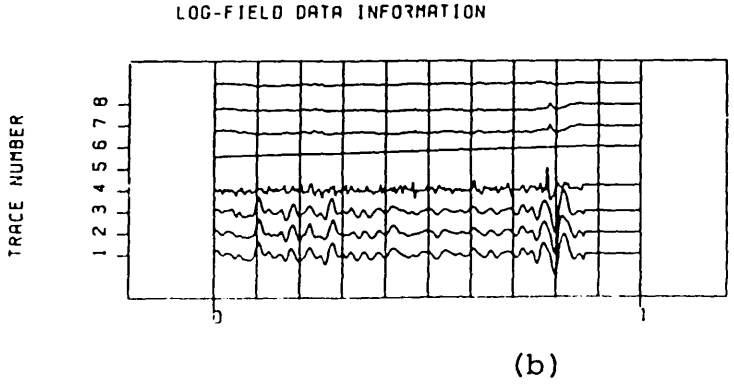


Fig. 5.15_1: Method of S Residuals, line, cpv-10A
(Yc = 0.4)

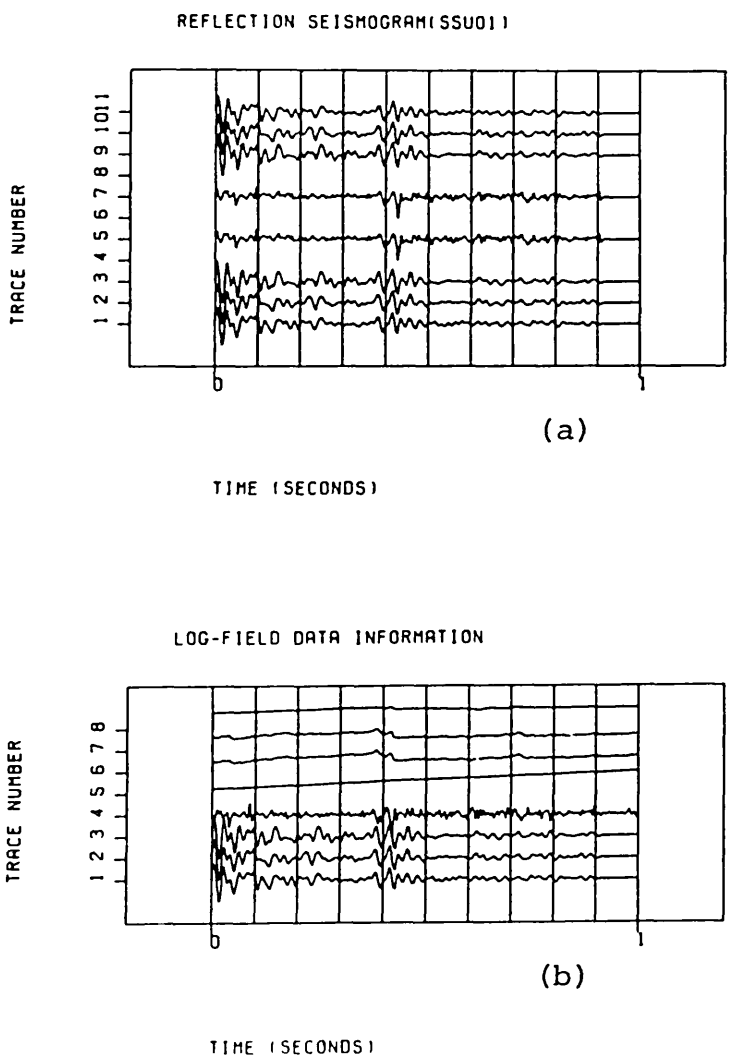


Fig. 5.16.1: Method of S Residuals well, cpv-03 (γ_c = 0.22)

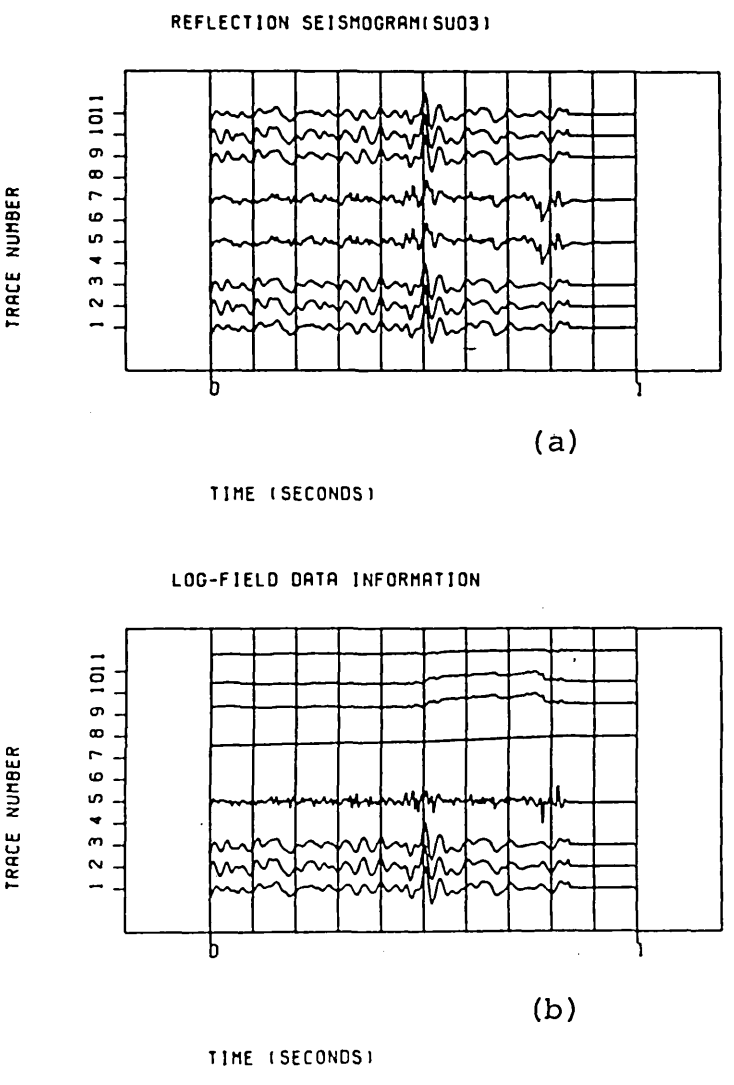
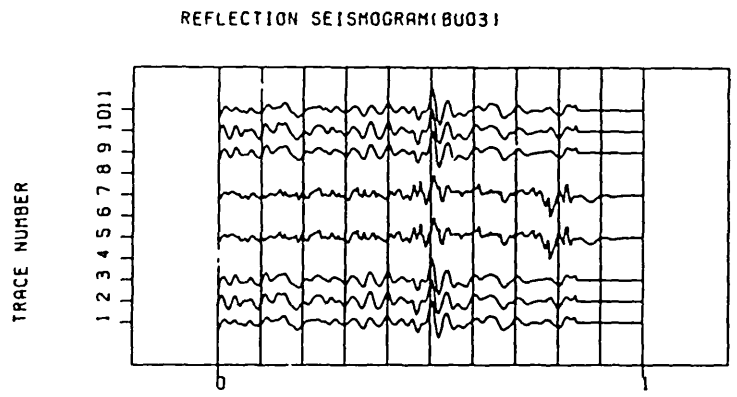


Fig. 5.17a: Synthetic, Primaries, well-cpv-03 (Matrix Analysis) (γ_c = 0.23)



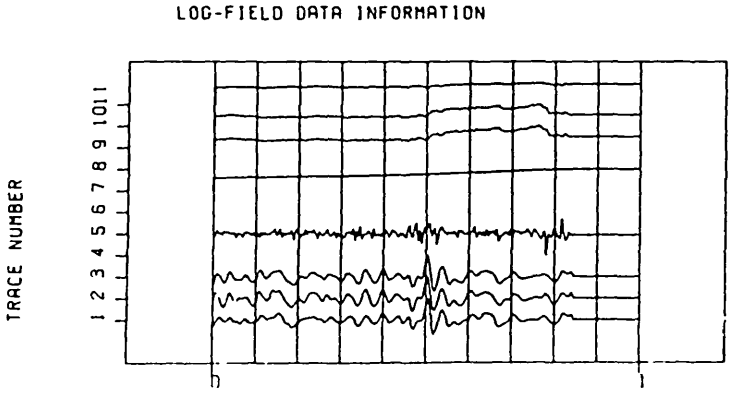
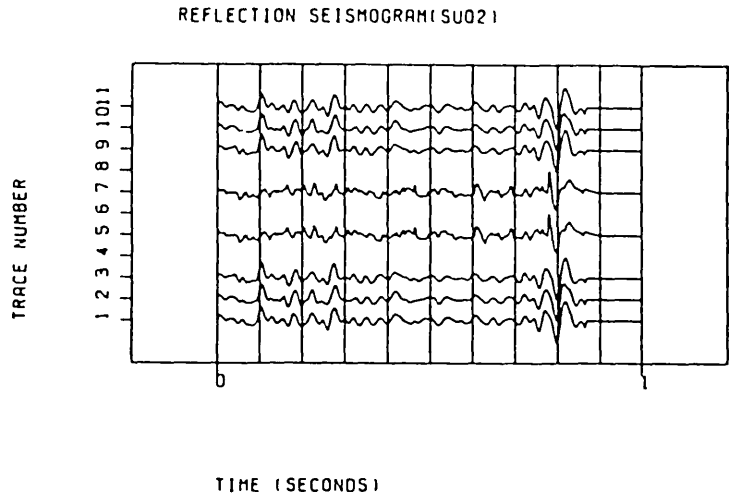


Fig. 5.17b: Subsurface Information (Log Analysis - well cpv-03).

Fig. 5.18a: Synthetic: Primaries only, multiples (Residual Analysis) $\gamma c = \emptyset.4$ (well, cpv-12)



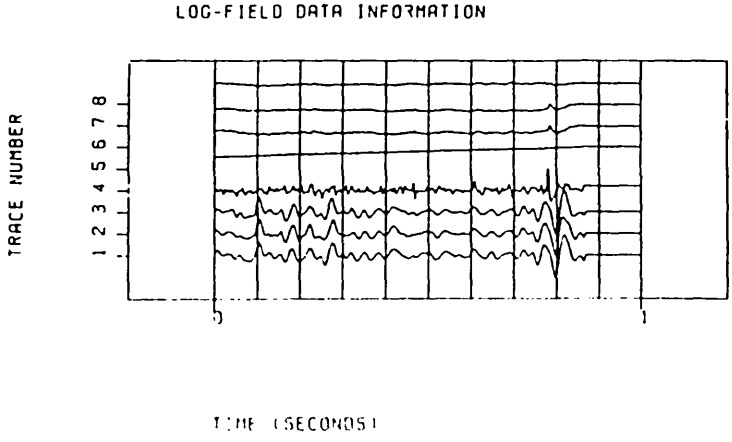
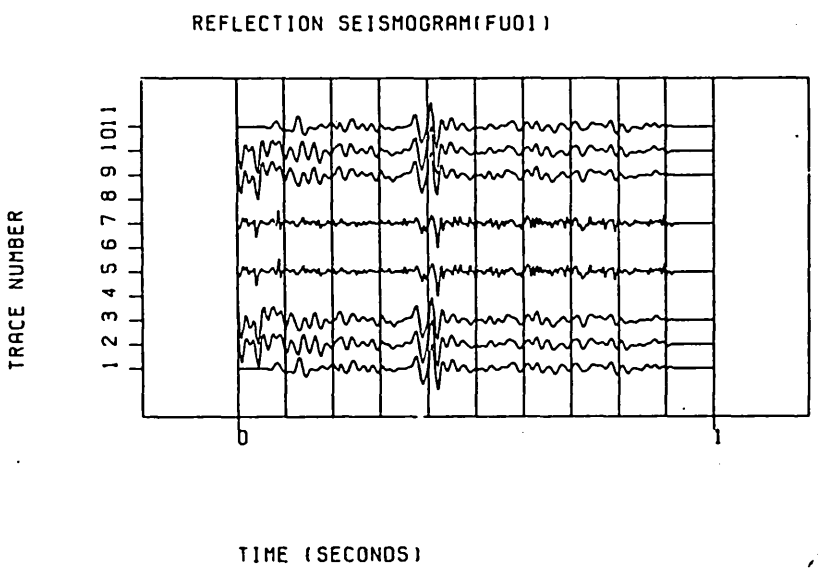


Fig. 5.18b: Subsurface Information (Log Analysis - cpv-12)

Fig. 5.19a: Synthetic Primaries, Multiples, (Whiteps model, Y_c = Ø.4O, Well cpv-1Ø, p. 4O, well, cpv-1Ø).



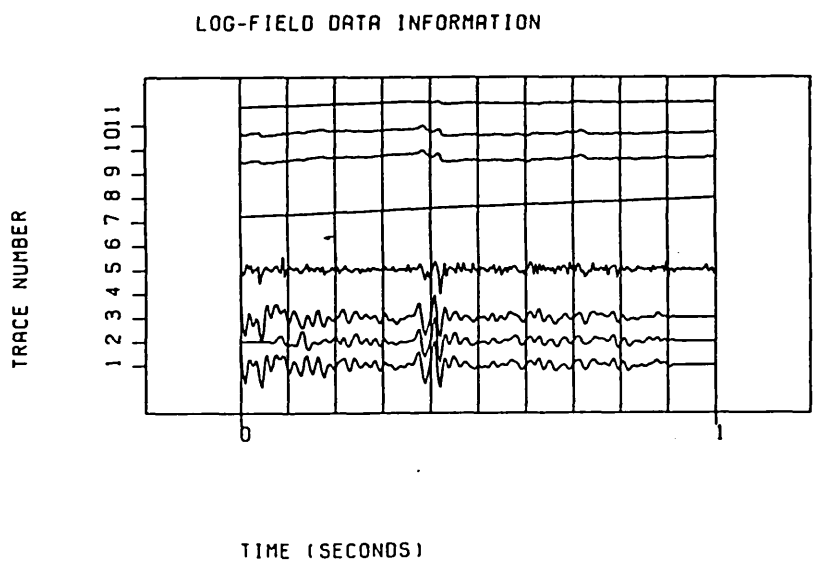


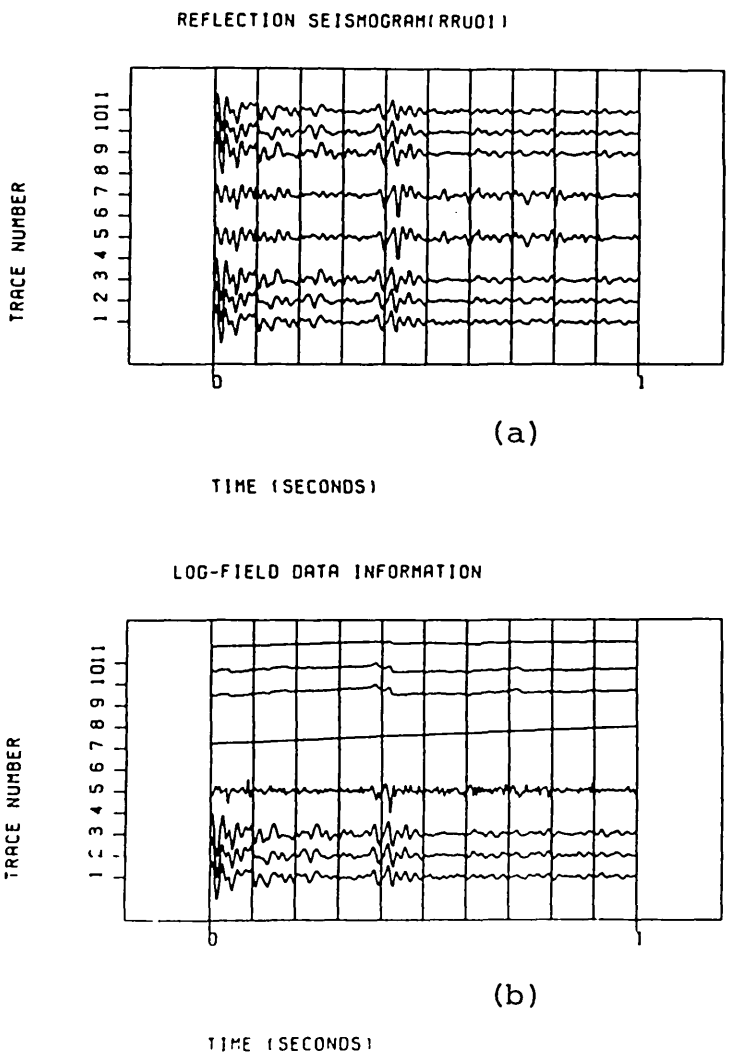
Fig. 5.19b: Subsurface Information (Log Analysis, well-cpv-1Ø).

Fig. 5.20: Least-square optimization line cpv-10A

$a_1 = 0.63 \quad \varphi_1 = 0.37$

$a_2 = 0.70 \quad \varphi_2 = 0.30$

$a_3 = 0.80 \quad \varphi_3 = 0.20$



the desired wavelet, generate the synthetic seismogram and compute other required parameters as necessary. There was no specific order in the choice of the programs, the corresponding wells and spec. lines. The only essence is to compare the existing with new results. Figure (5.17) - (5.20) relay the results as they were computed. The results suggest that wells cpv-1Ø and cpv-12 generate synthetics which match the corresponding field stacks much more closely than the match obtained by matching well cpv-Ø3 and its equivalent field stack. On the other hand, well cpv-1Ø, produces a better match than well cpv-12. All the deductions are made as in the first three experiments following the magnitude of the value of the correlation coefficients, CCOEF, α (the normalised mean square error), and Ω (the goodness measure) as well as the estimate of X^2 (chi-squared).

SUMMARY

Three efficient techniques, the matrix partition technique, the method of straight residuals and the optimum least-squares technique, have been developed and these compare relatively well with the method of White (1980) as far as wavelet estimation, synthetic seismogram generation, and matching of well log generated seismogram with field observed seismograms are concerned. The results show that the estimated synthetics sufficiently match the field observations.

The major advantages of the three introduced techniques over White's model are that they may be used

in the absence of complex variable evaluation routines. This is particularly important in installations where complex variable evaluation routines are not part of the computer software. The three techniques also can save a lot of computer time and space when compared to White's model. The estimate of the computer time is based on the number of multiplications involved in the computer evaluation of the necessary algorithms, while the computer space depends on the amount of core memory necessary for successful executions. Besides, the mathematical understanding and applications required for each of the three techniques are simple and straight forward, a medium mathematical ability is sufficient and enough to follow the three techniques and their methods of application. This may not be the case when using White's model.

However, if three or more input channels are absolutely necessary for our problem solution, then the method of White (1980) becomes indispensable, and the three methods we introduced demand modification. As far as seismic matching of seismograms, estimation of synthetic source wavelets and synthetic seismograms are concerned, solution of more than two-inputs is not a set back to using any of the three introduced techniques. This is because the present state of the art in seismic processing and analysis, can comfortably represent the entire seismic signal by two channel inputs, comprising the primaries in one channel and the noise (including all multiples) in the second channel. We therefore conclude that the techniques we have introduced are sufficient

CHAPTER 6

Further Developments.

The intention of this chapter is to investigate some other ways to improve our match. Many geophysicists are often inclined to suspect the well-log information as the more probable cause of mismatch (Thomas, 1977). Since we could not further improve the available field stacks, we decided to investigate more closely the synthetic seismogram components, V_{12} - the impulse responses.

The first step in this direction is to generate the impulse responses by a completely different approach. The new approach generates the impulse responses from a localised source, and includes the effect of attenuation and geometrical spreading, so that a set of synthetic traces are generated by convolution between the impulses and recorded far-field signature. The computations are done in the frequency - wavenumber domain so that the convolution becomes an ordinary multiplication process.

6.10 Impulse Responses Generated from localised source using double fast fourier synthesis, with attenuation included, in frequency-wavenumber domain.

We have already discussed techniques for the calculation of normal incidence synthetic seismograms. In such calculations generally, a vertically travelling plane P wave is allowed to interact with a multilayered model. The effects of seismic energy loss are all ignored

except those due to reflection and transmission. Trorey (1972) adopted an approach which permits the inclusion of attenuation. More often than not, shear wave influence is neglected in preference to an acoustic approximation of the layers. This form of approximation holds true for a plane P wave at normal incidence to the horizontal stratification but any oblique incidence generates shear waves. Seismic waves are better generated from concentrated sources. The use of a single plane P wave for even vertical reflections is inadequate. However, the superposition of a sufficiently large number of plane waves allows the simulation of a localised source. It is this localised-point source that accounts for the geometrical effect. This is the approach adopted by Kennett (1979) to generate his set of theoretical synthetic seismograms. A similar approach was earlier adopted by Fertig and Muller (1978, 1979), calculating seismograms at large offsets from a point source with particular interest in conversions from P and S waves. In their work, they constructed the full response of some coal measures including the effects of geometrical spreading in the computed theoretical seismograms. However, unlike, their approach, the method of Kennett (1979) makes it possible to compute the primaries and multiples independently.

In the present work, the two methods have been adapted such that a set of impulse responses is generated using the velocity, density, and depth, derived from a well-log. Using the computed responses, and the recorded

far-field signature (as source wave form), we show how a set of synthetic seismograms for small offsets may be constructed. The seismograms compare favourably with the field observed seismograms. All computations are done in the frequency and wave number domain so that the synthetic seismograms are finally recovered in the time domain by the use of the double fast Fourier transform.

6.20 Basic Theory of Analysis

In this section we do not intend to give full details of the methods of Kennett (1974, 1975, 1979) or of Fertig et al. (1978, 1979). An interested reader is referred to those references.

Now, using the method of Kennett (1979) and working in the frequency and wavenumber domain we can represent the wavefields interacting with a stack of layers and within a given half space in terms of their vertical and horizontal plane wave components, $W(x,z,t)$ and $U(x,z,t)$, as shown;

$$W(x,z,t) = \int_{-\infty}^{\infty}\int \bar{W}(k,z,w)\, e^{ikx-iwt}\, dkdw \qquad (6.01)$$

$$U(x,z,t) = \int_{-\infty}^{\infty}\int \bar{U}(k,z,w)\, e^{ikx-iwt}\, dkdw \qquad (6.02)$$

These wave components are connected to each other by a vector the surface displacement vector, $\bar{W}_o(k,w)$ which is also a function of frequency, w, and wavenumber, k, so that we define

$$\bar{W}_o(k,w) = \begin{pmatrix} \bar{U}(k,0,w) \\ \bar{W}(k,0,w) \end{pmatrix} \qquad (6.03)$$

or

$$\bar{W}_o(k,w) = \bar{W}(k,0,w) \qquad (6.04)$$

Equations (6.03) and (6.04) define the displacement vectors for cases where either the elastic or the acoustic approximation has been considered.

Similarly, if we decompose the wavefield within each layer into an up and downgoing part, V^u and V_D, then we can also define at each level in the medium a reflection matrix R^D, such that the up and downgoing waves are related as shown.

$$V^u = R^D V_D$$

where for elastic fields

$$R^D = \begin{pmatrix} R^D_{pp} & R^D_{ps} \\ R^D_{sp} & R^D_{ss} \end{pmatrix}$$

and for acoustic fields

$$R^D = R^D_{aa}$$

R^D, is expressed in terms of the acoustic reflection coefficients, and by definition, R^D_{pp} are the reflection coefficients from downgoing P to upgoing p waves, or R^D_{sp} are the reflection coefficients from downgoing P to upgoing S waves.

Following the method of Kennet (1974) the displacement $\bar{W}_o(k,w)$ may be written thus;

$$\bar{W}_o(\underline{k},w) = \left[MD+MuR^D\right]\left[ND+NuR^D\right]^{-1} S(k,w) \qquad (6.05)$$

The above relation expresses the displacement in terms of the overall reflection matrix R^D and the source function $S(k,w)$, where M_D, M_u are the transformation matrices from wave amplitudes to displacements and N_D,N_u are the corresponding transformation matrices from wave amplitudes to stresses. Actually, expression (6.05) includes all surface reflections but the expression can be decomposed further so that $\bar{W}_o(k,w)$ takes the form

$$\bar{W}_o(k,w) = \left[Mu+M_D \tilde{R} \right] R_D n_D^{-1} S(k,w) + \ldots \qquad (6.06)$$

where (6.06) includes only those waves which have been reflected once beneath the surface through the term R^D, while $\left[M_u+M_D\tilde{R} \right]$ is the modification of displacement due to the free surface, $\tilde{R}$ is the free surface reflection matrix defined;

$$\tilde{R} = - n_D^{-1} n_u$$

Thus for a given set of w,k we can represent the surface displacements according to the relations:

$$\bar{W}_o(k,w) = MN^{-1}S(k,w) \qquad (6.06)$$

so that depending on our type of approximation (elastic or acoustic), and on the choice of either free or no free-surface reflections, we can define the M, N parameters as shown:

(a) For elastic fields with all surface reflections included:

$$M = \begin{pmatrix} p(I+R_{pp}) + q_\beta R_{sp} & pR_{ps}+q_\beta(1+R_{ss}) \\ -q_a(I-R_{pp}) + pR_{sp} & -p(I-R_{ss})-q_\alpha R_{ps} \end{pmatrix}$$

$$N = \mu_{ow}{}^2 \begin{pmatrix} 2pq_a(R_{pp}-I)+rR_{sp} & 2pq_aR_{ps} + r(R_{ss}-I) \\ -[r(I+R_{pp})-2pq_\beta R_{sp}] & 2pq_\beta(I+R_{ss})-rR_{ps} \end{pmatrix} \qquad (6.07)$$

where $p = k/w$

$\mu_o = \rho_o \beta_o{}^2$

$q_a = (1/\alpha_o{}^2 - p^2)^{\frac{1}{2}}$

$q_\beta = (1/\beta_o{}^2 - p^2)^{\frac{1}{2}}$ $\qquad I_m q_a, q_\beta \geq 0$

$r = 1/\beta_o{}^2 - 2p^2$

(b) Elastic fields, no free surface reflections

$$M = iw \begin{pmatrix} pcR_{pp} + q_\beta dR_{sp} & pcR_{ps} + q_\beta dR_{ss} \\ -q_a dR_{pp} + pcR_{sp} & -q_a dR_{ps} + pcR_{ss} \end{pmatrix}$$

$$N = \mu_o w^2 \begin{pmatrix} -2pq_a & -r \\ -r & 2pq_\beta \end{pmatrix} \qquad (6.08)$$

and

$C = 4q_a q_\beta/(\beta^2 \Delta)$

$\Delta = 4p^2 q_a q_\beta + r^2$

$d = 2r/(\beta^2 \Delta)$

(c) Acoustic approximation - all surface reflections

$$M = q_a (I - R_{AA})$$
$$N = iw\rho (I + R_{AA}) \qquad (6.09)$$

(d) Acoustic Approximation - no free surface reflections

$$M = 2\, q_a R_{AA}$$

$$N = i\, w\rho \tag{6.10}$$

The next important step is to compute the total reflection matrix R^D for all the layering beneath the surface. This is accomplished using an iterative scheme for the reflection matrix (Kennet, 1974). By the application of this iterative technique, the total reflection matrix becomes;

$$R^{\Delta}_{j-1} = r^D + t^u \bar{R}^D_j \left[I + \sum_q (\underline{r}^u \bar{R}^D_j)^q \right] t^D \tag{6.11}$$

where t and r represent the interface transmission and reflection matrices, and the index attached to them denotes the direction of wave travel.

Equation (6.11) includes all internal multiples, though we can actually identify some specific contributions as desired. For example, if we desire only the primary reflections then

$$R^D_{j-1} = r^D + t^u \bar{R}^D_j t^D \tag{6.12}$$

while if we want to include the first multiples or the peg-legs, then

$$R^D_{j-1} \triangleq r^D + t^u \bar{R}^D_j (I + r^u \bar{R}^D_j) t^D \tag{6.13}$$

The total reflection matrix R^D is in reality the so-called complex reflectivity function $R_D(w,k)$ (Hughes et al., 1983), Fertig et al. (1978). Methods of computing the reflection and transmission coefficients have been

efficiently treated and made considerably faster with computer routines by the following authors; Čerevený et al. (1971), Braile et al. (1976) and Kind (1976). The general algorithm also allows one to take into account the reflection coefficients for reflected and incident s waves. The total reflection matrix (or otherwise the reflectivities) automatically incorporates all conversions from P to S waves or conversions from S to P waves in the reflecting medium. Once the total reflection matrix R^D is computed, and a suitable source term assigned, it becomes a simple matter to evaluate the expression (6.06) to obtain the surface displacements.

6.30 The theoretical Synthetic Seismogram Generation

We have discussed so far how we obtain the surface displacement response for a single plane wave component, though in the absence of attenuation. In this section we shall discuss how we can generate a set of theoretical seismograms by the superposition of these displacement responses. The method of inclusion of attenuation via a complex velocity profile is well treated in Kennett (1979).

Now, we can compute the surface displacements W_o from the plane wave components by superposition if we can evaluate the intergral:

$$W_o(x,t) = \int_{-\infty}^{\infty} dw\, e^{-iwt} \int_{-\infty}^{\infty} dk e^{ikw}\, \bar{W}_o(k,w) \qquad (6.14)$$

The details of integral evaluations, in addition to the introduction of velocity filtering to ease the

limits of integration may be found in the same paper as mentioned above.

As we may recall, our aim is to recover the vertical, horizontal or both displacement responses at the surface. These responses depend on the approximations (elastic or acoustic) and on the levels of reflection signals (primaries, multiples, etc.), hence equation (6.14) takes the form

$$W_o(x,t)e^{-\lambda|x|} \triangleq \int_{-wm}^{wm} dw e^{-iwt} \int_{0}^{w/a_o} dk \cos kx \; \bar{W}_o(k-i\lambda, w) \tag{6.15}$$

where the limits of integration and the necessary transformations have been deduced as stated earlier. Equation (6.15) can then be evaluated using the double fast Fourier transform, thus recovering the seismograms in the time domain. The use of the Fourier analysis is facilitated by the fast Fourier algorithm (Cooley and Tukey, 1965).

The frequency interval is $1/T$ and the frequency ranges from 0 to the Nyquist frequency defined f_m, where as usual

$$fm = 1/(2\Delta T)$$

ΔT is the time sampling interval. This frequency condition is necessary if we have to avoid the old problem of frequency aliasing. The choise of T on the other hand is limited by the computer time for a modest work. For example, a 512 time samples with 420 layers takes up to 600 cpu secs (- off-peak time) to run. The bandwidth therefore, is often adjusted. In the present work, the low and upper frequencies are taken

to correspond to the values determined from seismic field processing (8(hz) - 60 (hz)).

The aliasing problems in the wavenumber domain are generally more severe and every attempt was made to avoid a relatively coarse discretisation in terms of Δx (the distance sampling). In general Δx varies from one geophone spacing to a little less than half of it. Besides, the inclusion of attenuation into the velocity model (Kennett, 1979) leads to damping in both space and time hence reducing aliasing problems.

Now, returning to equation (6.14) we recall that the most important step in the evaluation of the integral equation is the computation of $\bar{W}_o(k,w)$, where $\bar{W}_o(k,w)$ contains the complex reflectivity function $R_D(k,w)$. Actually, the computation of $R_D(k,w)$, is the most time consuming step in the computations, though in reality the Fourier transformation is over the function $W_o(k,w)$. Equation (6.14) may be seen in terms of equation (4) of Fertig et al. (1978). On the basis of this relationship, we can then define two probable options in the evaluation of (6.15) viz:

(a) We can recover the displacements either by Fourier and inverse Fourier transformations of the displacement function $\bar{W}_o(k,w)$ or

(b) by similar transformations but using only a component of the displacement function, $\bar{W}_o(k,w)$. This component of the displacement function is the reflectivity function $R_D(k,w)$. The transformations of $R_D(k,w)$ alone produces the so-called impulse responses of the layered medium.

Such responses may be compared with those generated through the linear filter model by looking at the numerical values of the match between their synthetics and the corresponding field observations.

The above is actually the path adopted in this work. The computer program, KEN, for the evaluation of (6.15) was set such that any of the two options could be computed. To obtain the set of theoretical synthetic seismograms we convolved the reflectivity function with a defined source function (in the frequency domain). Further to the computations of the reflectivity function, options are set to include free-surface reflections, to compute only primaries, primaries plus first multiples, or primaries plus all possible multiples, in each layer or as desired. In this respect, the present method resembles the previous methods of synthesis but differs in the sense that attenuation has been included, besides the use of Fourier superposition of plane waves ensures the simulation of a point-localised source.

The log-information used in the synthesis is from well, cpv-1Φ defined in the last chapter. The closest line is cpv-1ΦB. The simplest way to test the relationship between the new generated seismograms and the field observations is by use of the Pearson's product moment correlation coefficient(γ_c). When computed, the value of γ_c for the theoretical and field trace came to a value of 0.49. Figure (6.01) shows some plots of the two sets of seismograms.

This value of γ_c, is the highest value so far computed in this work. This gives a change in magnitude

Fig. 6.Ø1 Kennett's Model (Source function included) Correlation (Y_c = Ø.49)

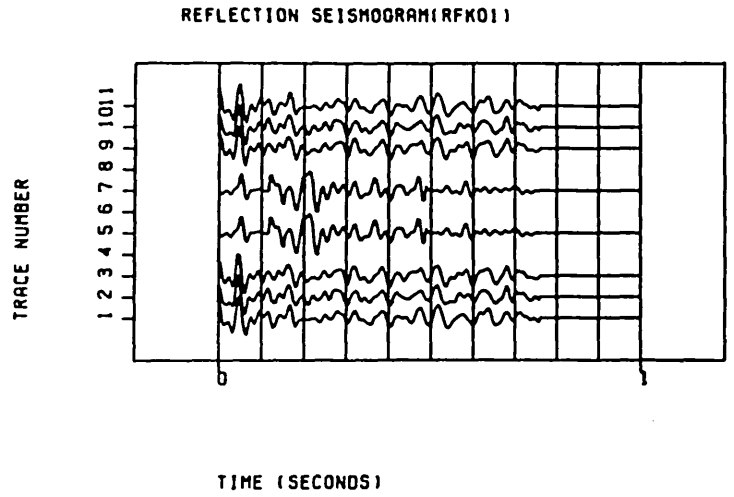
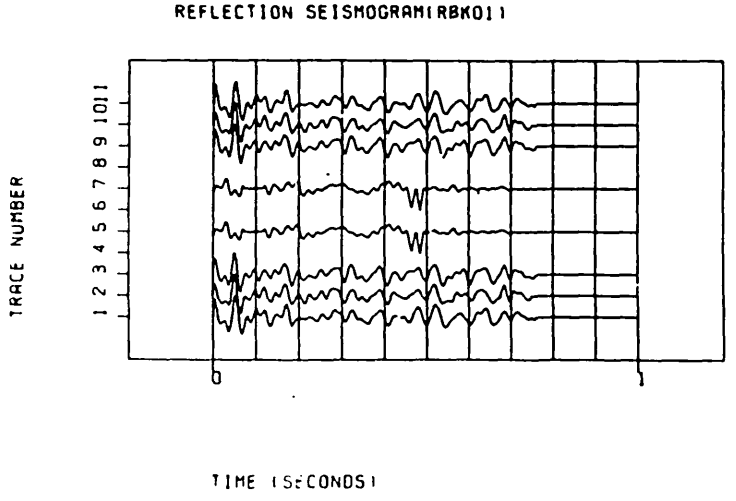


Fig. 6.Ø1.1: Kennett's Model (No source function) Correlation (Y_c = Ø.34)



of about 0.1 or more when compared to the values computed in the last chapter. This is encouraging. This change in γ_c suggests that we may not have reached the limit of accuracy in matching. It may be either that the old methods of synthetic generation are themselves deficient or that we have incorporated into the new approach a process which so far is not considered in the old techniques.

Kennett's model incorporate the following:

(1) Geometrical spreading

(2) Attenuation

(3) Elastic approximation

The first of these is corrected for in the field traces. We choose a constant attenuation for all the layers. Owing to the large computer time involved (600 cpu secs. in CDC, at off-peak) we could possibly cover less than 200 m offset-distance for the 420 layers. The elastic and acoustic approximations differ particularly at fairly large offsets and angles of incidence for which conversion to shear waves can become important (Kennett, 1979). This is also observed in the present work. Since the offset distance is comparatively low, the elastic and acoustic γ_c-values are virtually the same.

From the foregoing points, we decided to generate the same responses but without the source function. This enables us to investigate the effect of the source function. Besides, we can directly compare γ_c for this model with the linear filter model. Fig. (6.01-1), shows the results for the Kennett's theoretical seismograms without the source function. The value of γ_c is 0.34.

When source function was included, the value was Ø.49 We therefore conclude that the source function is probably more responsible for the high value of γ_c hence the approach adopted in the next section.

6.40 Filtering the Impulse Responses (From Linear Filter Models)

As we have seen, the last section suggested the need to use filtered reflection sequences as input parameters to our similarity measurements, and matching analysis deduced in chapter five.

The three main filtering processes which are usually common to routine seismic data processing are used in the present method of impulse filtering. These include;

(a) The minimum phase bandpass filtering, here the pass region ranges from 8(hz) to 60(hz) at (18-24) dB/OCT. This is in reality the desired output of the source signature compensation of the type often applied to most seismic data.

(b) The second filter was a time-variant zero phase bandpass. The parameters are as follows;

At 100 ms

f_1 = 14(hz)

f_2 = 60(hz)

S_1 = 24(dB/OCT)

S_2 = 36(dB/OCT)

where f_1, f_2, S_1, S_2 are the lower, upper, frequencies and slopes.

Similarly,

At 850 Ms	At 3200 Ms:
f_1 = 12(hz)	f_1 = 10(hz)
f_2 = 55(hz)	f_2 = 45(hz)
S_1 = 24(dB/OCT)	S_1 = 24(dB/OCT)
S_2 = 24(dB/OCT)	S_2 = 24(dB/OCT)

This second filter is the final time variant filter applied to the seismic field data.

(c) The third filter, is a time variant zero phase lowpass defined as follows:

At 100 Ms

Frequency cut-off = 60(hz)
slope = 36(dB/OCT)

At 1100 Ms

Frequency cut-off = 36(hz)
slope = 12(dB/OCT)

At 2300 Ms

Frequency cut-off = 30(hz)
slope = 18(dB/OCT)

To apply this third filter, the spectrum of seismic data is usually compared with that of the synthetic data after the application of (a) and (b) above. This comparison generally gives an insight into the degree of the earths attenuation. The third filter actually approximates to this earth filter effect.

The above filtering approach is typical of the type used in routine seismic analysis for visual correlation of field and synthetic data but has not been exploited quantitively.

In the above example we have only described the filtering steps as applied to well cpv-10. Similar filtering analyses have been applied to each of the remaining two wells so that as in chapter five we set the results as follows:

Figures (6.04) - (6.07) show the plots and related results obtained by estimating the wavelets (from the filtered impulse responses) and generating the synthetic seismograms using:

(i) The matrix partition technique

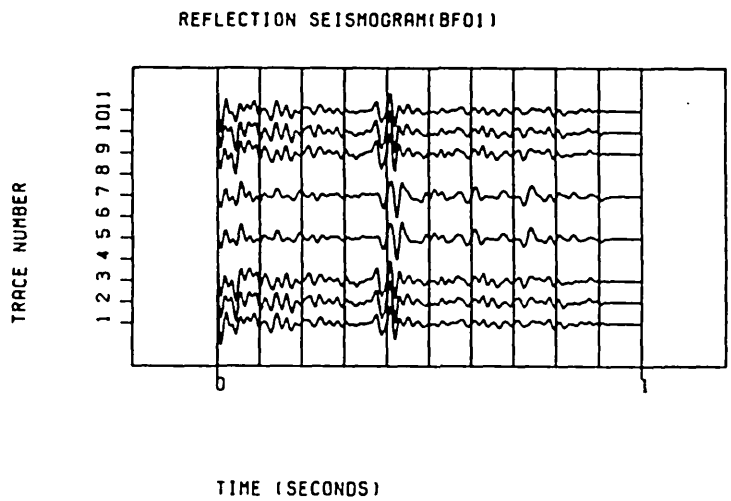
(ii) The method of straight residuals

(iii) The Whites model.

In figure (6.04) T_5 is the computed synthetic seismogram. As in chapter five, the synthetic has been plotted with the rest of the stack for visual analysis. The match between the synthetic and the field stack is very encouraging. This is seen from the value of the correlation coefficient which is 0.52 and it is about 0.2 higher than the unfiltered result in figure (5.00). The peaks and troughs of the synthetic and the field seismogram correspond more closely than in figure (5.00).

Similarly, and as expected, the results from figure (6.05) through (6.06) follow the same pattern as in chapter five, figure (5.01) through (5.02). The correlation coefficient in the two cases changes by 0.2 as compared to the unfiltered components in figure

Fig. 6.04a: Matrix Analysis (correlation = 0.52)
The two middle traces are computed synthetics (well-cpv-10).



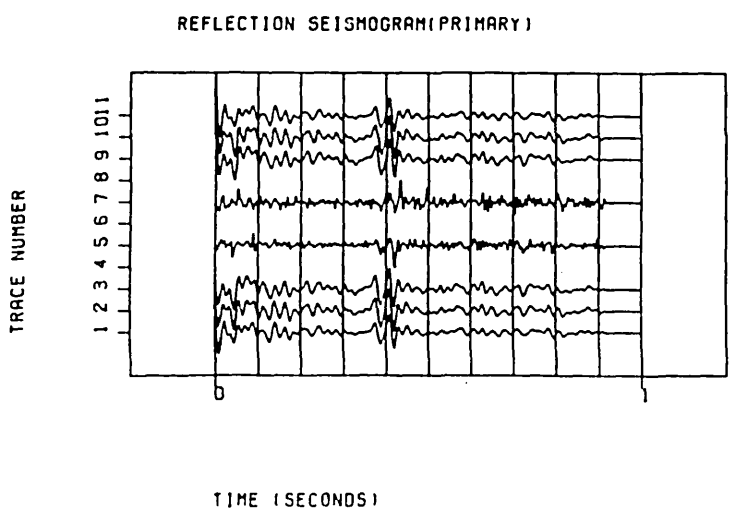
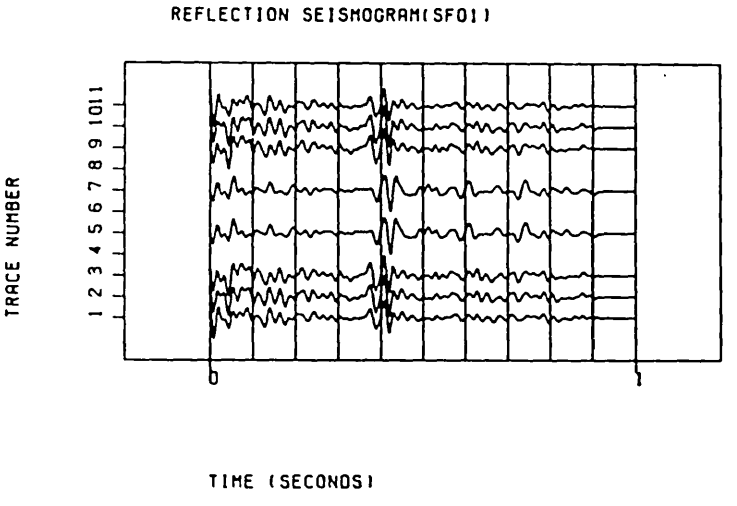


Fig. 6.04b: Matrix Analysis
The first three and the last three traces are the field stacks. The middle two traces are the computed responses (unfiltered).

Fig. 6.05a: Residual Analysis (correlation = 0.53)
X^2 = 50.94 (critical value = 124.34)



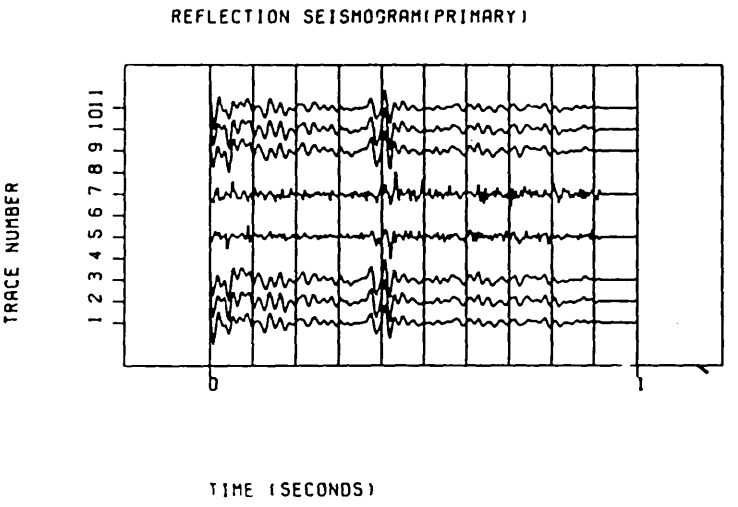
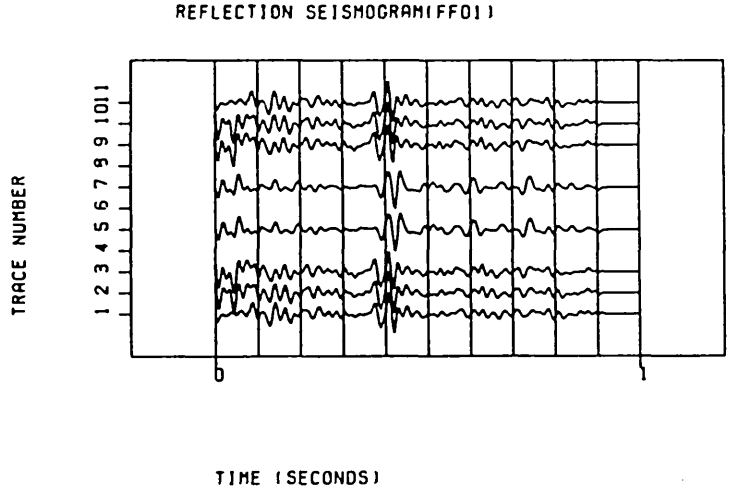


Fig. 6.05b: Field stacks and computed responses (cpv-10)

Fig. 6.06a: White's model (correlation = Ø.51). Line cpv-1ØB



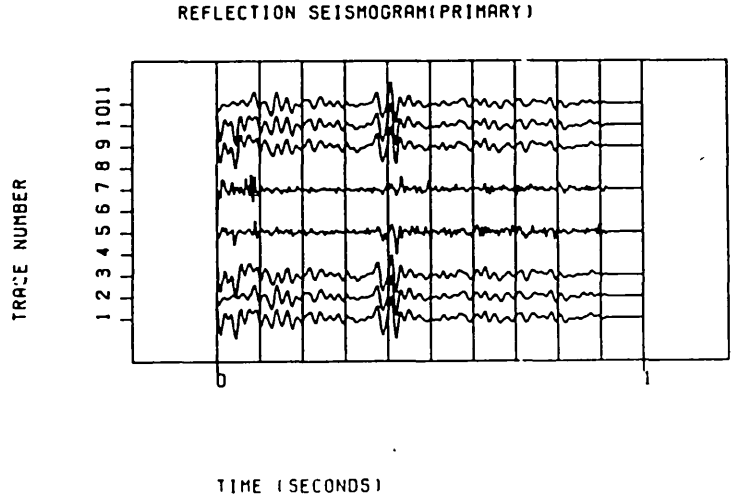


Fig. 6.06b: Field stacks and computed responses (cpv-10).

(5.01) and (5.02) (see the plots for details).

Again, and as in the last chapter, using the optimum least-squares technique, we set the values of α, and Ω, the comparing parameters as follows;

(1) Primaries only; $\alpha_1 = 0.41$ $\Omega_1 = 0.59$
(2) Primaries plus White Series; $\alpha_2 = 0.67$ $\Omega_2 = 0.33$
(3) Random White Series, $\alpha_3 = 0.80$ $\Omega_3 = 0.2$

Figure (6.07) shows the plotted results using this technique. The results are in agreement with the other three techniques, having a match change of approximately 0.2 in magnitude. This can be deduced from the difference between the old and new values of CCOEF, or (from the change in the values of α_1 and Ω_1) respectively.

Following a similar approach as in chapter five, we investigated for the effects of transmission losses and source ghosts. Figure (6.08) - (6.11) are the plots and related results from the computations. When the synthetic seismograms are computed (with primaries plus transmission losses included), the synthetics are then matched with the corresponding field stacks, the magnitude of the match changed by 0.02 as in the previous experiments. The transmission factor therefore, has not introduced a very remarkable change in this match.

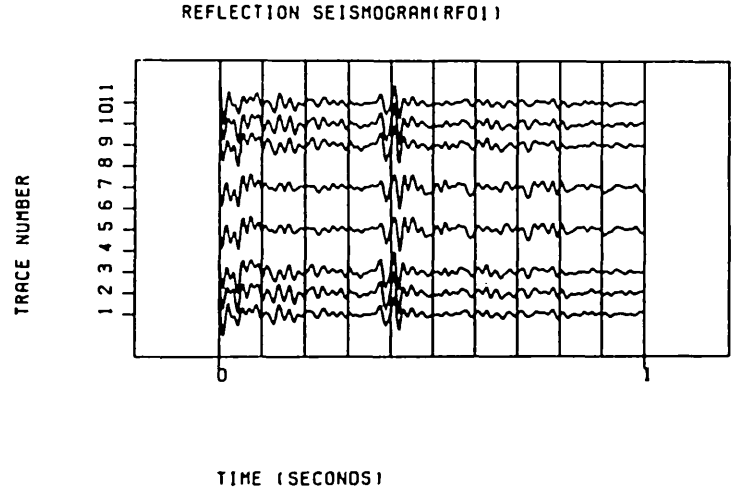
The effects of the source ghosts on the primaries is negligible, CCOEF, which measures the primary effects has changed only by a small amount about 0.02 (see Fig. (6.12) - (6.15).

In the fourth test, we used the method of straight

Fig. 6.07a - Least-square optimization

$a_1 = 0.41$ $a_2 = 0.67$ $a_3 = 0.80$

$\rho_1 = 0.59$ $\rho_2 = 0.33$ $\rho_3 = 0.20$



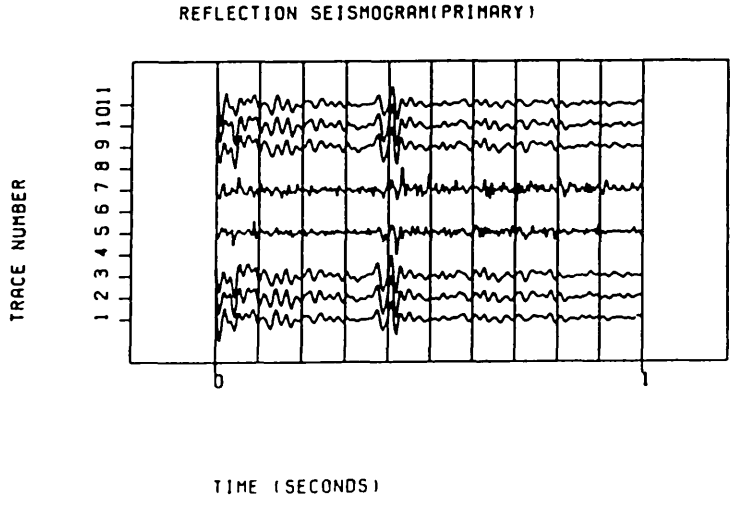
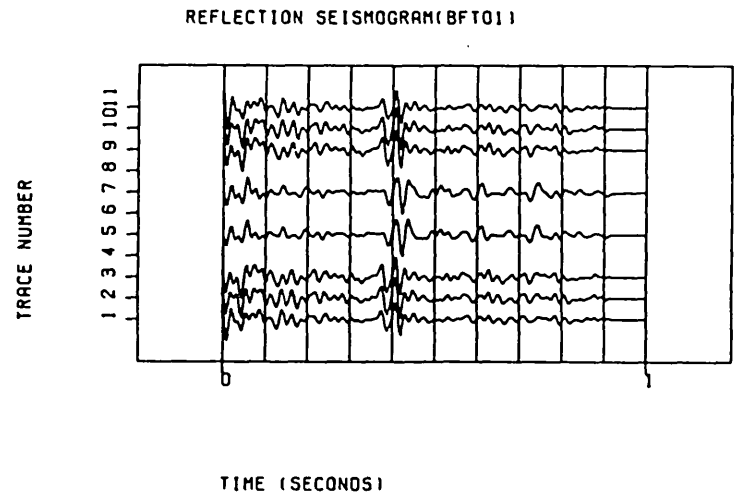


Fig. 6.07b Least-squares optimization showing field stacks and computed responses (unfiltered) - cpv-10.

Fig. 6.08a Matrix Analysis - primaries plus transmission loss correlation = 0.52



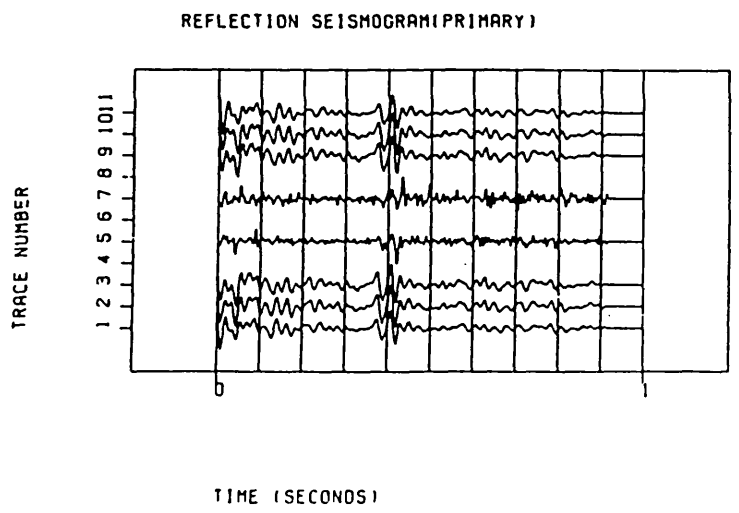


Fig. 6.08b: Matrix Analysis - comparing with unfiltered responses including transmission loss

Fig. 6.09a: Residual Analysis (Transmission loss included)
Correlation = 0.54
X^2 = 50.9 (124.34 - critical)

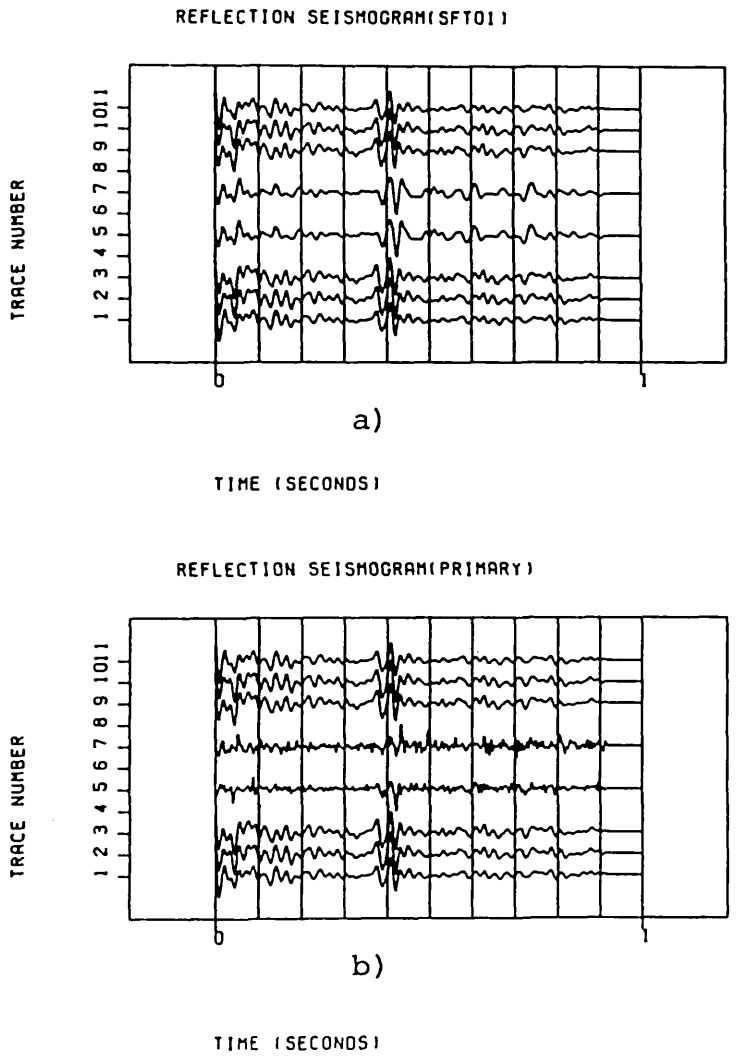


Fig. 6.10: White's Model (transmission loss)
correlation = 0.51

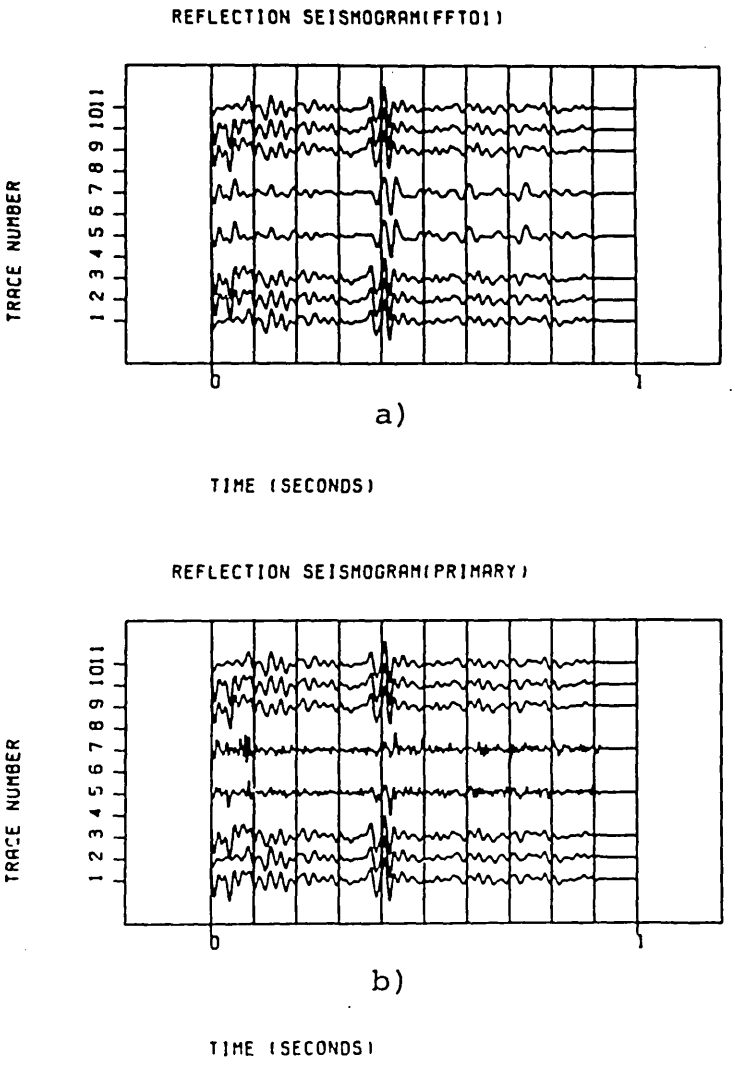


Fig. 6.11 Least-squares optimization (transmission loss)

$a_1 = .39$ $a_2 = 0.67$ $a_3 = 0.8$ $x^2 = 34.5$

$\Omega_1 = 61$ $\Omega_2 = 0.33$ $\Omega_3 = 0.2$

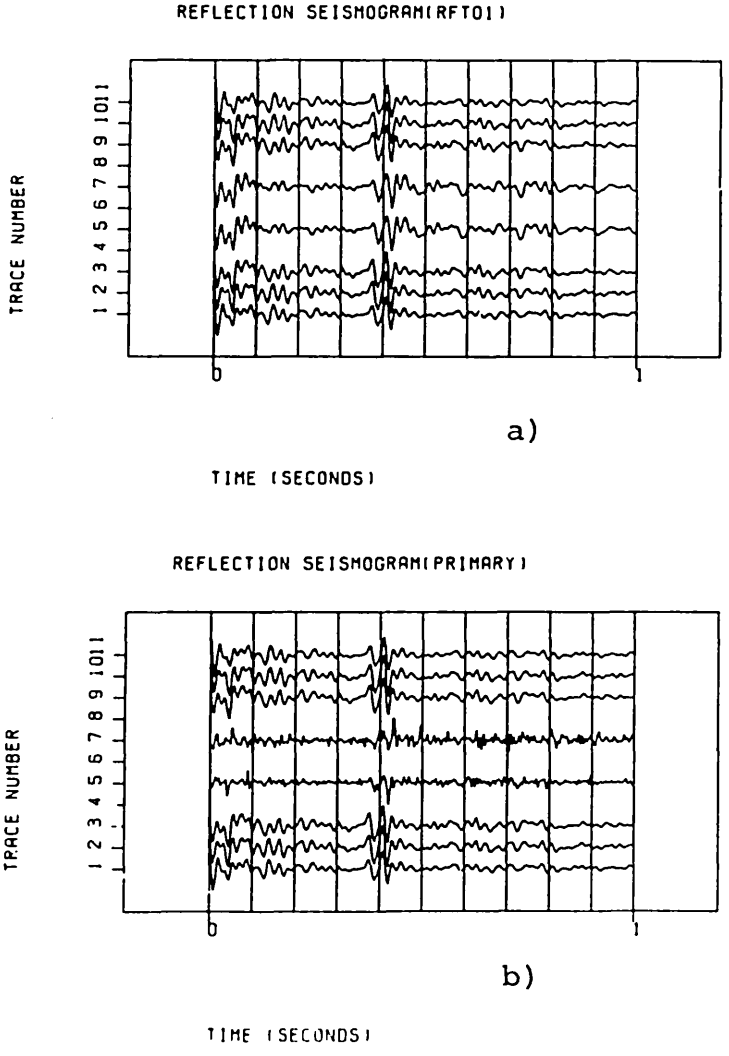


Fig. 6.12: Matrix Analysis (Source Ghosts)
Correlation = 0.51

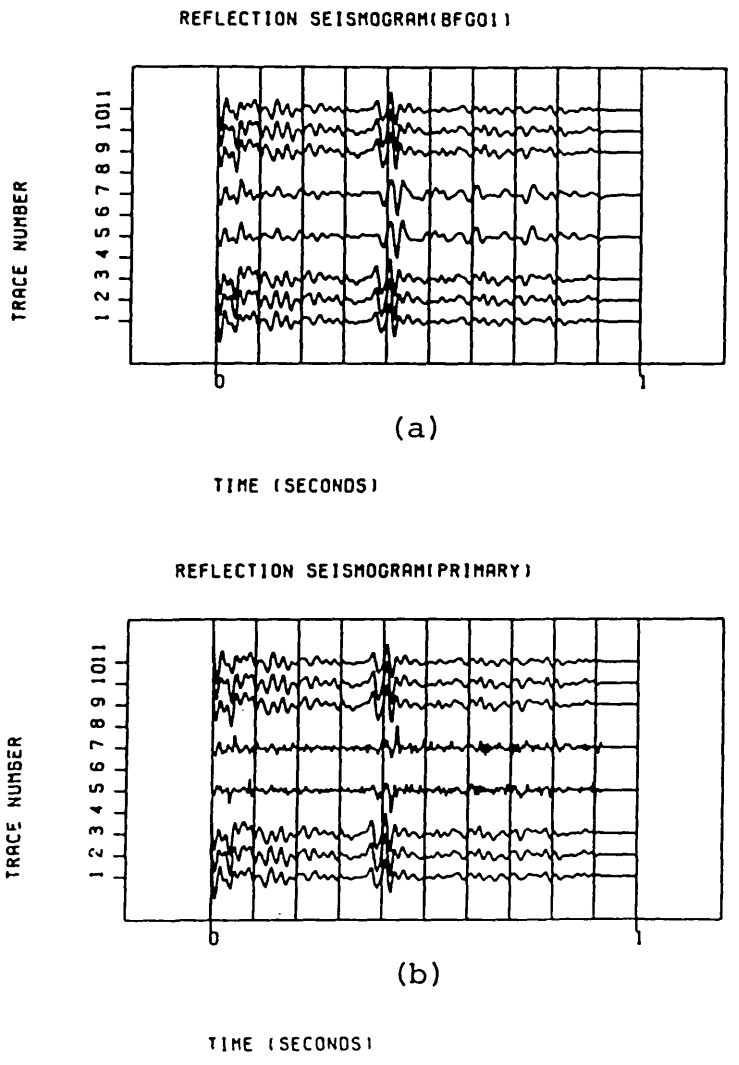


Fig. 6.13 Residual Analysis (Source ghosts)
Correlation = 0.53
X^2 = 50.9

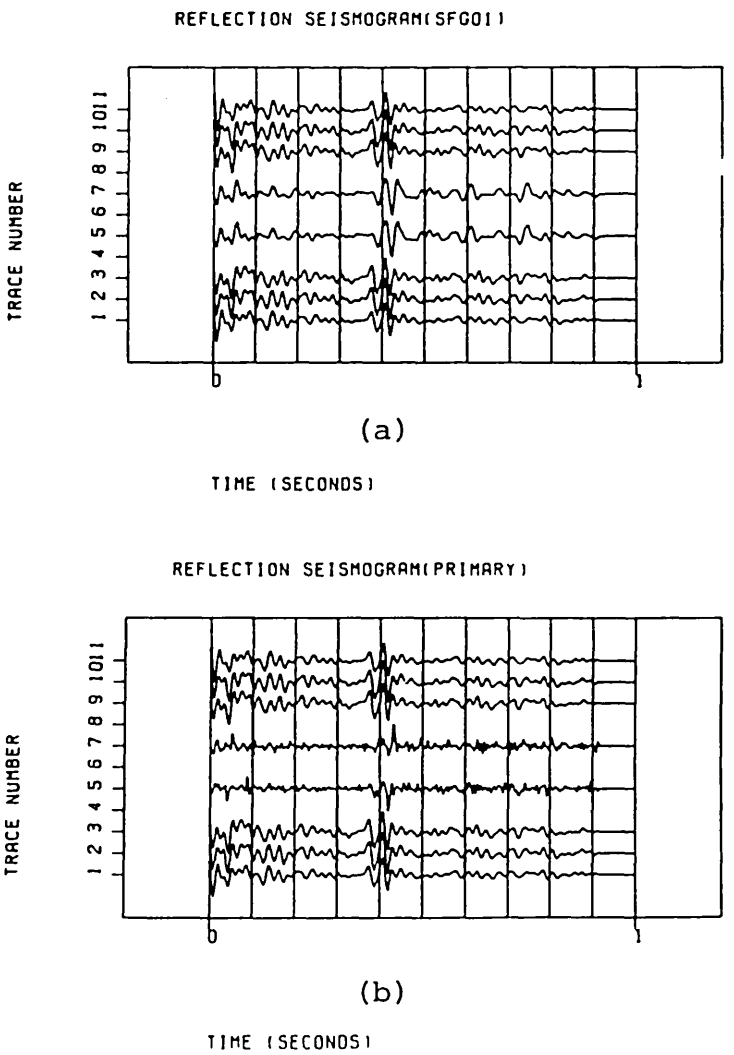


Fig. 6.14 White's Model (Source ghosts)
Correlation (0.50)

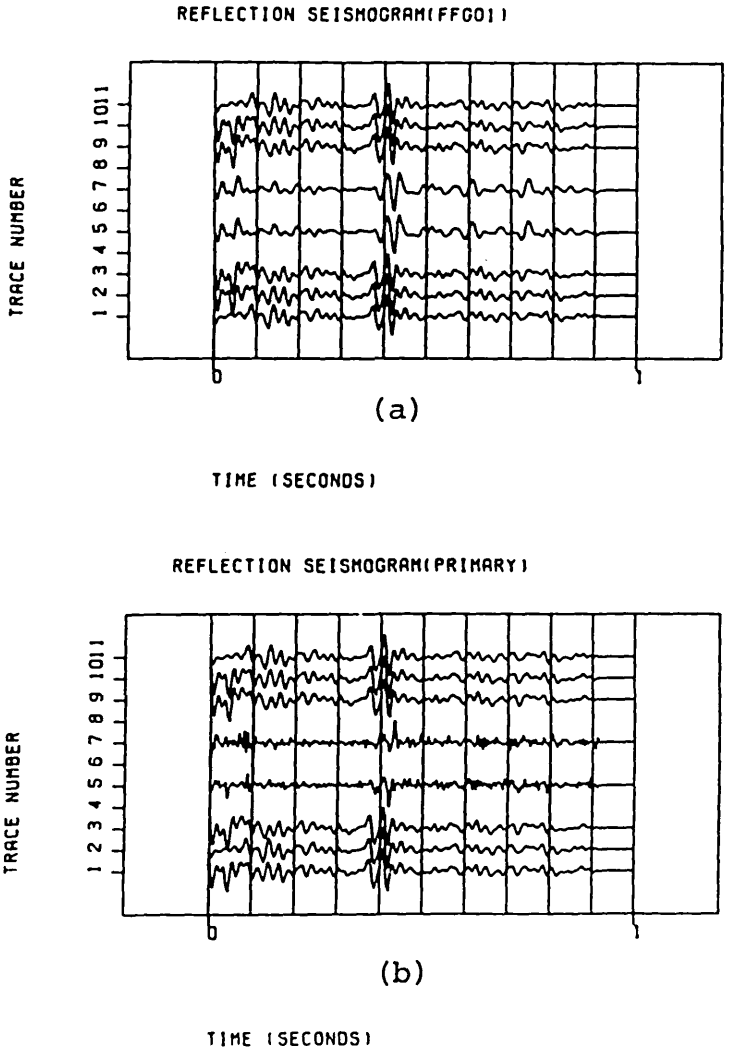


Fig. 6.15: Least squares optimization (source ghosts)

$a_1 = 0.41 \quad a_2 = 0.67 \quad a_3 = 0.80$

$\rho_1 = 0.59 \quad \rho_2 = 0.33 \quad \rho_3 = 0.20$

$X^2 = 40.02$

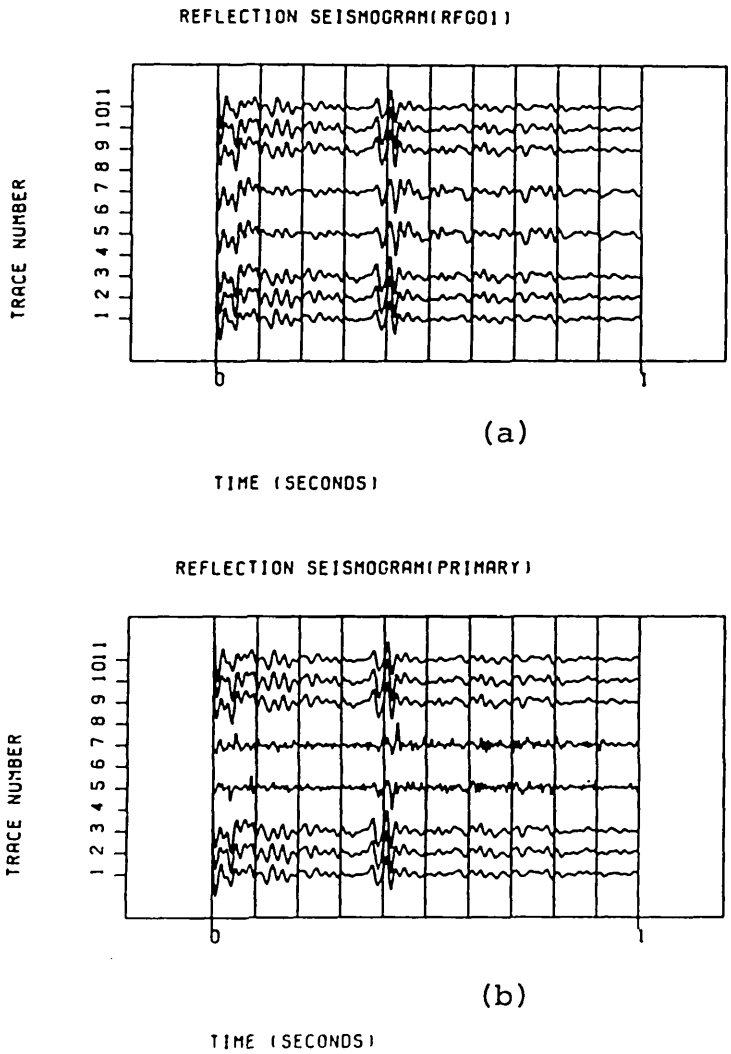


Fig. 6.12-1 Residual Analysis, all wells. Well, cpv-10 (γ_c = 0.53)

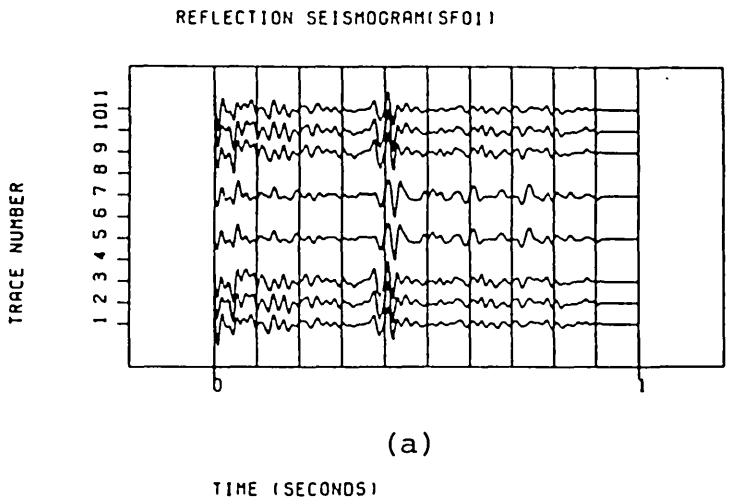


Fig. 6.13.1: Residual Analysis
Well, cpv-12 (γ_c = 0.49)

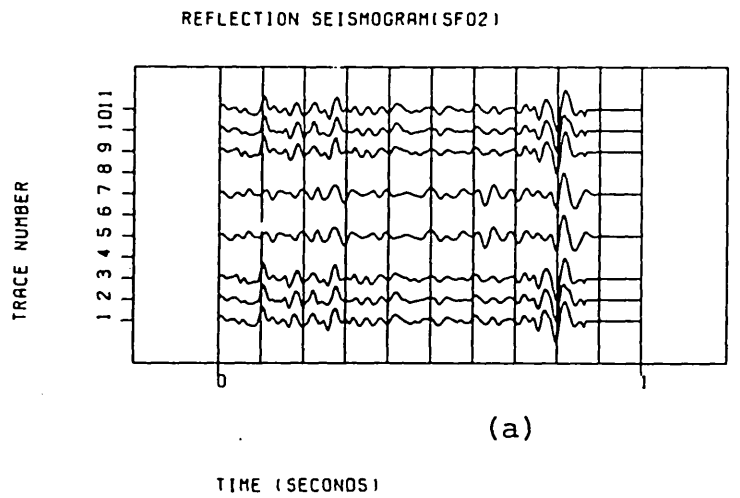


Fig. 6.14.1: Residual Analysis (cpv-10A)
(γ_c = 0.50)

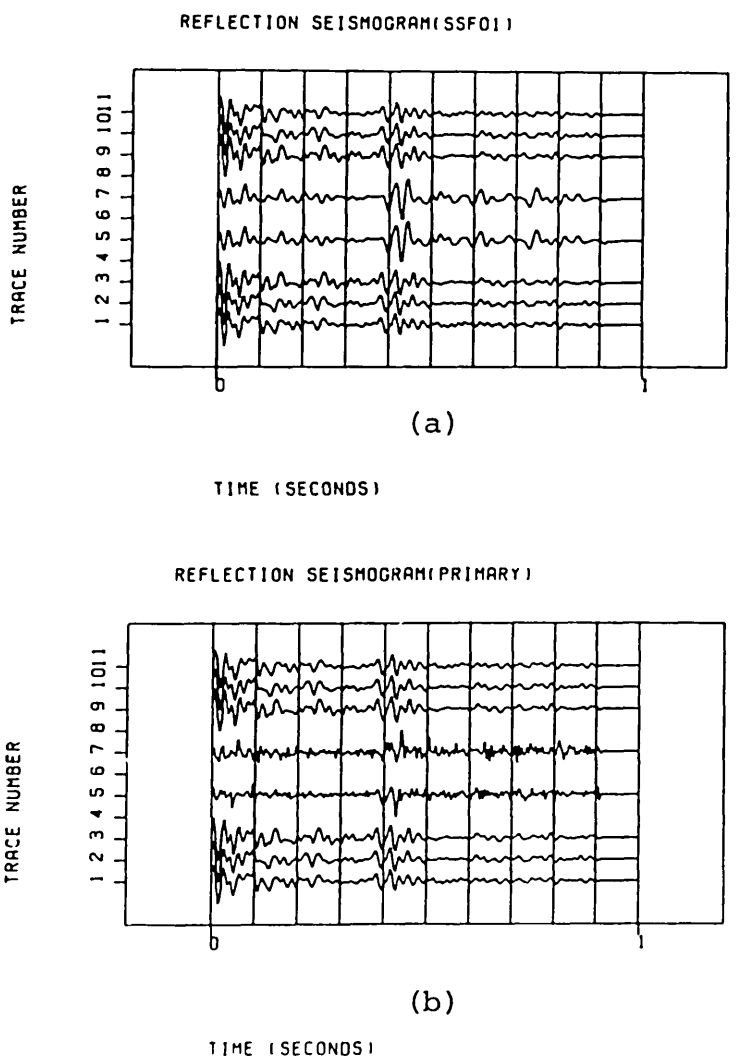


Fig. 6.15-1: Residual Analysis (cpv-03)
(γ_c = 0.3)

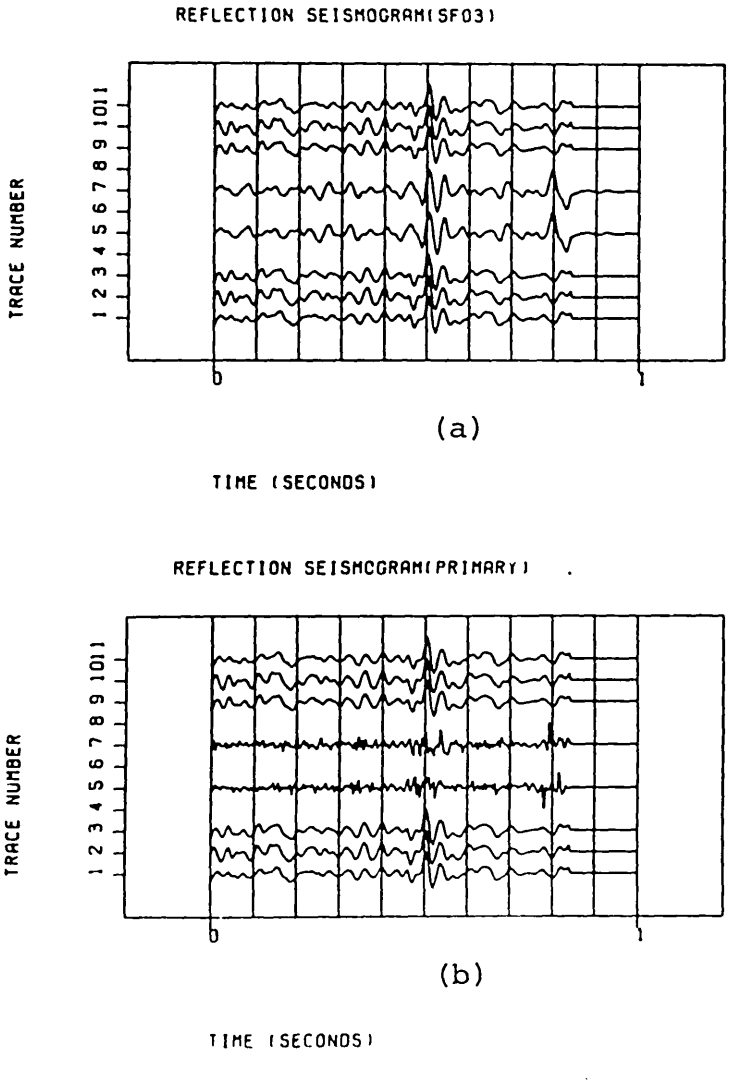


Fig. 6.16 Matrix Analysis - Well (cpv-03)
(γ_c = 0.30)

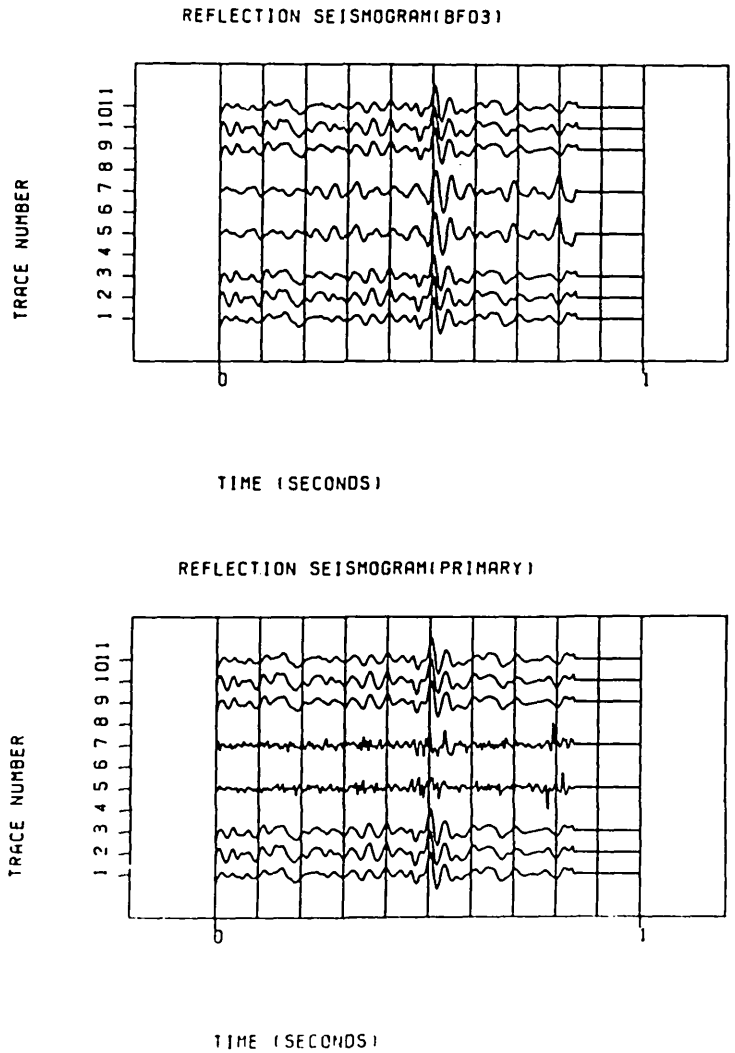


Fig. 6.17 Residual Analysis - well cpv-12
Correlation = 0.49

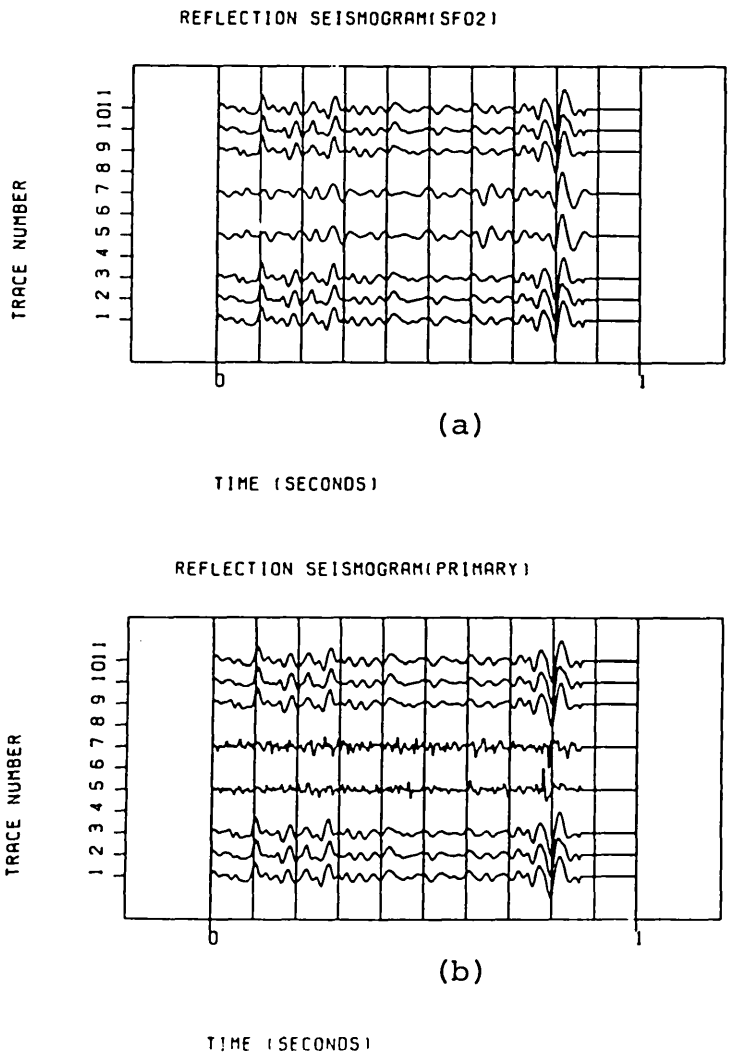


Fig. 6.18: White's model (cpv-10B)
(γ_c = 0.50)

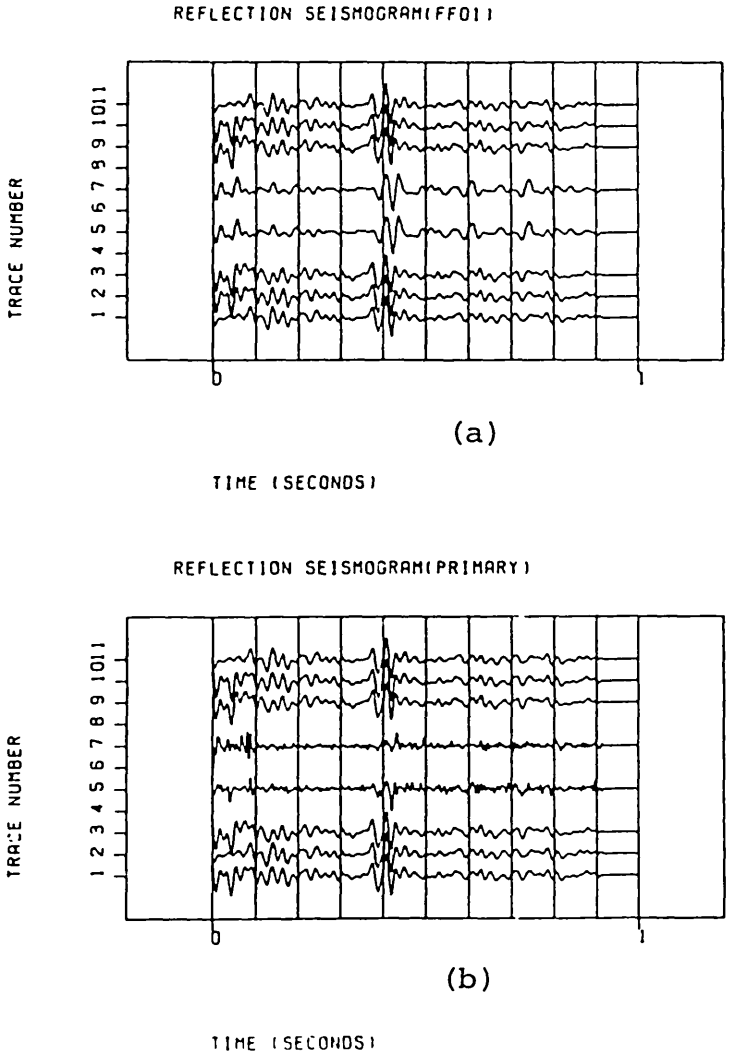
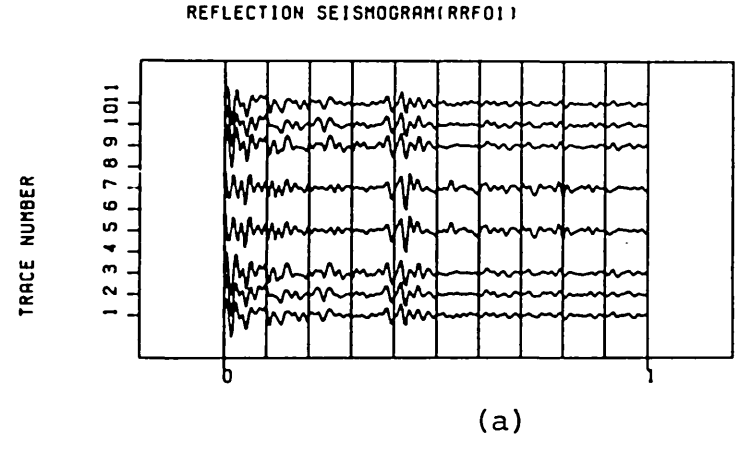
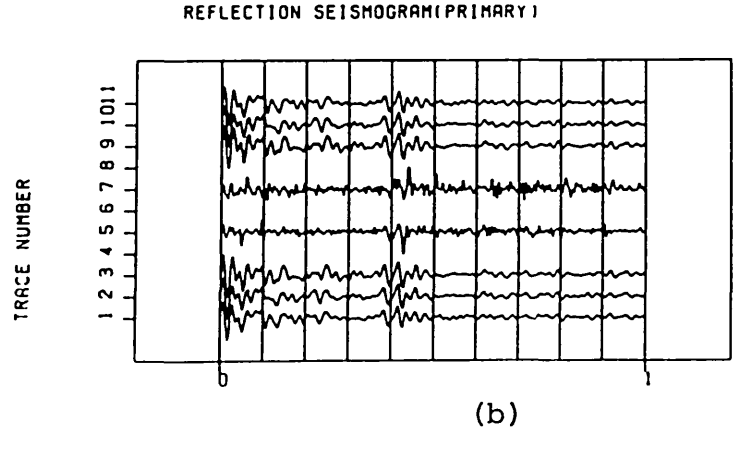


Fig. 6.19 Least squares optimization - line cpv-10A

$a_1 = 0.55 \quad a_2 = 0.70 \quad a_3 = 0.82$

$\Omega_1 = 0.45 \quad \Omega_2 = 0.30 \quad \Omega_3 = 0.18$





residuals on all the wells. Once more there is a marked improvement, γ_c changing to more encouraging values, (see fig. 6.12-1, — (6.15.1) for details. In the final test all the filtered well information were used simultaneously with all the seismic lines, again in the order shown:

(1) BENSOL - cpv-03 - cpv-03A

(2) OTNES - cpv-12 - cpv-12A

(3) FAITH - cpv-10 - cpv-10B

(4) DESIGN - cpv-10 - cpv-10A

The set up follows the same interpretation as in chapter five. The only reason for using the same configuration is to enable us compare the two results (from chapters five and six) without much confusion. We have also used only the filtered primaries and multiples in the analysis. The plots and related results are shown in figure (6.16) - (6.19). As we expected, the change in the matches improved by about 0.2. The conclusion follows from the calculated values of Pearson's product moment correlation coefficient recorded in each case as CCOEF.

Summary

When the well log generated impulse responses are filtered or are generated from Fourier synthesis, thereafter, the resulting synthetics match the field observed seismograms much better than when the impulse responses were generated only from unfiltered linear filter model. The change in magnitude is about 0.2.

This could be explained from the fact that the filtering procedures have most probably reduced some noise effects attributed to each of the various input components hence leaving us with more of pure signal components for our analysis.

The matching of well cpv-10 and line cpv-10B produced a much better match than that between the rest of the other wells and their corresponding seismic lines. The explanation here, is again straight forward. Well cpv-10 has the shortest offset-distance to line cpv-10B when compared to the distances of each of the other wells to their corresponding seismic lines.

Now, comparing the last two sections - matching with synthetics from Fourier analysis, and from filtered Impulse responses (linear filter model), one could say (judging from the magnitude of each match) that one method is as good as the other. However, the first method (Impulse generation via Fourier synthesis) involves a good deal of computer time. This is an obvious disadvantage. The second technique apart from being simpler in application has another advantage in that the filtering processes could be done side by side with the normal routine seismic field processing, otherwise both methods have good applicability.

Let us return to the results in chapters five and six. Considering the results of the match in chapter five, we would, for example, have concluded that the match between well cpv-10 and line cpv-10B is 0.4. The result and conclusion would probably have been

acceptable to the present state of the art. On the other hand, results from chapter six have shown that we can improve our probable limit of accuracy in matching analysis. By using the method of Fourier synthesis and far-field signature, or by filtering the reflection impulses generated via the linear filter model, we have been able to improve the magnitude of our match even by a value of 0.2. This indeed, is a very significant result, the limit of matching accuracy having been improved, when compared with our earlier results.

CHAPTER 7

CONCLUSIONS AND SUGGESTIONS FOR FURTHER WORKS

Throughout this work efforts have been made to give a conclusive presentation of all material under investigation. In this final chapter, we shall give only a short summary of points already covered in detail.

In order to obtain a suitable field trace which would most properly match the well-log generated synthetic seismogram, we must effectively tackle the seismic limitations as well as the synthetic generation problems. The most important problems are; Noise (especially the multiples), inaccurate well-logs and synthetic approximations, problems of velocity measurements in boreholes and in the field, NMO effects, aliasing, limited frequency bandwidth, and diffraction effects.

The accuracy of the synthetic seismograms is enhanced by proper estimation of the source wavelet. The matrix partition technique, method of straight residuals, optimum least-squares technique, and normal equations approach of White (1980), are found to be very effective. The first three are particularly advantageous in terms of computer time and ease of application, while the last technique is indispensable for multichannel input.

The various numerical methods of quantifying the similarity between the synthetic and field seismograms, such as γ_c (the product moment correlation coefficient), Ω (the goodness measure), α (the normalised

mean square error), coherence (the frequency dom in measure, and X^2 (chi-squared), add more credibility to the matching analysis.

When a synthetic seismogram is generated from reflection impulses using the double fast Fourier algorithm, and the far-field signature or when band-pass and time-variant filtering processes are applied to reflection impulses, computed from linear filter models, the numerical estimates of most matches change significantly.

It would be presumptious to claim that this research gives an exhaustive treatment of synthetic-field trace matching. That would be beyond the scope of the present work. For example, it would be interesting to match Kennett's theoretical seismograms containing (primaries and multiples) with pre-stack-field seismograms. The computation of the layer matrices or the total reflection matrix is the most time consuming step in Kennett's model. With better computer hardware, longer offsets could be computed and pre stack-matching might become an attractive approach. Such a match may account for the effects of NMO and stack, attenuation and geometrical spreading. It may even be worthwhile to investigate the effects of velocity anisotropy on the reflection and transmission coefficients with the hope of generating some synthetics from them (see Daley et al. 1979). With the rapid advances in computer technology the chances of improving seismi resolution and synthetic-field matching is undoubtedly high.

REFERENCES

G.: Geophysics, G.P.: Geophysical Prospecting)

ABELES, F., 1946. Nouvelles formules relative a la lumiere reflechie et transmisi par un empilement de lames a faces parallels. Comptes Rendue de L'Academie des Sciences, 223, pp. 891-893.

ALLEN, F. et al., 1952. The application of the Reflection seismograph to near-surface exploration: G.17, 859-866.

ANGONA, F.A., 1958. Seismic data producing system: American Patent No. 2, 834, 422.

ANSTEY, N.A., 1957. Modern Technique in Seismic Reflection recording: G.P., 5, pp. 44-60.

ANSTEY, N.A., 1960. Attacking the problems of the synthetic seismogram: G.P., 8, pp. 242-259.

BACKUS, M., BURG., J., BALDWIN, D., BRYAN, E., 1964. Wide band extraction of mantle p-waves from ambient noise: G. 29, 672-692.

BAKER, B.B., COPSON, E.T., 1939. The mathematical theory of Huggen's principles. Clarenden Press.

BANTHIA, B.S., KING, M.S., FATT, I., 1965. Ultrasonic Shear wave velocities in rocks subjected to simulation overburden press and internal pore press: G. 30, 117-121.

BARANOV, V., KUNETZ, G., 1960. Film Synthetique avec reflexions multiples; theorie et calcul pratique; G.P., 8, pp. 315-325.

BENDAT, J.S., PIERSOL, A.G., 1966. Measurement and Analysis of random data: Wiley Int. Sc. N.Y.

BENDAT, J.S., PIERSOL, A.G., 1971. Analysis and Measurement procedures: Wiley Int. Science, N.Y., Sydney, Toronto.

BERRYHILL, J., 1977, Diffraction Response from non-zero separation of source-receiver: G., 42, 1158-1176.

BERRYMAN, L.H., GOUPILLAUD, P.C., WATERS, K.H., 1958. Reflection from multiple transition layers - Part 1: Theoretical Results: G, 23.

BERZON, I.S., 1967. Analysis of the spectral characteristics of a thin bedded sequence in seismic wave propagation in real media: Consultants Bureau, N.Y. Lond.

BLAKE, F.G., 1952. Spherical wave propagation in solid media. Jour. Acoust. Soc. Am. Vol. 24, pp. 211-215.

BRACEWELL, R., 1965. The Fourier transform and its applications: McGraw-Hill, New York.

BUCHEN, P.W., HADDON, R.A.W., THENUWARA, A., 1980. On computing seismic diffractions: University of Sydney, Australia.

BUTTERWORTH, S., 1930. On the theory of filter amplifiers: Witeless Engr. 1, 536-541.

CHOLET, J., 1954. A test on Elastic Anisotropy measurements at Berriane: G.P., 2, 232-246.

CLAERBOUT, J.F., 1976. Fundamentals of Geophysical data processing: McGraw Hill B.K. Comp. Inc., New York.

CLAERBOUT, J.F., 1970. Coarse grid calculations of waves in Inhomogeneous Media: G., 35, 407-418.

CLAERBOUT, J.F., 1970. Downward continuation of moveout - corrected seismogram, G. 37, 741-768.

COOLEY, J., TUKEY, J., 1965. An algorithm for the machine calculation of complex Fourier Series. Mathm. Computation 19, pp. 297-301.

CRAWFORD, J.M., DOLY, W.E. and LEE, M.R., 1960. Continuous signal seismograph, G. 25, pp. 95-105.

ČRERVENRÝ, V., RAVINDRA, R., 1971. Theory of seismic head waves: U. of Toronto Press, Toronto.

CRESSMAN, S., 1968. How velocity layering and steep dip affect CDP: G. 33, 399-411.

CROOK, A.W., 1948. The reflection and transmission of light by any system of parallel isotropic films: Journal of the Optical Society of Am. 38, 954-964.

DALEY, P.F., HRON, F., 1979. Reflection and transmission coefficients for seismic waves in Ellipsoidally anisotropic media: G., 44, pp. 27-38.

DAVENPORT, A.G., 1961. The spectrum of horizontal gustiness near the ground in high winds, Q.J.R. Meteorol., Soc. 87, 194-211.

DELA PLANCHE, J., HAGEMANN, R.F., PIERRE, G., 1963. An example of the use of synthetic seismograms: G., 28, 842-854.

DENNISON, A.T., 1960. An introduction to synthetic seismogram techniques. G.P., 8, pp. 231-241.

DIX, C.H., 1952. Seismic prospecting for oil: Harper, New York.

DIX, C.H., 1955. Seismic Velocities from surface measurements: G.,20, pp. 68-86.

DIX, C.H., 1955. The mechanism of generation of long waves from explosions. G., 20, p. 87.

DOMENICO, S.N., 1974. Effects of Water Saturation on Seismic Reflectivity of Sand Reservoirs Encased in Shale: G., 39, 758-769.

DOMZALSKI, W., 1956. Some problems of shallow refraction investigations G.P., 4, 140-146.

DOUZE, E.J., 1971. Prediction Error Filters, White Noise and Orthogonal co-ordinates. G.P. 19, 253-264.

DUNKIN, J.W., LEVIN, F.K., 1973. The effect of normal moveout on a seismic pulse: G.38, pp. 635-642.

DURSCHNER, H., 1958. Synthetic seismograms from continuous velocity logs: G.P., VI, pp. 272-284.

DUNOYER DE SEGON ZAC, LAHERRERE, J., 1959. Application of the continuous velocity log to anisotropy measurements: G.P.7, No. 2.

EMBREE, P., BURG, J.P., BACKNS, M., 1963. Wideband velocity filtering - the pie-slice process; G. 28, 948.

FAUST, L.Y., 1953. A velocity function including lithologic variations: G.18, pp. 271-288.

FERTIG, J., MULLER, G., 1978. Computations of synthetic seismograms for coal seams with Reflectivity Method: G.P. 26, pp. 868-883.

FOSTER, M.R., SENGBUSH, R.L., WATSON, R.J., 1964. Design of subpotimum filter systems for multivariate seismic data processing: G.P., 12, 173.

FOSTER, M.R., GUINZY, N.J., 1967. The coefficient of coherence: its estimations and use in geophysical data processing: G. 32, pp. 602-616.

FOSTER, M.R., SENGBUSH, R.L., WATSON, R.J., 1968. Use of Monte Carlo Techniques in Optimum Design of Deconvolution process: G., 33, pp. 945-949.

FITCH, A.A., 1976. Seismic Reflection Interpretation. Geoexplanation monographs, Series I, No. 8.

GANTMACHER, F.R., 1959. The theory of Matrices: Vol. I, Chelsea publ. comp. N. York.

GEERSTMA, J., SMITH, D.C., 1961. Some aspects of Elastic waves propagation in Fluid Saturated porous solids: G., 26, 169-181.

GEORGE, E.F., SMITH, H.W., BOSTICK, F.X., 1964. Application of Inverse filters to Induction Log Analysis: G., 29, 93-104.

GRETENER, P.E.F., 1961. An Analysis of the observed time discrepancies between continuous and conventional well velocity surveys: G., 26, 7-11.

GOUPILLAUD, P.L., 1961. An approach to Inverse filtering of the near surface layer effects from seismic records: G., 26, 754-760.

HAMID, N., AL-SADI, 1980. Seismic Exploration Technique and Processing: Birkhauser Verlag, Basil.

HICKS, W.G., 1959. Lateral Velocity Variations near Boreholes: G.24, 780-806.

HILDERBRAND, F.B., 1962. Advanced calculus for Application: Prentice-Hall Inc., New Jersey.

HILTERMAN, F., 1970. Three-dimensional seismic modelling. G., 35, 1020-1037.

HILTERMAN, F., 1975. Amplitudes of seismic waves: A quick look: G., 40, 745;762.

HINICH, M., CLAY, C., 1968. Application of the discrete Fourier transform in the estimation of power spectra, coherence and bispectra of Geophysical data: Reviews of G., 6, 347-363.

HUGHES, V.J., KENNETT, B.L.N., 1983. The nature of seismic reflections from coal seams: First Break, 1.

JENNISON, R.C., 1961. Fourier transforms and convolutions for the experimentalist: Pergamon, London.

KANASEWICH, E.R., 1975. Time Sequence Analysis in Geophysics: University of Alberta Press.

KENNETT, B.L.N., 1974. Reflections, Rays and Reverberations: Bull. Seism. Soc. Am. 64, pp. 185-1696.

KENNETT, B.L.N., 1975. The Effects of Attennation on Seismograms. Bull. Seism. Soc. Am., 65, pp. 1643-1651.

KENNETT, B.L.N., 1979. Theoretical Reflection Seismogram: G.P., 27, pp. 301-321.

KENNETT, B.L.N., 1979. The suppression of surface multiples on Seismic records: G.P. 27, 584-600.

KIND, R., 1976. Computation of Reflection coefficient for Layered Media: G., 42, pp. 191-208.

KISSLINGER, C., 1963. The generation of the primary seismic signal by a contained explosion: Vesiac State of the Art Report. Univ. Michigan.

KOEFOED, O., 1954. Some observations on seismic weathering corrections: G.P. 2, 274-280.

KNUDSEN, V.O., ALFORD, R.S., EMILING, J.W., 1948. Underwater ambient noise. J. Mar. Res., 7, 410-429.

LEE, Y.W., 1960. Statistical theory of communication John Wiley, N.Y.

LEVINSON, N., 1946. The Wiener rms (root mean square) error criterion in filter design and prediction: Journal of Mathematics and Physics 25(4), p. 261.

LEVINSON, N., 1947. A heuristic exposition of Wiener's mathematical theory of prediction and filtering. Journal of mathematics and physics, 26(2), p. 110 (see also the Appendix of Wiener (1949) p. 149).

LINDSETH, R.O., 1979. Synthetic sonic-log. A process for stratigraphic interp. G., 44, pp. 3-26.

MARSH, H.W., 1963. Origin of the Knudsen spectra: J. Acous. Soc. Am. 35, 409-410.

McDONALD, J.A., GARDNER, G.H.F., HILTERMAN, F.J., 1983. Seismic studies in physical modelling. Broad oak press, Sussex, England.

NEIDELL, N.S., 1977. Stratigraphic modelling and interpretations: Geophysical principles and techniques: A.A.P.G. continuing: Ed. series No. 13.

O'BRIEN, P.N.S., 1967. Efficient use of large charges: S.E.G. Publications, 1967, pp. 152-162.

O'DOHERTY, R.F., ANSTEY, N.A., 1971. Reflections on Amplitudes, G.P., 19, pp. 430-458.

OLHOVICH, V.A., 1964. The causes of noise in seismic reflections and refraction work: G. 29, 1015-1030.

OTNESS, R.K., ENOCHSON, L., 1972. Digital Time Series Analysis: Wiley Inter. Science, N.Y. London.

OTNES, R.K., ENOCHSON, L., 1972. Digital Time Series Analysis: John Wiley and Sons, New York.

PASENICH, I.N., 1952. Experimental method of studying Resonance in the Geophone - Ground Vibrating System: .. Lzvestia Akademii Nauk USSR, No's. 1, 3, 5, (1952).

PETERSON, R.A., FILLIPONE, W.R., COKER, F.B., 1955. The synthesis of seismograms from well log data: G. 20, pp. 44-458.

RADAR, C.M., GOLD, B., 1967. Digital filter Design Techniques in the Frequency Domain: Proc. IEEE, 55, pp. 149-171.

RALSTON, A., 1965. A first course in numerical Analysis: International Series in pure and applied maths. McGraw Hill.

ROBERT, M.P., LUCAS, H.F., Jr. 1964. A rigorous least square analysis of complex Gamma-Ray spectra with partial compensation for instrumental instability: IEEE, Transaction on Nuclear Science, pp. 249-357.

ROBINSON, E.A., TREITEL, S., 1967. Principles of Digital Wiener filtering: F.P. 15, pp. 312-333.

ROBINSON, E.A., TREITEL, S., 1967. Principles of Digital Wiener filtering G.P.15 p. 309.

ROBINSON, E.A., 1967a. Statistical Communication and detection with special reference to digital data processing of Radar and Seismic Signal: Charles Griffin and Comp. London.

ROBINSON, E.A., 1967b, Multichannel Time Series Analysis with digital computer programs. Holden-Day Inc.

ROBINSON, E.A., 1967c. Predictive decomposition of time series with application to seismic exploration: G., 32, pp. 418-481.

ROBINSON, E.A. & TREITEL, S., 1980. Geophysical signal Analysis, Prentice-Hall, Inter. Inc. London.

ROBINSON, J.C., 1968. Noise Attennation on Common Depth Point Seismic Records by a Semideterministic approach: G. 33, 723-733.

RUDNICK, P., 1969. Wave directions from a large spar buoy. J. Mar. Res., 27, 7-21.

SAFAR, M.H., 1978. On the minimization of the distortions caused by the Geophone - Ground coupling: G.P., 36, p. 538.

SCHNEIDER, W.A., PRINCE, E.R., GILES, B.F., 1965. A new data processing technique for multiple attenation exploiting differential normal moveout. G.30, 348-362.

SCHOENBERGER, M. and LEVIN, F.I., 1979. The effects of subsurface sampling on one-dimensional synthetic seismograms: G., 44, pp. 1813-1829.

SENGBUSH, R.L., LAWRENCE, P.L., McDONALD, F.J., 1961. Interpretation of synthetic seismograms: G., 26, pp. 138-157.

SHARPE, J.A., 1946. The production of Elastic waves by explosive pressures: G., VII, 2 (144-154), VIII, 3 (311-321).

SHERIFF, R.E., 1975. Factors affecting seismic amplitudes: G.P. 23, 125-138.

SHERWOOD, J.W.C., 1962. The Seismoline. An analog. computer of theoretical seismograms. G., 27, pp. 19-34.

SHERWOOD, J.W.C., TROREY, A.W., 1965. Minimum phase and related properties of a horizontal stratified absorptive earth due to plane acoustic waves: G. 30, pp. 191-197.

THAMOS, D.H., 1977. Seismic Applications of Sonics: Communications No. 7, Fifth European Logging Symposium, Paris, (20-21, Oct., 1977).

TREITEL, S., ROBINSON, E.A., 1966. Seismic wave propagation in Layered Media in terms of communication theory: G., 31, pp. 17-32.

TROMBKA, J.I., SCHMADEBECK, R.L., 1968. A method for analysis of pulse height spectra containing gain-shift and zero-drift compensation: Nuclear Instruments and Methods, 62, pp. 253-261.

TROREY, A.W., 1962. Theoretical Seismograms with frequency and depth dependent absorption: G., 27, pp. 766-785.

TROREY, A.W., 1970. A simple theory for seismic diffractions: G., 35, pp. 762-784.

TROREY, A.W., 1977. Diffraction for Arbitrary source-receiver location: G.42, 1177-1182.

TUCKER, P.M., YORSTON, H.J., 1973. Pitfalls In Seismic Interpretation: SEG, Monograph Ser. (2).

UHRIG, J., 1955. Velocity Anisotropy in stratified media. G.20, pp. 774-779.

URSIN, B., 1978. Attenuation of coherent noise in Marine Seismic Exploration using very long arrays: G.P., 26, pp. 722-749.

URSIN, B., 1979. Seismic Signal Detection and Parameter Estimation: G.P., 27, 1-15.

VANDER STOEP, D.M., 1966. Velocity Anisotropy Measurements in Wells: G., 31, 900-916.

WADSWORTH, G.P., ROBINSON, E.A., 1953. Detection of Reflections on Seismic Records By Linear Operators: G.18, pp. 539-586.

WALDEN, A.T., WHITE, R.E., 1983. On the errors of fit and Accuracy in Matching Synthetic Seismograms and Seismic traces: Paper presented at 45th E.A.E.G. Meeting Oslo.

WATERS K.H., 1979. Reflection Seismology: Wiley - Interscience publications. New York, London.

WHITE, R.E., O'BRIEN, P.N.S., 1974. Estimation of the primary seismic pulse, G.P., 22, pp. 627-651.

WHITE, R.E., 1980. Partial coherence matching of synthetic seismograms with seismic traces: G.P., 28, pp. 323-332.

WIDESS, M.B., 1973. How thin is a thin bed? G. 38, pp. 1176-1180.

WIENER, N., 1949. Extrapolation Interpolation and Smoothing of Stationary time series: The M.I.T. Press, Cambridge, Massachusetts.

WIGGINS, R.A., 1966. W-K filter Design G.P., 14, p. 427.

WIGGINS, R.A., 1969. Uses of the Expected Error in the Design of least-squares optimum filters. G. 289-310.

WOLF, A., 1944. The Time Delay of a wave group in the weathered layer: G., 4, 367.

WOODWARD, P.M., 1953. Probability and Information theory with application to Radar: Pergaman, London.

WUENSCHEL, P.E., 1960. Seismogram Synthesis including multiples and transmission co-efficient: G., 25, pp. 106-129.

WYLLIE, M.R., GREGORY, A.R., GARDNER, G.H., 1958. An experimental Investigation of factors affecting elastic wave velocity in Porous media: G., 23 pp. 459-493.

YOUNG, G.B., BRAILE, L.W., 1976. A computer program for the application of Zoeppritz's Amplitude Equation and Knott's Energy Equations: Bull. Seism. Soc. Am. 66, 1881-1885.

Appendix A-1

Appendix A-1 gives a brief summary of the well-logs and seismic lines used in this thesis.

Like most logs, the well-logs used in this work do not contain information from the upper layers. A suitable ramp replaces the missing upper layer information. A surface reflection coefficient of 0.3, sample interval of 4ms, source-detector depths of 7.5m and 10.0m, are used for all synthetic computations. The following parameters describe the well information.

Well	Depth Range(ft)	Time Samples
cpv-10	3138-7525	420
cpv-12	3391-7225	524
cpv-03	3465->7000	588

Each of the wells is drilled closest to at least one of the four main seismic lines with the essential parameters shown in table A-1. Line cpv-10B is the nearest line to cpv-10. In section, Reflections are observed up to 5.6 secs. our analysis is confined to the first 1.7 secs. wich is the time corresponding to the limit of the available log data. The seismic horizons for the first 2 secs. show a good reflection alignment. Some prominent flat horizons are shown between 0.9 and 1.0 sec., while between 1.0 and 2.0 secs., the horizons dip gently to the right (see cpv-10B-1). Refflction alignments are better for the migrated than for the unmigrated sections. Sections from cpv-10A is very similar to

cpv-10B. This is expected since both lines lie very close to each other. (see event lying between 0.9 and 3.3 secs. in the two different sections).

Sections from cpv-12A show reduced continuity in reflection alignments than sections from the first two lines. The time segment (4.8- 7.0 secs) is dominated by reflection and diffraction events typical of folded structures (cpv-12A). Migration removes much of the diffraction events. The nearest CDP to the well is 503, and the synthetic seismogram has a time depth of about 2.1 secs. Continuity is preserved within this time depth and the effect of structural deformation did not seriously mar the result of our match.

For line cpv-03, reflection continuity in the section is comparatively good. A series of flat events and split reflections are observed. The split reflections and discontinuous horizons are probably due to changing and thickening sequences, interruption by geological phenomenon such as faulting or even poor data. The effects could have shown better on an unmigrated section. However, neither the geological section for the area nor the unmigrated section is available at the time of writing. The chance of picking the wrong CDP or shot point is small, otherwise our matching analysis is accurate.

Well	Spec line	Nearest CDP	Nearest SP	CDP Gather	CDP Range	Sampling
cpv-10	cpv-10A	1485	1464	Trace weighted	64-1485	4
	cpv-10B	126	101		64-1003	4
cpv-12	cpv-12A	503	485	3000% Coverage	64-833	4
cpv-03	cpv-03A	801	780	for all gathers.	64-2949	4

Table- A-1: Parameters used in synthetic-field analysis.

The above parameters are as contained in the original field tapes, only the necessary segments are enclosed in this thesis.

APPENDIX A-2

Derivation of Expected Error Minimum e_m

The expected error e is defined by the relation:

$$e = E\left\{(D_t - \sum_{s=0}^{n} a_s C_{t-s})^2\right\} \qquad A(2.1)$$

If we let τ be another summation index, then:

$$e = E\left\{Dt^2\right\} - 2E\left\{Dt \sum_{s=0}^{n} as\, C_{t-s}\right\} + E\left\{\sum_{s=0}^{n} as C_{t-s} \sum_{\tau=0}^{n} a_\tau C_{t-\tau}\right\} \qquad A(2.2)$$

$$\Rightarrow e = E\left\{Dt^2\right\} - 2\sum_{s=0}^{n} asE\left\{D_t C_{t-s}\right\} + \sum_{s=0}^{n} as \sum_{\tau=0}^{n} a_\tau E\left\{C_{t-s}C_{t-\tau}\right\} \qquad A(2.3)$$

By setting

$$R_{D(0)} = E\left\{Dt^2\right\}$$

$$G(s) = E\left\{DtC_{t-s}\right\}$$

$$R(\tau-s) = E\left\{Ct-sC_{t-\tau}\right\}$$

$$= E\left\{Ct+\tau-sC_t\right\}$$

then we can define $R_D(0)$ as the autocorrelation of the desired output at zero lag, and G(s) and $R(\tau-s)$ are in agreement with our earlier definitions of cross correlation and autocorrelation. Substituting the last three equations into A(2-3) we have

$$e = R_D(0) - 2\sum_{s=0}^{n} asG(s) + \sum_{s=0}^{n} as \sum_{\tau=0}^{n} a_\tau R(\tau-s) \qquad A(2.4)$$

Now, if we substitute equation (5.42) - the normal equations into equation A(2.4) then e will be at a minimum. Since $R(\dot{T}-s) = R(s-\dot{T})$, we can see with little or no difficulties, the relationship between the left-most summation in equation (5.42) and the right-most summation in A(2.4), hence we can replace the right-most summation in A(2.4) with the right of (5.42) to obtain ℓ_{min}, so that

$$\ell_{min} = R_D(0) - \sum_{s=0}^{n} as\ G(s) \qquad A(2.5)$$

Equation A(2.5) is equivalent to equation (5.44) used in the text (chapter five) and from whence the normalised mean square error α was calculated.

APPENDIX A-3

Computations of Residuals

To show how residuals may be computed from a set of inputs and one output (the inputs of which may be correlated, let us have a look back at figure (5.01).

For simplicity we shall meanwhile consider just one input and the output. Suppose, we call then $X_x(t)$, and $Y_y(t)$, we also assume $X_x(t)$ and $Y_y(t)$ are random variables.

Now, a linear prediction: $\bar{Y}_y(t)$ and $Y_y(t)$ from $X_x(t)$ may be defined according to the relation:

$$\bar{Y}_y(t) = KX_x(t) \qquad A(3.1)$$

where k is a constant.

Least-squares prediction ensures that if K is well chosen, then the mean square error is a minimum for all possible chosen values of K.

$$\Rightarrow \quad e = E\left[(Y_y(t) - \bar{Y}_y(t))^2\right]$$

$$= E\left[\bar{Y}_y{}^2(t)\right] - 2\,KE\left[X_x(t)\,Y_y(t)\right] + K^2E\left[X_x{}^2(t)\right]$$

..A(3.2)

K, is well chosen if our partial derivative with respect to K satisfies the relation;

$$de/dk = 0 \qquad A(3.3)$$

Using simple calculus we have from A(3.2)

$$K = E\left[X_x(t)\ Y_y(t)\right] / E\left[X_x^2(t)\right] \qquad A(3.4)$$

where E, denotes expectation, and we can recognize the numerator and denominator as the cross correlation and the auto-correlation of the random processes at zero lag (T = 0). We therefore define our correlations thus:

$$\begin{aligned} \phi_{xy} &= \phi_{xy}(o) \\ &= E\left[X_x(t)\ Y_y(t)\right] \end{aligned} \qquad A(3.5)$$

$$\begin{aligned} \text{and}\quad \phi_{xx} &= \phi_{xx}(O) \\ &= E\left[X_x^{+2}(t)\right] \end{aligned} \qquad A(3.5b)$$

where the low cases (xx, and yy) in ϕ_{xx}, and ϕ_{xy} are chosen to simplify notations.

We can now define the residual $DY_r(t)$ of $Y_y(t)$ from $X_x(t)$ following the method of Bendat et al. (1972); so that

$$\begin{aligned} DY_r(t) &= Y_y(t) - \bar{Y}_y(t) \\ &= Y_y(t) - KX_x(t) \\ &= Y_y(t) - \left[\frac{\phi_{xy}}{\phi_{xx}}\right] X_x(t) \end{aligned} \qquad A(3.6)$$

Equation A(1.6) is the residual computed for two random variables $X_x(t)$ and $Y_y(t)$. The expression can be extended for say three random variables, two inputs (primaries, and multiples) and one output (the field observed seismogram).

If we call the three variables, $X_{x1}(t)$, $X_2(t)$, and $Y_y(t)$, we can remove the effects of $X_{x2}(t)$ on both $X_{x1}(t)$ and $Y_y(t)$, just by computing the respective residuals as in equation A(1.6).

$$DX_1(t) = X_{x1}(t) - \left[\frac{\phi_{21}}{\phi_{22}}\right] X_{x2}(t) \qquad A(3.7)$$

$$DY_1(t) = Y_y(t) - \left[\frac{\phi_{2y}}{\phi_{22}}\right] X_{x2}(t) \qquad A(3.8)$$

where ϕ_{21}, ϕ_{2y}, ϕ_{22}, are the respective cross and auto-correlations of the variables, $DY_1(t)$ is the output residual, $DX_1(t)$, the input residual. Similarly, residuals may be calculated by removing the effects of $X_{x1}(t)$ on $X_{x2}(t)$ and $Y_y(t)$. From these residuals, it becomes a simple matter to compute say the frequency response function H(f), or the partial coherences, using the relations,

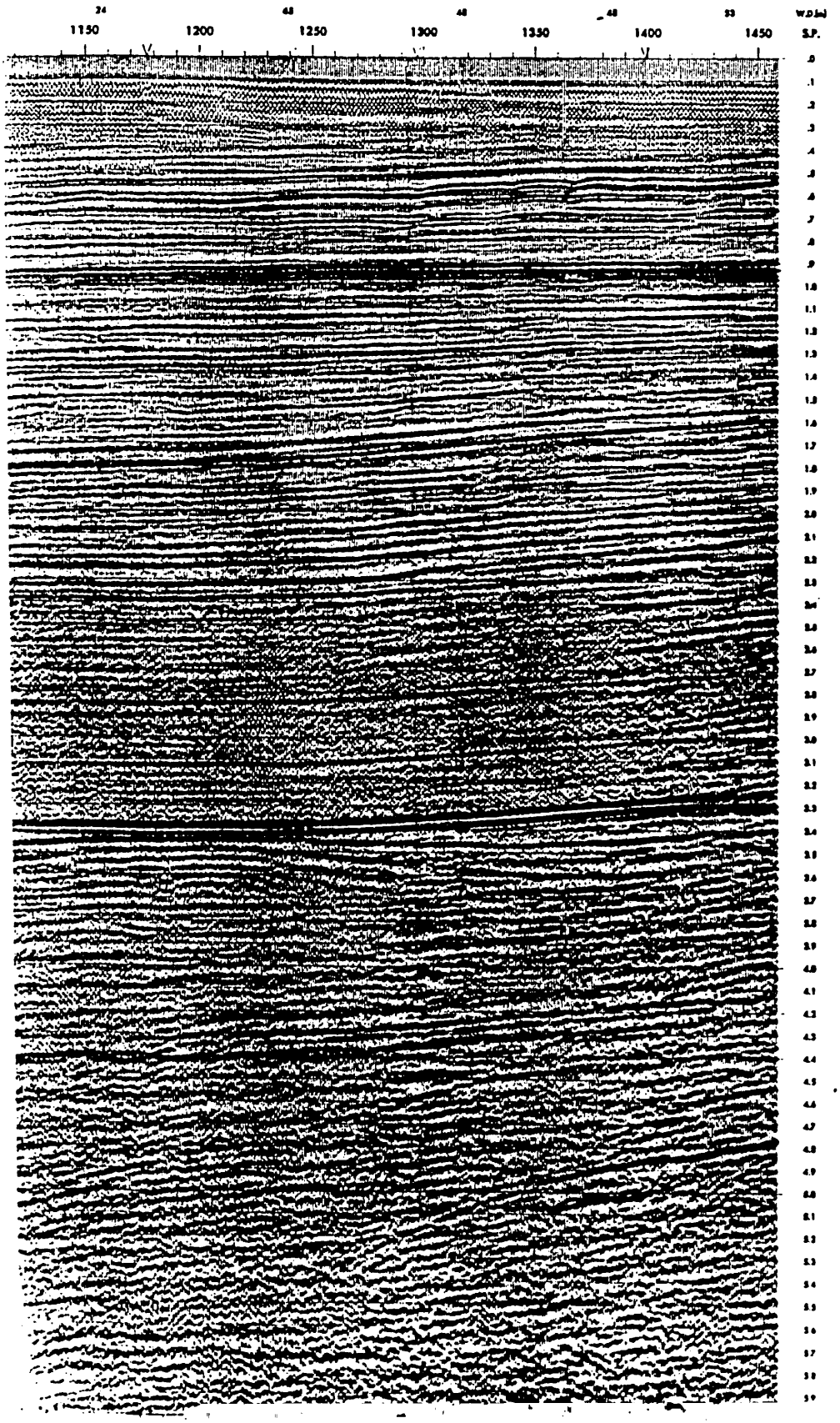
$$H_1(f) = \frac{G_{1y.2}(f)}{G_{11.2}(f)} \qquad A(3.9)$$

and $$\gamma^2_{1y.2}(f) = \frac{\left|G_{1y.2(f)}\right|^2}{G_{11.2(f)} G_{yy.2}(f)} \qquad A(3.9B)$$

where $G_{11.2}(f)$ for example implies that the power spectrum of say $X_{x1}(t)$ was computed after the effects of $X_{x2}(t)$ have been removed (i.e. $G_{11.2}(f)$ is the power spectrum of $DX_1(t)$ and $G_{1y.2}(f)$, is the cross power spectrum of $DX_1(t)$ with $DY_1(t)$.

LINE: CPV-10A-1



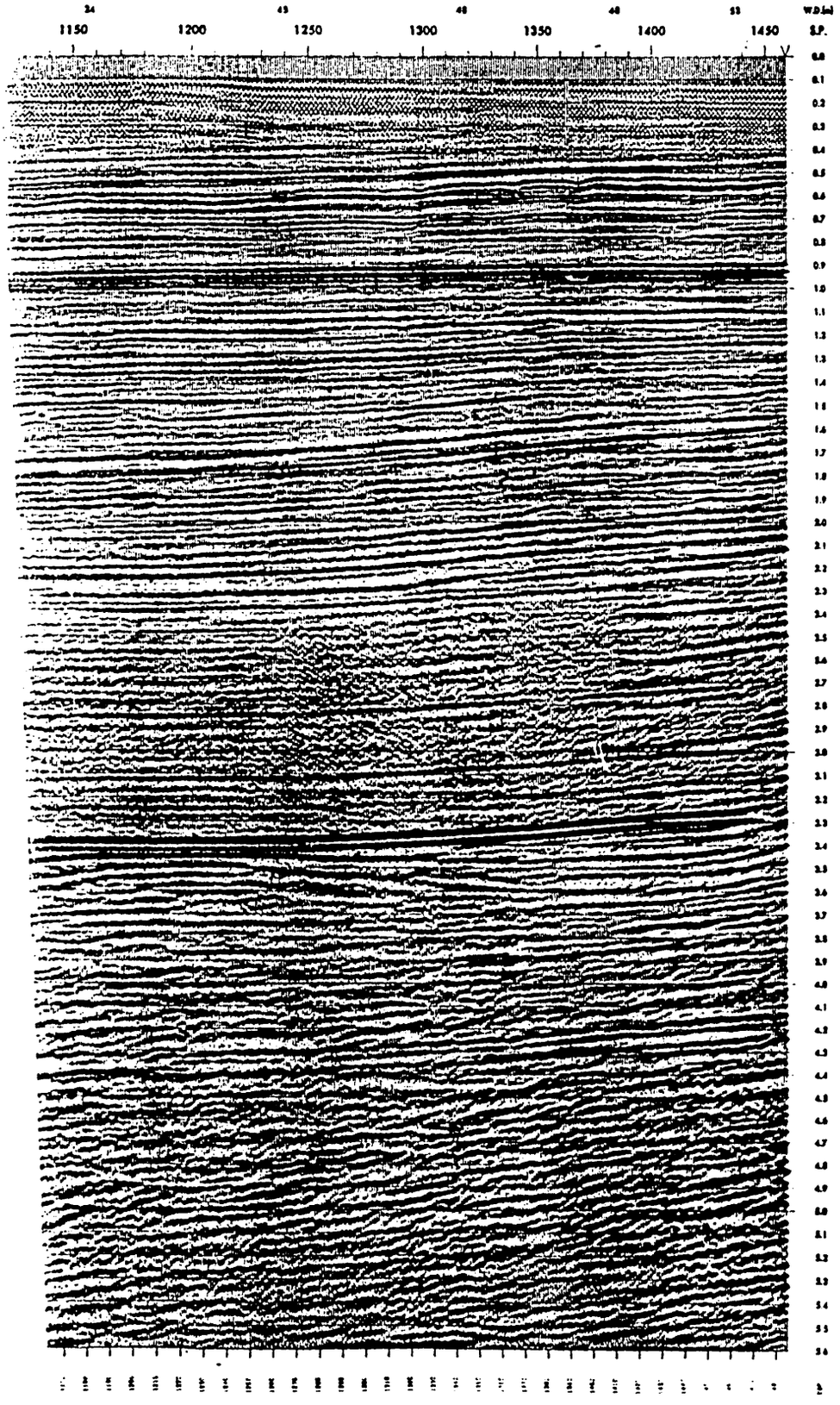


MERLIN GEOPHYSICAL COMPANY LTD.

line: SP82-56A sp 101-1484
area: OFFSHORE DENMARK
filter: 3000% FILTERED STACK
direction: ⟶ (NNE)

SPECULATIVE SURVEY
not to be sold or traded without permission

LINE: CPV-10A-2



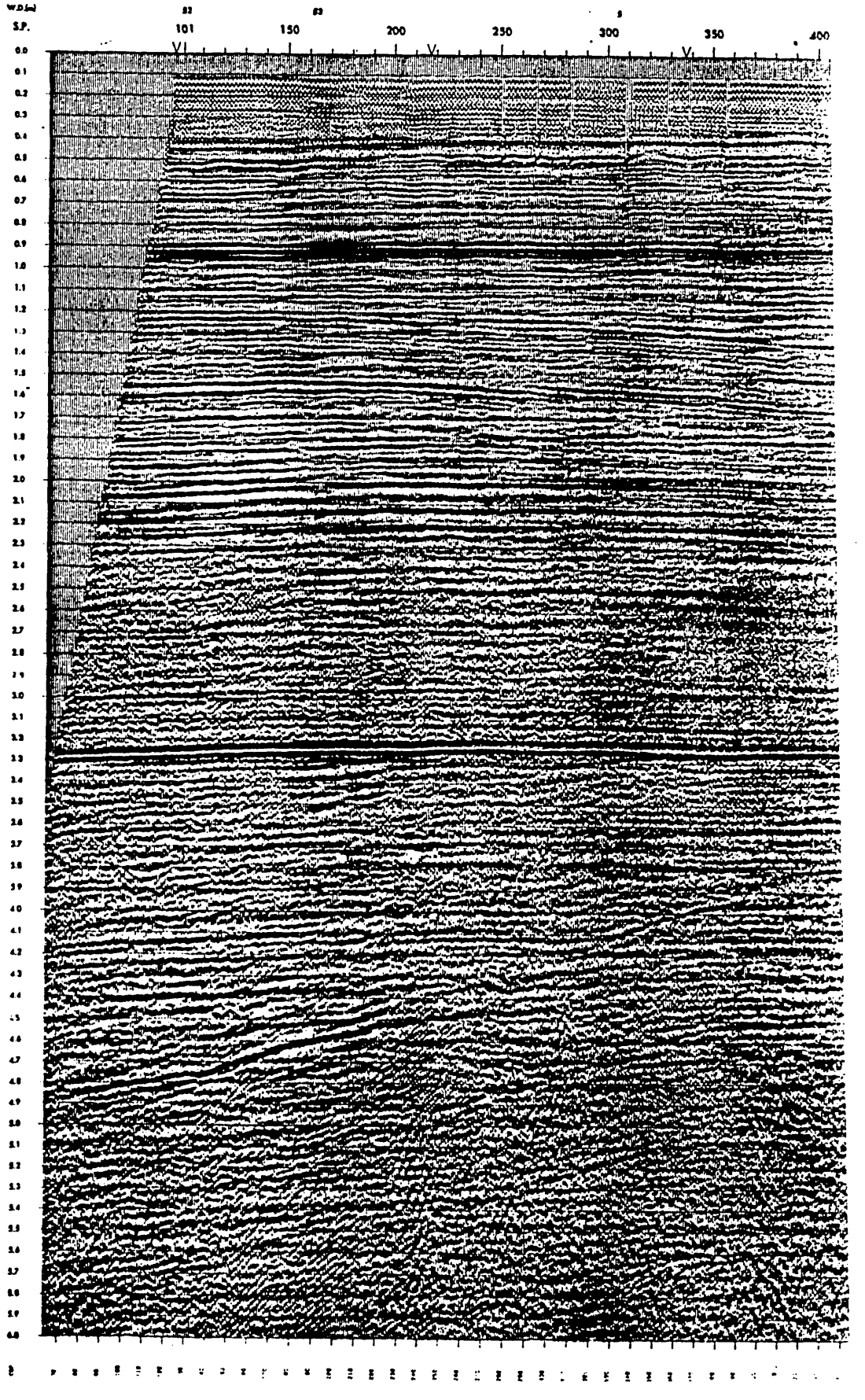
MERLIN GEOPHYSICAL COMPANY LTD.

line: SP82-86A sp 101-1484
area: OFFSHORE DENMARK
title: 3000% FILTERED MIGRATION
direction: → (NNE)

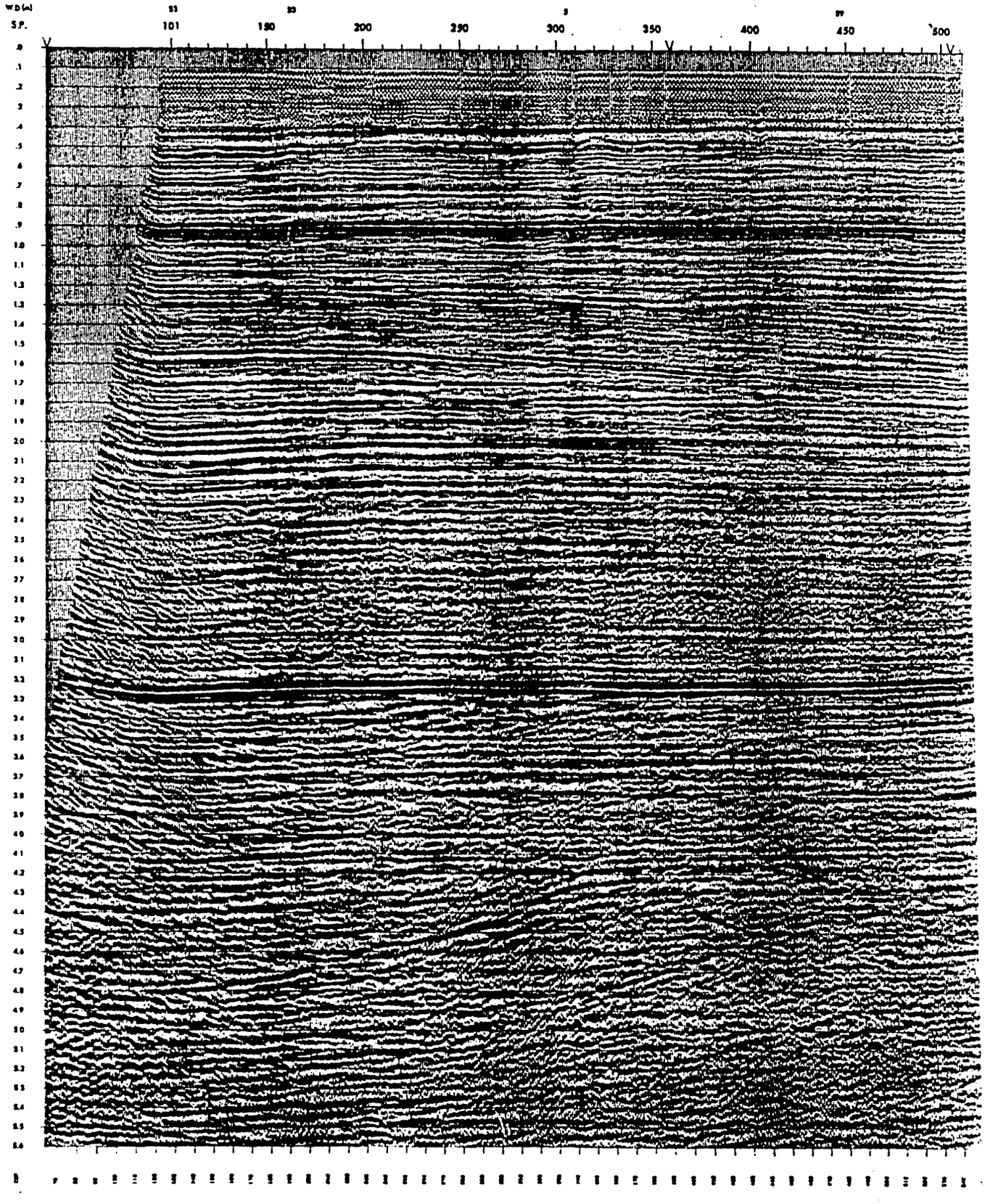
SPECULATIVE SURVEY

not to be sold or traded without permission

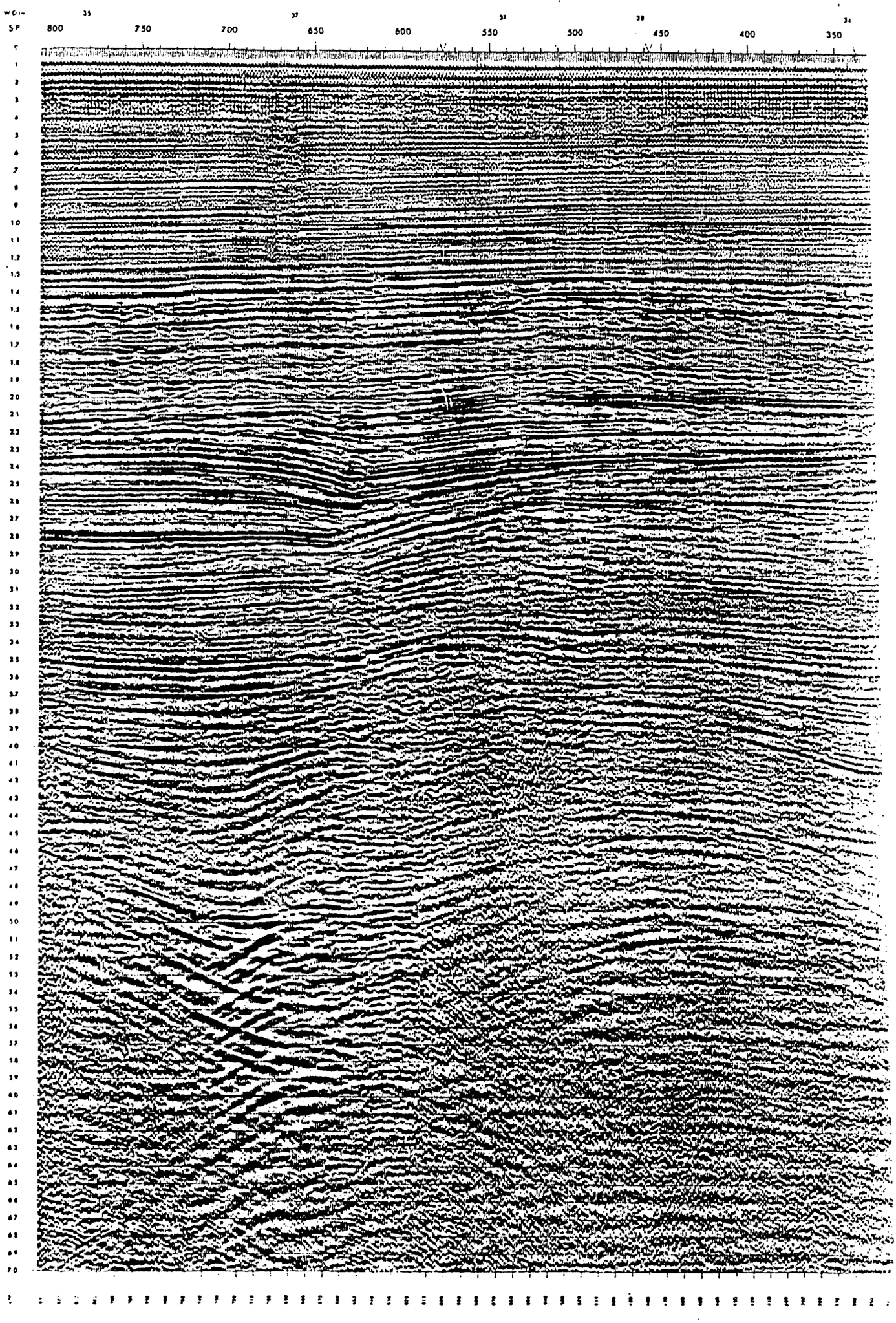
LINE: CPV-10B-1



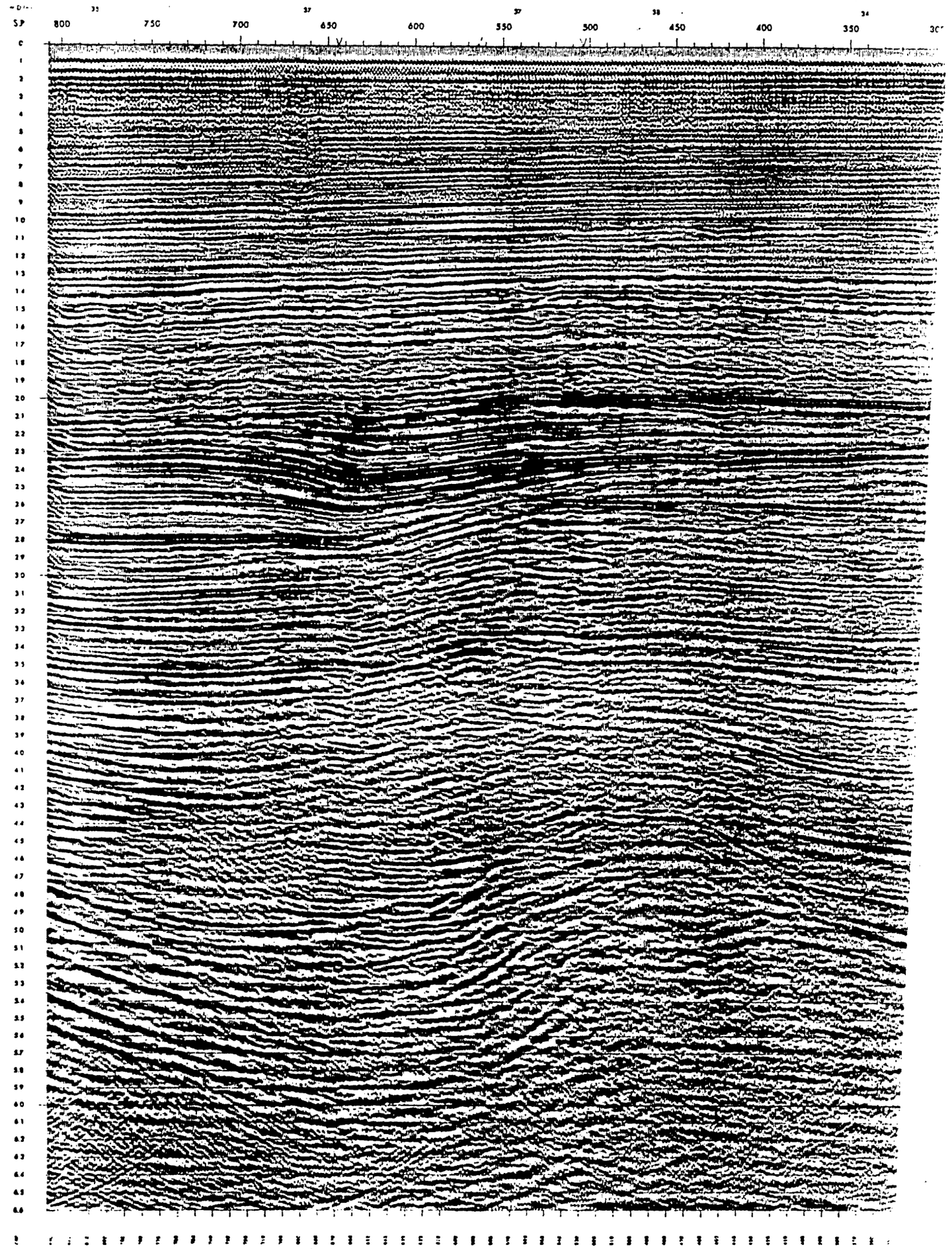
LINE: CPV-10B-2



LINE: CPV-12A-1



LINE: CPV-12A-2



LINE: CPV-03A-2

650 700 750 800 850 9(

